VAN BILJON, W J

MODELING THE TDEM RESPONSE FOR A LATERAL CHANGE IN CONDUCTIVITY

MSc UP 1997

Modeling the TDEM response for a lateral change in conductivity

by

Willem J van Biljon

Submitted in partial fulfillment of the requirements for the degree MSc. Exploration Geophysics
in the Faculty of Science
University of Pretoria
Pretoria
November 1997

ABSTRACT

The solution of the transient response of a layered earth excited by a vertical magnetic dipole is well known and used. Expansion of the solution for a 2D or 3D earth, where the conductivity changes in not just the z-direction, is extremely difficult and has only been done by way of numerical schemes, which are laborious even on powerful computers.

In this study a current fillament is used to generate magnetic fields and its derivative. This current filament diffuses like a smoke ring, downwards and outwards through the earth in time, and is defined by the following parameters: a current amplitude, a horizontal expansion velocity and a vertical or downward velocity. The influence of the conductivity and layer thickness are investigated and it is found that the parameters of the moving current filament is an integrated function of the total resistivity distribution of the layered earth model. For this study a current ring in different environments is used and the results compared. This process indicates that the current filament can be used to model differences in apparent conductivity without considering the thicknesses of layers.

The parameters of the current filament are changed one at a time, keeping the other constant, to investigate the influences of each. This technique is then applied to a 2D case, where transient sounding data is generated in the center of the transmitter loop. The 2D model consists of a vertical geo-electrical boundary which is infinite in strike. The resistivity ratio between the two regions is low and it is assumed that only a primary field is present, as is the case with a layered earth. A qualitative approach is used to determine if and when there are significant changes in the measured temporal field.

The apparent resistivity is calculated using the derivitave of the magnetic field as defined in Kaufman and Keller, 1983. This has also been applied to the magnetic field and it has been found that there is no difference for this qualitative model between the two approaches.

It has been found that the distortion of the current filament is dependent on the locality of the transmitter loop, with a larger distortion when the transmitter loop is located on the more conductive side of the discontinuity.

Lastly, this study proven has the feasability of using the concept of a moving current filament to formulate forward models for 2D and 3D models, if the proper velocity functions are known.

OPSOMMING

Die oplossing van die tydverval van 'n gelaagde aarde as gevolg van 'n vertikale magnetiese dipool is bekend en word algemeen gebruik. Om hierdie oplossing uit te brei vir 2D of 3D gevalle, waar die geleiding verander in meer as net die z-rigting, is uiters moeilik en word gedoen deur numeriese oplossings, wat selfs op baie kragtige rekenaars tydsaam kan wees.

In hierdie studie word 'n stroomfilament, wat uit- en afwaarts beweeg soos 'n rookkring, gebruik om magnetiese velde en hul afgeleides te genereer. Die invloed van die resistiviteit en diktes van lae word ondersoek en daar word gevind dat die weerstandsverspreiding van 'n gelaagde aarde 'n geïntegreerde funksie is, wat die parameters van 'n bewegende stroomring beheer. Hierdie parameters bestaan uit 'n stroomamplitude en 'n radiale en vertikale snelheid. Vir die doeleindes van hierdie studie word 'n stroomring in verskillende omgewings gebruik en die resultate word dan vergelyk. Hierdie proses dui daarop dat die stroomfilament aanvaarbaar is om verskille in skynbare weerstande aan te dui sonder om die diktes van lae in ag te neem.

Die parameters wat die posisie, grootte en stroom van die ring beheer, word afsonderlik verander, terwyl die ander konstant bly, om die invloed van elke verandering te ondersoek. Hierdie tegniek word dan toegepas op 'n 2D geval, waar tydvervaldata in die middel van die lus gegenereer word. Die 2D-model bestaan uit 'n vertikale geo-elektriese grens wat oneindig in strekking is. Die weerstandsverhouding tussen die twee gebiede is laag, sodat daar aangeneem word dat slegs 'n primêre veld, soos ook die geval vir 'n gelaagde aarde, teenwoordig is. 'n Kwalitatiewe proses word gevolg om vas te stel of daar beduidende veranderinge in die tyddata van die gemete veld is.

Die skynbare weerstand word bereken vir die afgeleide van die magneetveld soos gedefinieer in Kaufman en Keller, 1983. Hierdie proses is ook toegepas op die magneetveld en daar is geen verskil gevind tussen hierdie twee gevalle vir die kwalitatiewe voorwaartse model nie.

Die resultaat is dat die vervorming van 'n stroomfilament afhanklik is van die posisie van die bronlus, met 'n groter afwyking wanneer die bronlus op die meer geleidende deel van die diskontinuïteit is.

Hierdie studie het laastens die bruikbaarheid van die konsep van 'n bewegende stroomfilament om voorwaartse modelering vir 2D of 3D aardmodelle te doen, bewys.

ACKNOWLEDGMENTS

I would like to thank the following:

My promoter Prof W J Botha for his patience, guidance and continued support throughout this study. Drs E Stettler and A du Plooy who presented an electromagnetic honours course with enough enthusiasm and clarity to prompt my further study in the field and Dr M N Nabighian who suggested the use of a current ring to investigate this problem.

For financial support the Foundation for Research Development which provided me with a bursary and the Department Physics: UP, where I had a tutor job for two years. For my pregraduate studies the University of Pretoria provided me with a bursary of achievement. My father, Stef van Biljon, without whose monetary assistance all my years of study would have been much more difficult.

My fellow students Francois, Magdel, Petro, Riana and Jacques who provided helpful hints, conversation and encouragement over the years when it was needed. Also Pille who introduced me to geophysics. For mathematical discussions Rudolph and, especially, Gustav who provided the idea of using vectors to calculate the total magnetic field of different line elements.

The family Van Biljon for their support and concern as well as the family Louw, specifically Prof W J Louw for providing advice on the structure of this presentation.

Irma and Andries for companionship and meaningful discussions, also about the contents of a masters thesis.

Dorette for her part in this work, for always loving, encouraging and supporting me as well as providing for me in France.

TABLE OF CONTENTS

Chapter 1

Chapter 2

Chapter 3

Chapter 4

Chapter 6

Appendix A

Chapter 1

Introduction

The popularity of the time domain electromagnetic (TDEM) method has increased over the years and is now routinely applied outside the sphere of mineral exploration. Applications can be seen in engineering geology, sinkhole detection (Nelson and Haigh, 1990), groundwater prospecting as well as polution monitoring and detection. Unfortunately, the interpretation techniques have not kept pace and a need exists for more versatile interpretation techniques that can handle complex geological situations without having to use a CRAY or CONVEX main frame. The purpose of this study is therefore to investigate the applicability of emulating the behaviour of the subsurface induced current with that of a simple current filament.

Electromagnetic techniques induce current flow in the subsurface by an alternating current flow in the transmitter loop. In the frequency domain (FDEM) sinusoidal alternating current is used to energize the subsurface and in the time domain (TDEM) a step function or pulse function is used.

The TDEM technique is usually applied to two ideal geological scenarios, namely a) mapping the lateral change in electrical conductivity or resistivity of the rock mass and this is referred to as profiling, and b) mapping the vertical variation in electrical conductivity or resistivity and called transient sounding (TS) (Swift, 1988). In this study the emphasis will be on the TDEM sounding technique.

The presence of a conductive surface layer can prohibit the detection of deeper conductors and although the TDEM technique provides better results in such situations, the EM techniques work best at locating a conductor situated in a resistive host rock (Swift, 1988). Examples of such geological scenarios are the location of water-bearing structures in the gneissic terrain of northern South Africa, or in the Kalahari desert, situated at the common border between South Africa, Botswana and Namibia. Here potable groundwater can be located on the edge of conductive glacial deposits, covered by sometimes considerable thicknesses (80 to 150m) of high resistivity Kalahari sand (Van der Walt, 1991). If such features could be accurately resolved from routine TDEM soundings, the acute water shortage of this arid area could be somewhat alleviated.

The thrust of this study will therefore be to obtain more information from TS data, than that available from the conventional, one dimensional (1D), layered earth model. By studying the analogy of the movement of a current filament through the country rock, it is to be investigated whether the 2D or even 3D structure can be ascertained.

THE TIME DOMAIN ELECTROMAGNETIC METHOD

The response of a horizontally layered earth, excited by a vertical magnetic dipole, is well known and commercial software for forward and inverse calculation of data exist. These usually estimate the depth and resistivity of layers and thus treat the earth as a simple layered 1D structure, which is not always the case. Although the use of mainly 1D modeling has been fairly successful in modeling a 3D earth, there is a need to develop simple forward modeling techniques for more complex 2D and 3D situations. By forward modeling, it is meant that the structure of the earth is postulated, the response of the postulated model calculated and altered until the model and measured response agree in significant detail.

To be able to predict a realistic geological model, the geophysicist must be able to understand the processes that govern the TDEM response in simple terms. This is even more true for a multi-dimensional than for a 1D case, because the number of variables increase significantly.

The solution for the response of a 1D earth, as it is shown in Chapter 2, is fairly straightforward, because of the symmetry of the situation. The reader should note that the wave equation is solved directly, without using a vector potential.

In Chapter 3 various previous attempts to develop forward models for 2D and 3D situations are discussed. Removing the symmetry results in a system of equations which, to date, could not be solved directly. Thus various numerical solutions have been proposed. Unfortunately these techniques are very time consuming, even for powerful computers.

In Chapter 4 a forward model, based on a concept by Nabighain (1979) that the induced currents in the earth can be modeled using a single filament, moving downwards and outwards like a smoke ring, is proposed and compared to results of a vertical dipole on a layered earth.

The shape and orientation of a moving current filament are changed in Chapter 5 to investigate the possibility of applying this method to the detection of semi-vertical geo-electrical boundaries. It is assumed that the response of a laterally inhomogeneous earth will be an integrated one, in the sense that it is not possible to distinguish between a primary and secondary field, which can be superimposed to give the total response. This is usually the case with strong conductors. First, all the different parameters that govern the size and position are changed separately, as well as tilting the current ring, to determine what the effect of each change is on the measured field. Two forward models to approximate physical situations are suggested and investigated, changing all the variables simultaneously. Lastly, the results of the magnetic field definition of apparent resistivity are compared with those of the derivative of the field.

Chapter 6 concludes this study with a discussion of the results of Chapter 5, followed by the conclusions and recommendations for possible further research. The one advantage of this model is that it provides the geophysicist with a physical understanding of the electromagnetic processes that take place in the earth, something which is very difficult when faced with the numerical solution of a set of integral equations.

Appendix A contains the computer algorithms used to produce the results of Chapter 5.

Chapter 2

The Time Domain Electromagnetic (TDEM) field of a vertical dipole on a horizontally layered earth due to a step function excitation

To investigate any aspect of TDEM sounding phenomena it is important to first consider the theory for a layered earth (1D solution). This highlights the importance of a symmetrical approach. It will become apparent that it is very difficult to extend this method to more intricate 2D and 3D geological situations, because the lack of symmetry does not allow analytical solution in closed form.

This chapter gives a brief overview for solving the horizontally layered earth as follows from Du Plooy (1985), starting with Maxwell's equations, finding the Helmholz equation for the electric field, solving it directly in the frequency domain without use of a vector potential, transforming it to the time domain and defining an apparent resistivity.

Various possible definitions of apparent resistivity are investigated along with their implications.

2.1 THE HELMHOLZ EQUATION

Faraday's Law (Feynman et. al., 1975) states that the induced emf in a closed path is equal to the temporal change of magnetic flux through a surface bounded by the closed path.

$$\oint_c \bar{E}.d\bar{l} = -\frac{\partial\Psi}{\partial t} = -\frac{d}{dt}\int_s \bar{B}.d\bar{A} \qquad (2\text{-}1)$$

where E is the electrical field (V/m), Ψ is the total magnetic flux and B is the magnetic induction (T).

Ampere's Law states that the line integral of the magnetic field around any closed path is directly proportional to the net current through any area bounded by the path.

$$\oint_c \bar{H}.d\bar{l} = \int_s \bar{J}.d\bar{A} \qquad (2\text{-}2)$$

Where H is the magnetic field (A/m) and J the current density (A/m^2).

From Coulomb's law (Feynman et. al., 1975) we have

$$\int_s E.ds = \frac{Q}{\varepsilon} \qquad (2.3)$$

and

$$\int_s B.ds = 0 \qquad (2.4)$$

where Q is the total charge enclosed by the surface s.

Equations 2.1 to 2.4 are called the Maxwell equations in integral form. Although these equations are valid throughout space, they are difficult to solve for a specific problem and it is easier to work with them in differential form. These are obtained by using the theorems of Stokes and Gauss.

Stokes' law:

$$\oint_c \bar{F}.d\bar{l} = \int_s \nabla \times \bar{F}.d\bar{A} \qquad (2\text{-}5)$$

Gauss' law:

$$\oint_s \bar{F}.d\bar{A} = \int_v \nabla.\bar{F}dv \qquad (2\text{-}6)$$

Using eq 2-1 and 2-5, it follows:

$$\oint_c \bar{E}.d\bar{l} = \int_s \nabla \times \bar{E}.d\bar{A}$$

$$= -\frac{d}{dt}\int_s \bar{B}.d\bar{A}$$

$$= -\int_s \frac{\partial \bar{B}}{\partial t}.d\bar{A}$$

for a stationary surface S.

$$\int_s (\nabla \times \bar{E} + \frac{\partial \bar{B}}{\partial t}).d\bar{A} = 0$$

If S is any arbitrary nonzero surface, it means that the terms in brackets must be zero for this equation to be valid.

$$\Rightarrow \nabla \times \bar{E} + \frac{\partial \bar{B}}{\partial t} = 0$$

$$\therefore \nabla \times \bar{E} = -\frac{\partial \bar{B}}{\partial t}$$

Similarly it is possible to show from Ampere's law:

$$\nabla \times \bar{H} = \bar{J}$$

Taking into account the conservation of charge:

$$\nabla.\bar{J} + \frac{\partial q}{\partial t} = 0$$

Maxwell stated:

$$\nabla \times \bar{H} = \bar{J} + \frac{\partial \bar{D}}{\partial t}$$

where D is the displacement current (C/m^2).

Thus Maxwell's equations in a charge free homogenous medium are:

$$\nabla \times \bar{E} = -\frac{\partial \bar{B}}{\partial t} \qquad (2\text{-}7)$$

$$\nabla \times \bar{H} = \bar{J} + \frac{\partial \bar{D}}{\partial t} \qquad (2\text{-}8)$$

$$\nabla.\bar{B} = 0 \qquad (2\text{-}9)$$

$$\nabla.\bar{E} = 0 \qquad (2\text{-}10)$$

Equations 2-7 to 2-10 are called Maxwell's equations in differential form and are only valid where the various functions are continuous. Where discontinuous boundaries exist, the integral form of Maxwell's equations is used to deduce the following boundary conditions.

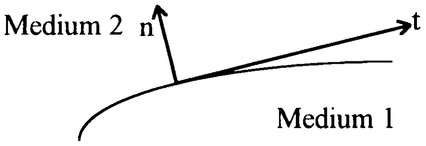

Figure 2.1 Illustration of boundary condition components with n the normal and t the tangential components.

$$E_t^1 = E_t^2 \qquad (2\text{-}11)$$

$$H_t^1 = H_t^2 \qquad (2\text{-}12)$$

$$J_n^1 = J_n^2 \qquad (2\text{-}13)$$

$$B_n^1 = B_n^2 \qquad (2\text{-}14)$$

where *n* denotes the normal component and *t* the tangential component and the superscript number the different media. When solving the Maxwell equations, one uses the following constitutive equations: $\overline{B} = \mu\overline{H}$, with μ the permeability (H/m), $\overline{D} = \varepsilon\overline{E}$, with ε the permitivity (F/m) and $\overline{J} = \sigma\overline{E}$, with σ the conductivity (S/m) of the medium.

It is further assumed that there is a zero charge density throughout the medium and that the time under consideration is long enough that displacement currents can be ignored. When a sinusoidal source current is assumed, the Maxwell equations reduce to:

$$\nabla \times \overline{E} = i\omega\overline{B} \qquad (2\text{-}15)$$

$$\nabla \times \overline{H} = \overline{J} + (-i\omega)\overline{D} \qquad (2\text{-}16)$$

$$\nabla . \overline{B} = 0 \qquad (2\text{-}17)$$

$$\nabla . \overline{E} = 0 \qquad (2\text{-}18)$$

Taking the curl of eq 2-15 and substituting 2-16:

$$\begin{aligned} \nabla \times \nabla \times \overline{E} &= i\omega\nabla \times \overline{B} \\ &= i\omega\mu\nabla \times \overline{H} \\ &= i\omega\mu(\overline{J} - i\omega\overline{D}) \\ &= i\omega\mu(\sigma\overline{E} - i\omega\varepsilon\overline{E}) \\ &= (i\omega\mu\sigma + \omega^2\mu\varepsilon)\overline{E} \end{aligned}$$

and applying the identity $\nabla \times \nabla \times \overline{F} = \nabla\nabla.\overline{F} - \nabla^2\overline{F}$ gives:

$$\nabla\nabla.\overline{E} - \nabla^2\overline{E} = (i\omega\mu\sigma + \omega^2\mu\varepsilon)\overline{E}$$

from eq 2-18 this simplifies to:

$$\nabla^2\overline{E} + (i\omega\mu\sigma + \omega^2\mu\varepsilon)\overline{E} = 0 \tag{2-19}$$

Taking into account that the frequencies used in exploration geophysics (excluding ground penetrating radar and radio wave tomography) are usually less than 100kHz, it is possible to make the quasi-static assumption:

$$i\omega\mu\sigma + \omega^2\mu\varepsilon \approx i\omega\mu\sigma = k^2 \tag{2-20}$$

Applying this assumption to eq 2-19 gives:

$$\nabla^2\overline{E} + k^2\overline{E} = 0 \tag{2-21}$$

which is the Helmholz equation. The equation indicates that the electromagnetic wave propagation is by diffusion and that reflection plays only a minor role.

2.2 A VERTICAL MAGNETIC DIPOLE ABOVE A CONDUCTING HALF-SPACE

2.2.1 The electrical field

Consider a magnetic dipole on the surface of a conductive infinite medium (half space). Assume that the conductivity of air is zero (σ=0) and that the permeability of both free air and the medium is that of free space namely $\mu=\mu_0=4*10^{-7}$H/m.

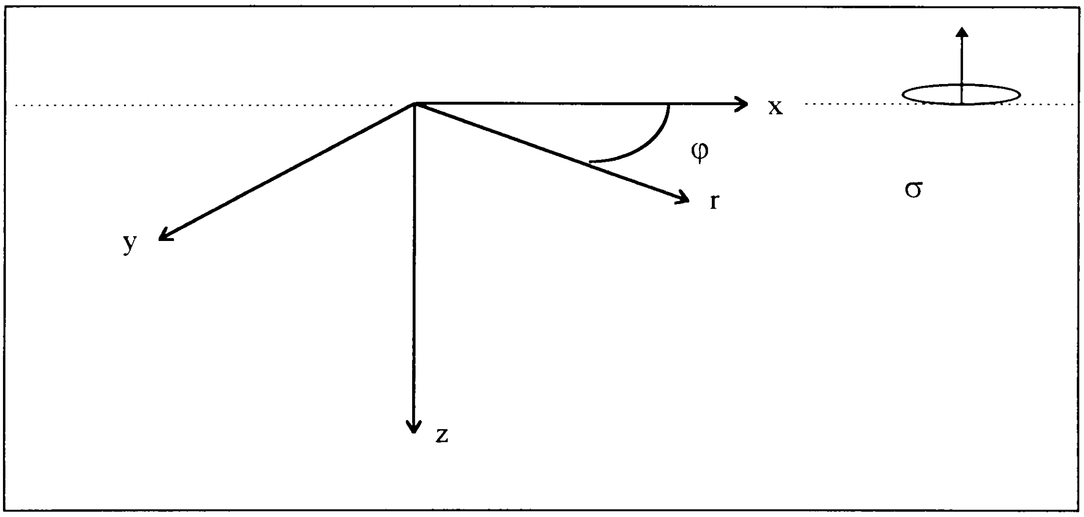

Figure 2.2 Cartesian and cylindrical system of axis with z=0 and vertical dipole at the surface of the half-space.

Due to the symmetry of the magnetic field of a magnetic dipole and by implication also the electrical field, it is preferable to work in cylindrical coordinates.

For the electric field:

$$\overline{E} = E_r\hat{r} + E_\varphi\hat{\varphi} + E_z\hat{z}$$

But looking at the symmetry of the fields generated by the vertical dipole, it is possible to see that the electrical field will only have a component in the angular direction and that that component will be independent of the angle:

$$\begin{aligned} &\bar{E} = E_\varphi \hat{\varphi} \\ &\frac{\partial \bar{E}}{\partial \varphi} = 0 \end{aligned} \qquad (2\text{-}22)$$

Thus from eq 2-21 and 2-22:

$$\nabla_\varphi^2 \bar{E} + k^2 E_\varphi = 0 \qquad (2\text{-}23)$$

For cylindrical coordinates:

$$\begin{aligned} \nabla_\varphi^2 \bar{E} &= \nabla^2 E_\varphi - \frac{1}{r^2} E_\varphi + \frac{2}{r^2}\frac{\partial E_r}{\partial \varphi} \\ &= \nabla^2 E_\varphi - \frac{1}{r^2} E_\varphi \end{aligned} \qquad (2\text{-}24)$$

because E_r=0. Substituting into eq 2-23:

$$\nabla^2 E_\varphi - \frac{1}{r^2} E_\varphi + k^2 E_\varphi = 0 \qquad (2\text{-}25)$$

Using the fact that $\nabla^2 u = \frac{1}{r}\frac{\partial}{\partial r}(r\frac{\partial u}{\partial r}) + \frac{1}{r^2}\frac{\partial^2 u}{\partial \varphi^2} + \frac{\partial^2 u}{\partial z^2}$ gives:

$$\frac{1}{r}\frac{\partial}{\partial r}(\frac{1}{r}\frac{\partial E_\varphi}{\partial r}) + \frac{\partial^2 E_\varphi}{\partial z^2} + (k^2 - \frac{1}{r^2})E_\varphi = 0 \qquad (2\text{-}26)$$

Let us try to solve eq 2-26 by proposing a solution of the form:

$$E_\varphi = R(r)Z(z) \qquad (2\text{-}27)$$

and substituting back into eq 2-26:

$$\frac{1}{Rr}\frac{dR}{dr} + \frac{1}{R}\frac{d^2 R}{dr^2} - \frac{1}{r^2} = -\frac{1}{Z}\frac{d^2 Z}{dz^2} - k^2 \qquad (2\text{-}28)$$

Because eq 2-28 must be valid for any arbitrary r and z, both sides of the equation must be constant. Choose this constant to be $-m^2$:

$$\begin{aligned} &\frac{d^2 Z}{dz^2} + (k^2 - m^2)Z = 0 \\ &\frac{d^2 Z}{dz^2} - u^2 Z = 0 \end{aligned} \qquad (2\text{-}29)$$

where $u = \sqrt{m^2 - k^2}$ and only real values when u>0 are considered. The solutions of eq 2-29 are combinations of e^{uz}, e^{-uz}.

$$r^2\frac{dR}{dr} + r\frac{dR}{dr} + (r^2 m^2 - 1)R = 0 \qquad (2\text{-}30)$$

Possible solutions of eq 2-30 are the Bessel functions $J_1(mr)$ and $Y_1(mr)$. In air k^2=0, because σ=0 and eq 2-29 becomes:

$$\frac{d^2 Z}{dz^2} - m^2 Z = 0 \qquad (2\text{-}31)$$

and the solutions become combinations of e^{mz}, e^{-mz} and eq 2-30 remains unaltered. The electrical field in air consists of two parts $E_\varphi = E_\varphi^p + E_\varphi^s$ where the p denotes primary and the s secondary. The primary field is due to the source (the magnetic dipole) while the secondary field is the result of the interaction of the source with the earth.

$$E_\varphi^s : (Ae^{mz} + Be^{-mz})(CJ_1(mr) + DY_1(mr))$$

$$E_\varphi^p : \frac{i\omega\mu M}{4\pi}\int_0^\infty e^{-m|z|} J_1(mr) m dm \tag{2-32}$$

To solve the constants for the secondary field in eq 2-32, apply the boundary conditions at z=0:

$$E_\varphi^0 = E_\varphi^1 \tag{2-33}$$

$$\frac{dE_\varphi^0}{dz} = \frac{dE_\varphi^1}{dz} \tag{2-34}$$

The electromagnetic field must always be bounded and therefore any solution that tends to infinity at any stage is not valid. The Bessel function $Y_1(mr) \xrightarrow{r\to 0} -\infty$ and the logarithmic function $e^{-mz} \xrightarrow{z\to -\infty} -\infty$ do not give rise to proper solutions for the electrical field in air (z<0). From eq 2-31 and 2-32 the electrical field is:

$$E_\varphi = \frac{i\omega\mu M}{4\pi}\int_0^\infty e^{-m|z|} J_1(mr) m dm + \int_0^\infty Ae^{mz} J_1(mr) dm \tag{2-35}$$

In the ground (z>0) the solution $e^{uz} \xrightarrow{z\to\infty} \infty$ is not applicable and the electrical field becomes:

$$E_\varphi^{'} = \int_0^\infty Be^{-uz} J_1(mr) dm$$

At the air-surface interface (z=0) eq 2-33 must be valid:

$$\frac{i\omega\mu M}{4\pi}\int_0^\infty J_1(mr) m dm + \int_0^\infty AJ_1(mr) dm = \int_0^\infty BJ_1(mr) dm$$

$$\int_0^\infty (m\frac{i\omega\mu M}{4\pi} + A - B) J_1(mr) dm = 0$$

$$\frac{i\omega\mu Mm}{4\pi} + A = B \tag{2-36}$$

To complete the solution, use the boundary condition of eq 2-34:

$$\begin{aligned} \frac{-i\omega\mu Mm^2}{4\pi} + mA &= -uB \\ &= -u(\frac{i\omega\mu Mm}{4\pi} + A) \end{aligned} \tag{2-37}$$

Set $\rho = \frac{i\omega\mu M}{4\pi}$:

$$
\begin{aligned}
A &= \left(\frac{m-u}{m+u}\right) m\rho \\
B &= \frac{2m^2\rho}{m+u} \qquad (2\text{-}38) \\
E_\varphi(z=0) &= \frac{i\omega\mu M}{2\pi}\int_0^\infty \frac{m^2}{m+u} J_1(mr)\,dm
\end{aligned}
$$

2.2.2 Explicit form of E_φ in relation with $\partial B_z/\partial t$

From eq 2-38 and $\dfrac{1}{m+u} = \dfrac{m-u}{k^2}$ it follows:

$$
E_\varphi = \frac{M\rho}{2\pi}\left(\int_0^\infty m^3 J_1(mr)\,dm - \int_0^\infty m^2 u J_1(mr)\,dm\right) \qquad (2\text{-}39)
$$

Making use of the Sommerfeld integral:

$$
\begin{aligned}
\frac{e^{ikR}}{R} &= \int_0^\infty \frac{m}{u} e^{-u|z|} J_0(mr)\,dm \qquad (2\text{-}40) \\
R &= \sqrt{r^2+z^2}
\end{aligned}
$$

and applying the differential operator $\dfrac{\partial}{\partial r}\dfrac{\partial^2}{\partial z^2}$ to both sides of eq 2-40 it is possible to write the two integrals in eq 2-39 in explicit form:

$$
E_\varphi(t) = \frac{3M\rho}{2\pi r^4}\left((1-ikr-\frac{k^2r^2}{3})e^{ikr}-1\right) \qquad (2\text{-}41)
$$

From Maxwell's equation (eq 2-15) $\nabla\times\overline{E} = i\omega\overline{B}$ follows:

$$
\Delta\times E_\varphi(t) = \frac{1}{r}\frac{\partial}{\partial r}\left(rE_\varphi\right) = i\omega B_z(t)
$$

Hence:

$$
i\omega B_z(t) = \frac{9M\rho}{2\pi r^5}\left(1-\left(1-ikr-\frac{4}{9}k^2r^2+\frac{1}{9}k^3r^3\right)e^{ikr}\right) \qquad (2\text{-}42)
$$

2.3 $\partial B_Z/\partial t$ FOR A HOMOGENEOUS HALF-SPACE

Regard the earth as a linear system which transforms the input *f*(ω) to *g*(ω) by way of function *h*:

$$
\begin{aligned}
& f(\omega)\rightarrow h\rightarrow g(\omega) \\
\Rightarrow\ & g(\omega) = f(\omega)h(\omega)
\end{aligned}
$$

Assume that the input current is a step function:

$$
\tilde{I}(t) = \begin{cases} 1 & t<0 \\ 0 & t\geq 0 \end{cases}
$$

$$\therefore I(\omega) = \frac{1}{i\omega}$$

Thus the time domain output would be:

$$\tilde{B}(t) = \frac{1}{2\pi}\int \frac{\overline{B}(\omega)}{i\omega} e^{-i\omega t} d\omega \tag{2-43}$$

But the Fourier transform of a derivative is $\Im(f') = -i\omega f$ and therefore the transformation of the magnetic induction in the z-direction, B, is done as follows:

$$\frac{\partial B_z}{\partial t} = \frac{1}{2\pi}\int_{-\infty}^{\infty} B(\omega)_z (-i\omega) e^{-i\omega t} d\omega \tag{2-44}$$

Substituting eq 2-44:

$$\frac{\partial B_z}{\partial t} = \frac{9M\rho}{2\pi r^5}\frac{1}{2\pi}\int_{-\infty}^{\infty}\left(1-(1-ikr-\frac{4}{9}k^2r^2+\frac{1}{9}k^3r^3)e^{ikr}\right)\frac{e^{i\omega t}}{i\omega} d\omega \tag{2-45}$$

By making use of the probability integral:

$$\frac{1}{2\pi}\int_{-\infty}^{\infty}\frac{e^{ikr}}{i\omega} e^{-i\omega t} d\omega = \Phi(u)$$

$$\Rightarrow \Phi(u) = \sqrt{\frac{2}{\pi}}\int_0^u e^{\frac{-x^2}{2}} dx$$

$$u = r\sqrt{\frac{\sigma\mu}{2t}}$$

it can be shown that:

$$\frac{\partial B_z}{\partial t}(t) = -\frac{9M\rho}{2\pi r^5}\left(\Phi(u) - \sqrt{\frac{2}{\pi}} e^{\frac{-u^2}{2}} u(1+\frac{u^2}{3}+\frac{u^4}{9})\right) \tag{2-46}$$

2.4 PRESENTATION OF TIME DOMAIN DATA

2.4.1 General

Spies and Eggers (1986) note that the term apparent resistivity has a long history and that it is traditionally defined as the resistivity of a homogenous half-space which will produce the same response as that measured over the real earth. They also point out that apparent resistivity is merely a normalizing procedure with little physical significance, except for a homogeneous half-space and that there are other methods of normalization suitable to some cases.

They compare early and late time apparent resistivity definitions for the magnetic field and voltage responses. It is clearly shown that, because the voltage response is the derivative of the magnetic field response, 'ambiguities' can arise in the apparent resistivity curves, so that the apparent resistivity can give higher values than are possible for any homogeneous earth, or that the curves can even oscillate.

These so-called ambiguities only arise because they do not seem to conform to the intuitive understanding of apparent resistivity curves.

Furthermore they argue against Macnae and Lamontagne (1984) who stated that measurements based on the magnetic field, step response, are inherently superior to voltage (impulse response) measurements, because characteristic features of the first type occur earlier. Spies and Eggers (1986) consider that both types of systems measure the same phenomenon, i.e. the decay of the secondary EM field and must both be affected by the same earth layering, although the shape of the voltage curve will be different, being the time derivative of the magnetic field. However, Newman, et. al., (1987) find that there are cases for a 3D earth where the magnetic field definition of apparent resistivity is superior.

Spies and Eggers (1986) suggest using alternative normalizations such as:

$$\frac{V\sigma a^3}{mI}$$

which is dimensionless and can be used with the in-loop voltage response, and

$$\frac{V\sigma a}{I}$$

with the coincident loop voltage response. These relations normalize for the transmitter loop size, current and receiver moment and is useful for displaying layered earth data, because the conductivity of the upper layer can be found directly. The expression for the magnetic field in-loop measurement is:

$$\frac{ha}{I}$$

which is dimensionless and does not involve conductivity.

Raiche and Gallagher (1985) attempted to calculate transient electromagnetic (TEM) vertical diffusion velocity as a function of resistivity, time and transmitter loop size. This diffusion velocity is used to calculate apparent resistivity pseudodepth sections from apparent resistivity time sections.

The vertical diffusion velocity was defined as the rate of propagation of the maximum of dB/dt, the rate of change of the magnetic field. When the transmitter is switched off, the constant magnetic field that was set up in the earth, collapses. The TEM diffusion process is the rate at which this collapse occurs. The apparent resistivity as a function of pseudodepth is plotted. After applying this method to different layered earth models they conclude that apparent resistivity is associated with a smoke disk which can be present in different layers at once. This smoke disk is presented against the smoke ring concept introduced by Nabighain (1979).

The conventional apparent resistivity definition is not the only way by which TEM data can be presented. Macnae and Lamontagne (1987) investigated another form of data transformation to try and find a conductivity section of the earth. This method is a forward solution scheme with only one step as opposed to the inversion of data which is a dual step process, where forward models are normally also necessary, to compare the inverted model with.

The process consists of two parts: the first step is to transform the data at each time delay to an apparent depth to which the currents have diffused at that time. They also found a transformation that is independent of the source receiver geometry by representing the response in the form as source images as first applied by Maxwell. The second step is to find a reasonable conductivity function from the apparent depth function. A simple conductivity estimator was found by using the concept of 'slowness' of diffusion. Although the method could not be explained theoretically, empirical evidence proves its validity.

2.4.2 Apparent resistivity

The asymptotic values for the electrical field, from eq 2-41 are:

$$E_\varphi \xrightarrow{t\to 0} \frac{3M\rho_1}{2\pi r^4}$$
$$E_\varphi \xrightarrow{t\to\infty} \frac{\mu^{5/2}\sigma_N^{3/2} rM}{40\pi^{3/2} t^{5/2}} \qquad (2\text{-}47)$$

The apparent resistivity can now be defined (Kaufman and Keller, 1983) as either:

$$\rho_a = \frac{2\pi r^4 E_\varphi}{3M}$$
$$\rho_a = \left(\frac{\mu^{5/2} rM}{40\pi^{3/2} t^{5/2} E_\varphi}\right)^{2/3} \qquad (2\text{-}48)$$

Looking at the asymptotic values of eq 2-48 in the light of eq 2-47 it is clear that the first definition will only give the apparent resistivity of the first layer, while the second definition contains information over the range of conductivities in the earth converging to the last layer's value. It is important to note that apparent resistivity is only a definition to highlight certain features of a measured field in the earth to aid in the interpretation of a possible geological structure. It is usually more practical to measure the emf caused by a changing magnetic flux (derivative of magnetic flux) through a coil.

The apparent resistivity definition most frequently used is (Kaufman and Keller, 1983):

$$\rho_a = \frac{\mu}{4\pi t}\left(\frac{2\mu M}{5t\dot{B}_z}\right)^{2/3} \ (\Omega.\mathrm{m}) \qquad (2\text{-}49)$$

This formula enables one to draw apparent resistivity curves for the central loop configuration, where the apparent resistivity is plotted against a normalized time variable. Forward models for a variety of physical situations can be calculated and compared to field data. This method is called transient sounding (TS), because the magnetic field, or its derivative, is displayed as an apparent resistivity value as the magnetic field decays with time.

Similar to the case for a magnetic dipole on a conducting half space, the behaviour of a magnetic dipole on a layered earth is also relatively easy to calculate. This is due to the fact that the response of the dipole is symmetrical and lends itself well to mathematical treatment in the cylindrical or even spherical coordinate system.

Lateral or horizontal change in resistivity does not normally display such symmetrical behaviour and cannot be mathematically described in closed form, except for special cases. The next chapter takes a look at some attempts at solving such problems.

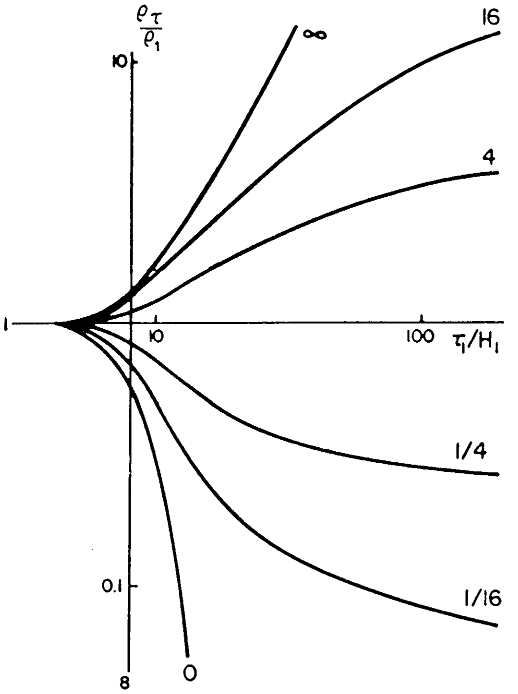

Figure 2.3 Two layer apparent resistivity curves (after Kaufman and Keller, 1983).

Chapter 3

The transient sounding (TS) technique and lateral changes in resistivity

This chapter describes briefly the theoretical background of previous work done in this field. It is divided into three parts: mathematical models, physical models and case studies. Although it is not complete with respect to 3D modeling of EM theory in general, care was taken to include specific studies which attempted to solve the situation of low contrast lateral changes in resistivity, with the TS technique. Some studies present only a forward model while others also include case studies, or interpretations of synthetic data.

3.1 MATHEMATICAL MODELS

3.1.1 Axially symmetric earth

In the mid-seventies several procedures were presented that enabled the solution of localized 3D structures in the frequency domain, but these could not be directly Fourier transformed to the time domain as the response was only limited over a bandwidth of frequencies. To calculate the time domain response, the response at many frequencies must be known (Goldman and Stoyer, 1983). Consequently a finite difference scheme was formulated by Goldman and Stoyer (1983) to solve the integral equation of the electrical field over an axially symmetric earth. The model consists of a buried cylindrical conductor whose axis coincide with that of the field system.

The reason for choosing this model is that it supports the formulation of a boundary value problem. The finite difference grid is not extended to include the half-space above the earth and the basement is taken to be perfectly conducting; this means that there is no field present here. The boundary condition at the air-earth interface is replaced by an integral equation. If the basement is not perfectly conducting, the boundary condition there will also have to be replaced by an integral equation.

Goldman and Stoyer (1983) employed the variable-directions method, which reduces each advance of one step in time from one 2D calculation to a large number of one-dimensional calculations. Thus, for one time step forward, two sets of 1D finite-difference equations and one Fredholm integral equation are solved. The solution shows excellent agreement with an analytical solution for a four layer earth.

Buried cylinders are best resolved if their radii are between 0.5 and two times the overlying sediment thickness as can be seen in Figures 3.1 to 3.3. If the radius of a conductive cylindrical body is more than twice the sediment thickness, it appears to be of infinite lateral extent. The interpreted conductivity, using 1D inversion, of smaller bodies is significantly less than the true conductivity, while the interpreted thickness is about the same.

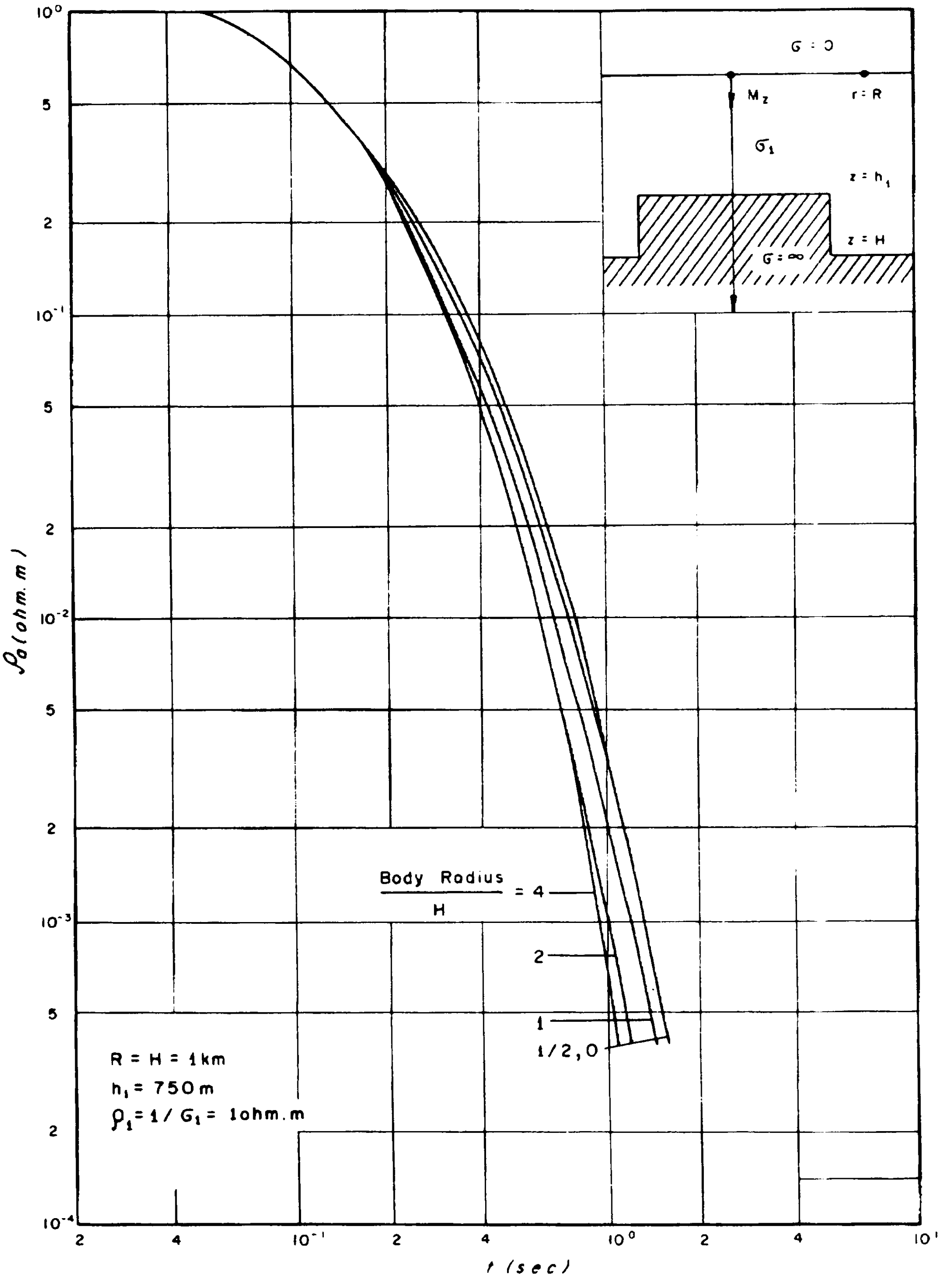

Figure 3.1 Transient (total field) response of a cylindrical topographic high on the perfectly conducting basement. Note that features with a radius less than the sediment thickness are not detectable (after Goldman and Stoyer, 1983).

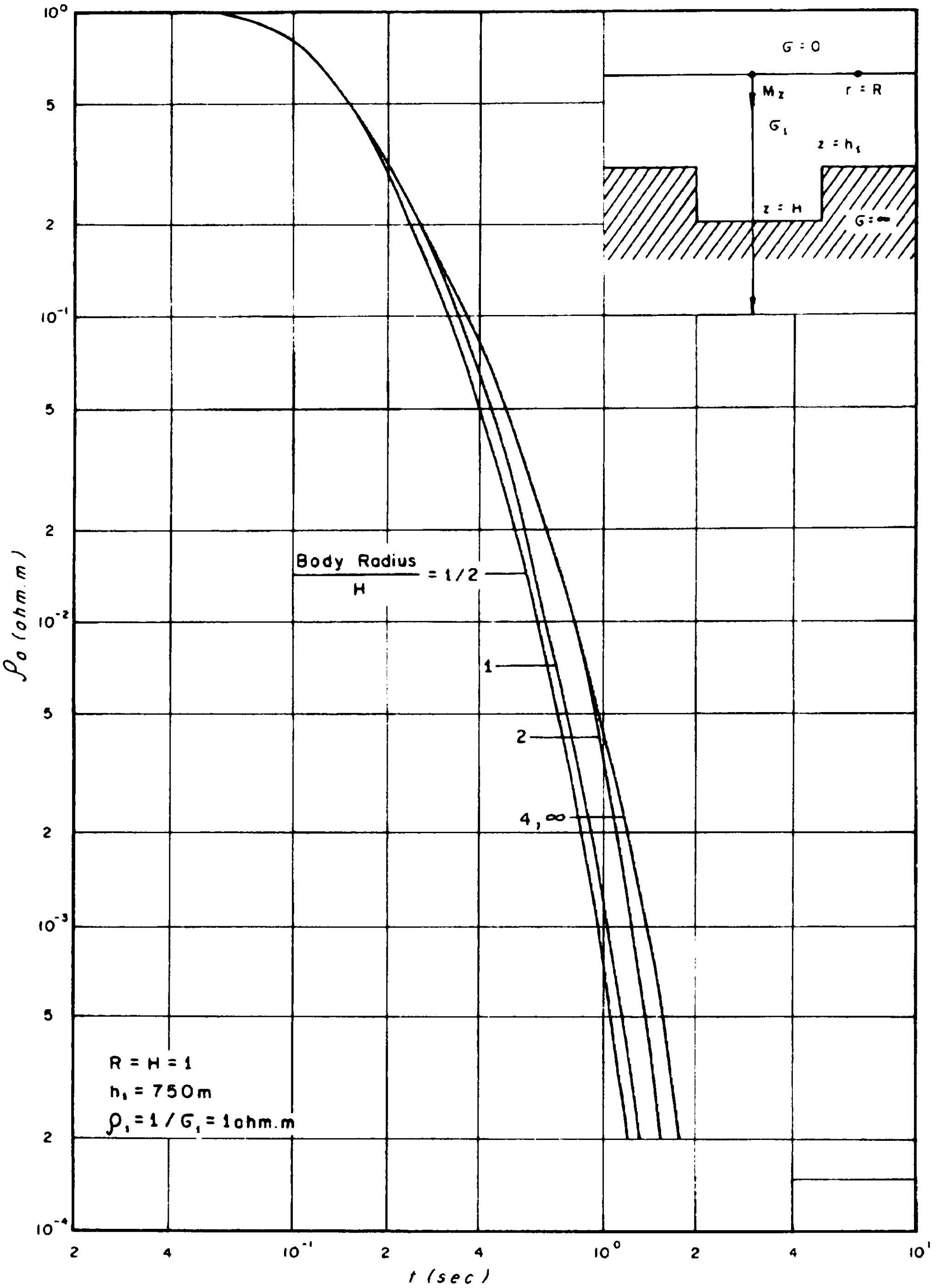

Figure 3.2 Transient (total field) response of a cylindrical topographic depression on the perfectly conducting basement. Note that features with a radius greater than about twice the sediment thickness appear to be infinite in extent (after Goldman and Stoyer, 1983).

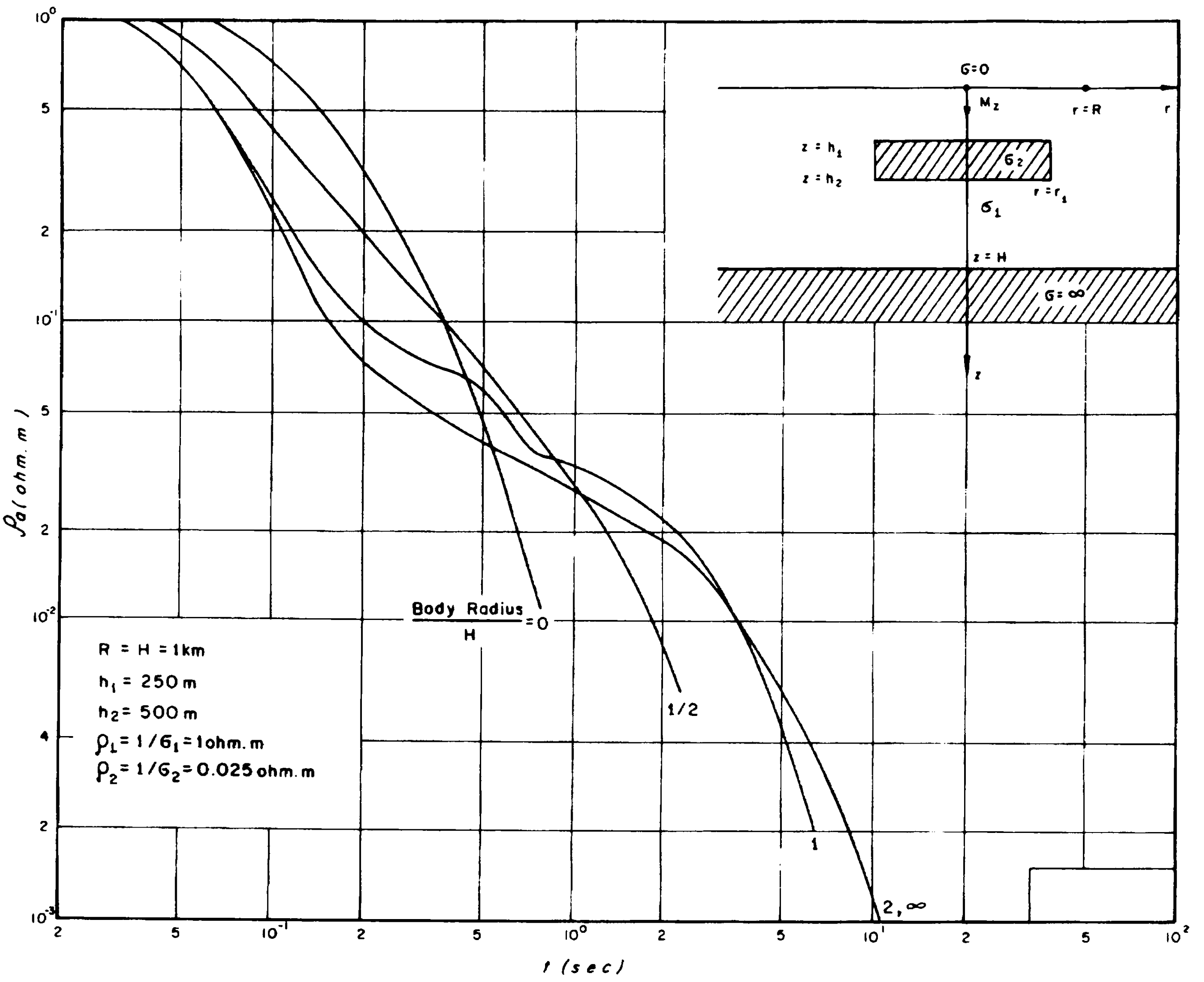

Figure 3.3 Transient (total field) response of a cylindrical conductor buried in the sediments with perfectly conducting basement. Note that features with radius greater than the sediment thickness appear to have infinite lateral extent (after Goldman and Stoyer, 1983).

3.1.2 Spatial and temporal analysis of EM data

To try and interpret EM data collected over an earth with 3D structures, Garg and Keller (1986) applied a filtering technique used in magnetic methods. One of the reasons for this is that calculating the response of 3D structures is expensive, whereas a filtering method is easily done. The method was applied to data from a so-called long offset transient electromagnetic method (LOTEM) survey. The LOTEM system consists of a long grounded wire through which a square wave of current is flowing. Measurements of the transient magnetic field accompanying each edge of the step wave in the source are done at some distance from the source.

Traditionally, data of this type was interpreted by assuming the variation of resistivity only to be that of a layered earth. Garg and Keller (1986) found that the distortion of data as a result of 3D structures can be so severe that no acceptable fit can be found by means of a 1D inversion and also that the distortion is not necessarily diagnostic. Measurements were made over a wide range of parameters.

Examination of the model response revealed that the effects of 3D structures are more clearly indicated in the spatial structure than in the temporal structure of the EM field.

Firstly they determined the best layered earth fit to the data at all the stations and then subtracted these apparent resistivity values at each station and time to obtain modified time-slice apparent resistivity maps, given the assumption that the EM field consists of separate superimposed contributions. The primary secondary field is considered the result of the layered structure of the earth and the further perturbations of the field originates from induction and counter induction of areas where the resistivity deviates from that of a layered earth.

Selected anomalies were downward continued. The peak-to-trough amplitude of the anomaly is then plotted as a function of the depth of continuation. The point of maximum curvature of this plot is the approximate depth of the body. Although the interpretation could not be tested, the authors are satisfied that enough evidence is produced that continuation methods for static potentials can be applied just as successfully to EM data.

Fitterman and Stewart (1986) investigated the TS method for exploration of groundwater. They note that the following equation must be valid:

$$\frac{\sqrt{2\pi 10^{7} t\rho_1}}{h_1} \approx 7 - 11$$

to be able to estimate the resistivity of the first layer reliably; thus taking into account the propagation of EM fields in the earth. Using a forward calculation algorithm, they formulated their groundwater problems like gravel lenses and salt water and fresh water interfaces as 1D problems. Although these are 1D models, it shows that the spatial structure of the EM field is very important when investigating responses of 3D bodies or vertical geo-electric contacts.

3.1.3 Modeling and interpretation of 3D TS data

Newman, et. al. (1986) developed an algorithm to calculate the TEM response of a 3D body in a layered earth. The problem is solved in the frequency domain and the imaginary part is Fourier transformed to the time domain. This is done by way of a digital filter technique to yield sufficient data for a transient which is reliable over at least six decades.

The method does not lend itself to resistivity contrasts higher than 200:1. They investigated models of an overburden with variable thickness and a sedimentary structure beneath volcanics as applied to the central-loop method. These forward calculations were interpreted by means of a 1D inversion scheme.

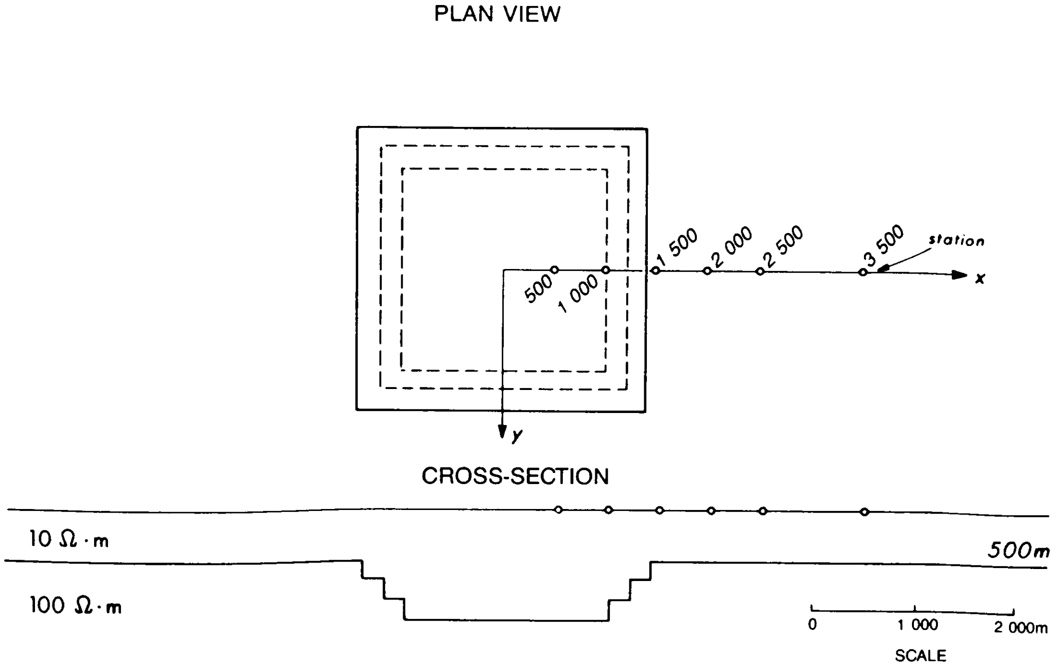

FIG. 15. Structure model of an overburden layer with variable thickness.

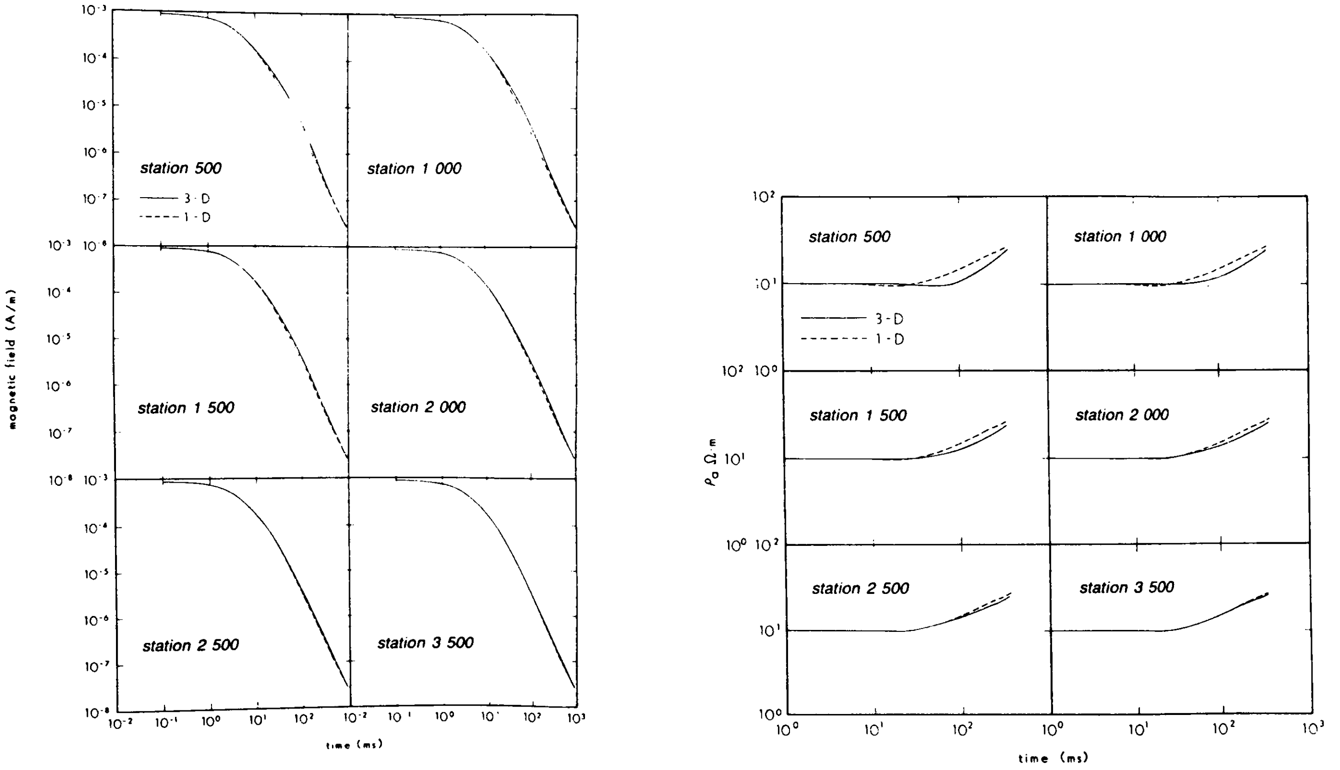

Figure 3.4 Model and results of an overburden with variable thickness (after Newman, et. al, 1986).

The 1D response in Figure 3.4 is defined as the response of a layered earth without the depression. As a result of the depression, the magnetic field is increased and the apparent resistivity is lowered relative to the 1D response. There is a slower decay over the depression. The anomaly of the 3D data with respect to the 1D data is band limited in time and disappears eventually so that the 3D data approach the layered earth case. 1D inversion resulted in a depth to the basement of 700m as opposed to the real depth of 1100m. The result is not accurate, but does locate the deepest part of the depression.

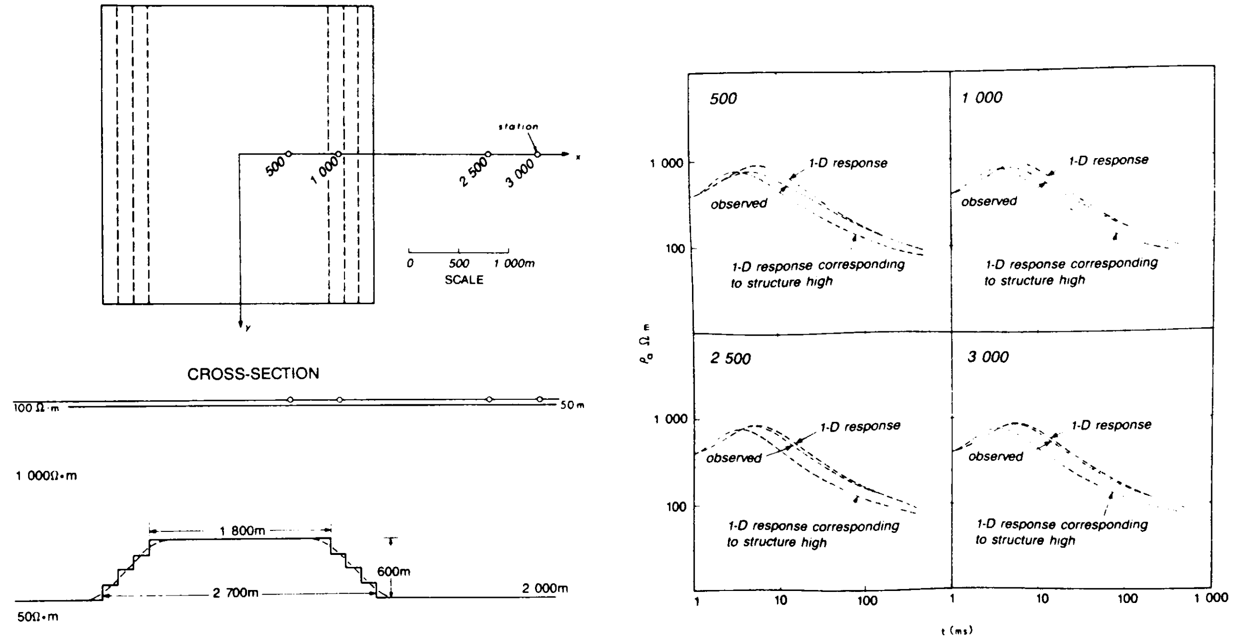

Figure 3.5 Simulation of sedimentary structure beneath volcanics. Central-loop stations are located at x=500, 1000, 2500 and 3000 (after Newman, et. al., 1986).

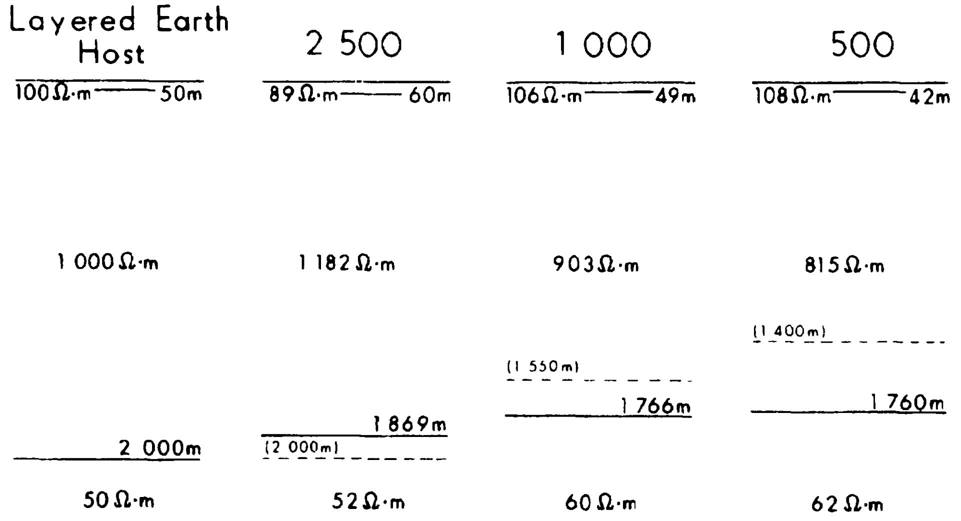

Figure 3.6 Three-layer 1D interpretations of model in Figure 3.5 (after Newman, et. al., 1986).

Another model studied by Newman, et. al. (1986) is shown in Figure 3.5 with 1D three-layer interpretations in Figure 3.6. The three-layer interpretation does indicate a volcanic unit whose resistivity changes laterally. A rise in the basement is detected. Real depth to basement is indicated by dashed lines. The volcanic unit has a resistivity of 815 Ω.m at station 500, but at station 2500 the resistivity increases to 1182 Ω.m. The interpretation also shows that the minimum depth to conductive basement is 1760m at station 500, whereas the correct depth is 1400m.

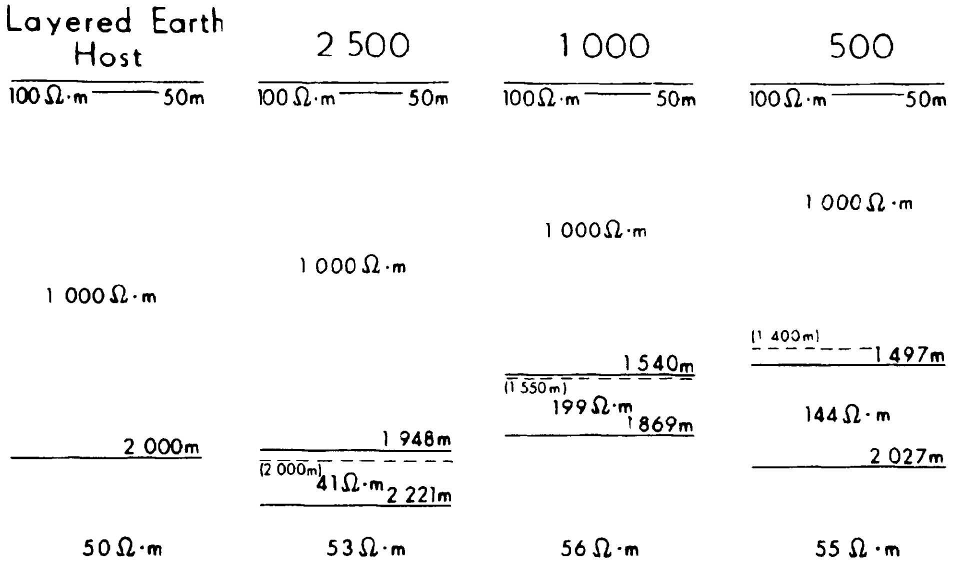

Figure 3.7 Constrained four-layer interpretation of model in Figure 3.5 (after Newman, et. al., 1986).

A constrained four-layer interpretation is shown in Figure 3.7 and it shows a thinning in the volcanic unit as the sounding station approaches the basement high. The volcanic unit is constrained at 1000Ω.m. This method of using a constrained four-layer model replaces the basement high with an equivalent conducting layer which has variable resistivity and thickness at similar depth. In practice it will be difficult to apply a constrained layer case, because the control of a known overburden resistivity will not be known.

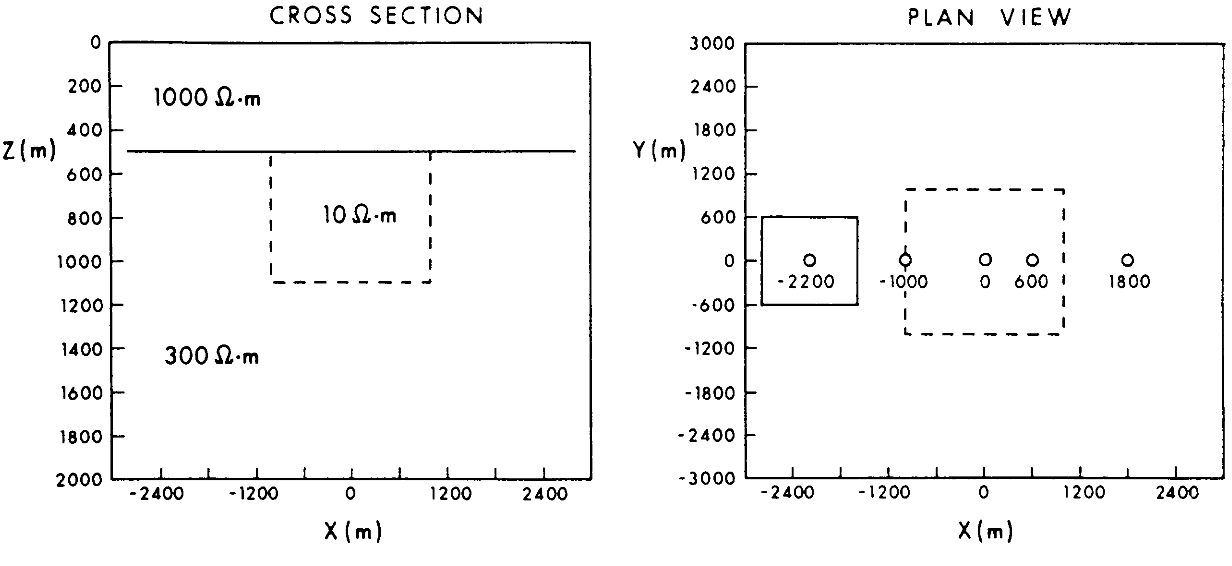

Figure 3.8 3D conductive body in a two-layer earth. The body is typical of a geothermal exploration target. The body is outlined by the dashed lines. The transmitter loop is only shown at -2200. Central-loop soundings are calculated at -2200, -1000, 0, 600 and 1800 (after Newman, et. al., 1987).

Furthermore Newman, et. al. (1987) investigated how the interpretation of TS over 3D structures can best be made with optimum use of layered earth models. The forward model used by Newman, et. al. to investigate a 3D conductive structure in a layered earth is shown in Figure 3.8 and the comparison of the layered earth apparent resistivity curves at station 600, with and without the 3D structure, is made in Figure 3.9. It is clear that the voltage apparent resistivity definition yields over- and undershoots of the data which do not correspond with the magnetic field. As mentioned before (Spies and Eggers, 1986) this is due to the fact that the measured voltage is the derivative of the magnetic field and not solely the result of the 3D situation.

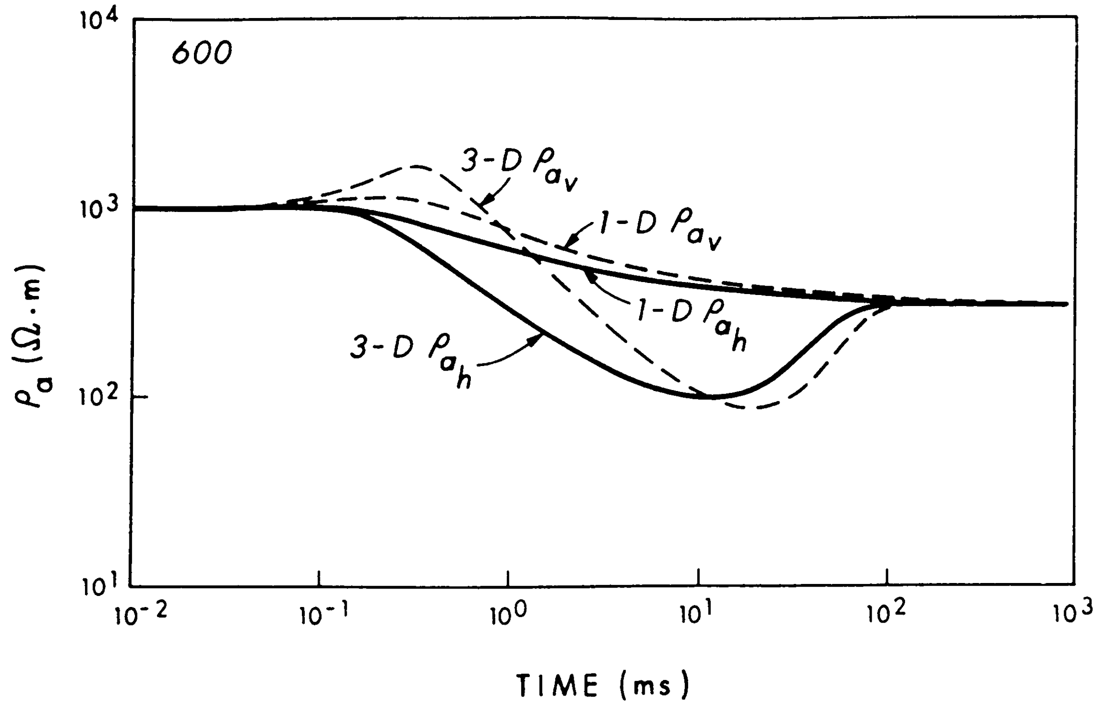

Figure 3.9 3D apparent resistivity responses at station 600. The 1D responses are shown for comparison. Subscripts v and h refer to apparent resistivity calculated with the voltage and magnetic data, respectively (after Newman, et. al., 1987).

They then attempted 1D models fits and inversion of the data at the stations indicated in Figure 3.8, based on the magnetic field definition of apparent resistivity. Four layers were the minimum that yielded satisfactory results. Increasing the number of layers did not significantly reduce the root mean square error of the fits. The first and last layer were constrained at 1000Ω.m and 300Ω.m respectively. Figure 3.10 depicts the results of the inversion. At stations 0 and 600 the observed soundings change too rapidly with time to be matched with a realistic layered earth model. It is known that an insulating basement could cause a steep rise of the apparent resistivity curve, but such an interpretation would not fit the data at a late time - after 100ms.

Figure 3.11 is the final interpretation of magnetic apparent resistivity curves. The 3D structure is indicated by a second conductive layer and a third resistive layer. The conductance of the second layer underestimates the conductivity-thickness product of the body and the high resistivities of the third layer are not well resolved, while the thicknesses seem to be quite accurate. The thickness of the second layer is estimated very closely to the real depth of 500m. The same procedure was followed using the voltage definition of apparent resistivity and very similar results were obtained.

They also calculated the horizontal magnetic and voltage responses for the conductive model in Figure 3.8. Although this method clearly indicates the presence of a 3D structure, it is difficult to make accurate measurements of the horizontal field, because the receiver must be located precisely at the center of the transmitter loop. The calculated results are shown in Figure 3.12.

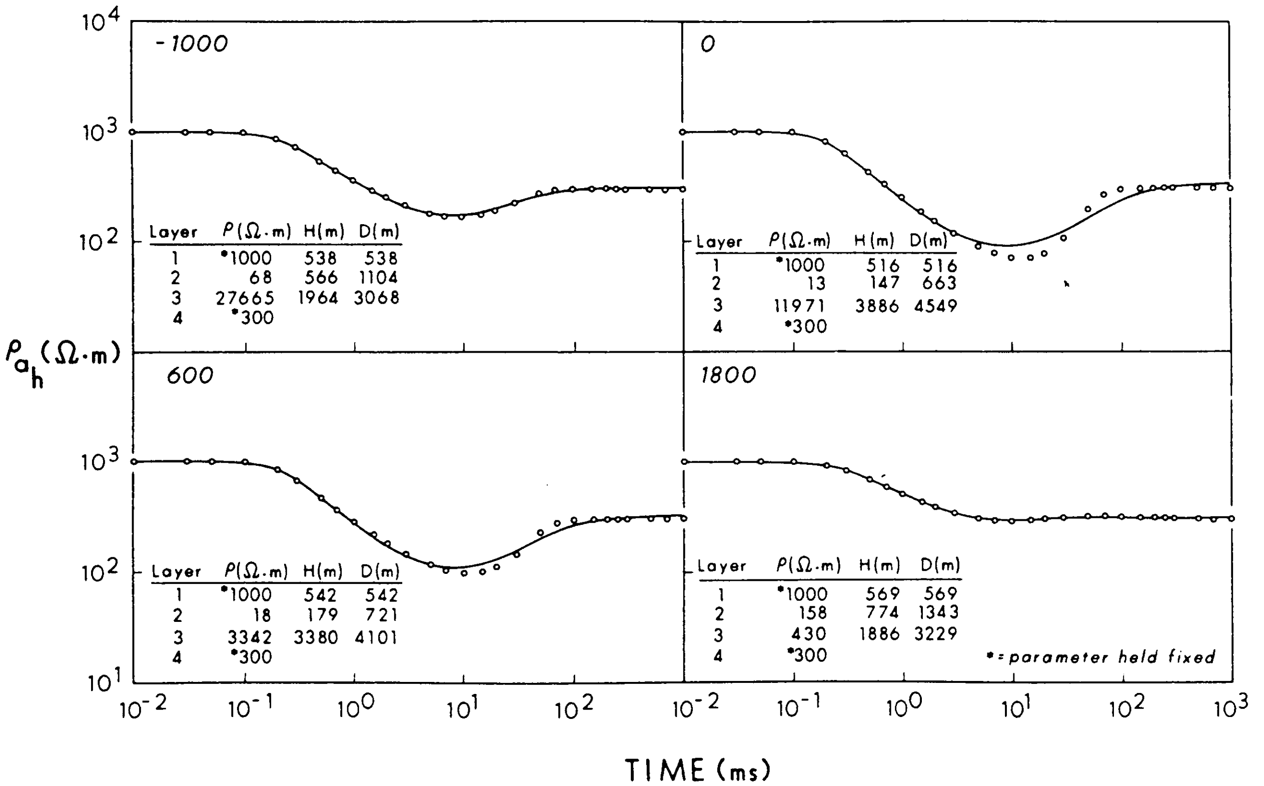

Figure 3.10 Layered-earth fits to the ρ_{a_h} data calculated from the 3D model in Figure 3.8. The open circles are the synthetic data and the solid lines the layered-earth fits (after Newman, et. al., 1987).

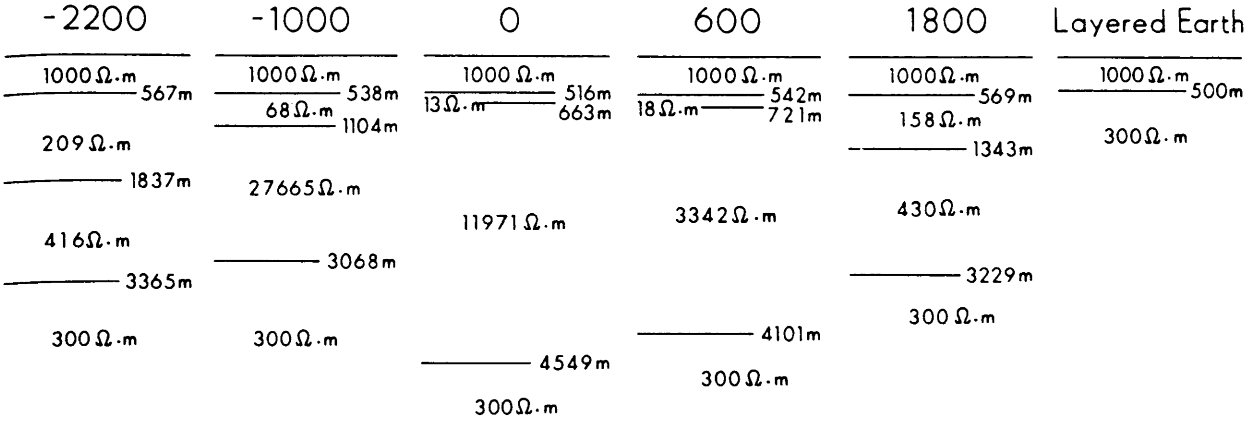

Figure 3.11 Interpreted ρ_{a_h} section for the 3D model in Figure 3.8 (after Newman, et. al., 1987).

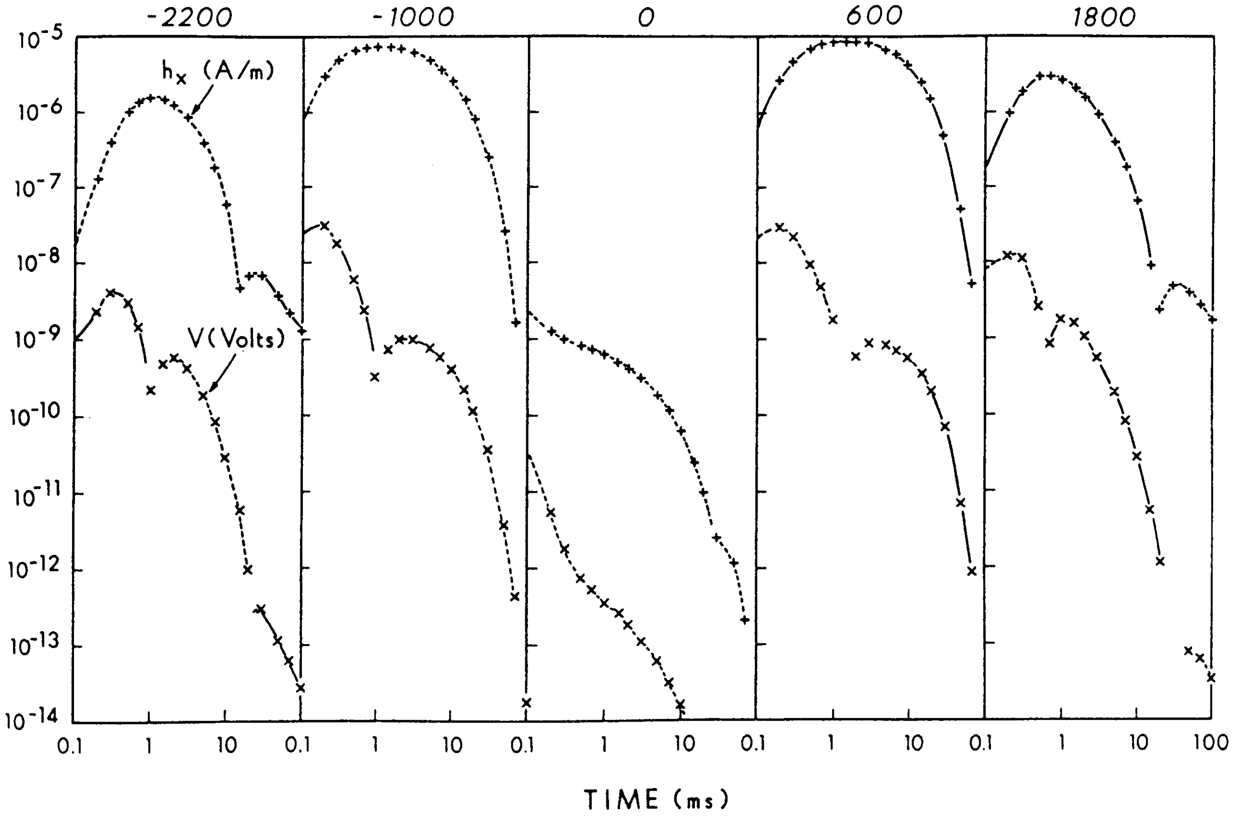

Figure 3.12 Horizontal magnetic field and voltage responses (h_x and V_x). Solid curves define positive responses and dashed curves negative responses. The magnetic field responses are depicted by plus signs and the voltage responses by crosses (after Newman, et. al., 1987).

It can be seen from Figure 3.12 that the horizontal responses on the left side of the conductor are opposite in sign to the responses on the right side. The change in sign of both the voltage and magnetic response happen when channeled and return currents are maximized around the 3D conductor.

Again, exactly the same method was followed, but with a 3D resistive structure (300Ω.m) this time. Figure 3.13 shows the ρ_{a_h} interpreted section, which corresponds well with the forward model (compare Figure 3.8 where the conductive body was replaced with a resistive one). The depth of the first layer is estimated accurately, while the basement depth under the 3D body is considerably underestimated; around 800m while the real depth is 1100m. The resistivity of the body is underestimated at 29Ω.m, 71Ω.m and 45Ω.m, compared to the real value of 300Ω.m, while the basement resistivity is found to be very accurate at between 8Ω.m and 9Ω.m, which is very close to the real value of 10Ω.m.

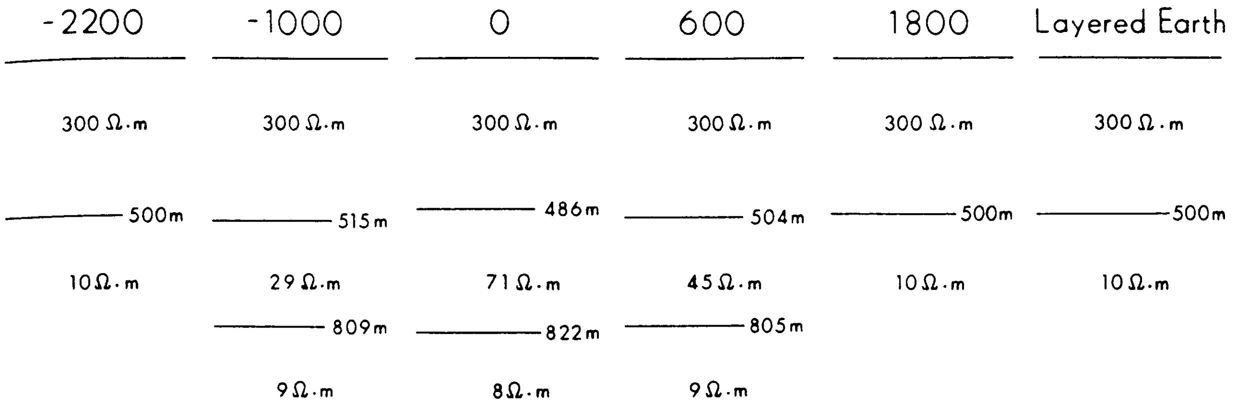

Figure 3.13 Interpreted ρ_{a_h} section for the same model as in Figure 3.8, except that the conductive structure was replaced by a resistive one. The data at stations -2200 and 1800 show only the background layered-earth (after Newman, et. al., 1987).

Interestingly enough, four layers are needed to give satisfactory results if interpretations are done by using the ρ_{a_v} method. A thin conductive layer has to be added above the basement to give good fits at late times. Compare the results in Figure 3.14 with that of Figure 3.13.

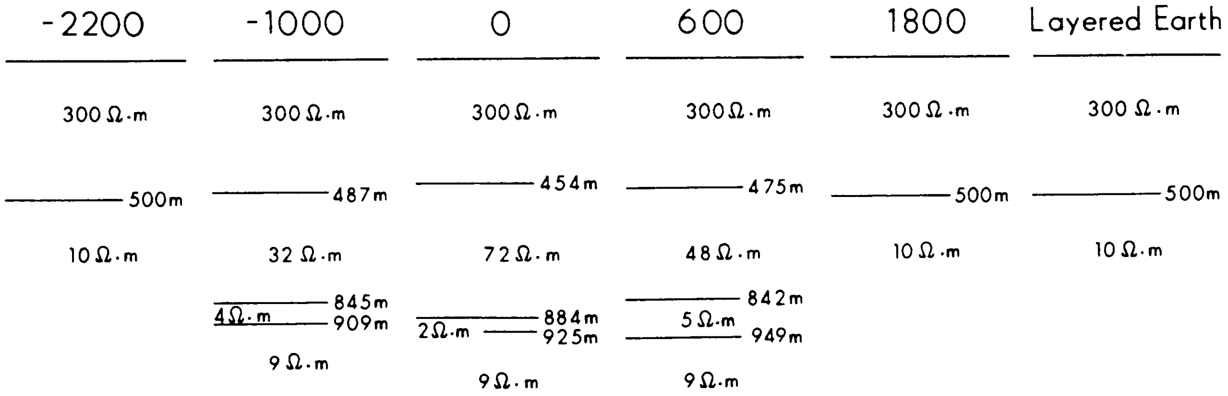

Figure 3.14 Interpreted ρ_{a_v} sections for the same model as used in Figure 3.13 (after Newman, et. al., 1987).

Increasing the resistivity of the first layer to 1000Ω.m and interpreting the data based on the voltages lead to poorer fit of the data at late times. Thus the estimated depths of the resistive body become increasingly unrepresentative of the forward model as shown in Figure 3.15. The interpretation using the magnetic data (Figure 3.16), on the other hand, gives very much the same type of results as in Figure 3.13. Newman, et. al. (1987) remark that interpretations of layered earth data are identical for magnetic and voltage data, whereas this is clearly not necessarily the case with a 3D earth.

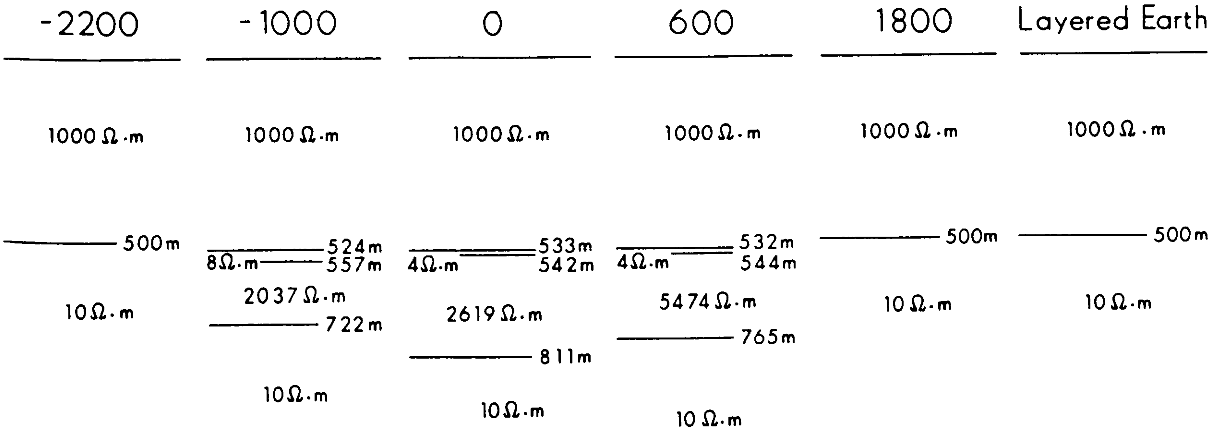

Figure 3.15 Interpreted ρ_{a_v} section for the same model as used in Figure 3.13 where the first layer's resistivity was changed to 1000Ωm. The data at stations -2200 and 1800 show only the background layered-earth response (after Newman, et. al., 1987).

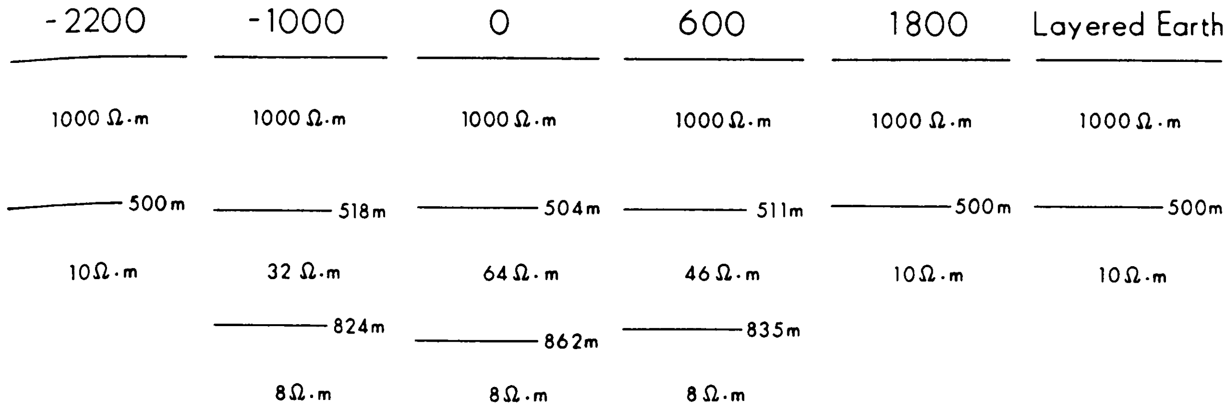

Figure 3.16 Interpreted ρ_{a_h} section for the same model as used in Figure 3.13 where the first layer's resistivity was changed to 1000Ωm. The data at stations -2200 and 1800 show only the background layered-earth response (after Newman, et. al., 1987).

Poddar and Anderson (1992) applied the forward modeling developed by Newman, et., al. (1986) to shallow A-type sections to see if it will be possible to resolve lateral variation in a resistive layer. 1D interpretation of data near a 3D body was not satisfactory, while applying the 1D interpretation over such a body yielded sufficient evidence of the 3D body. This was done specifically for the horizontal electric dipole (HED), to show that the method can be used to some advantage when direct current (DC) resistivity soundings are not sufficient.

3.1.4 Calculating the response of a laterally varying overburden

Smith and West (1987) formulated frequency and time domain techniques for calculating the response of a thin flat inhomogeneous conductive sheet. The time domain step response is calculated by time-stepping the vertical component of the magnetic field. They plotted the calculated vertical magnetic field values as a function of position (profile) and found that the symmetry of the field is severely distorted as a result of near-surface inhomogeneities. Figure 3.17 shows the field as a function of position for different time values. They also present a field example which shows that a response which could be attributed to a dipping conductor, might just as well be due to lateral variations in the overburden.

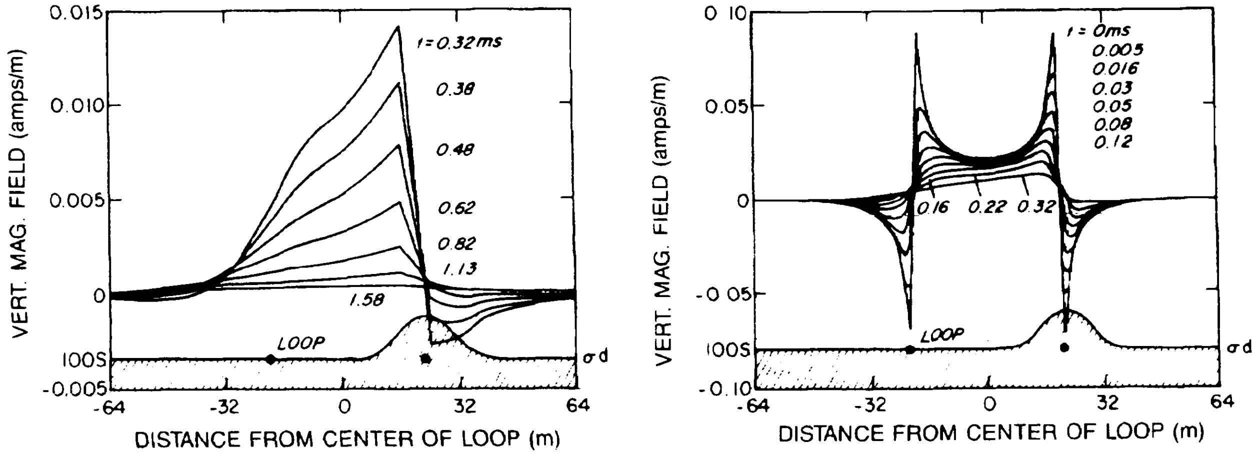

Figure 3.17 Decay of the vertical magnetic field as a function of time and position. The delay time of each curve is shown and the bottom part of the graph is the conductivity distribution (after Smith and West, 1987).

3.2 PHYSICAL MODEL STUDY

Spies and Parker (1984) investigated current channeling and gathering in models of resistive host rock and step discontinuities in a horizontal conductive sheet. Figure 3.18 depicts responses over a resistive discontinuity and it can be seen that the response is a function of transmitter position. They explain that for the transmitter situated over the discontinuity, separate currents are set up in each conductor and the final field closely resembles that of an uniform layer. Moving the transmitter away from the discontinuity results in current being concentrated at the boundary and thus an anomalous field.

The same was done with a step discontinuity as shown in Figure 3.19. The results are a much more subtle difference with the response of a uniform layer. When the loop is centered over the discontinuity (Figure 3.19b) there is a migration of the maximum amplitude with time in the direction of increased thickness. The step is most easily observed with the loop position as it is in Figure 3.19c. At the position in Figure 3.19a there is again a migration of maximum amplitude toward the thicker section with time.

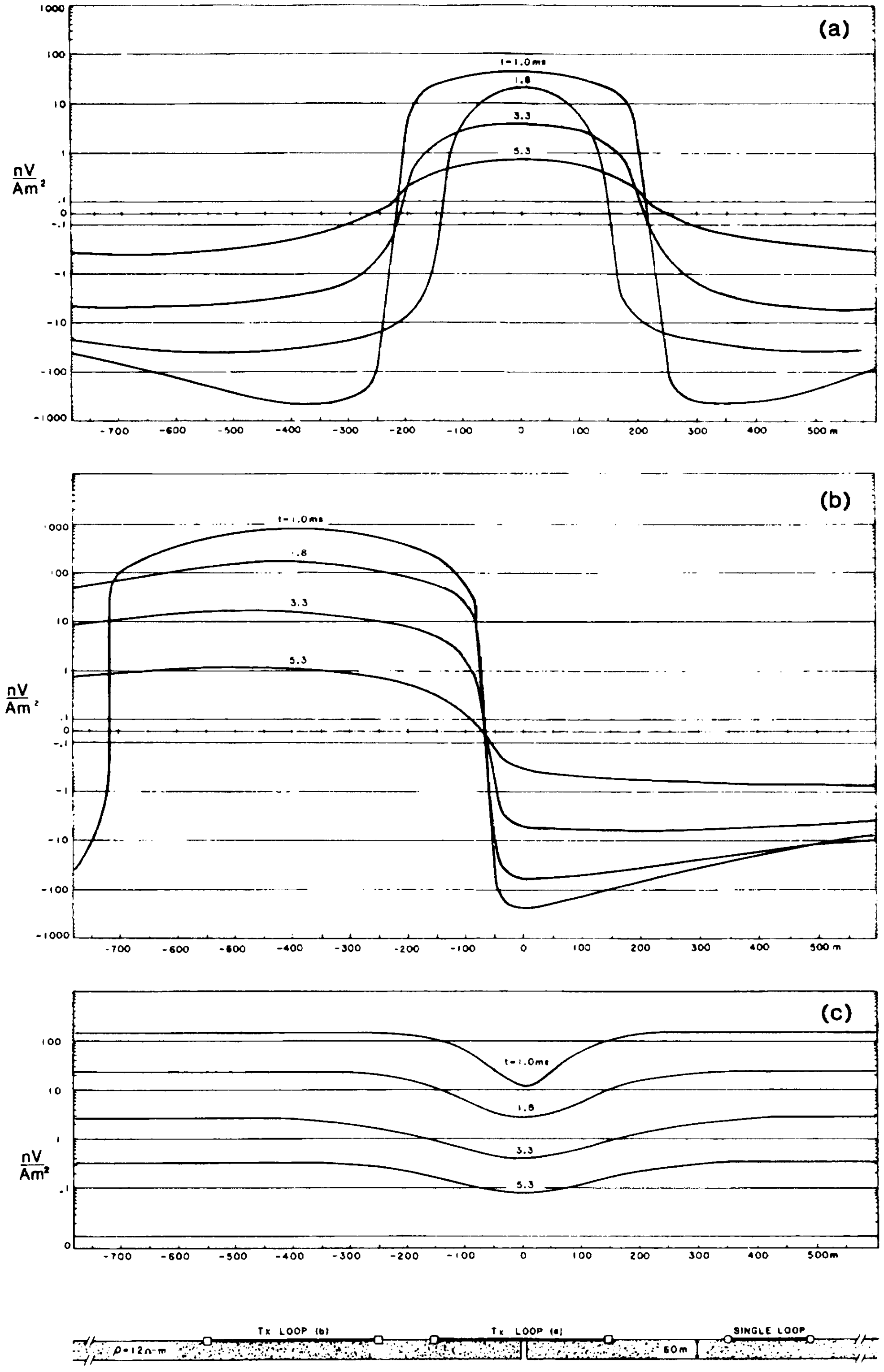

Figure 3.18 TEM profiles over a resistive discontinuity in a horizontal slab: (a) transmitter loop centered over the resistive break; (b) transmitter loop located away from the resistive break; (c) TEM profiles obtained with the coincident loop configuration (after Spies and Parker, 1984).

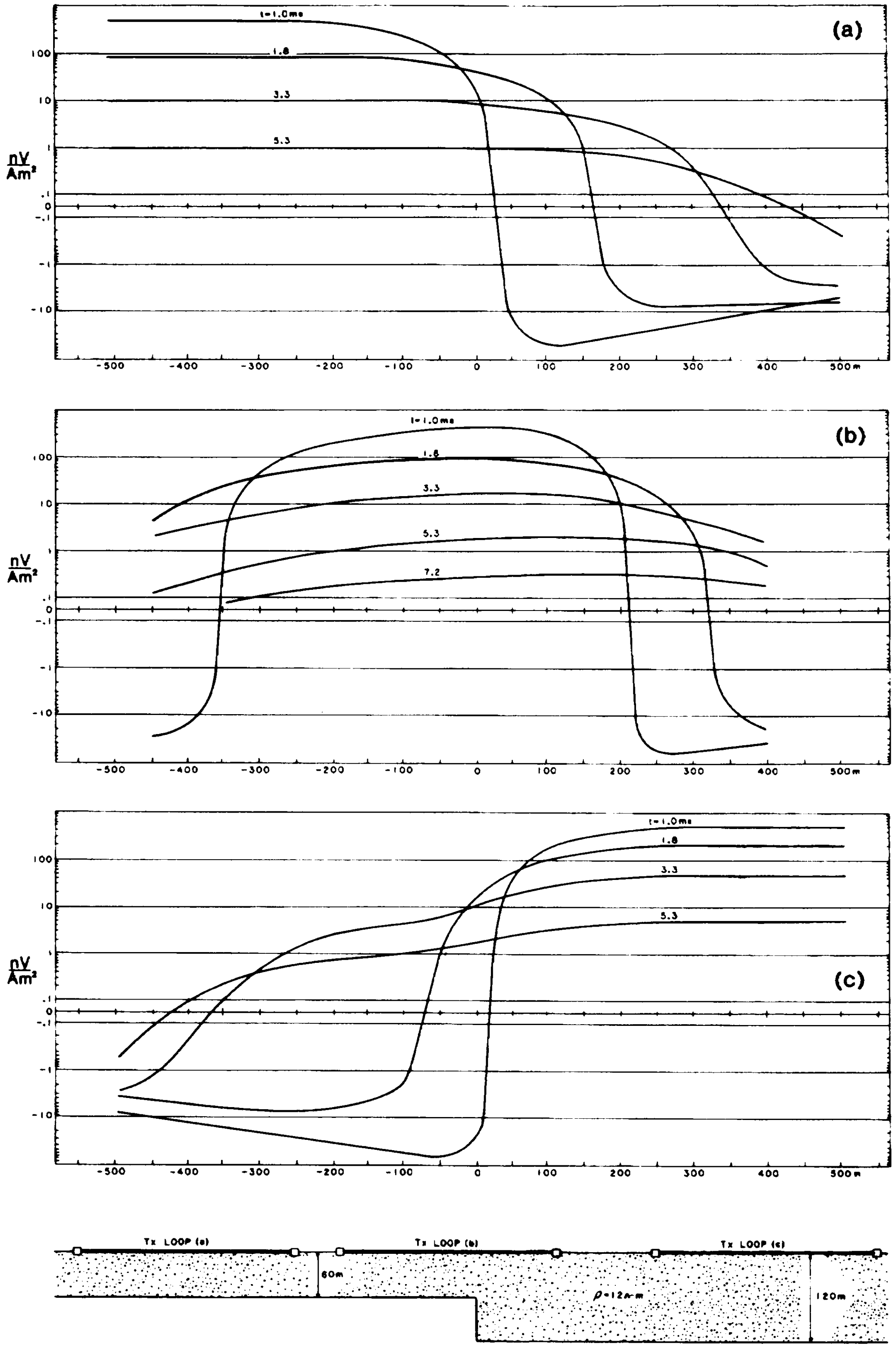

Figure 3.19 TEM profiles over a step discontinuity in the thickness of a horizontal slab with different loop positions (after Spies and Parker, 1984).

3.3 CASE STUDIES

Frischknecht and Raab (1984) used the short-offset TDEM method in a geologically complex region. They found the TDEM method to be less sensitive to lateral variations and giving deeper information than the FDEM or DC methods. However, it proved to be very useful in determining the general layering of the situation by 1D inversion. Stations close to the vertical boundaries did not yield good 1D results which confirmed the change in layering. Compare the apparent resistivity emulation in Figure 3.20 at stations 17 and 18, 18 and 19, 13 and 14, where interpreted vertical boundaries occur as shown in Figure 3.21.

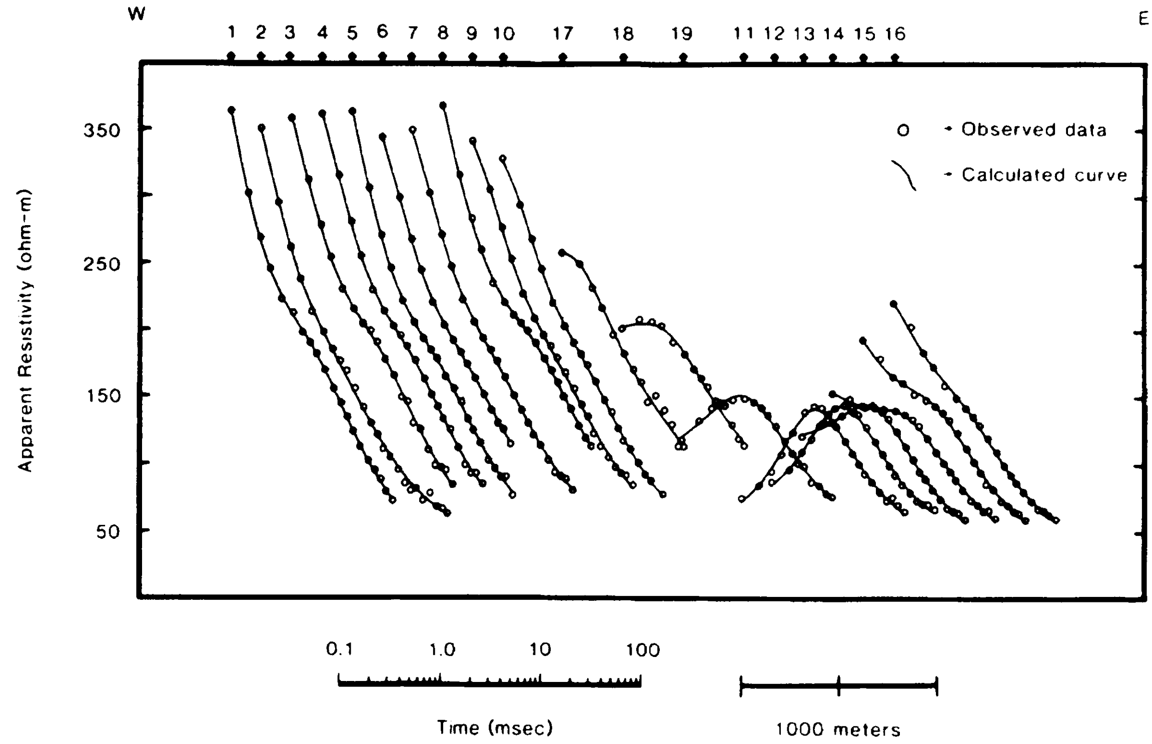

Figure 3.20 Observed TDEM apparent resistivity data and calculated curves. Note the poor fits at stations where interpreted vertical boundaries occur as shown in Figure 3.21 (after Frischknecht and Raab, 1984).

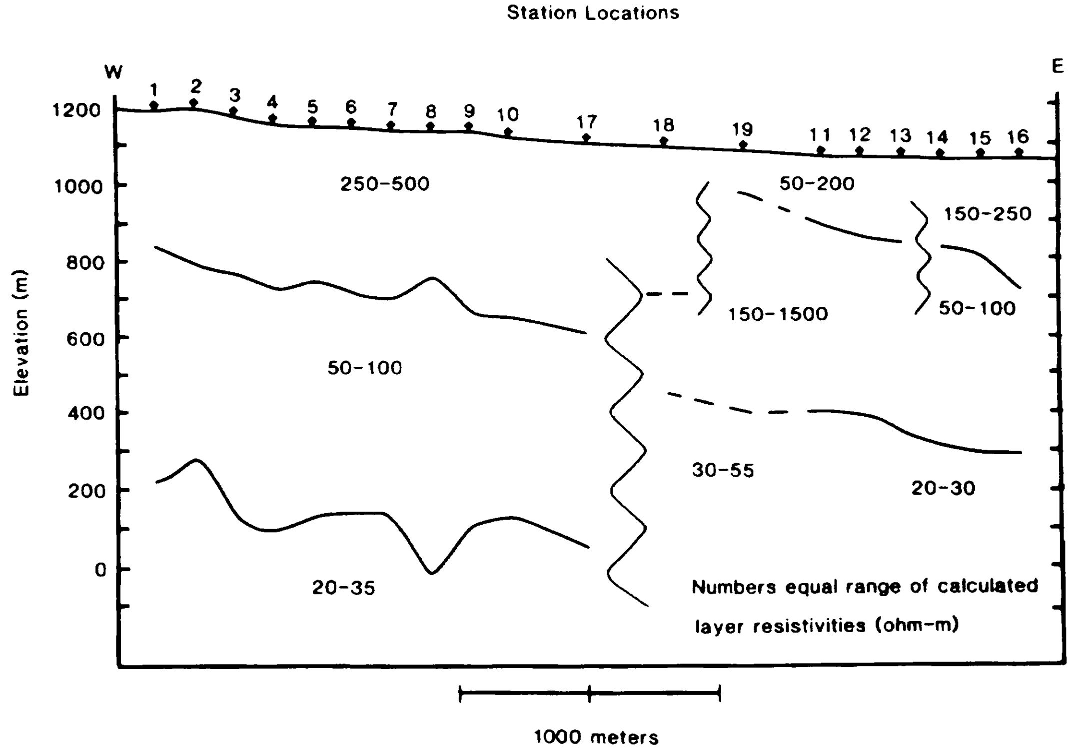

Figure 3.21 Calculated resistivity versus depth cross-section of data shown in Figure 3.20. Vertical exaggeration 2:3 (after Frischknecht and Raab, 1984).

Nelson and Haigh (1990) studied the use of geophysical methods in the detection of sinkholes. During preliminary investigations they employed microgravity, seismic fan shooting, electrical resistivity, shallow electromagnetic and ground radar methods. They concluded that detecting dolines were most effective using high resolution seismic reflection and deep sounding electromagnetic methods, namely the SIROTEM.

They termed dolines as a generic collective name for broad shallow depressions, deep steep-sided sinkholes and piping structures or cavities which may lead to sinkhole formation. They concluded that these targets, in a geophysical sense, were not only air and water filled cavities but also zones of silica leaching which produced zones of electrical conductivity. The reason for this is that the dolines contained clay rich material which absorbed ions and became conductive.

Another interesting observation they made is that the forming of these dolines were structurally controlled and connected to faults and fractures zones. Differential weathering produce the clay rich zones where holes or depressions might form, or it surrounds cavities. TDEM methods are not very sensitive to these type of cavities situated in highly resistive host rock, so the targets were the highly conductive clay zones. This summary of their results will only consider the electromagnetic methods used as the seismic methods have no bearing on the current study.

They found the central loop method where the measurements are made in the center of the transmitter more effective than the so-called Turam method where measurements are made across the transmitter loop. In Figure 3.22 a pseudosection of their data can be seen. This pseudosection is plotted as apparent resistivity values against time channels. Because the currents diffuse in time through the earth, the vertical axis is an indication of depth. They point out that the values seem to represent a heterogeneous earth, while it is difficult to detect a well structure situated at 1000N. In Figure 3.23 the well coincides with a pronounced narrow near surface resistivity low on Line 1012.5E which is 12.5m to the east of Figure 3.22.

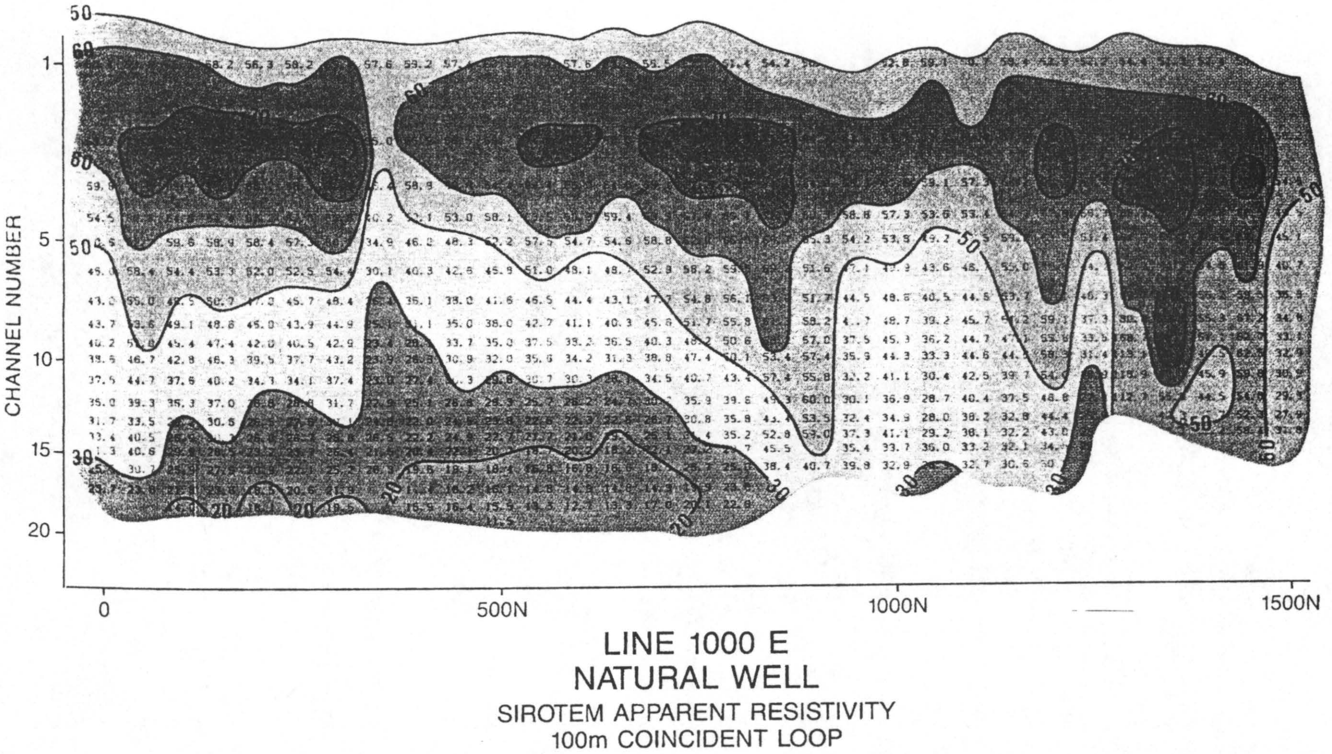

Figure 3.22 Coincident loop SIROTEM pseudosection at Natural Well test site. The well is located at 1000N, but has only small effects on the data. (After Nelson and Haigh, 1990.)

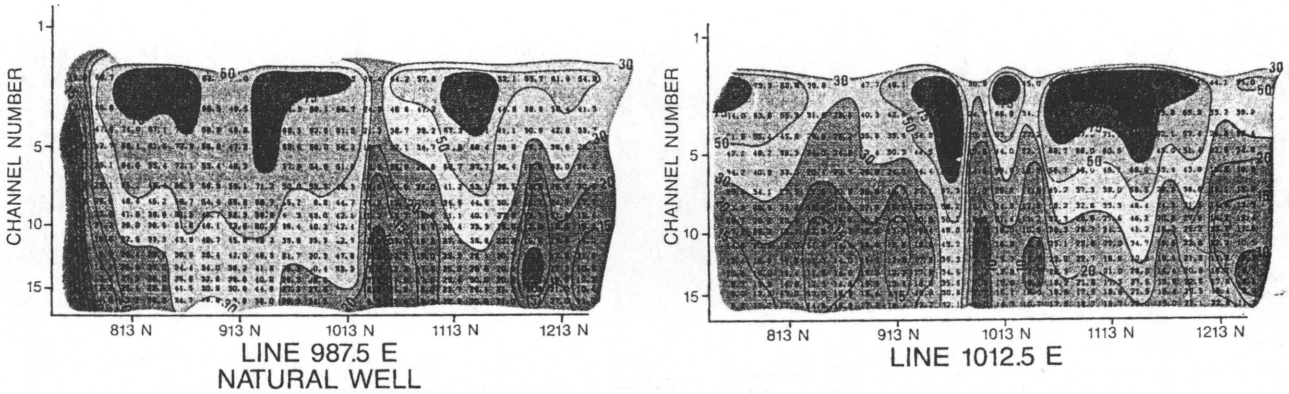

Figure 3.23 Coincident loop SIROTEM data from Natural well on lines adjacent to 1000E. The well is situated at 1000N and 1000E and coincides with the pronounced narrow, near surface resistivity low. (After Nelson and Haigh, 1990.)

Comparing this to Figure 3.24, which they considered to be the response of a layered earth, it is evident that it is possible to detect anomalous zones with the TDEM method. They concede that the work done resulted in different complex anomalies for which they could not provide a theoretical explanation. These were:

a) Complex (multiple peaks within a generally broad zone) conductive anomalies occur in a moderately resistive background.

b) Complex conductive anomalies occur in complex conductive background; the contrast with the background is generally small.

c) A singular conductive anomaly appears in moderately resistive background.

d) A singular moderately conductive anomaly appears in conductive background with moderate contrast.

e) A singular conductive anomaly occurs in conductive background with a small contrast.

The geomorphological model used to explain sinkhole formation, which accounts for the geophysical anomalies, was not proven at the time.

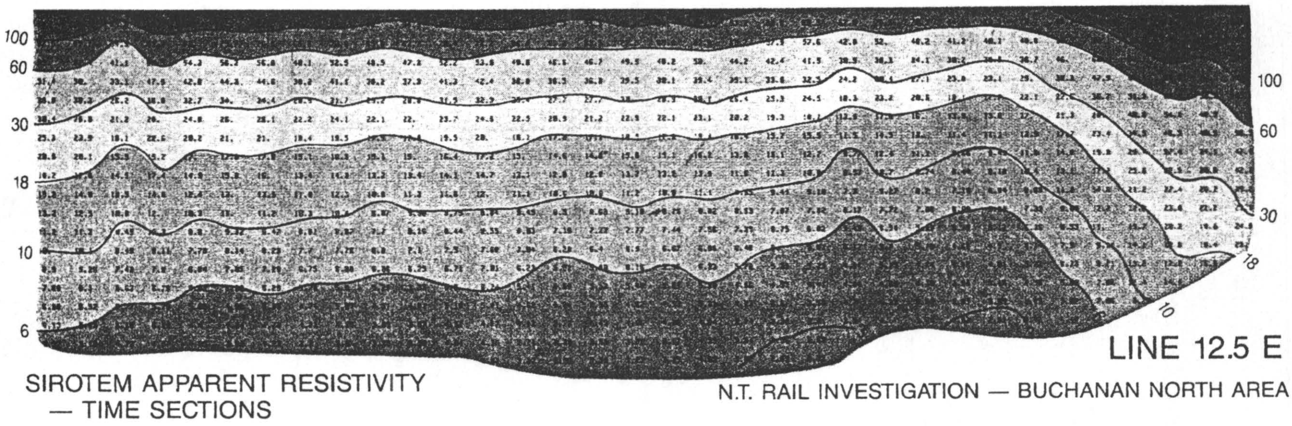

Figure 3.24 SIROTEM coincident loop apparent resistivity pseudosection which exhibits a more layered response and is not considered to be sinkhole prone. (After Nelson and Haigh, 1990.)

3.4 SUMMARY

Lateral changes in resistivity manifest both temporally and spatially in TDEM data. The temporal character of a 2D or 3D earth response could seem to be very close to that of a layered earth. However, it is impossible to find a perfect fit to 2D or 3D data when a 1D model is used for inversion (Newman, et. al., 1987), but constrained four layer interpretations of the calculated magnetic field yielded satisfactory results in determining the position of a 3D body in a two layer earth.

Smith and West (1987) showed that the symmetry of the TDEM field can be severely distorted by near surface inhomogeneities. Spies and Parker (1984) state that the change in spatial TDEM data is a function of the transmitter position, while Frisknecth and Raab (1984) found the TDEM method to be less sensitive of lateral variations than FDEM or DC methods. Nelson and Haigh (1990) conclude that variations in spatial TDEM data can be used effectively to detect sinkhole prone areas.

Chapter 4

Modeling the transient electromagnetic (TEM) step response of a vertical dipole with a moving current filament

This chapter starts off with the introduction of the current filament concept by Nabighian (1979) and other relevant historical works. The model for a forward program calculating the derivative of the magnetic field of a moving current ring is stated as well as assumptions for the diffusion velocity.

4.1 THE CURRENT FILAMENT CONCEPT

Nabighian (1979) showed that for a step-function excitation, the observed TEM-field over a conducting half-space or layered earth can be represented by a simple current filament of the same shape as the transmitter loop: moving downward and outward, as shown in Figure 4.1. This theory was supported by work done by Lewis and Lee (1978) and Hoversten and Morrison (1982). At first it may seem as if Lewis and Lee (1978) were the pioneers, but Nabighian first formulated the idea in a lecture at the US-Australia Electromagnetic workshop in 1978. The investigation of lateral inhomogeneities by Smith and West (1987) also proved that it could be advantageous to conceptualize TEM-fields as a system of smoke rings moving through the earth.

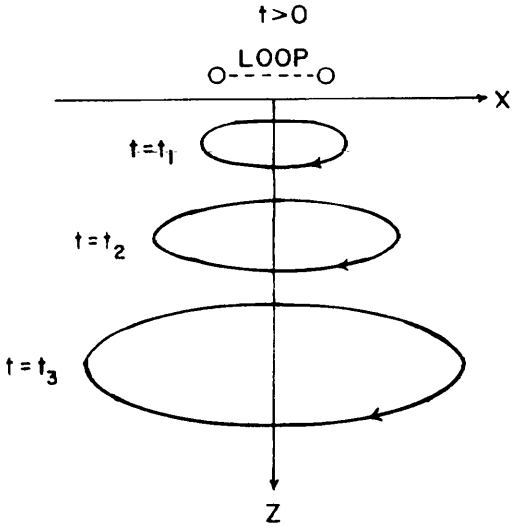

Figure 4.1 System of smoke rings established after current interruption showing its downward and outward movement (after Nabighian, 1979).

Nabighian (1979) did a series expansion of the perturbation kernel of the magnetic Hertz potential of an aperiodic magnetic dipole. He came to the conclusion that the potential could be written in such a way that it represented the magnetic Hertz potential of a circular current of radius $a = \lambda\sqrt{8C_2}$, situated at a depth $z = \left(4/\sqrt{\pi}\right)\lambda$ and of current intensity $I_i = 1/\left(4\pi C_2\lambda^2\right)$ where C_2 is a constant and $\lambda = \sqrt{t/\sigma\mu}$.

Figure 4.2 shows the computed current density for a central section through a rectangular loop of dimensions 400*800m. The current density maximum travels downward at an angle of approximately 30 degrees. To get the same field with the equivalent single-current filament it will have to travel downward with an angle equal to $z/a = 4\sqrt{\lambda/\pi}/\sqrt{8C_2\lambda} \approx 47°$

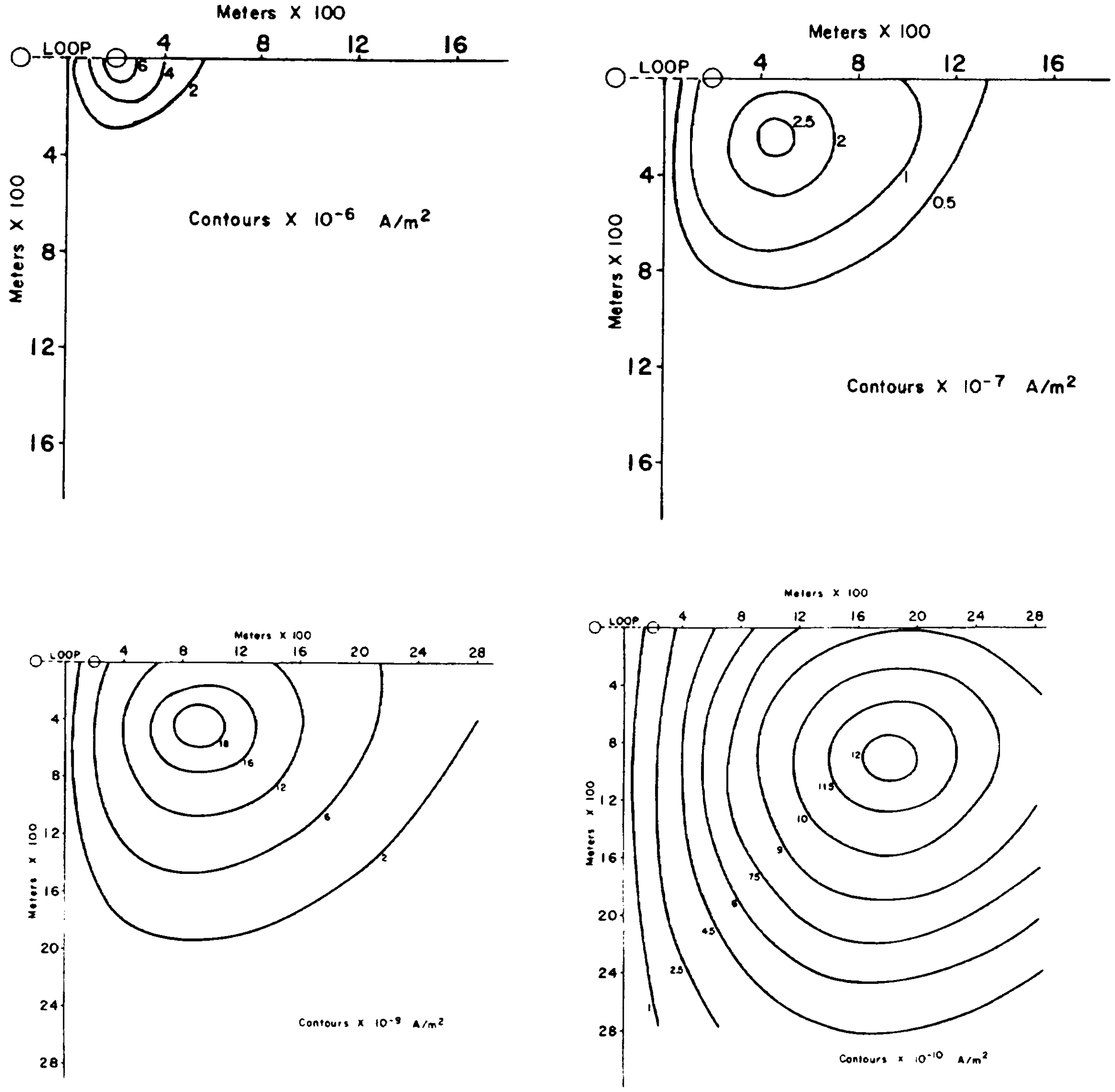

Figure 4.2 Computed contour plots of the normal component of current density in the earth. Starting top left and from left to right plots are for $t/\sigma=0.01$, 0.1, 0.4 and 1.6 sec/mho/m respectively (after Nabighian, 1979).

Lewis and Lee (1978) formulated a dimensionless expression for the electric field in a half space due to a current step in a transmitter loop. They found that the locus of the electric field initially moves slightly inward before following the downward angle of 30 degrees as shown in Figure 4.3.

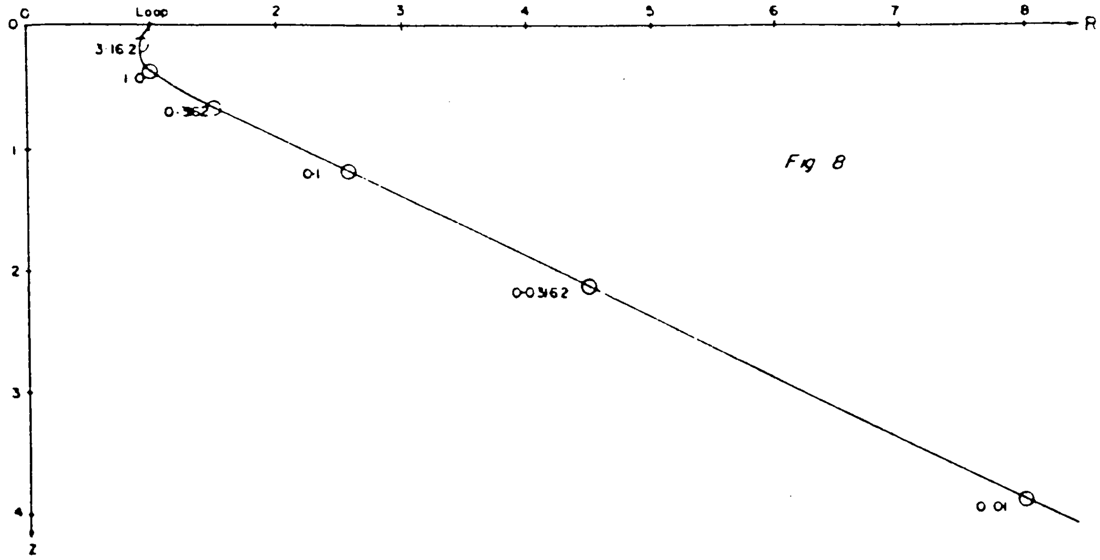

Figure 4.3 The locus of the maximum of the electric field. The numbers correspond to values of τ *(after Lewis and Lee, 1978).* $\tau = \dfrac{\sigma\mu_0 a^2}{4t}$

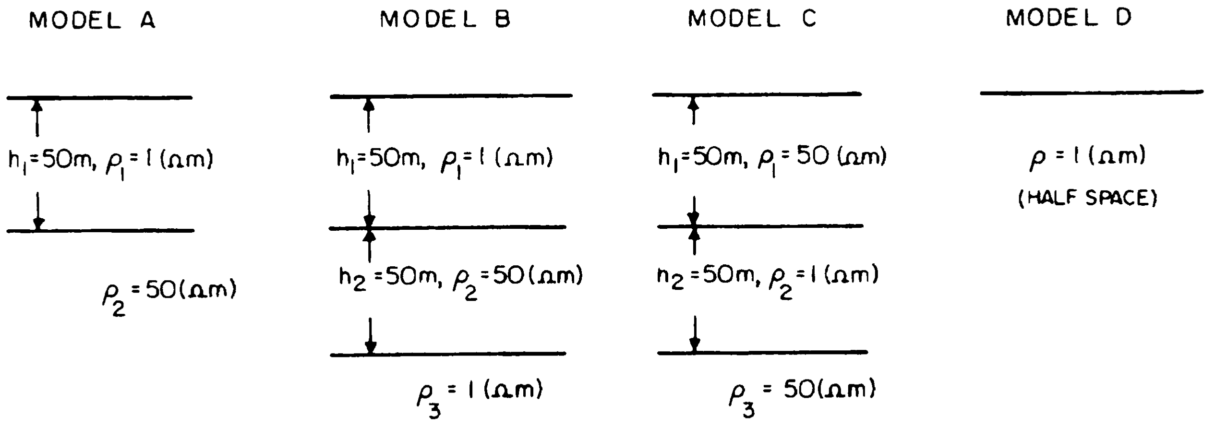

Figure 4.4 The four models used by Hoversten and Morrison (1982).

Hoversten and Morrison (1982) present the induced electric field in four layered earth models. They found an explanation for the sign reversal of the vertical magnetic field as well as proving empirically that there is only one fictitious current ring. Four different models (Figure 4.4) were used to calculate the electrical field. The results for the half-space (model D) are similar to that of Figure 4.2. They note that the sign reversal of the vertical field happens because the current ring moves under the receiver position and because the magnetic field on different sides of a horizontal conductor is opposite in sign.

Model A is a two layer earth with a conductive first layer. In contrast with the uniform half-space, the maximum of the electrical field is confined to the first layer and does not penetrate the lower resistive layer in the section shown in Figure 4.5. The total current in the two layer model is less than that of the half-space and the horizontal velocity of the maximum of the latter is less than that of model A, which results in a lower magnetic field response for model A when compared to model D.

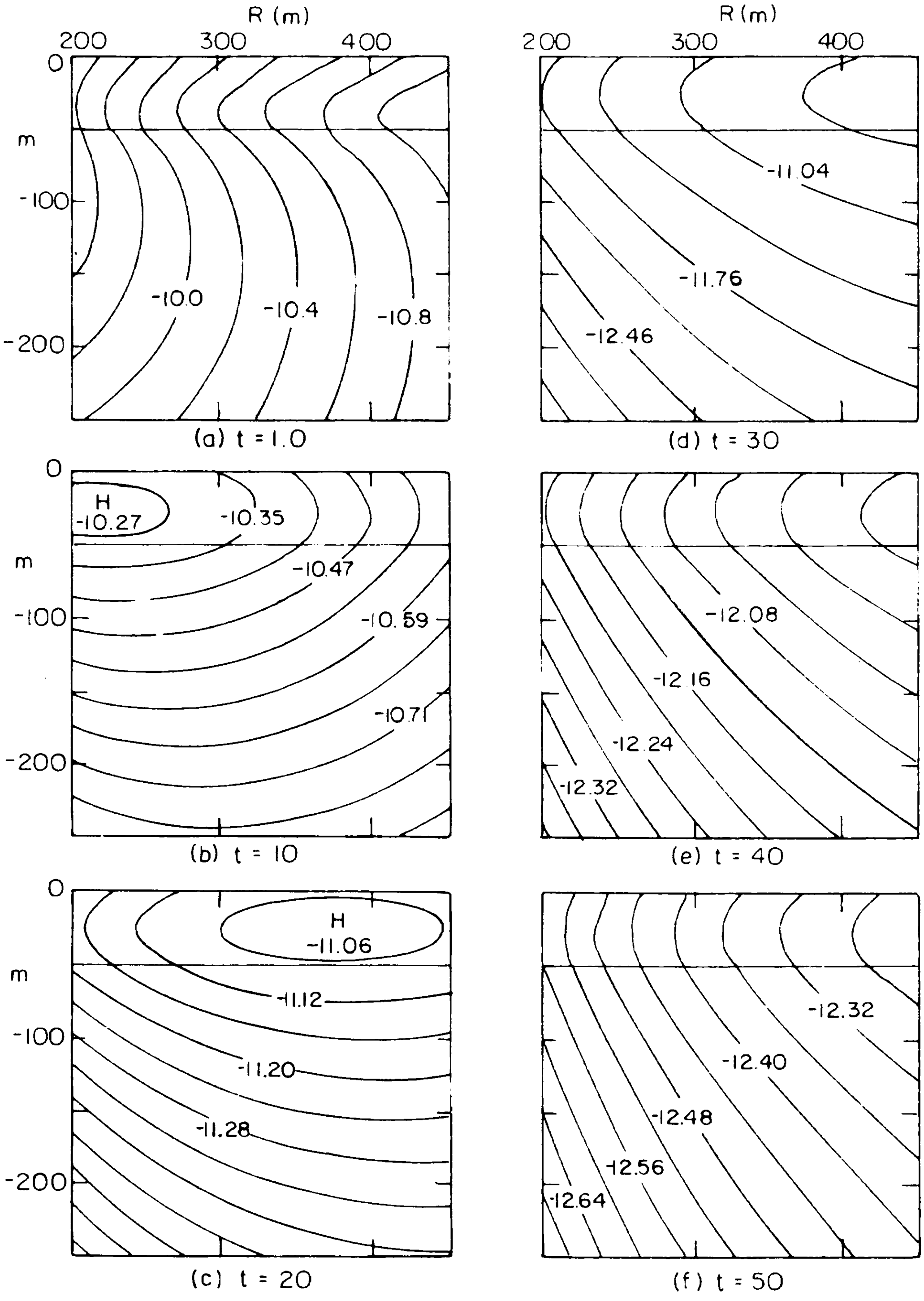

Figure 4.5 Induced electric field (volts/m) within model A shown in Figure 4.4 (after Hoversten and Morrison, 1982).

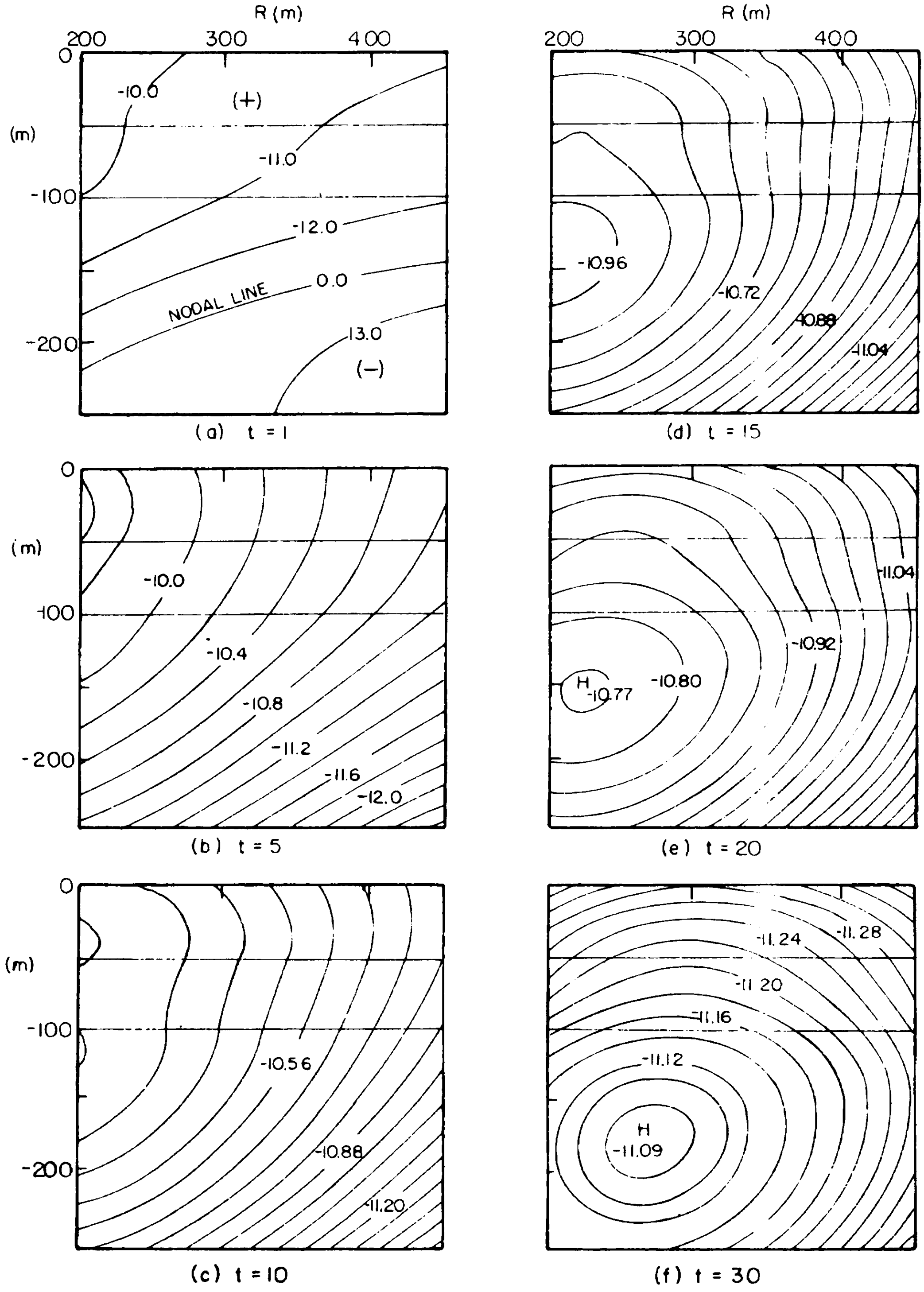

(a) t = 1

(d) t = 15

(b) t = 5

(e) t = 20

(c) t = 10

(f) t = 30

Figure 4.6 Induced electric field (volts/m) within model B shown in Figure 4.4 (after Hoversten and Morrison, 1982).

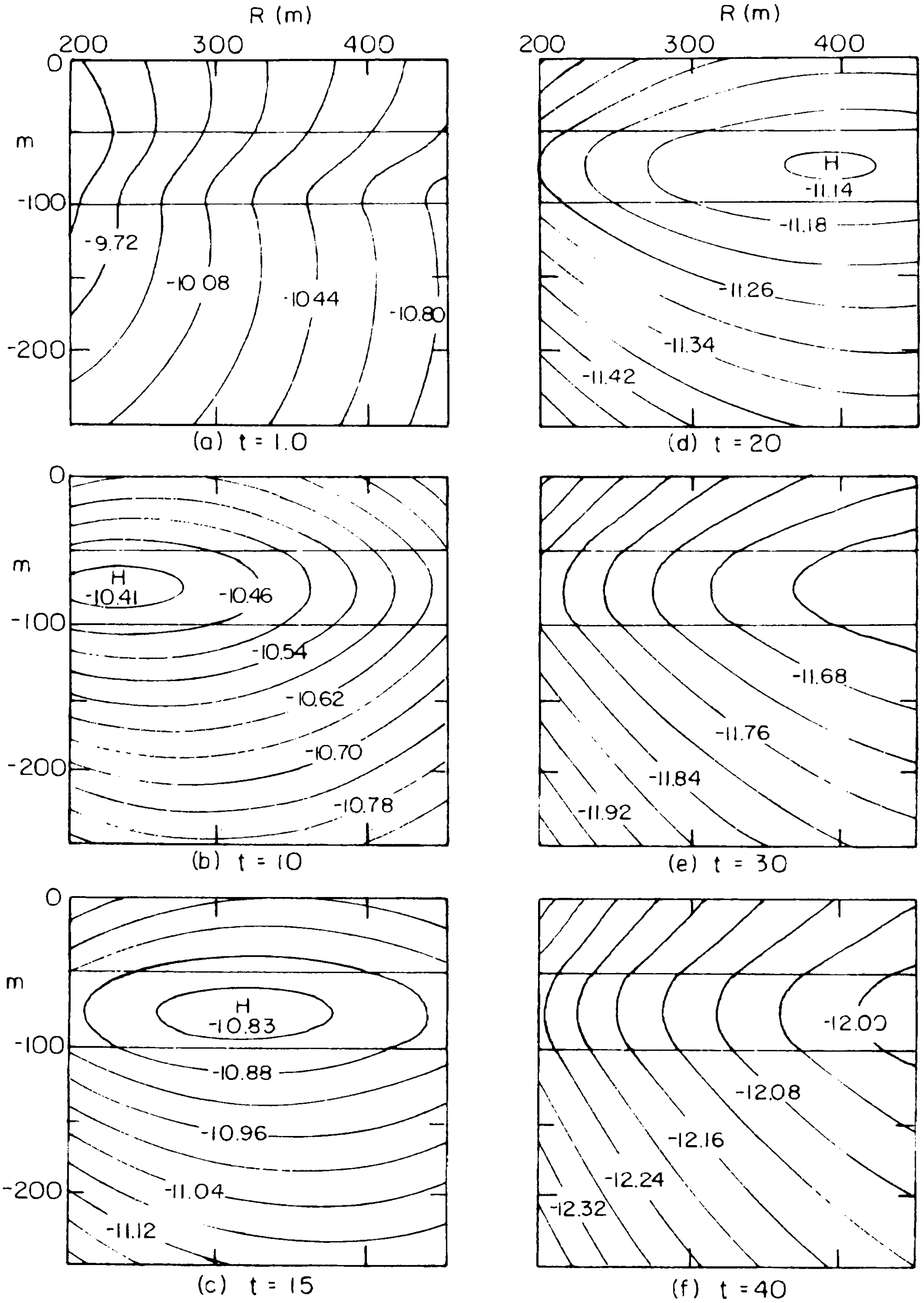

Figure 4.7 Induced electric field (volts/m) within model C shown in Figure 4.4 (after Hoversten and Morrison, 1982).

The presence of the conductive basement of model B (Figure 4.6) seems to pull the current filament through the resistive layer into the basement as time progresses. This keeps the maximum from propagating only horizontally in the first layer as it does in models A and C and results in a lower average horizontal velocity for model B.

For model C (Figure 4.7) the higher propagation velocity in the first layer and the conductive second layer results in the highest average horizontal velocity. The maximum of the electric field is confined to the top two layers, as is the case with model A.

4.2 FORWARD ALGORITHM

Thus it should be possible to model the TEM response of the earth by making use of a moving current filament in the earth. A forward algorithm was developed for an arbitrary shape current filament. This was achieved by adding the TEM field of short straight line elements, i.e. electric dipoles with a step current, situated at the origin directed in the positive x-direction, from Ward and Hohmann (1988), Wait (1958):

$$\bar{h} = \frac{Ids}{4\pi r^2}\left[\frac{2}{\sqrt{\pi}}\theta r e^{-\theta^2 r^2} + erfc(\theta r)\right]\left[-\frac{z}{r}\bar{u}_y - \frac{y}{r}\bar{u}_z\right] \qquad (4\text{-}1)$$

Or more generally the emf induced in a coil at z=0 is measured, which is proportional to the derivative of the magnetic field, Ward and Hohmann (1988):

$$\frac{\partial \bar{h}}{\partial t}(x,y,z,t) = \frac{Ids\theta^3 r}{2\pi^{2/3} t} e^{-\theta^2 r^2}\left(-\frac{z}{r}\bar{u}_y - \frac{y}{r}\bar{u}_z\right) \qquad (4\text{-}2)$$

where I is the current, ds is length, $r = \sqrt{x^2 + y^2 + z^2}$ and $\theta = \sqrt{\mu\sigma / 4t}$.

To be able to calculate the field of a system of transient electric dipoles (TED) the observer position relative to each TED, situated at the origin along the x-axis, must be calculated. The total field is just the sum of all the contributions, positive and/or negative, of all the dipoles constituting the current filament, as shown in Figure 4.8.

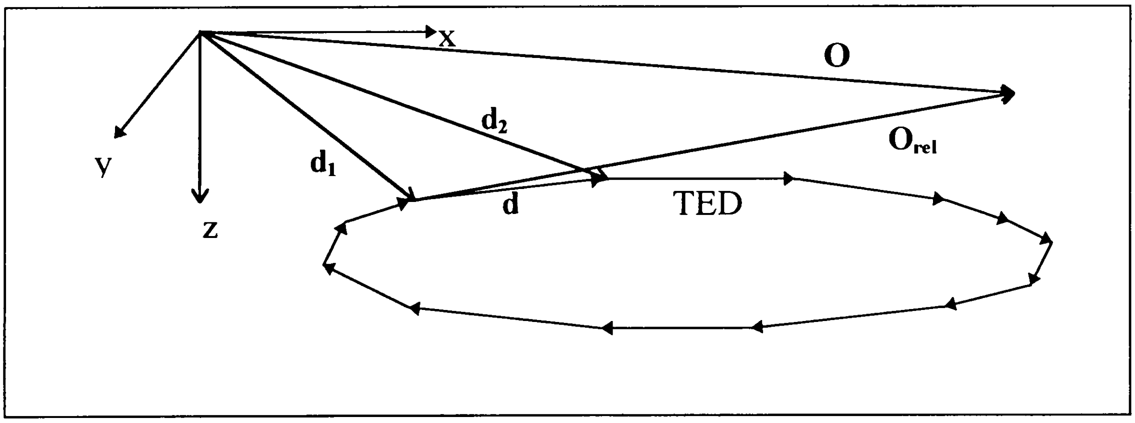

Figure 4.8 System of axes with the position of observation, O, with a current ring approximated by transient electric dipoles.

The first step is to find the components of the vector along the direction of the dipole, in the xyz-system of axes by taking the dot product with the unit vectors along the axes and forming a unit vector $\hat{d}$:

$$\hat{d}_x = \frac{\overline{D} \cdot \hat{x}}{\left|\overline{D}\right|}$$
$$\hat{d}_y = \frac{\overline{D} \cdot \hat{y}}{\left|\overline{D}\right|} \qquad (4.3)$$
$$\hat{d}_z = \frac{\overline{D} \cdot \hat{z}}{\left|\overline{D}\right|}$$

Find the unit vector perpendicular to the plane formed by the vectors $\overline{d}_1$, $\overline{d}_2$ and $\hat{d}$ by taking the cross product:

$$\hat{f} = \frac{\overline{d}_2 \times \overline{d}_1}{\left|\overline{f}\right|} \qquad (4.4)$$

And to form a new right hand set of axes:

$$\hat{e} = \hat{d} \times \hat{f} \qquad (4.5)$$

Find the components of $\overline{O}_{rel}$ in the new set of axes:

$$O_d = \overline{O}_{rel} \cdot \hat{d}$$
$$O_e = \overline{O}_{rel} \cdot \hat{e} \qquad (4.6)$$
$$O_f = \overline{O}_{rel} \cdot \hat{f}$$

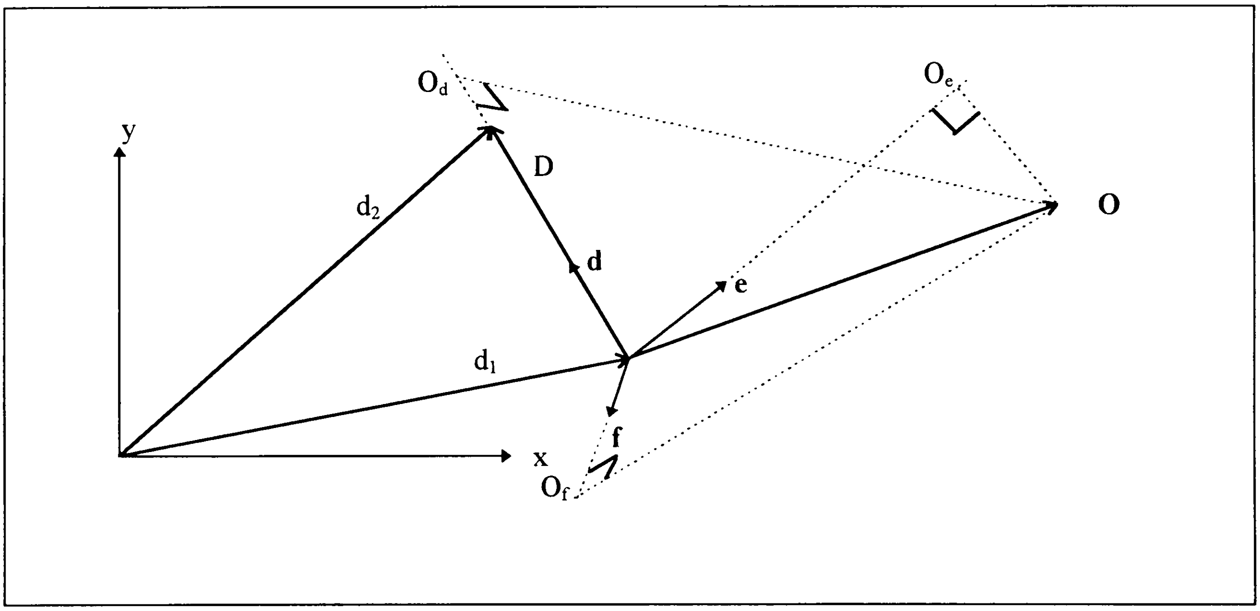

Figure 4.9 The new set of axes and the components of O_{rel} in it. Bold letters depict unit vectors.

Using eq 4.2 and the results from eq 4.6 the derivative of the magnetic field of the dipole can be found in the def-system:

$$\frac{\partial \overline{h}}{\partial t}(O_d, O_e, O_f) = \left(\frac{\partial h_d}{\partial t}, \frac{\partial h_e}{\partial t}, \frac{\partial h_f}{\partial t} \right) \qquad (4.7)$$

Note that the d-component will be zero, because there is no component of the magnetic field in the direction of the dipole. All that is left to do, is to find the components of eq 4.7 in the xyz-system and the derivative of the magnetic field of the dipole will be known.

$$\begin{aligned}\frac{\partial h_x}{\partial t} &= \frac{\partial \bar{h}}{\partial t}\cdot\left(x_d, x_e, x_f\right)\\ \frac{\partial h_y}{\partial t} &= \frac{\partial \bar{h}}{\partial t}\cdot\left(y_d, y_e, y_f\right)\\ \frac{\partial h_z}{\partial t} &= \frac{\partial \bar{h}}{\partial t}\cdot\left(z_d, z_e, z_f\right)\end{aligned} \tag{4.8}$$

where $x_d = \hat{x}\cdot\hat{d}, x_e = \hat{x}\cdot\hat{e}, x_f = \hat{x}\cdot\hat{f}$ etc.

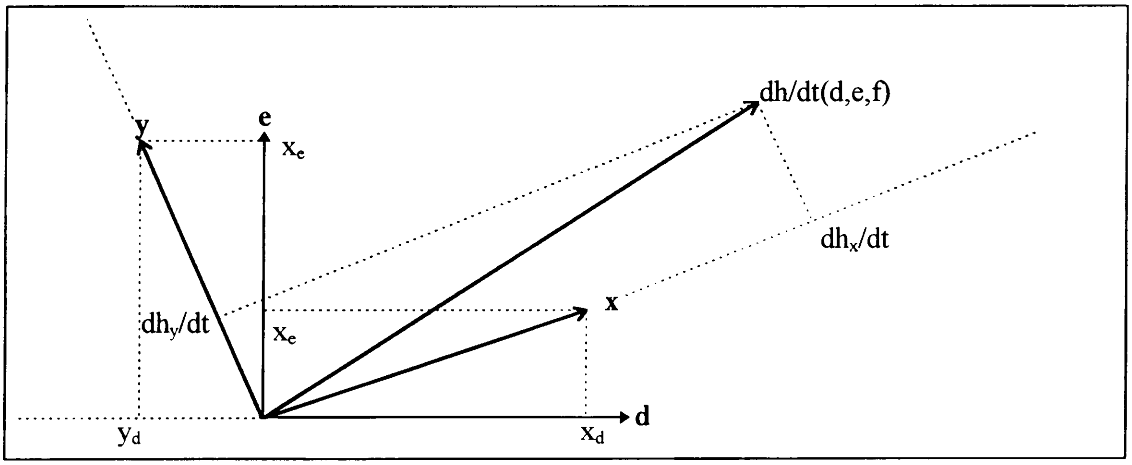

Figure 4.10 The components of the derivative of the magnetic field in the def-system is found in the xyz-system to be able to add the contribution of each TED making up the current ring. Only a 2D case is shown for simplicity.

This process is repeated for the whole system of dipoles and time stepped to simulate a ring of current moving through the earth. The current, position and radius of the current ring in the homogeneous half-space follows directly from Nabighian (1979).

4.3 COMPARISON OF CURRENT FILAMENT WITH ANALYTICAL RESULTS

4.3.1 Homogeneous half-space

Nabighian (1979) gives the velocity of the smoke ring due to a magnetic dipole on the surface of a homogeneous earth as:

$$\frac{4}{\sqrt{\pi}}\sqrt{\frac{t}{\mu\sigma}} \tag{4.9}$$

Looking at Figure 4.11 it is evident that the smoke ring decreases in velocity with time and eq 4.9 shows that an increase in resistivity of the half space will have a corresponding increase in velocity.

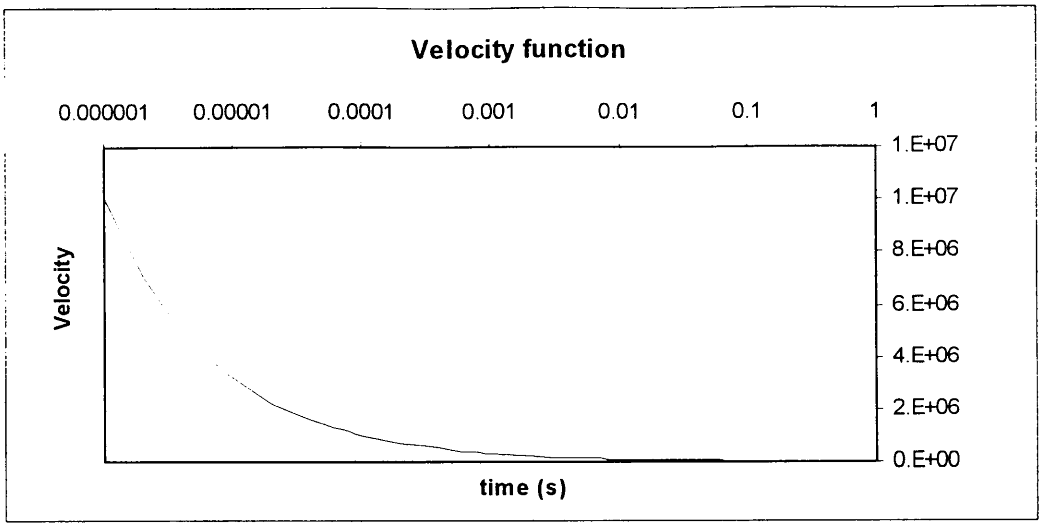

Figure 4.11 The velocity function of the smoke ring due to a vertical dipole for a 100 Ωm half-space as given by Nabighian(1979).

Using this velocity function and the formula for the radius and current with time:

$$a = \sqrt{\frac{t8C_2}{\mu\sigma}} \qquad t = \frac{1}{4\pi C_2 \lambda^2} \tag{4.10}$$

as well as the forward algorithm procedure described in Section 4.2, it is possible to calculate the derivative of the magnetic field of a moving ring of current. In Figure 4.12 the derivative of the magnetic field is shown over a 100Ω.m half space as a profile and in Figure 4.13 as a function of time. These results decay faster than those given in Ward and Hohmann (1988) and TN-7 (McNeill) shown in Figures 4.14 and 4.15, but the profile data in Figure 4.12 correspond well.

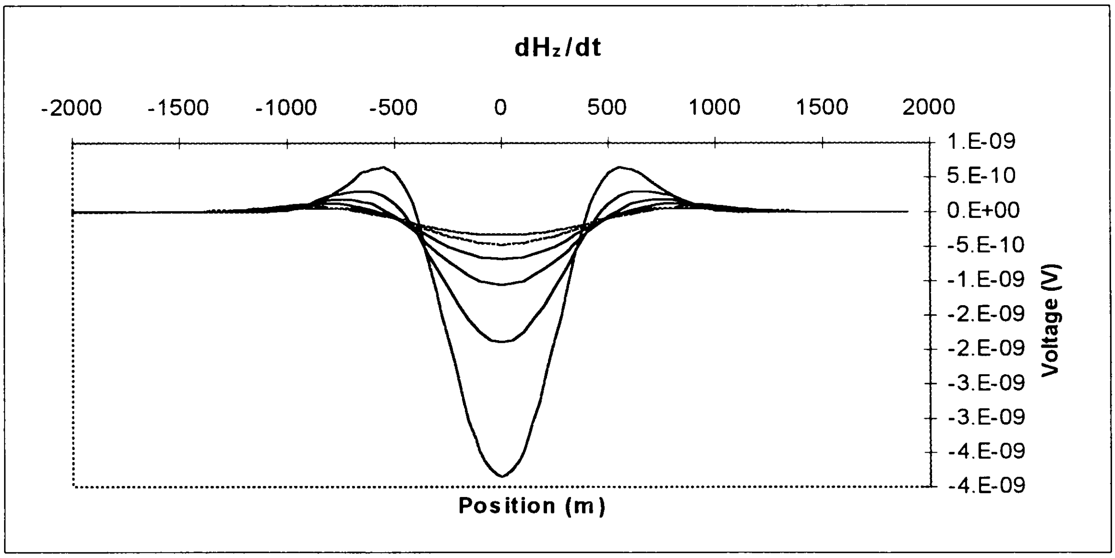

Figure 4.12a Profiles of the vertical component $\partial B_z / \partial t$ at consecutive times over a 100Ωm half-space calculated by making use of the forward algorithm of Section 4.2. Lower amplitudes correspond to later times.

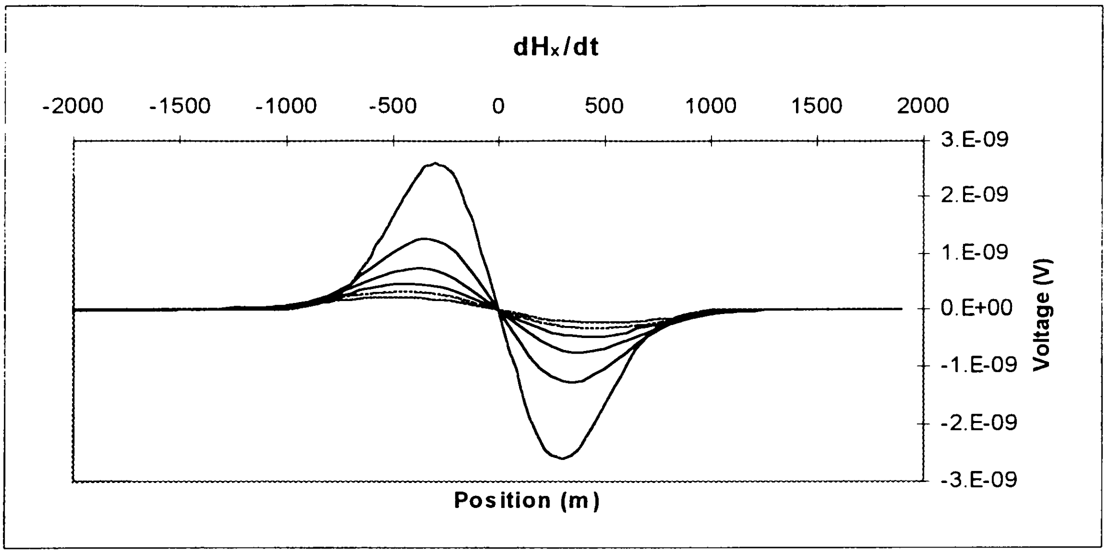

Figure 4.12b Profiles of the horizontal component $\partial B_r / \partial t$ *at consecutive times over a* $100\Omega m$ *half-space calculated by making use of the forward algorithm of Section 4.2. Lower amplitudes correspond to later times.*

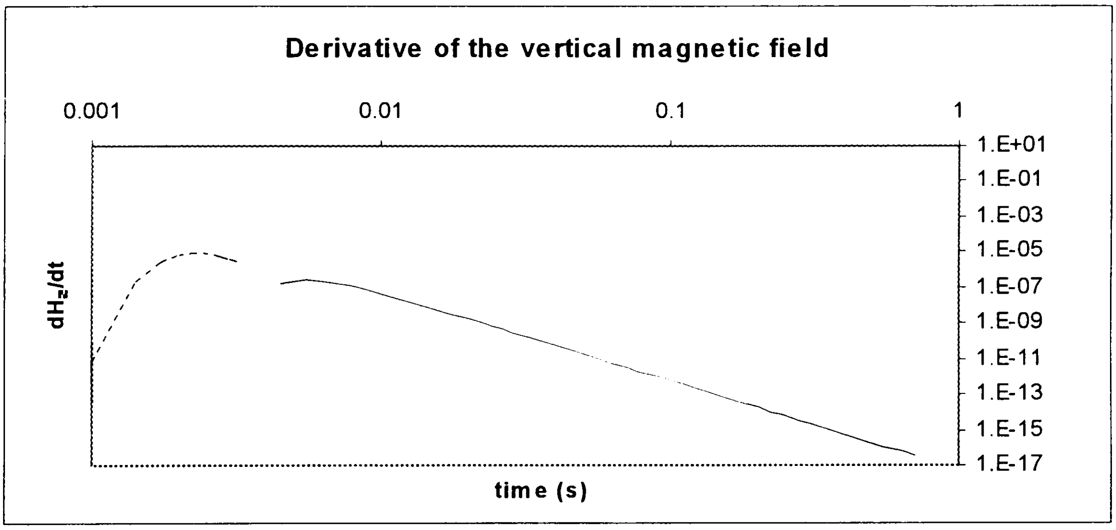

Figure 4.13 The decay of the magnetic field 100m from a vertical dipole as evident in the calculated derivative of the magnetic field, using the forward algorithm of Section 4.2. The dotted and solid lines depict opposite sign data.

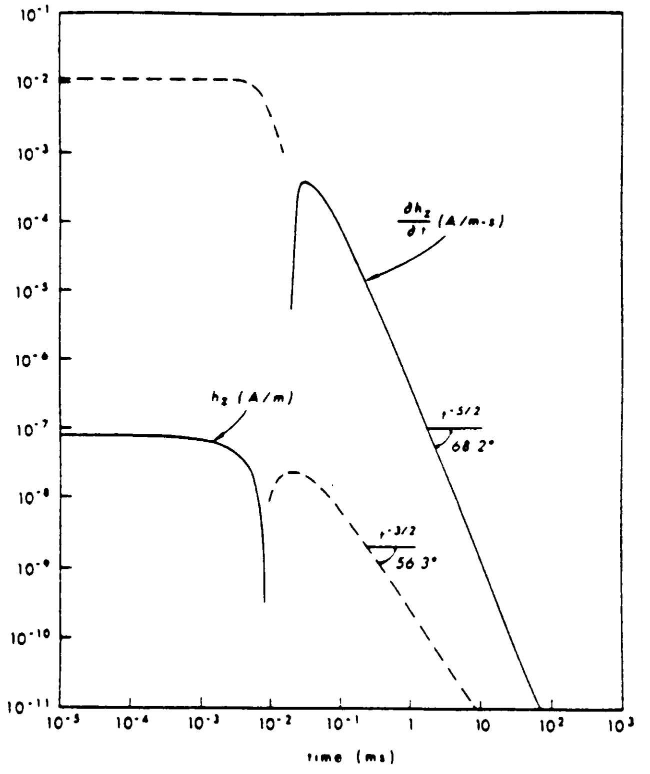

Figure 4.14 Vertical magnetic field and its derivative 100m from a vertical magnetic dipole that is terminated abruptly. Source and receiver at the surface of a 100Ωm half-space, after Ward and Hohmann (1988).

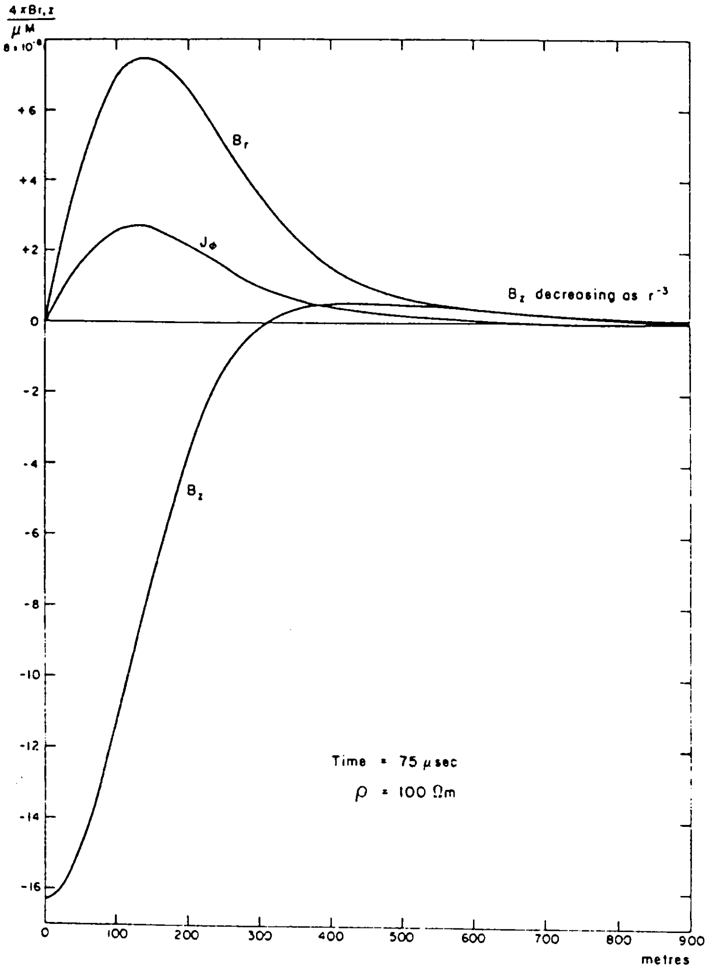

Figure 4.15 Magnetic field components at surface of homogeneous half-space, after TN-7 (McNeill).

4.3.2 Two layer earth

Thinking about a filament of current moving through the earth it is possible to imagine it moving with a certain speed which is a function of the conductivity of the layer it is situated in. At some stage the speed and radius will be affected by the second layer in the case of a two layer earth. If this layer is more conductive, the current ring will move slower vertically and horizontally and if the layer is less conductive, it will have the opposite effect. A model that can be suggested is shown in Figure 4.16 where the velocity changes abruptly.

To use the forward model, the depth and radius of the current ring must be known at all times. After eq 4.9 and 4.10 the following model is used with the velocity function shown in Figure 4.16:

$$z_1 = \frac{4}{\sqrt{\pi}}\sqrt{\frac{t}{\sigma_1 \mu}} \qquad a_1 = \sqrt{\frac{8C_2 t}{\sigma_1 \mu}} \tag{4-11}$$

where z_1 and a_1 are the depth and radius in medium 1 for $t<t_{con}$, the time the current ring passes through the contact between the two layers.

And when $t>t_{con}$ assume an abrupt change in velocity:

$$z_2 = h_1 + \frac{4}{\sqrt{\pi}}\left(\sqrt{\frac{t}{\sigma_2 \mu}} - \sqrt{\frac{t_{con}}{\sigma_2 \mu}}\right) \qquad a_2 = \sqrt{\frac{8C_2}{\mu}}\left(\sqrt{\frac{t_{con}}{\sigma_1}} + \sqrt{\frac{t}{\sigma_2}} - \sqrt{\frac{t_{con}}{\sigma_2}}\right) \tag{4-12}$$

These functions are shown in Figure 4.17 for a resistivity contrast of 1:100. All the functions are plotted against $\tau = \sqrt{t}$.

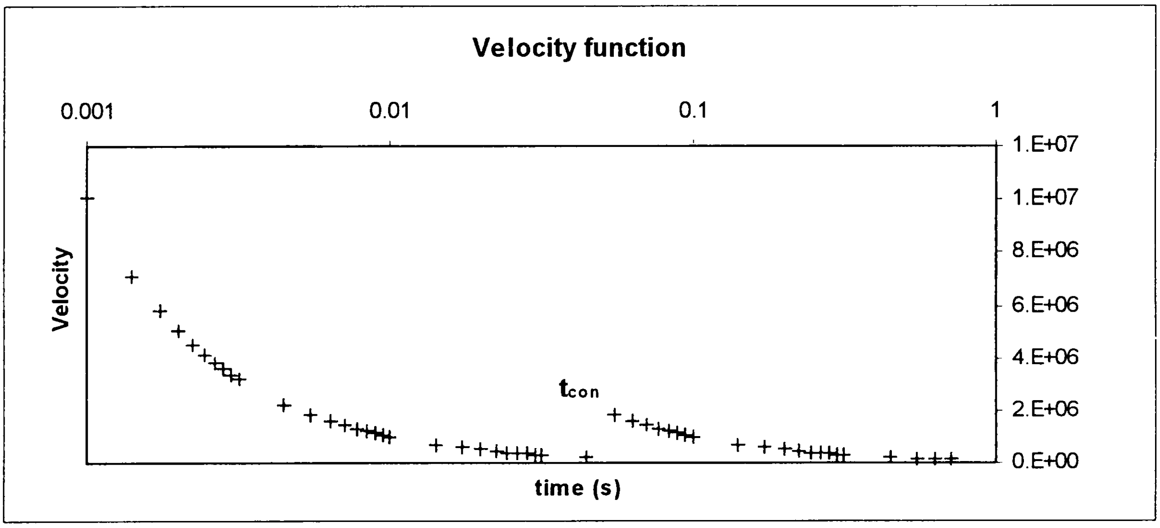

Figure 4.16 Simple velocity function for different media where t_{con} is the time when the current ring passes through a conductivity boundary as in a two layer earth.

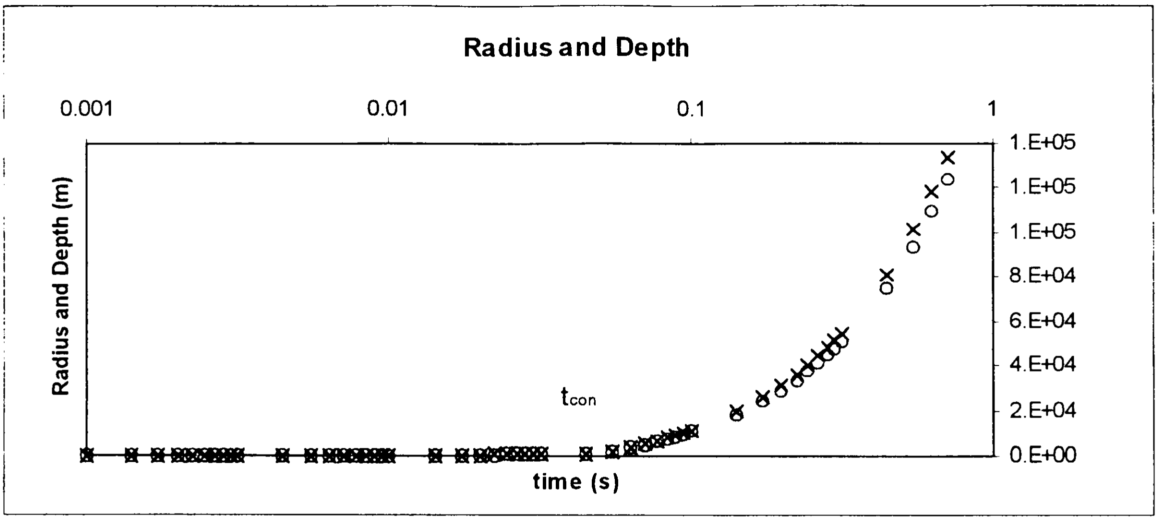

Figure 4.17 Radius and depth functions with time for the velocity model shown in Figure 4.16.

If the velocity changes abruptly, it has the effect that the measured magnetic field also has a discontinuity as shown in Figure 4.18, which is not really evident in the depth and radius functions in Figure 4.17. This is a situation which is rather far from the truth, because it would remove the reasons for formulating apparent resistivity, since it was developed to accentuate very small variations in the measured field. These variations are definitely not discontinuities as shown in Figure 4.18 and 4.19. Compare the apparent resistivity curves in Figure 2.3.

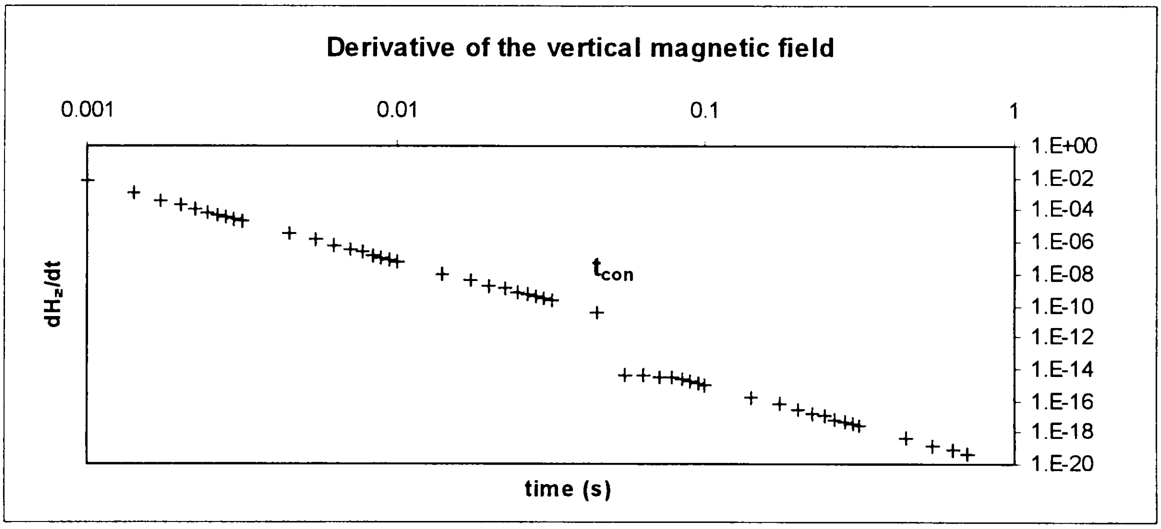

Figure 4.18 Measured vertical magnetic field calculated for the velocity function shown in Figure 4.16. Note the discontinuity associated with t_{con}.

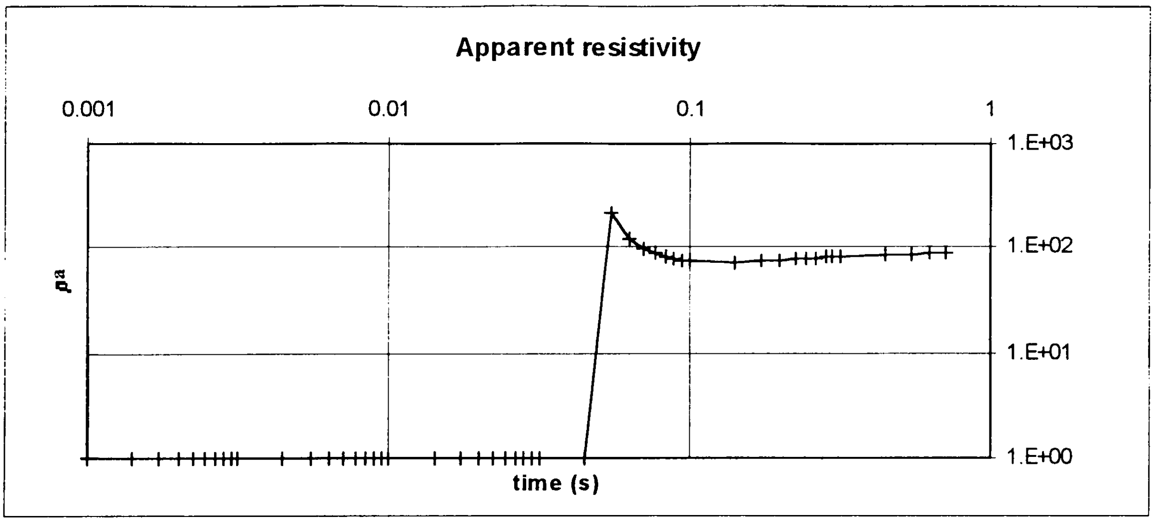

Figure 4.19 Apparent resistivity curve calculated using the results of Figure 4.17 and eq 2-53.

4.4 SUMMARY

Considering the results of Hoversten and Morrison (1982) it is clear that the velocity function is influenced by the total resistivity distribution and not just the layer the current filament is in. This fact could explain why Raiche and Gallagher (1985), when they were attempting to calculate TEM vertical diffusion velocity as a function of apparent resistivity, found that there was not a filament of current but a disc of current. Smith and West (1987) also found that a filament of current with a weighted average velocity function could explain the phenomena of near surface inhomogeneities as calculated by them on the edge of a horizontal conductor. Together with Hoversten and Morrison's (1982) findings of a single current ring, it seems more probable that it is not possible to define the velocity directly as a function of the resistivity distribution, but rather that some weighted average function should be found. Looking at Figure 2.3 it should now be quite evident that there is gradual change from the apparent resistivity of the one layer to the next.

Chapter 5

Approximating the response of a vertical geo-electrical boundary using a moving current filament

In Chapter 4 it became evident that it is possible to develop a qualitative model of a layered earth using the functions described by Nabighian (1979). The calculated apparent resistivities of different layered geo-electric models show clearly that it will be theoretically possible to detect and resolve a layered earth system by recording the derivative of the vertical magnetic field in the center of an approximately circular transmitter. The calculations were done for a vertical magnetic dipole, but using the concept of reciprocity it is possible to apply this to a large closed transmitter wire with a small receiver coil at the center. This chapter looks at the different components of the equations governing the diffusion of a current smoke filament through the earth in an attempt to isolate the characteristic responses of a distorted and tilted current filament. The purpose is to determine a possible closed solution for a vertical geo-electrical boundary response.

TDEM methods are usually employed in two different ways, namely profiling and sounding. For the first method, measurements of more than one component of the transient field are made along a traverse extending over the transmitter loop. This method is generally used for vertical conductor location. Measurements of the vertical component of the transient field for the second method are usually taken in the center of the transmitter loop and are used to interpret the layered structure of the earth underneath. For interpretation purposes the data is plotted differently.

The profile data are displayed as measured emf against position, for each time channel with separate plots for the x, y and z-components. From the profile plot the response of a homogenous or layered earth model is subtracted and the resulting anomaly interpreted. The layered earth response can also be removed by assuming a symmetrical response through the loop in the absence of an anomaly. Assuming the anomaly to be situated on one side of the loop, the opposite side can be mirrored and subtracted, (Slee 1988).

Sounding data are plotted as an apparent resistivity versus the square root of time graph. Illustrated in Chapter 2 the whole concept of using apparent resistivity to determine the layering of a system follows from a radial symmetry approximation. In this case the x and y-components will be zero anyway, given that measurements were made exactly in the center of the transmitter.

The object of this chapter is to attempt to approximate a situation with a vertical geo-electrical boundary formed by a fault or geological contact, for example, but which is not a vertical conductor. The question is what the effect of such a situation will be on a smoke ring of current and if it is possible to find characteristics which will present an acceptable interpretation. In much the same way that vectors are broken up into components, the different aspects of a smoke ring are changed one at a time. Because this is not a symmetrical case anymore, the data is evaluated both as profiles and as soundings.

Firstly, the shape and orientation are changed and presented as profiles and apparent resistivity plots. Consequently the current, radius and depth of a circular current are changed and presented as apparent resistivity plots, calculated from the values generated by the forward model. The current filament is then moved along a horisontal plain and the resulting field presented as profile and apparent resistivity plots. Lastly, two different possible physical models are presented and compared to the data above. The same is repeated for the magnetic field.

5.1 CHANGING THE SHAPE AND ORIENTATION OF A CURRENT FILAMENT

The shape of a moving current filament is changed by forming an ellipse shown in Figure 5.1. It is elongated in the x-direction by compressing it in the y-direction. The axis indicated as **a** is calculated using eq 4-10 as the current radius for a homogeneous half-space of 100Ω.m. Thus, to elongate it in the x-direction, the radius indicated as **b** is calculated with eq 4.10 for lower resistivities. To elongate the current filament in the y-direction, **a** is still calculated as being that of a 100Ω.m half-space, but now **b** is calculated with eq 4-10 as a function of higher resistivities.

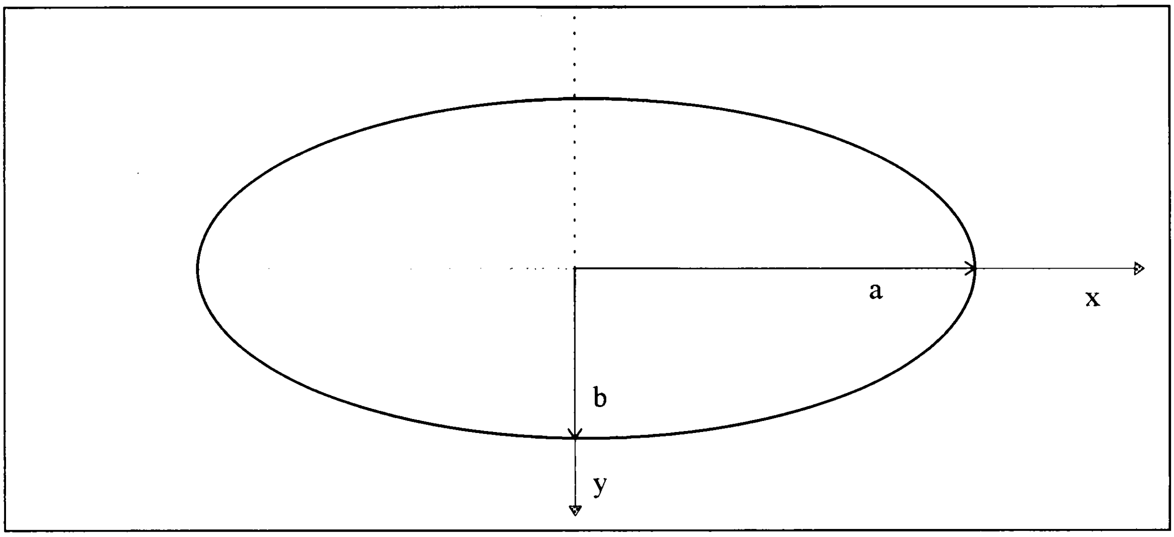

Figure 5.1 The current ellipse used to approximate a distorted circle. The axis indicated as a ***is calculated as the current radius of a 100Ωm homogeneous half-space. This ellipse is then elongated in the x or y-direction by calculating*** b ***for appropriate resistivities. Profiles plotted are calculated along the x-axis from -500m to 500m for y=0. The z-axis points into the page to conform to a right hand system. The ellipse is also tilted from the x to the z-axis for different angles up to π/4.***

For an untilted horizontal circular current filament, the x and z-components of the emf, directly proporsional to the derivative of the magnetic field, are symmetrical around the vertical magnetic dipole situated at 0m, as seen in Figure 5.2. The headings of the graphs refer to the displayed components, i.e. x and z, while R(100ohm.m) indicates that the b-axis of the ellipse was calculated for 100Ω.m. The a-axis is always calculated for 100Ω.m and thus the displayed results are for a circular current. The y-component of the emf is zero. The legend entries refer to the degree (in radians) of tilt from the x to the z-axis. Tilting this circular current filament results in an unsymmetrical emf when plotted as profiles. All the plotted profiles are for the same instant in time.

The x-component is no longer zero in the centre of the loop for an unsymmetrical earth, a fact that can be used to determine the presence of an unsymmetrical earth. For a tilt of pi/6 (30°) the z-component already displays a characteristic anomaly typical of a vertical conductor. Note that the zero cross-over is not situated over the center of the tilted current filament, but towards the upturned side of the current filament. For a tilt of pi/4 (45°) the zero cross-over is situated over the center of the current filament, but the amplitude of the anomaly is half that of the pi/6 tilt. Also important is the fact that the z-component does not change sign.

The legend in Figure 5.3 refers to different tilts from the x to the z-axis. The calculated apparent resistivity value is divided by apparent resistivity ($\rho 1$) for a horizontal circular current in a 100Ω.m half-space. Considering the apparent resistivity shown in Figure 5.3 it can be seen that the difference between the apparent resistivity values for a horizontal current filament and one tilted pi/36 (5°), pi/18 (10°) is negligible. Even for a tilt of pi/6 the ratio of apparent resistivity to that of a 100Ω.m earth is less than two. Thus tilting a circular filament of current changes the profile plots significantly, but not the apparent resistivity plots with the exception of a drastic tilt of pi/4. An apparent resistivity ratio of 10 to 1 is significant.

Note that the depth, radius and current used, were those corresponding to a 100Ω.m halfspace and that all the following presented results will take this model as the standard to be compared to.

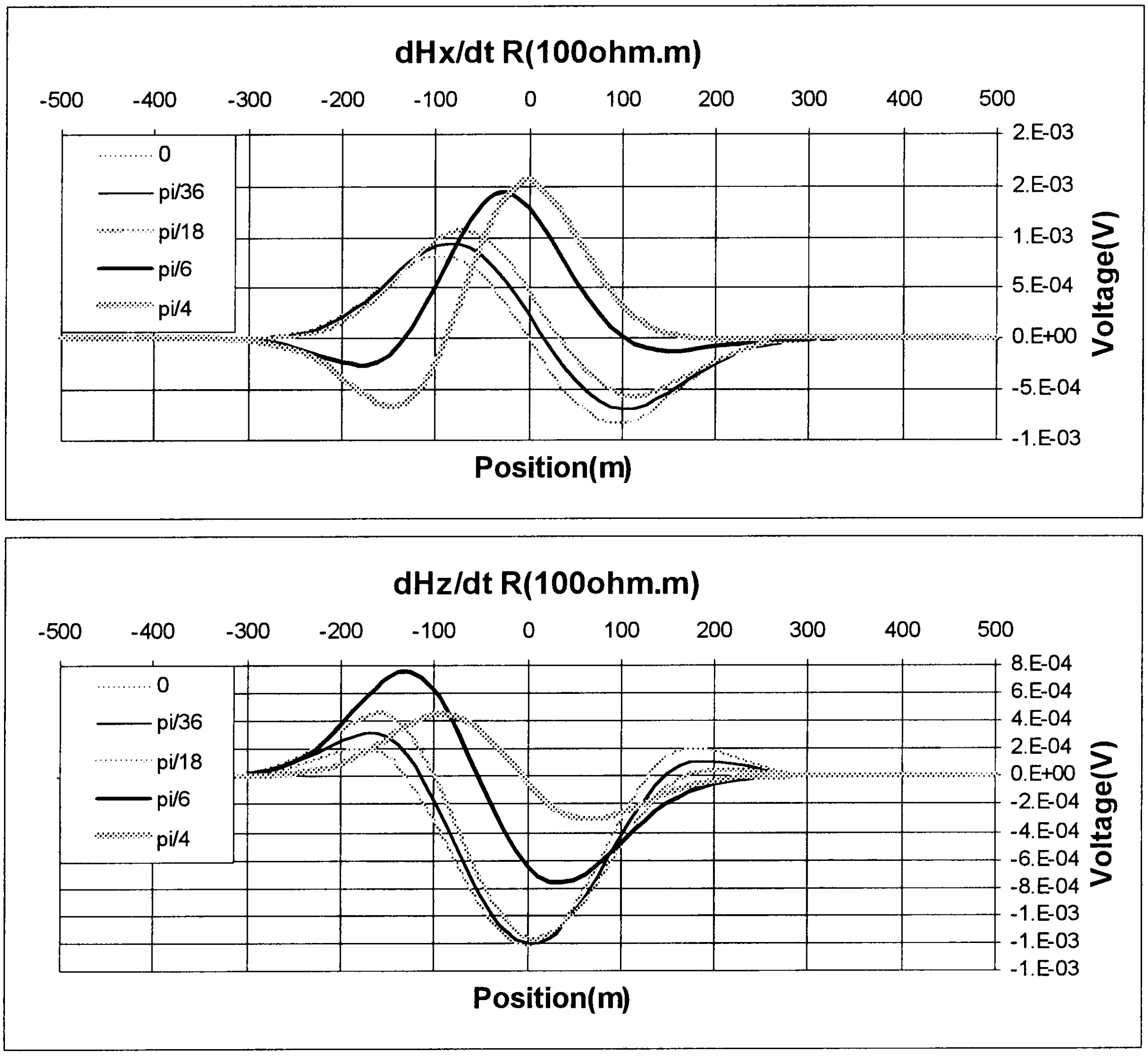

Figure 5.2 Profile plots of calculated models.

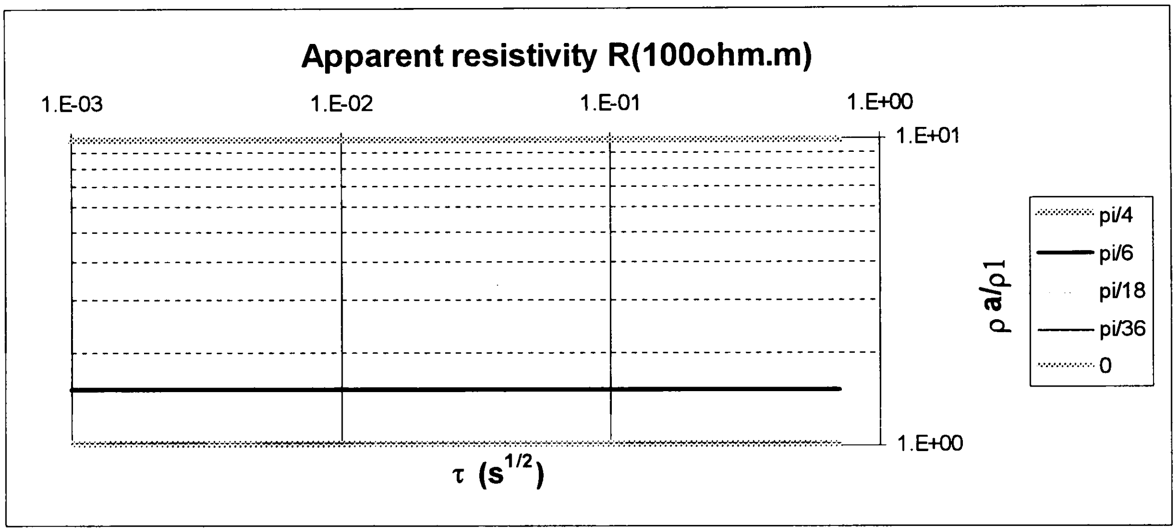

Figure 5.3 Apparent resistivity plots for b calculated with R(100Ωm) which means that the current is circular for a 100Ωm half-space.

5.1.1 Current filament compressed in the y-direction

In Figures 5.4 to 5.6 the x and z-components of a current filament compressed in the y-direction are shown. As stated before, the compression is achieved by calculating the b-axis in Figure 5.1 with lower resistivities than 100Ω.m. The form of both components do not change for different compressions when compared to Figure 5.2. It is only the maxima and minima of the graphs that become progressively lower for more compression. Therefore, if the responses for different compressions were plotted on the same profile, that of the 100Ω.m earth would overshadow the rest. The z-component of the compressed current filaments, tilted pi/4, do not have the zero cross-over at position 0m anymore, but to the left of the center for the time channel plotted.

Figure 5.7 shows that compression in the y-direction of a horizontal current filament yields progressively higher apparent resistivities than that of a 100Ω.m earth. The legend refers to b calculated for the noted resistivities. The calculated apparent resistivity value is divided by apparent resistivity (ρ1) for a horizontal circular current in a 100Ω.m half-space, which explains why R(100Ω.m) is plotted at 1. Theoretically there is a difference between the apparent resistivity values, but it is still relatively minor. For the 1Ω.m compression, which means that the a:b ratio is 10:1, the apparent resistivity ratio is 3:1.

This is a qualitative model and the fact that 1Ω.m is supposed to indicate a conductor in which separate (secondary field) currents will be induced, is ignored for the sake of a resistivity ratio.

The a:b ratio is calculated as follows, from eq 4-10:

$$
\begin{aligned}
r_b &= \sqrt{8C_2}\sqrt{\frac{t}{\sigma_b \mu}} = A\sqrt{\frac{t\rho_b}{\mu}} \\
&= B\sqrt{\rho_b} = B\sqrt{\rho_a f} \\
&= B\sqrt{\rho_a}\sqrt{f} \\
&= r_a\sqrt{f}
\end{aligned} \tag{5-1}
$$

where f is the factor between the resistivity values for a and b. For b(1Ω.m) $f=1/100$ and would $r_b=r_a/10$.

Figures 5.8 to 5.10 show the deformed current filament tilted from the x to the z-axis for the angle displayed in the legend. Because the apparent resistivity values are calculated in the center of the current filament, there would not be a difference if it were tilted from y to the z-axis, for example. Tilting the deformed current filament results in even higher apparent resistivities as each graph clearly shows, although it is hardly visible for the first two tilts. Comparing Figures 5.8 to 5.10 with Figure 5.3, where a circular current filament is tilted, leads to the conclusion that tilting a current filament compressed in the y-direction results in a smaller relative apparent resistivity change. When compared to Figure 5.3 none of these tilted deformed current rings has a difference of 10:1 between a horizontal and pi/4 tilt.

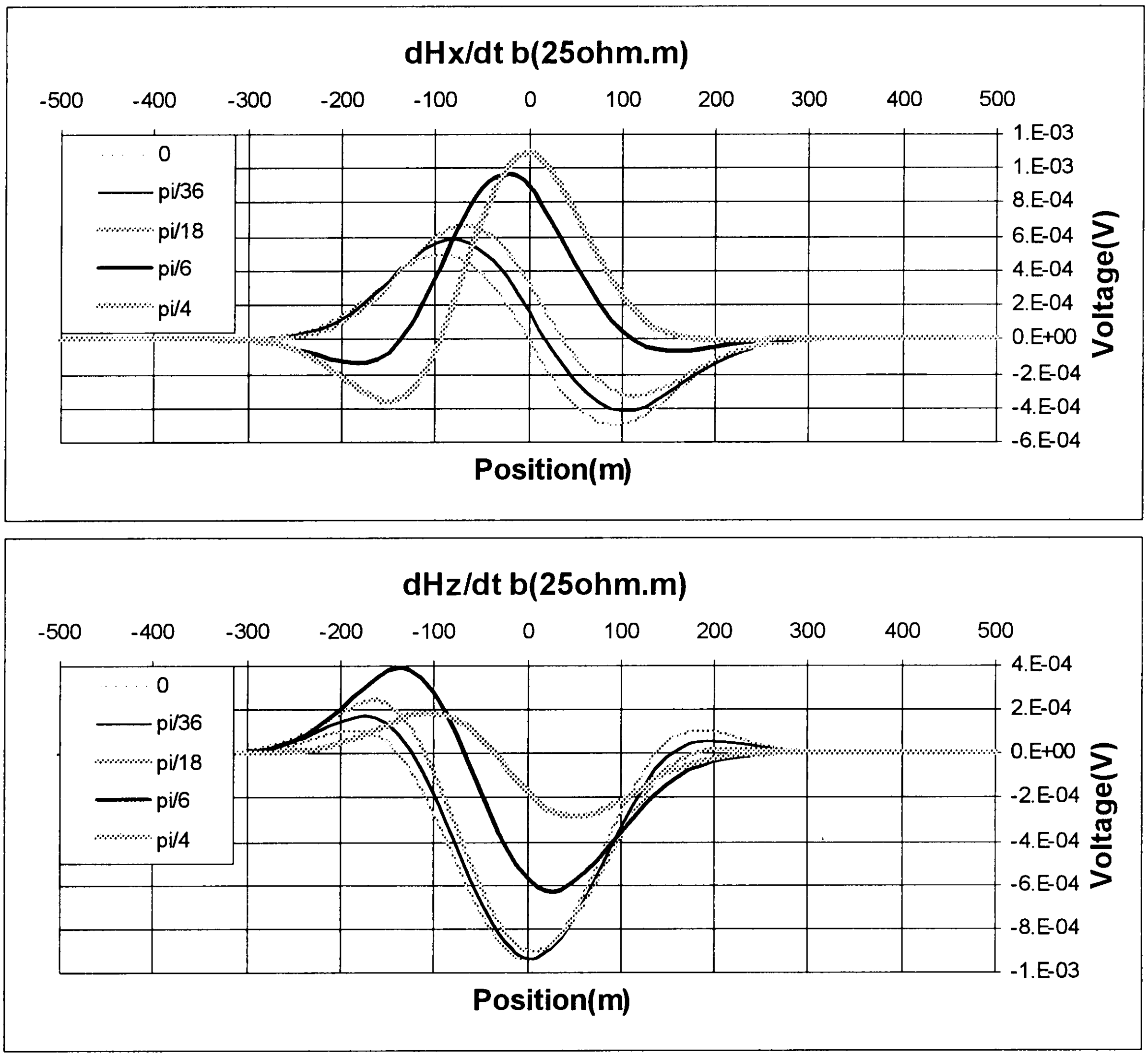

Figure 5.4 ***Profile plots for b calculated with R(25Ωm) resulting in an elongated current filament forming an ellipse in the x-direction. The y-component is zero.***

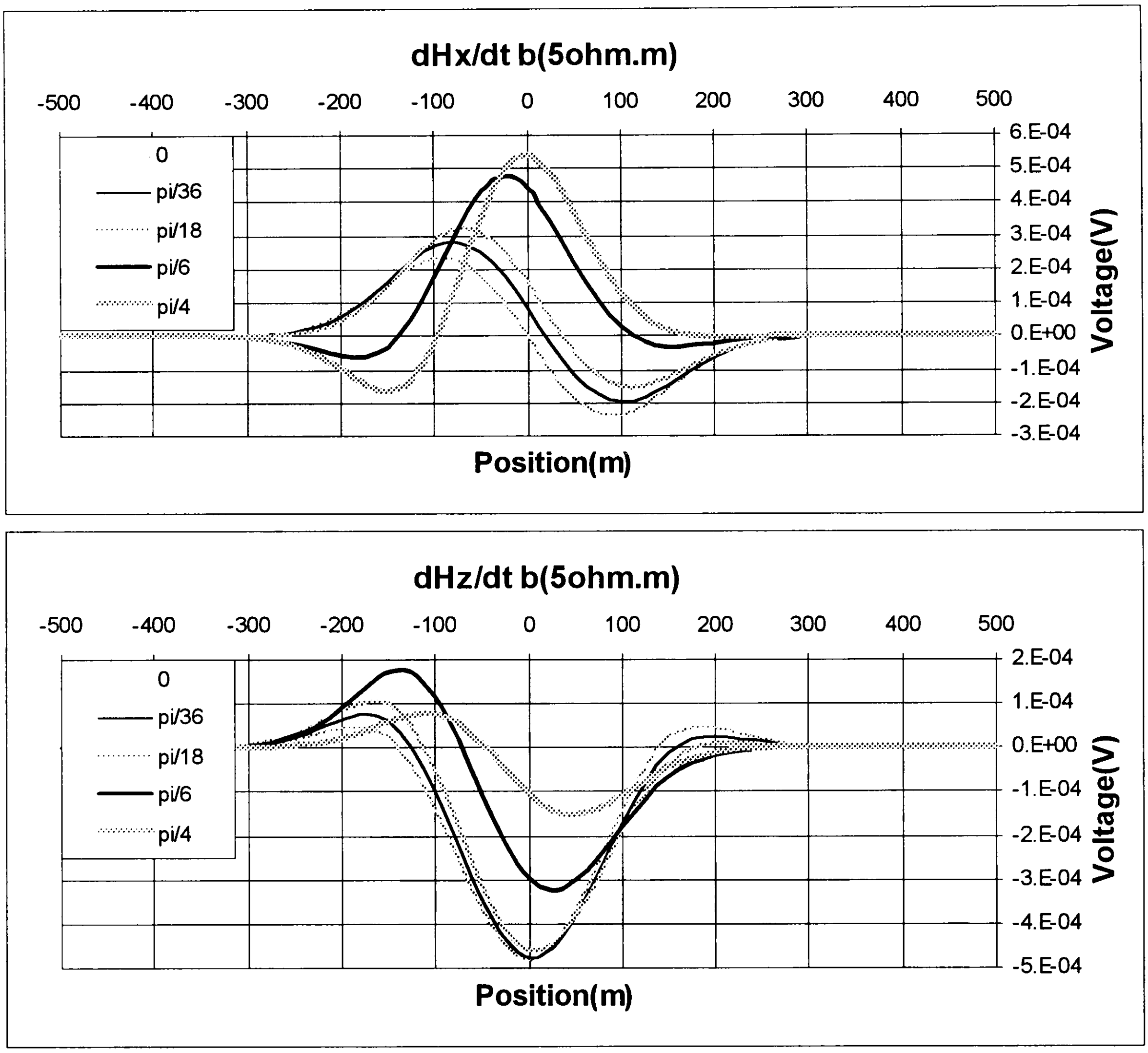

Figure 5.5 Profile plots for b calculated with R(5Ωm) resulting in an elongated current filament forming an ellipse in the x-direction. The y-component is zero.

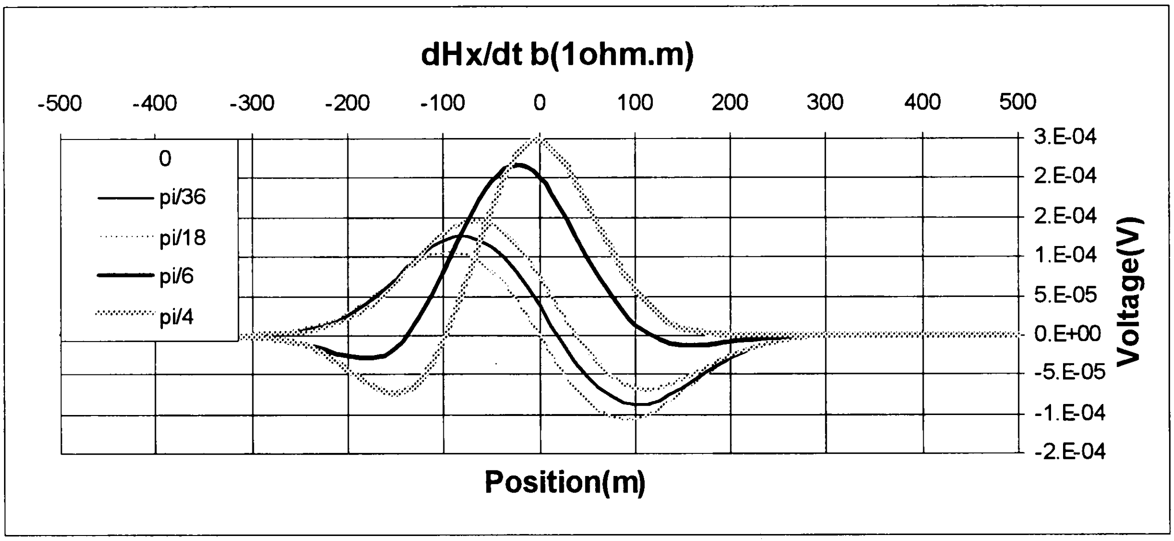

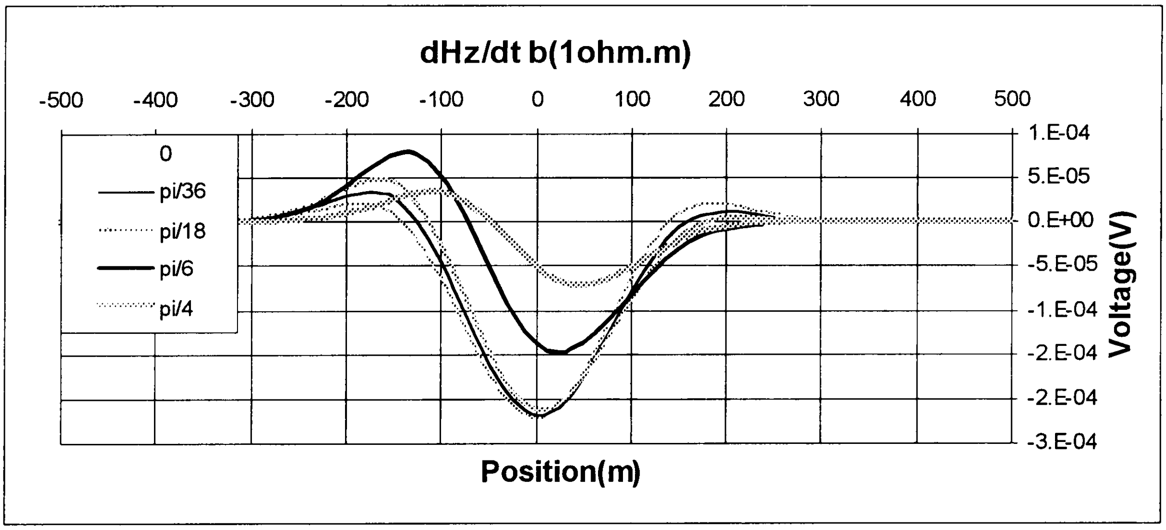

Figure 5.6 Profile plots for b calculated with R(1Ωm) resulting in an elongated current filament forming an ellipse in the x-direction. The y-component is zero.

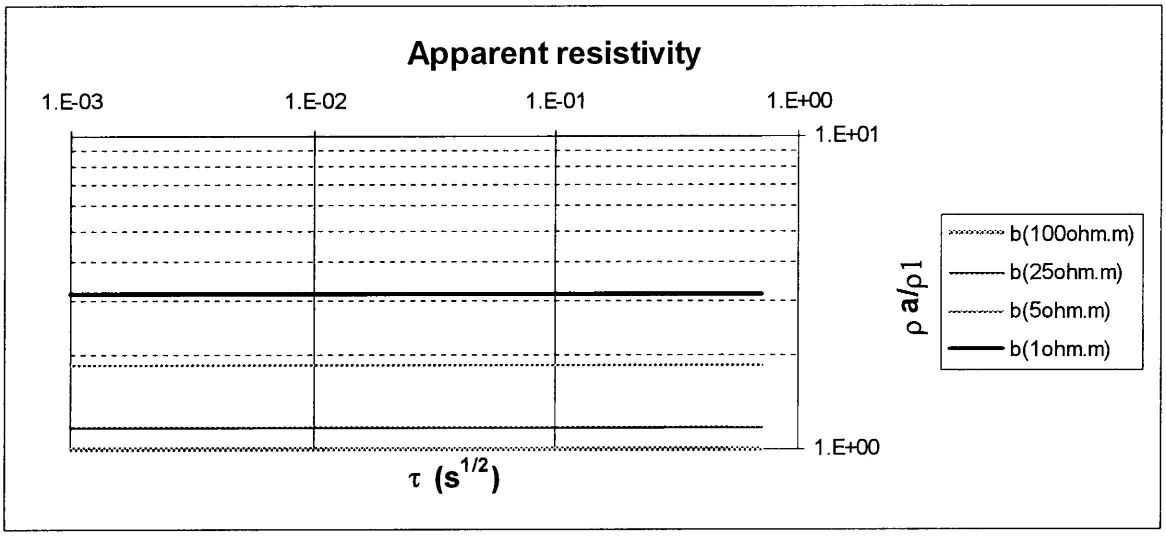

Figure 5.7 Apparent resistivity plots for horizontal currents and compression of the current filament in the y-direction.

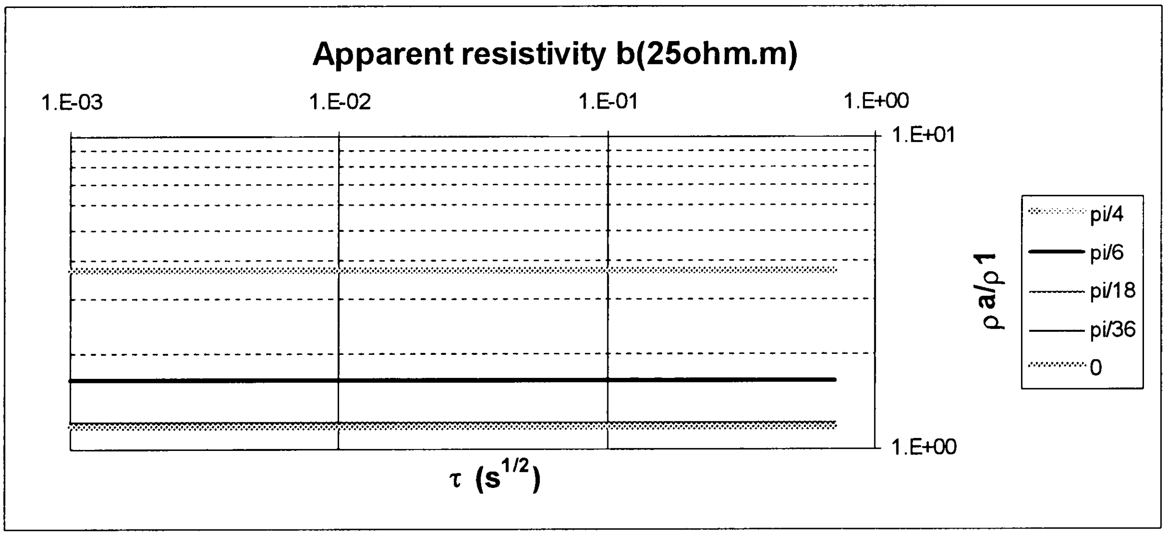

Figure 5.8 Apparent resistivity plots for b calculated with R(25Ωm) and tilted from the x to the z-axis as indicated in the legend (radians).

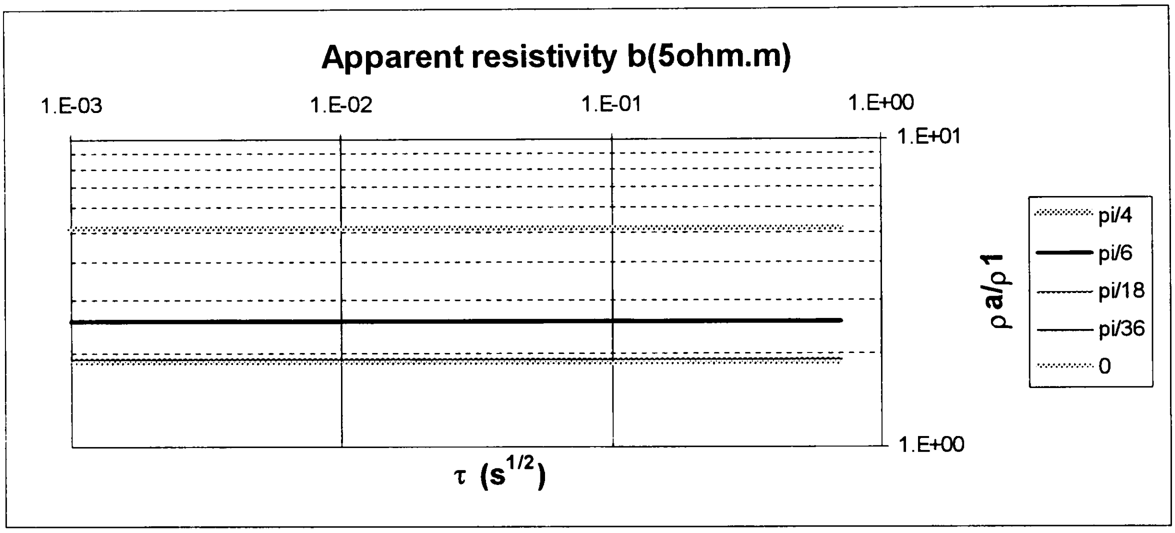

Figure 5.9 Apparent resistivity plots for b calculated with R(5Ωm).

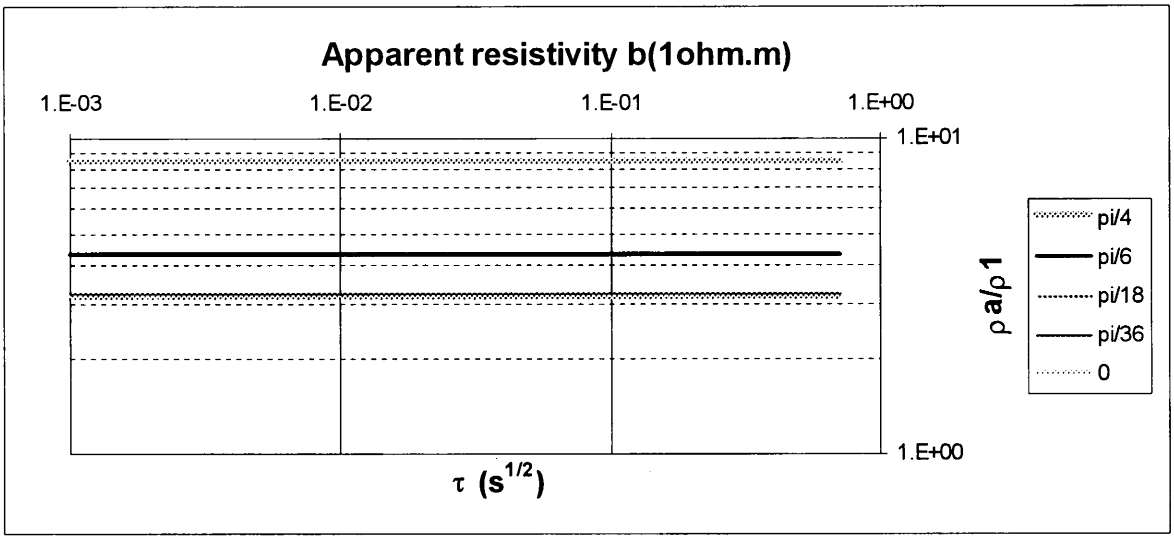

Figure 5.10 Apparent resistivity plots for b calculated with R(1Ωm).

5.1.2 Current filament elongated in the y-direction

The current filament is elongated in the y-direction by calculating b in Figure 5.1 with higher resistivities than 100Ω.m. Looking at Figures 5.11 to 5.13 it is clear that the x-components look very similar to those of a circular tilted current filament in Figure 5.2. Again the minima and maxima become progressively smaller with more elongation. The z-components also do not display extraordinary differences with a circular current filament. The zero cross-over of the pi/4 tilt is now just displaced to the right of 0m which means that the z-component values at 0m change sign between pi/6 and pi/4; this is the case for all the time channels. There are no other significant characteristics associated with a current filament elongated in the y-direction. As profiles, a distorted horizontal filament still has a symmetrical response, because the filament is deformed in a symmetrical manner.

Note that for b(10000Ω.m) in Figure 5.13 there is a distorted y-component of the emf. Compared to the calculated values for the x and z-components this emf is approximately 10^5 times smaller.

In Figure 5.14 the different apparent resistivity values for horizontal currents and different elongations in the y-direction are shown. The legend refers to b calculated for the noted resistivities. The calculated apparent resistivity value is divided by apparent resistivity (ρ1) for a horizontal circular current in a 100Ω.m half-space, which explains why b(100Ω.m) is plotted at 1. Again, as in Figure 5.7, distortion leads to higher apparent resistivities. The amount of change is very small compared to the distortion. Using the procedure in eq 5-1, it means that for b(10000Ω.m) the ratio a:b is 1:10, the apparent resistivity ratio is 3.5:1.

Tilting the deformed current filament up to pi/6 also manifests itself in an even higher apparent resistivity than that for the horizontal deformed filament, as seen in Figures 5.15 to 5.17. Note that for the tilt, pi/4, the apparent resistivity value is lower than for the pi/6 tilt, because the z-component has changed sign from negative to positive. The higher the deformation, the closer the apparent resistivity for pi/4 is to the untilted deformed apparent resistivity value.

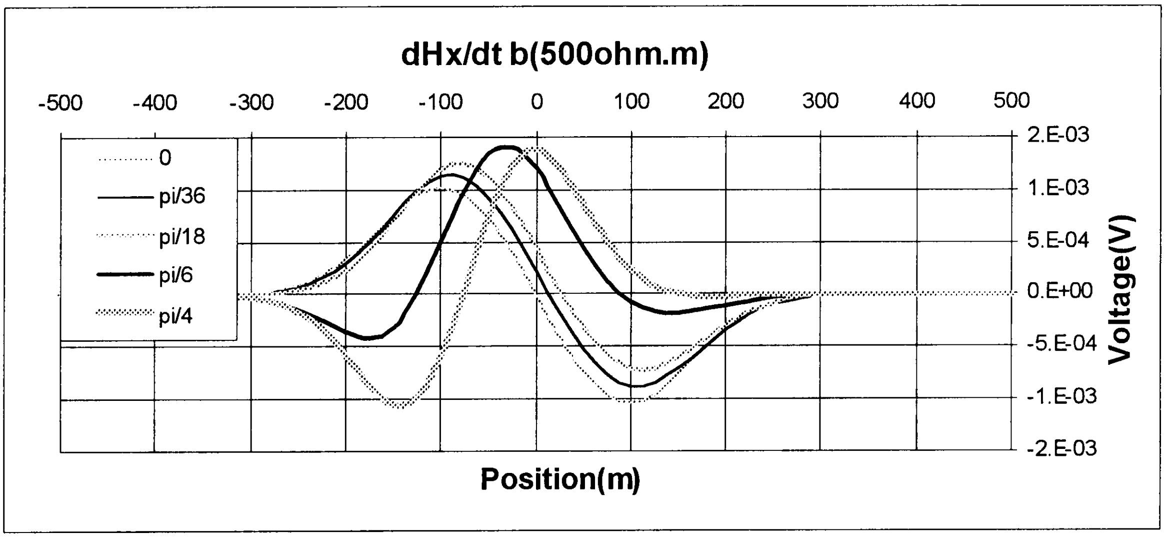

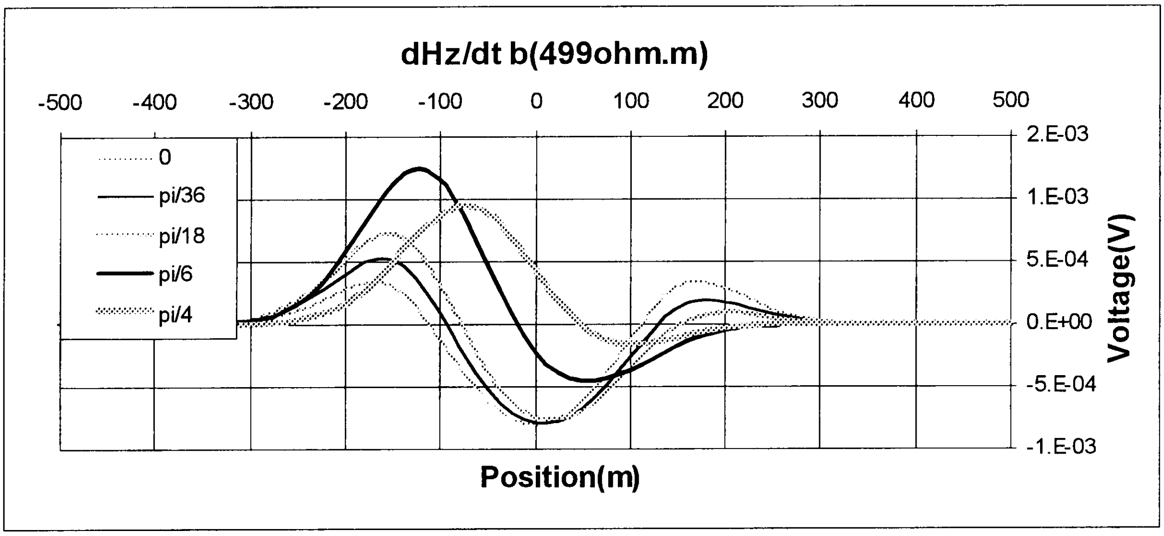

Figure 5.11 Profile plots for b(500Ωm) resulting in an elongated current filament forming an ellipse in the y-direction. The y-component is zero.

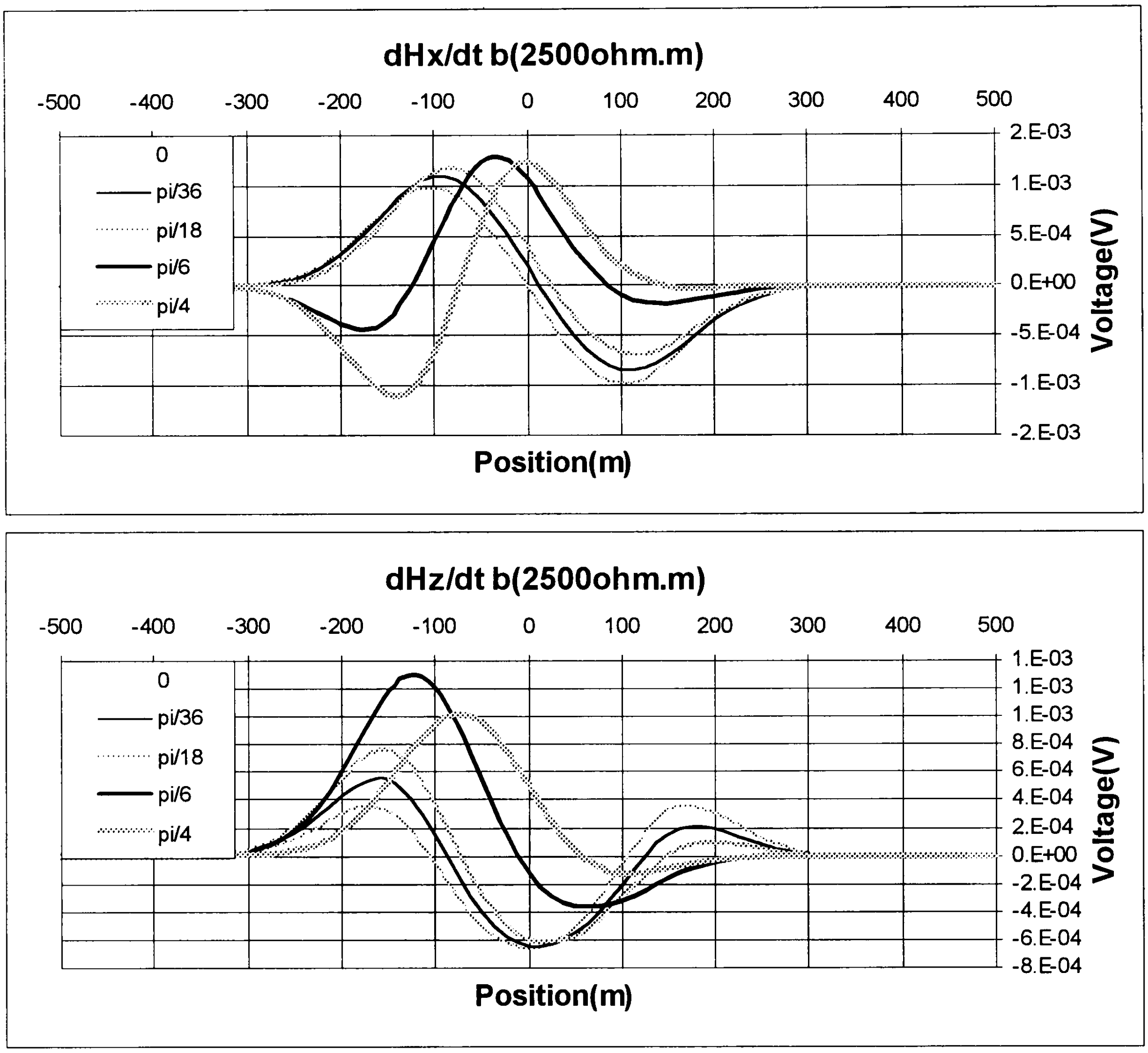

Figure 5.12 Profile plots for b(2500Ωm) resulting in an elongated current filament forming an ellipse in the y-direction. The y-component is zero.

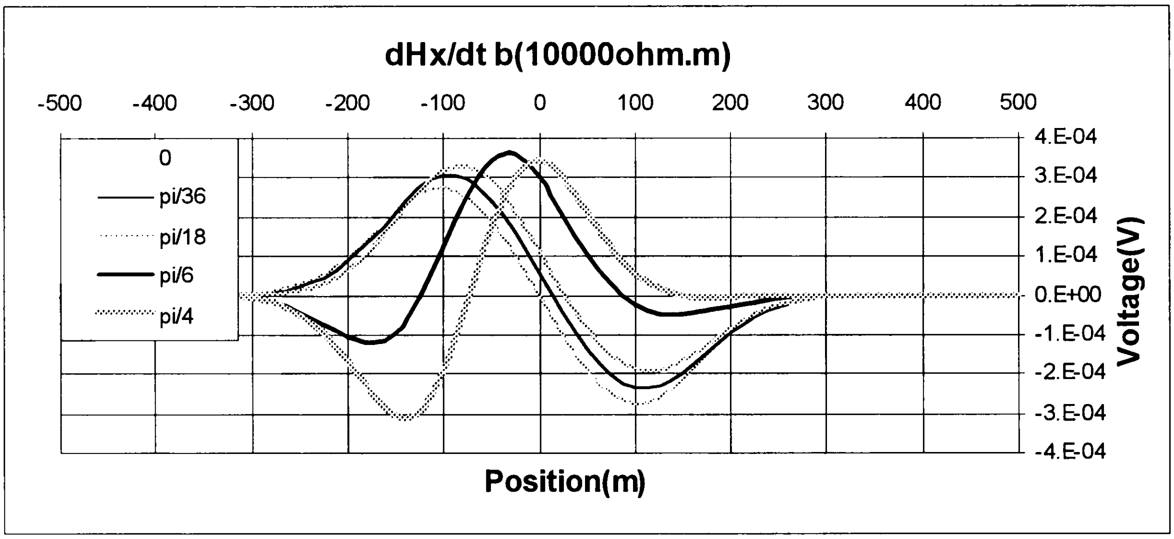

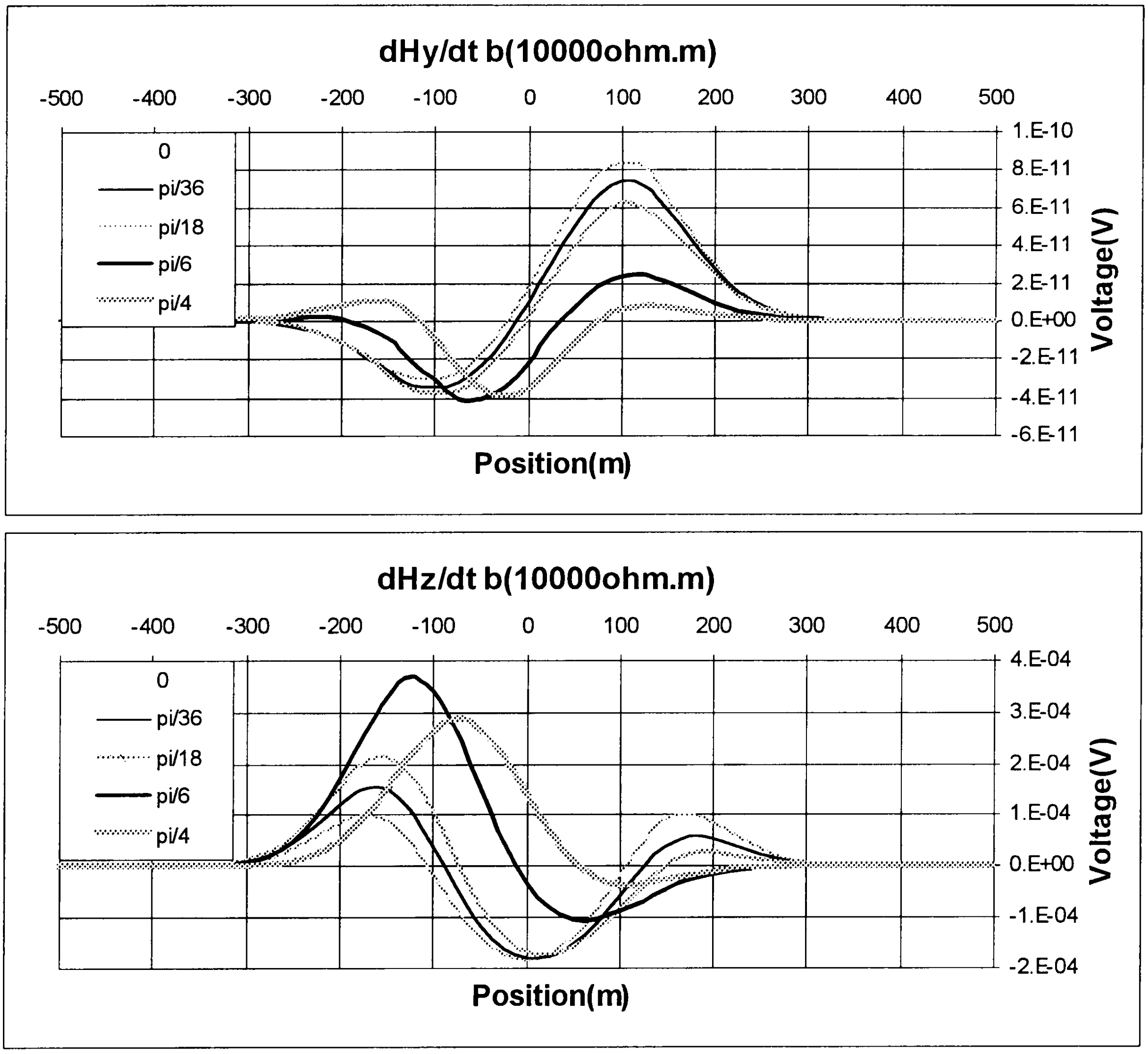

Figure 5.13 Profile plots for b(10000Ωm) resulting in an elongated current filament forming an ellipse in the y-direction. Note that the y-component is not zero anymore, although its values are negligible when compared to the x and z-components.

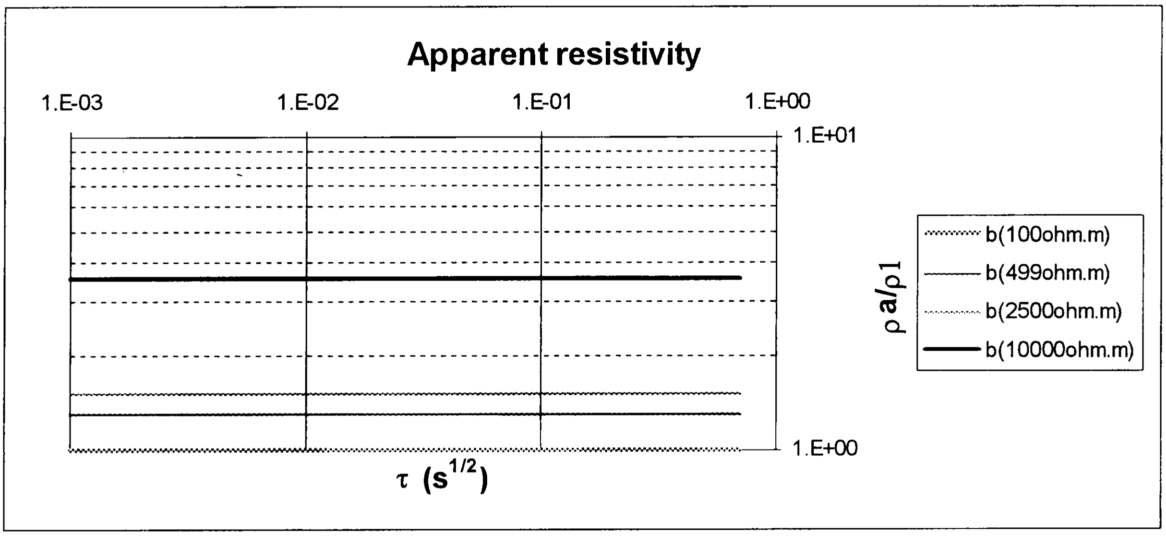

Figure 5.14 Apparent resistivity plots for horizontal currents and elongation of the current filament in the y-direction.

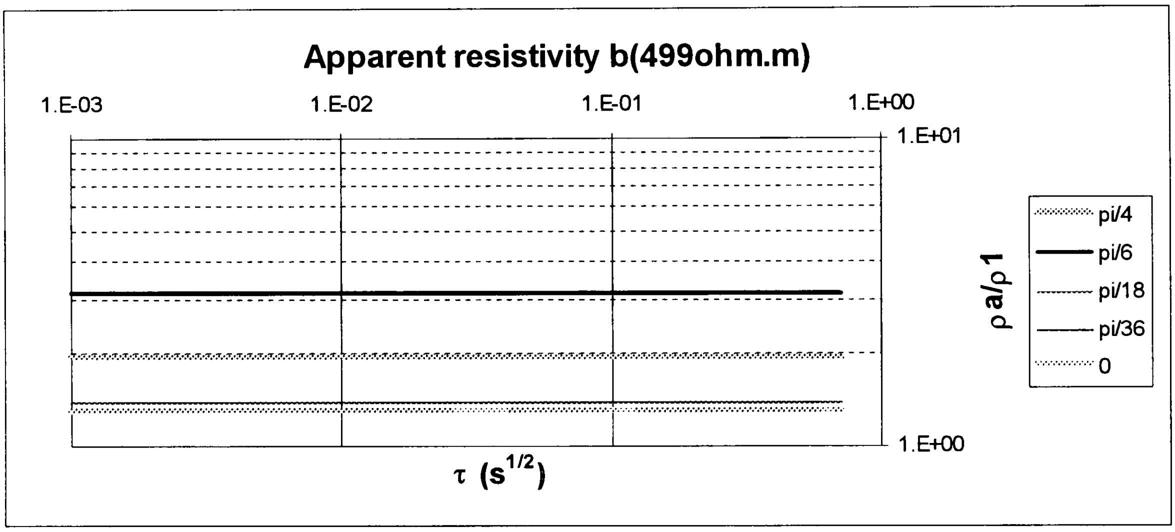

Figure 5.15 Apparent resistivity plots for b=rad(500Ωm) and tilted from the x to the z-axis as indicated in the legend (radians). Note that the emf for pi/4 is opposite in sign compared to the other tilts.

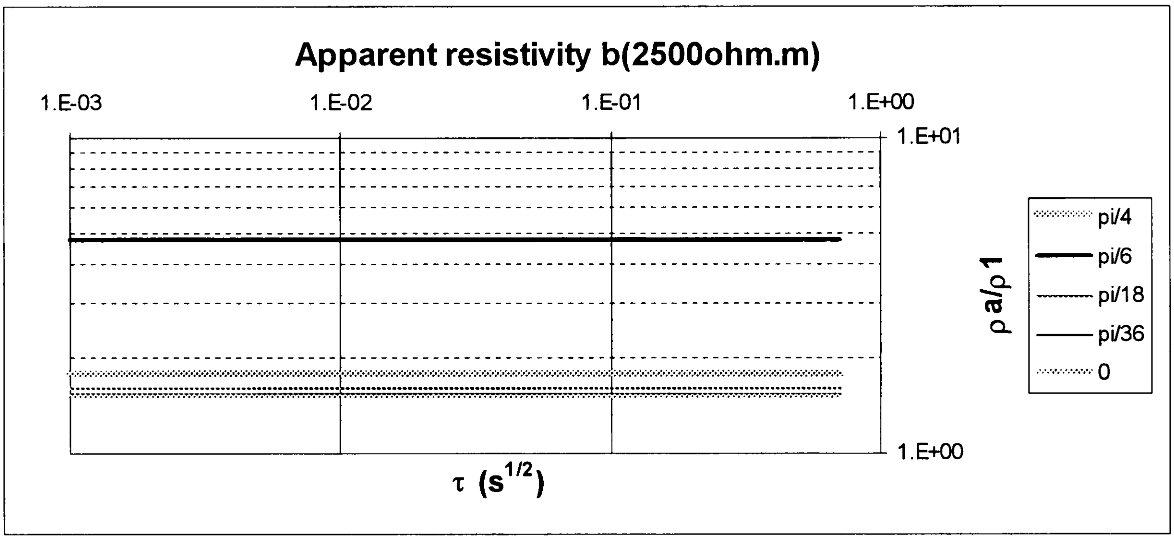

Figure 5.16 Apparent resistivity plots for b=rad(2500Ωm) and tilted from the x to the z-axis as indicated in the legend (radians). Note that the emf for pi/4 is opposite in sign compared to the other tilts.

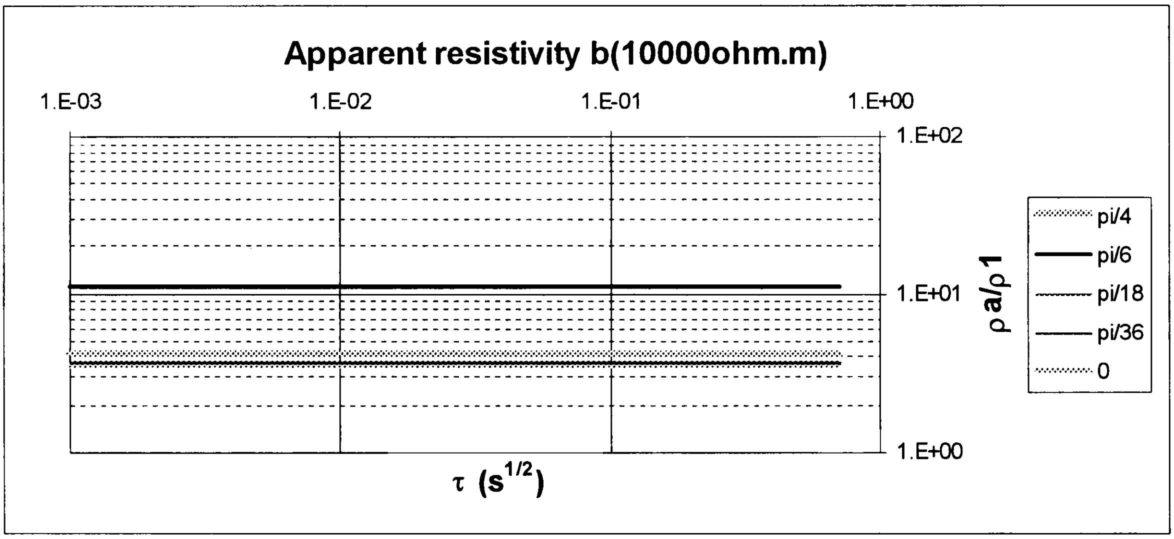

Figure 5.17 Apparent resistivity plots for b=rad(10000Ωm) and tilted from the x to the z-axis as indicated in the legend (radians). Note that the emf for pi/4 is opposite in sign compared to the other tilts

5.2 CHANGING THE CURRENT OF A CIRCULAR CURRENT FILAMENT

The amplitude of the current in the current filament is a function of the subsurface resistivity (Nabighian, 1979). It was therefore decided to investigate the influence of various current amplitudes.

The current for a circular horizontal smoke ring $I_i = 1/\left(4\pi C_2 \lambda^2\right)$, where $\lambda = \sqrt{t/\sigma\mu}$, is changed by changing σ and keeping all the rest of the parameters, like the depth and radius, as if for a 100Ω.m earth. This is performed for currents corresponding to 100Ω.m and less and the process is repeated for higher resistivities. The current filament is circular and horizontal. Profile plots of the x and z-components for the different current functions are presented for comparison. The y-component is zero, because the values are calculated for a traverse along the x-axis.

5.2.1 Currents calculated for 100Ω.m and less

First rewrite the equation for I_i as a function of resistivity (ρ):

$$I_i = \left(4\pi C_2 \frac{t}{\sigma\mu}\right)^{-1} = \frac{\mu}{4\pi C_2 t}\left(\frac{1}{\rho}\right) \qquad (5\text{-}2)$$

Thus the smaller the resistivity, the larger the current will be, as is obvious in Figure 5.18. The effect on the apparent resistivity can be seen in Figure 5.19, where a lower resistivity results in a lower apparent resistivity. For a current calculated for 1Ω.m the relative apparent resistivity ratio of ρ_a:ρ_1 is 1:20, which is significant.

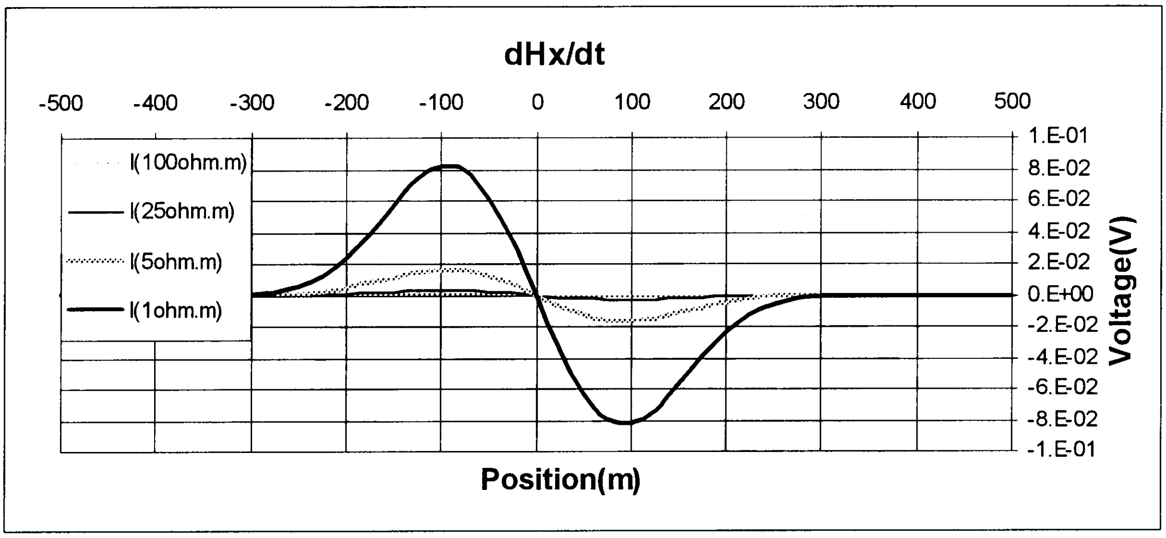

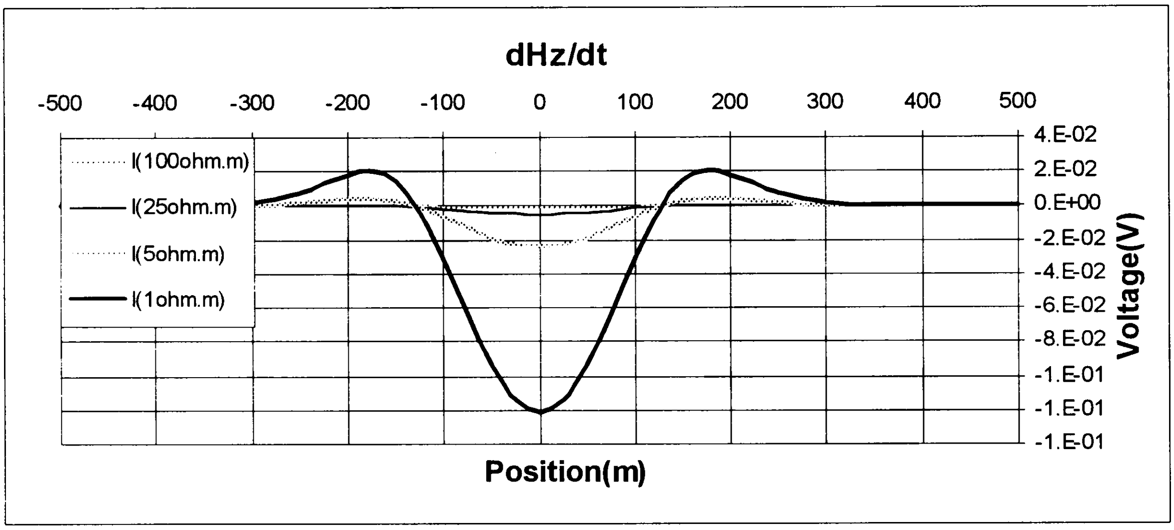

Figure 5.18 Profile plots for the indicated components and current functions. The depth and radius are kept as if for a 100Ω.m earth.

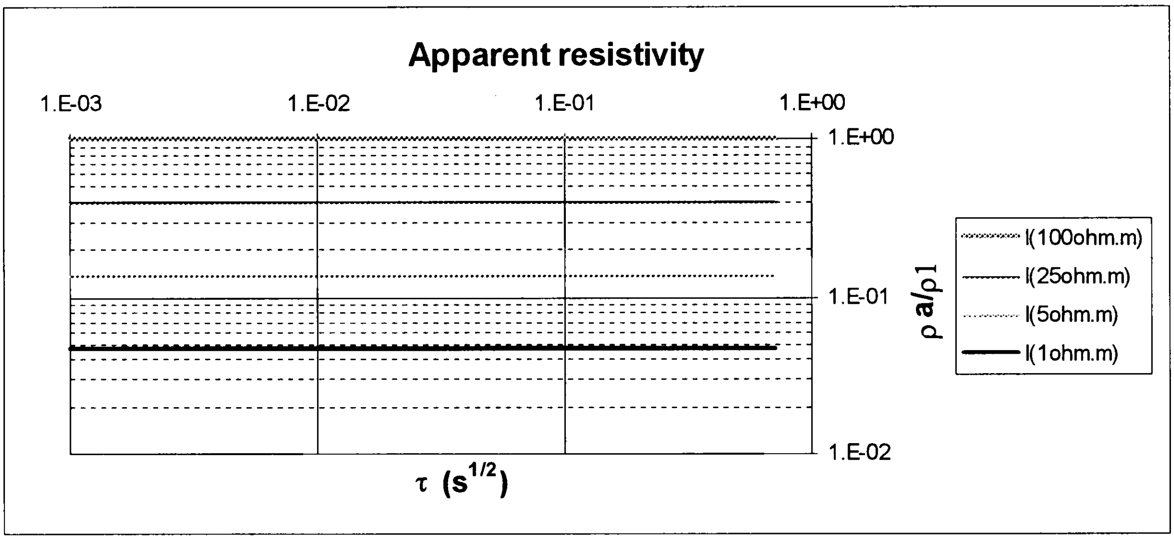

Figure 5.19 Apparent resistivity plots for different currents functions. The depth and radius are kept as if for a 100Ω.m earth.

5.2.2 Currents calculated for 100Ω.m and more

Eq 5-2 states that the current will become lower with a higher resistivity, which can be seen in Figure 5.20. In Figure 5.21 it is evident that for a higher resistivity, higher apparent resistivity will result. For an apparent resistivity ratio, ρ_a:ρ_1 9:1, the real resistivity ratio was 25:1, which is significant. Note that for this and the previous case the resulting apparent resistivity reflect the difference in resistivities used for calculation. A resistivity higher than 100Ω.m gives an apparent resistivity higher than 100Ω.m and for a resistivity higher than 100Ω.m a higher apparent resistivity follows.

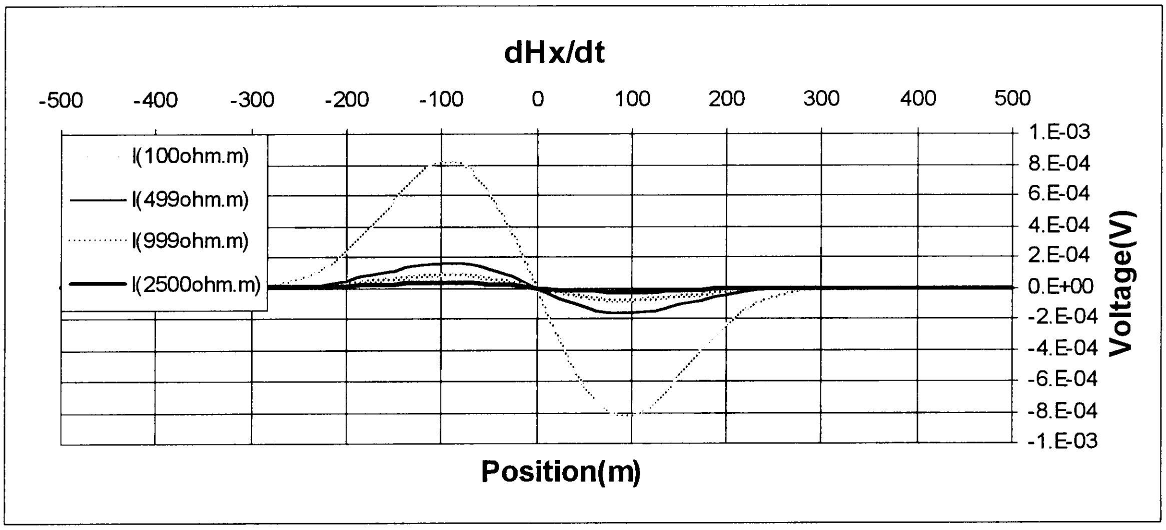

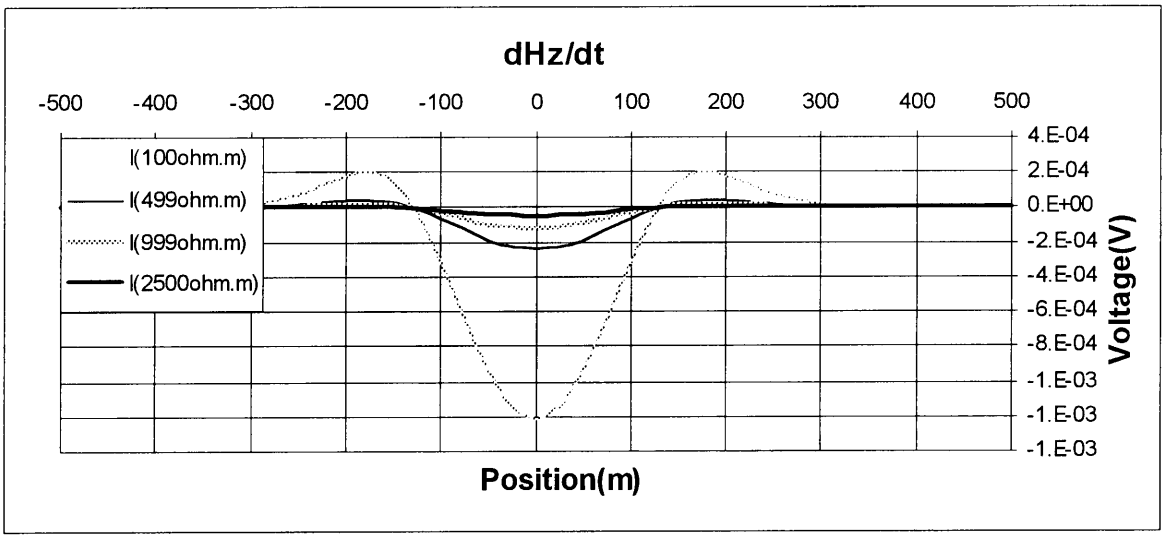

Figure 5.20 Profile plots for the indicated components and current functions. The depth and radius are kept as if for a 100Ωm earth.

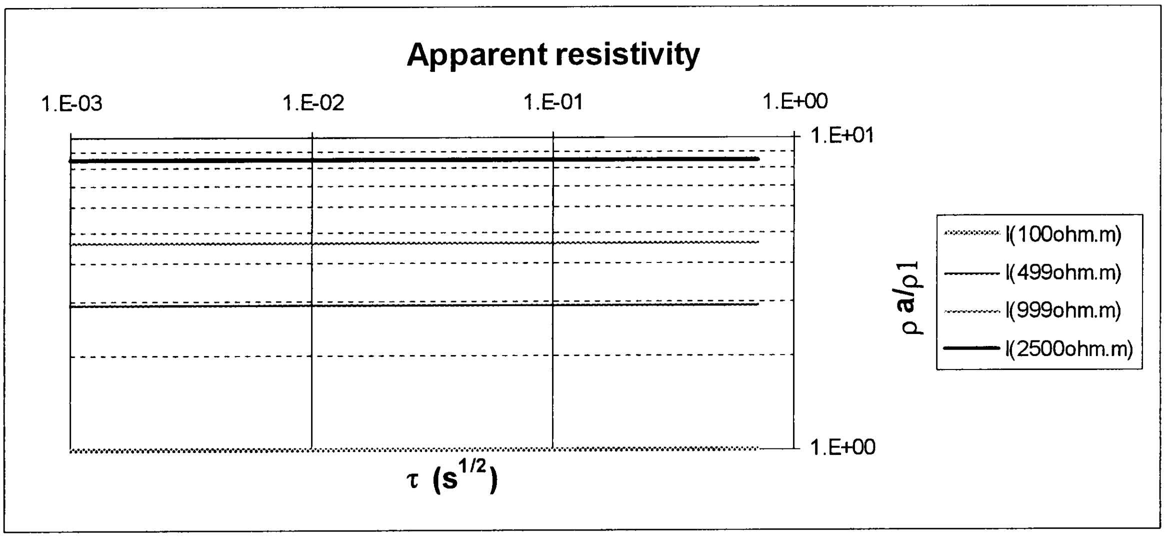

Figure 5.21 Apparent resistivity plots for different currents functions. The depth and radius are kept as if for a 100Ωm earth.

5.3 CHANGING THE DEPTH OF A CIRCULAR CURRENT FILAMENT

The depth for a circular horizontal smoke ring $z = \left(4/\sqrt{\pi}\right)\lambda$, where $\lambda = \sqrt{t/\sigma\mu}$, is changed by changing σ and keeping all the rest of the parameters, like the current and radius, constant. Note that this function is multiplied by λ where the current function was divided by its square:

$$z = \frac{4}{\sqrt{\pi}}\sqrt{\frac{t}{\sigma\mu}} = \frac{4}{\sqrt{\pi}}\sqrt{\frac{t\rho}{\mu}} \tag{5-3}$$

Thus the depth will change as the square root of the resistivity.

5.3.1 Depths calculated for 100Ω.m and less

The effect on the x-component in Figure 5.22 of changing the depth is not a linear function. Starting with the Z(100Ω.m), the Z(25Ω.m) gives a bigger response, while the Z(5Ω.m) and Z(1Ω.m) become respectively smaller. The z-component on the other hand has a direct relationship with resistivity.

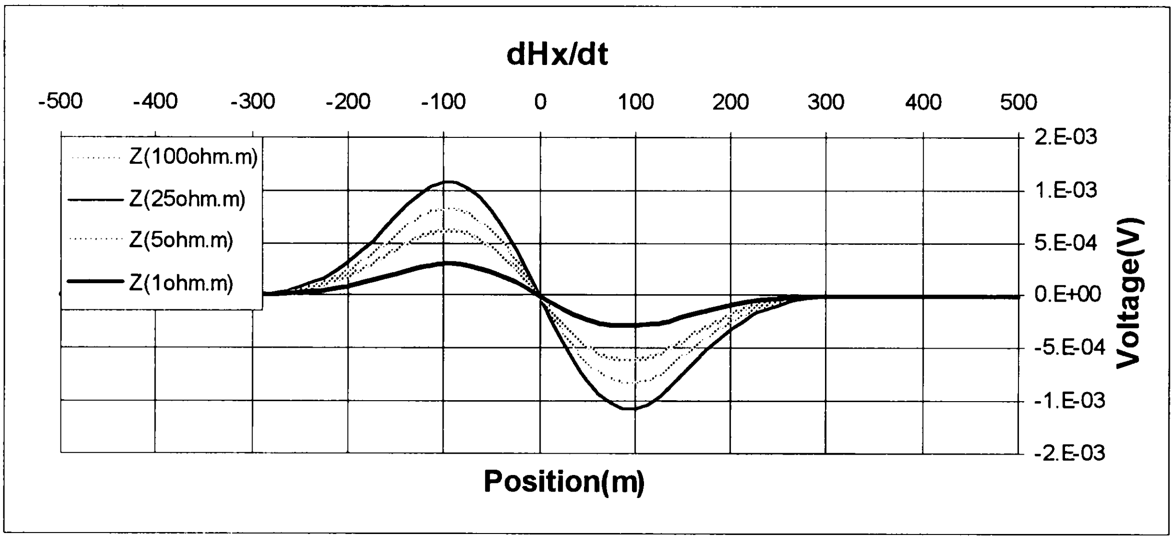

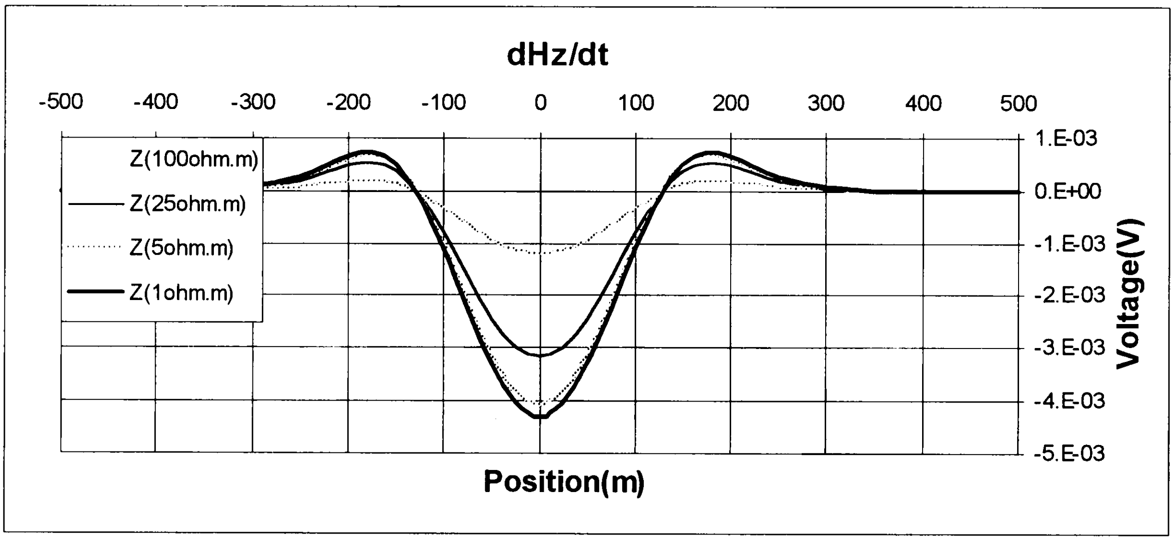

Figure 5.22 Profile plots for the indicated components and depth functions. The current and radius are kept as if for a 100Ωm earth.

Figure 5.23 shows the apparent resistivity plots where lower resistivities result in lower apparent resistivity as 100Ω.m, but the effect is very small. Thus for Z(1Ω.m), following a similar process than eq 5-1, the current filament is 10 times closer than for Z(100Ω.m), but the apparent resistivity ratio is 1:2.

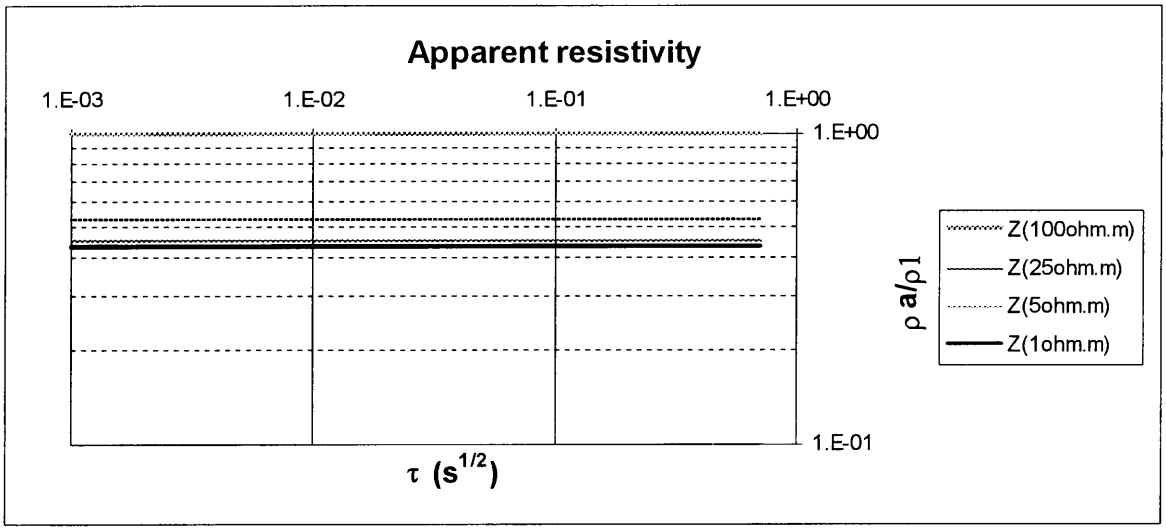

Figure 5.23 Apparent resistivity plots for different depth functions. The current and radius are kept as if for a 100Ω.m earth.

5.3.2 Depths calculated for 100Ω.m and more

Using depths calculated for more than 100Ω.m results in significant changes in the emf as can be seen in Figure 5.24. The form of the different components still looks the same, but the values are negligible when compared to those of Z(100Ω.m). This is also reflected in the apparent resistivities in Figure 5.25 where a resistivity contrast of 5:1 results in an apparent resistivity contrast of around 30:1. The next resistivity contrast of 10:1 results in a contrast of 2000:1 for the apparent resistivities. Thus the depth function is very sensitive to high resistivities which lead to serious apparent resistivity changes.

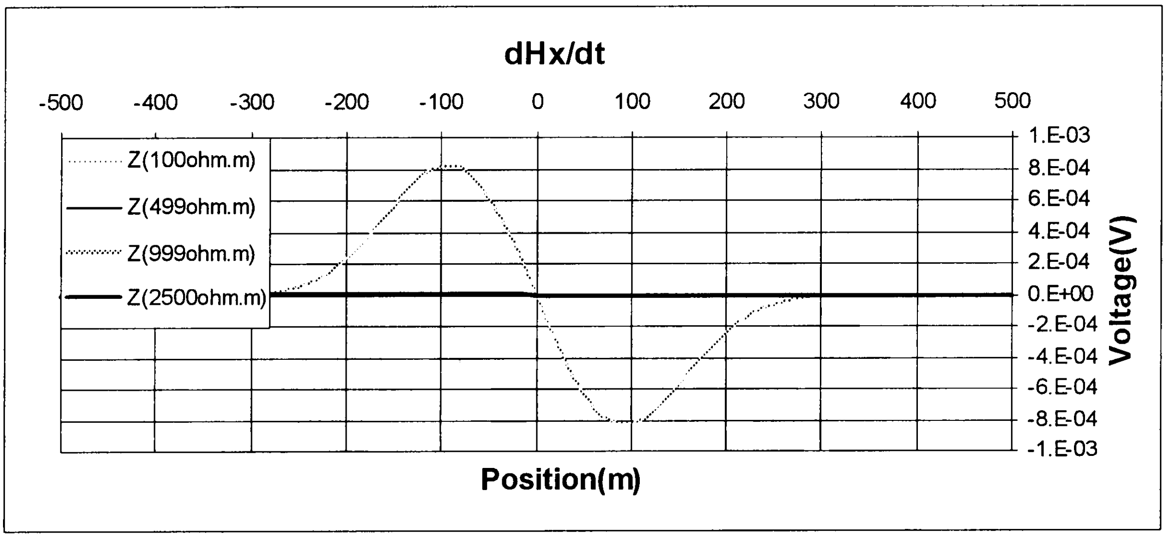

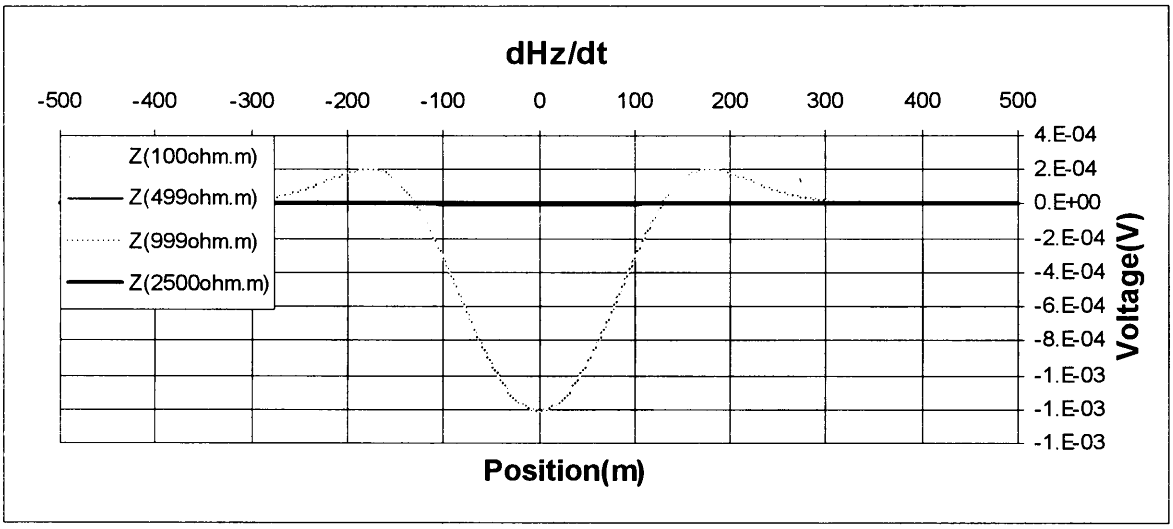

Figure 5.24 Profile plots for the indicated components and depth functions. The current and radius are kept as if for a 100Ω.m earth.

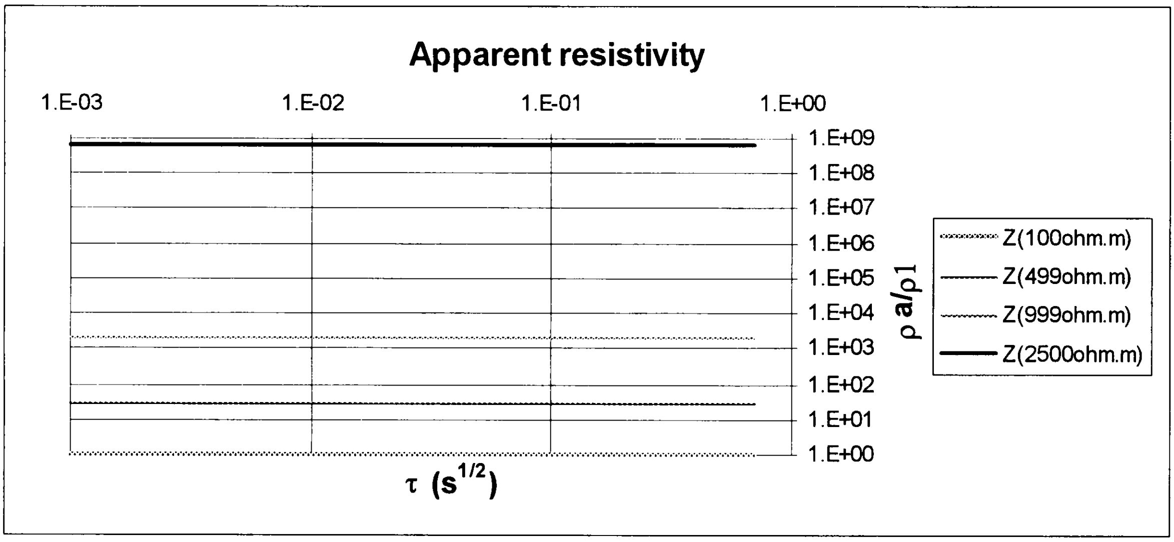

Figure 5.25 Apparent resistivity plots for different depth functions. The current and radius are kept as if for a 100Ω.m earth.

5.4 CHANGING THE RADIUS OF A CIRCULAR CURRENT FILAMENT

The radius for a circular horizontal smoke ring $a = \lambda\sqrt{8C_2}$, where $\lambda = \sqrt{t/\sigma\mu}$, is changed by changing σ and keeping all the rest of the parameters, like the depth and current, constant. Note that this function is multiplied by λ where the current function was divided by its square. This function is very similar to eq 5-3, there is only a difference in the constant. The results of changing the radius for different resistivities should thus be along similar lines than those for the depth.

5.4.1 Radii calculated for 100Ω.m and less

The smaller the radius becomes, the smaller the amplitude of the maxima and minima are, as seen in Figure 5.26. In this case the apparent resistivities calculated for lower resistivity radii are higher than that of 100Ω.m, which is the opposite effect than changing the depth. Making the radius 10 times smaller - Z(1Ω.m) - has the result of an apparent resistivity that is 10 times bigger.

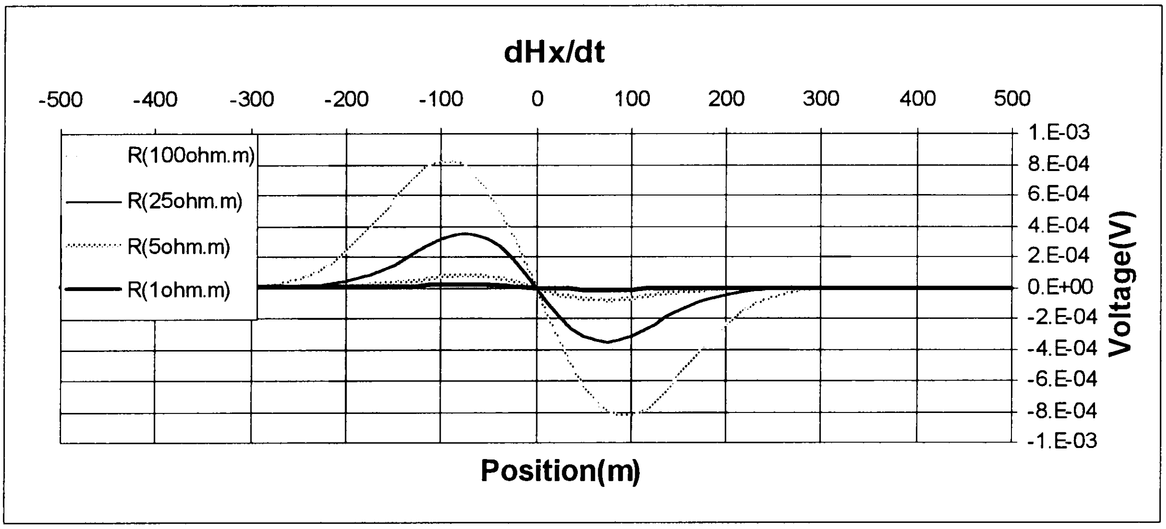

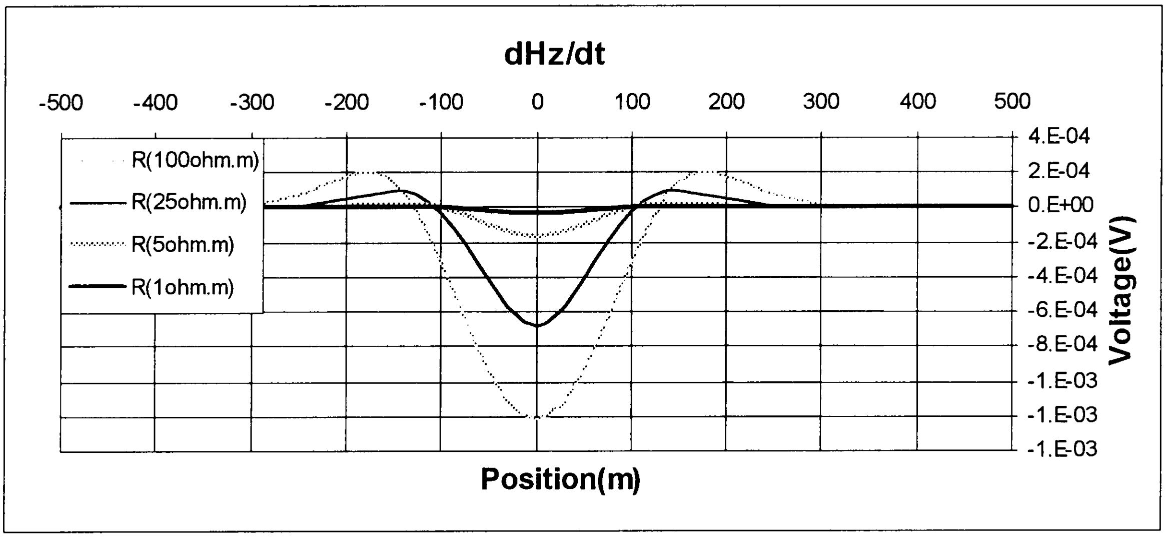

Figure 5.26 Profile plots for the indicated components and radius functions. The current and depth are kept as if for a 100Ωm earth.

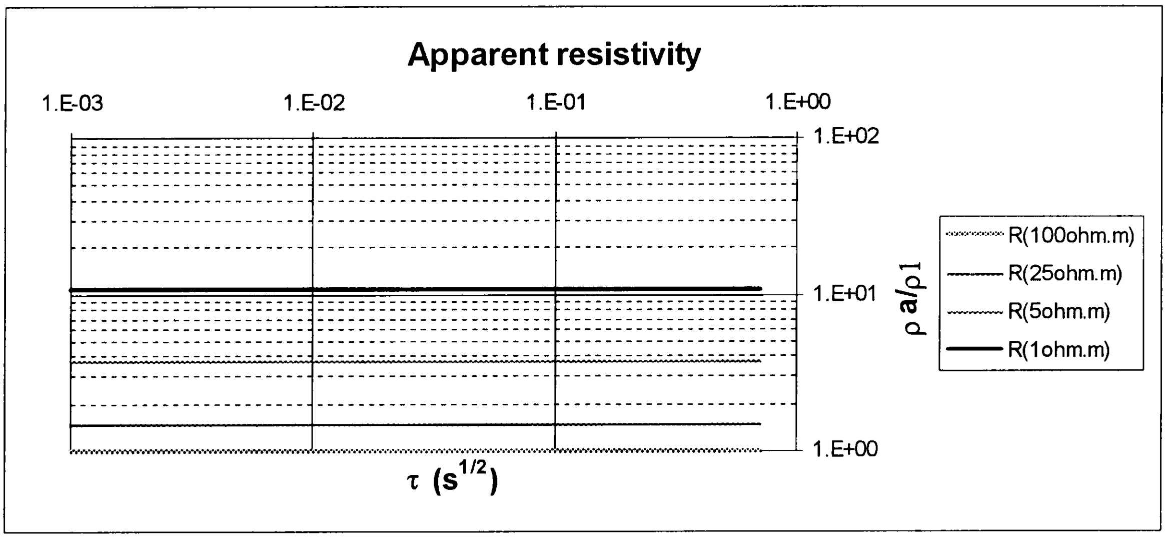

Figure 5.27 Apparent resistivity plots for different radius functions. The current and depth are kept as if for a 100Ωm earth.

5.4.2 Radii calculated for 100Ω.m and more

Making the radii bigger significantly changes the expected profile plots as shown in Figure 5.28. The responses of the sides of the loop are becoming separated from the total effect. Similar to changing the depth function, the apparent resistivities are significantly changed. For a resistivity contrast of 10:1 the resultant apparent resistivity contrast is 200:1. Thus, both changes of the radius resulted in higher apparent resistivity values.

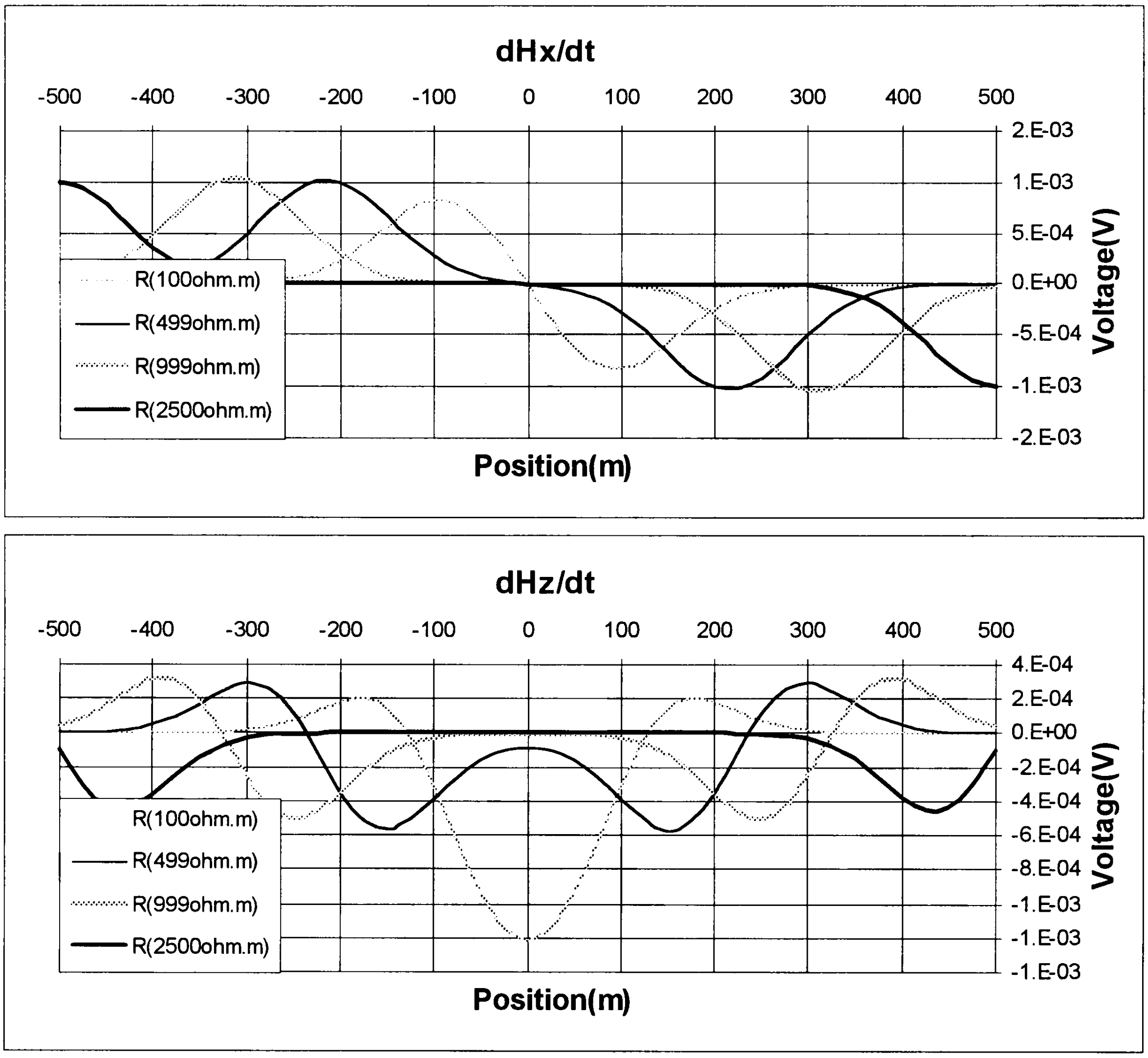

Figure 5.28 Profile plots for the indicated components and radius functions. The current and depth are kept as if for a 100Ωm earth.

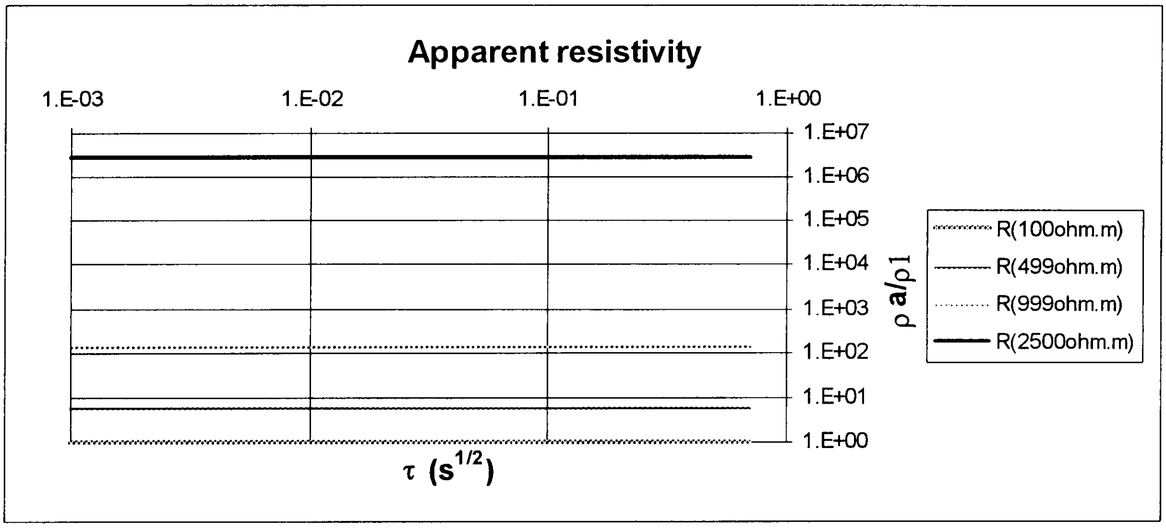

Figure 5.29 Apparent resistivity plots for different radius functions. The current and depth are kept as if for a 100Ωm earth.

5.5 SHIFTING A CURRENT FILAMENT HORIZONTALLY

A circular horizontal smoke ring for a 100Ω.m earth is shifted to the right as indicated in the legends of Figures 5.30 and 5.31. The process is then repeated for an ellipse elongated and compressed in the y-direction respectively.

The profile plots of Figure 5.30 show the x and z-components of the emf which are displaced horizontally. In the heading the entry b(100Ω.m) refers to length of the b-axis as shown in Figure 5.1. The a-axis is always calculated for ρ=100Ω.m. In this case it follows that the current filament is circular.

The apparent resistivity values in Figure 5.31 show no difference between each other at all, except for very early times when the steep slope of the z-component is close to 0m. But the downward and outward diffusion process happens so quickly that the distortions disappear for these small offsets. The sharp point for the 50m shift in Figure 5.31 is the result of a sign change of the z-component. The steep slope for the 25m shift is also the result of a sign change that happened just before $10^{-3}s^{1/2}$. Imagine recording at position -100m, for example. As the currents diffuse away the values at that position will change from positive to negative. If this happens for recorded values in the center of the loop, at position 0m, it is evident that a serious distortion of the traveling current filament has taken place, because a layered earth will always generate symmetrical fields where z values decay to zero in the center without a sign change.

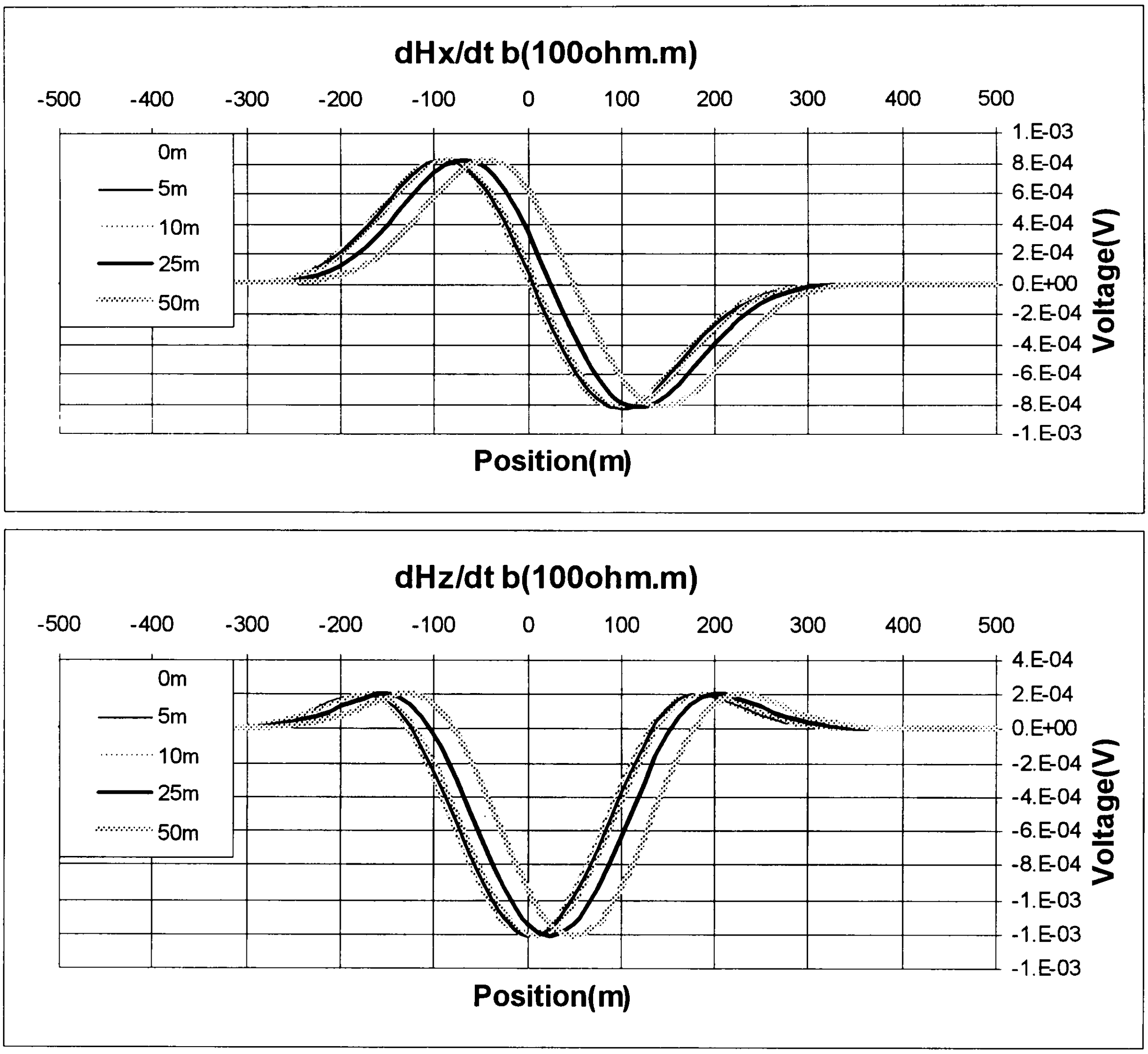

Figure 5.30 Profile plots for the indicated components, when a horizontal current filament is shifted to the right for the distances shown in the legend.

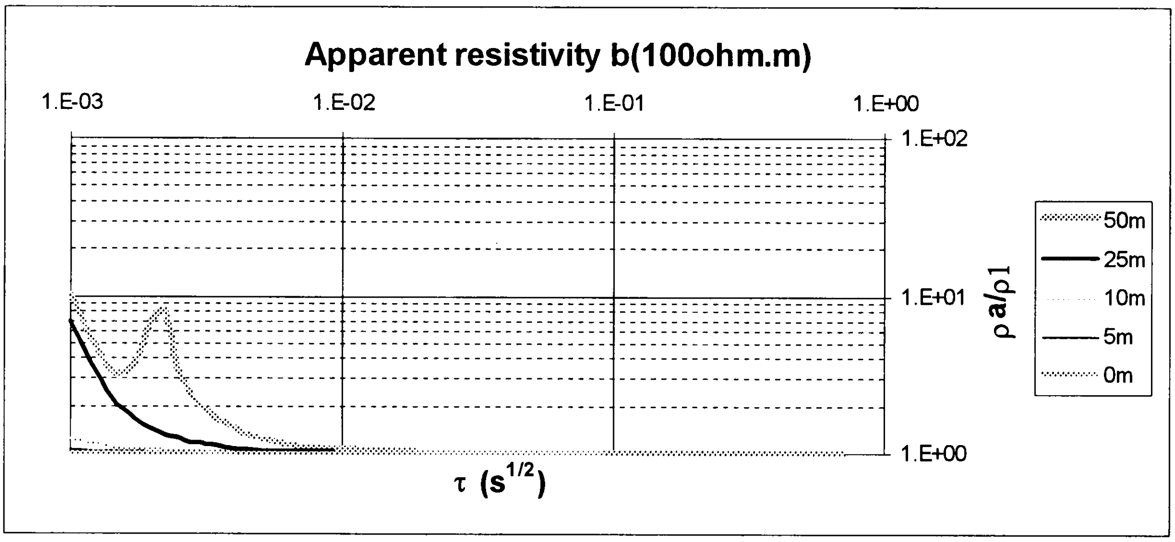

Figure 5.31 Apparent resistivity plots for the indicated b and shifted to the right for the distances shown in the legend. For a more complete explanation of b, see Figures 5.1 and 5.30.

5.5.1 Current filament compressed in the y-direction and shifted

Compressing the current filament and shifting it horizontally up to 50 m results in apparent resistivities shown in Figures 5.32 to 5.34. Except at very early times when the emf changes sign, the only change in apparent resistivity of that of 100Ω.m is because of the compression and not because of the horizontal shift. (Compare Figure 5.7)

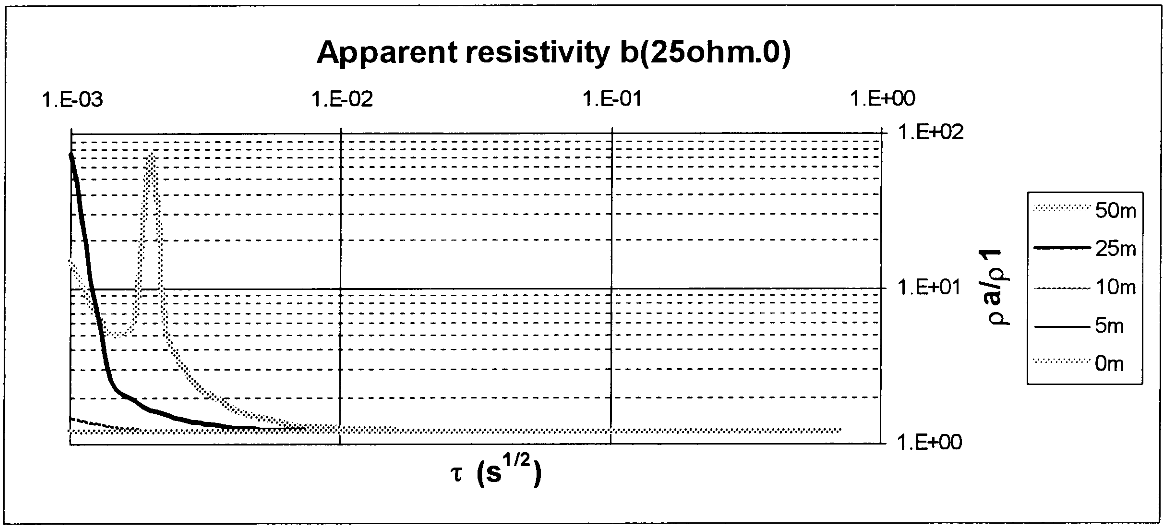

Figure 5.32 Apparent resistivity plots for the indicated b and shifted to the right for the distances shown in the legend.

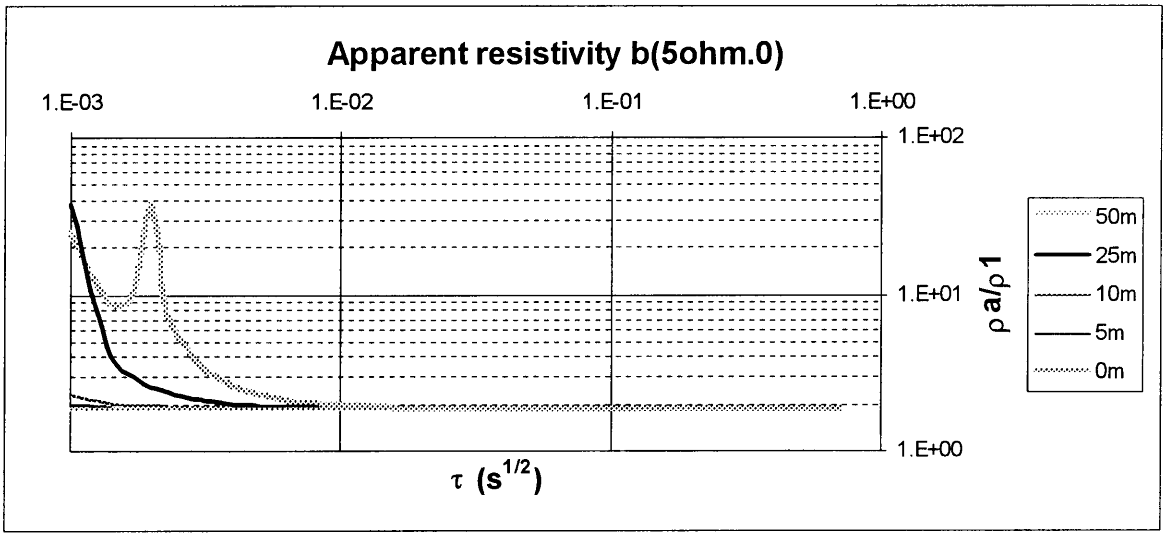

Figure 5.33 Apparent resistivity plots for the indicated b and shifted to the right for the distances shown in the legend.

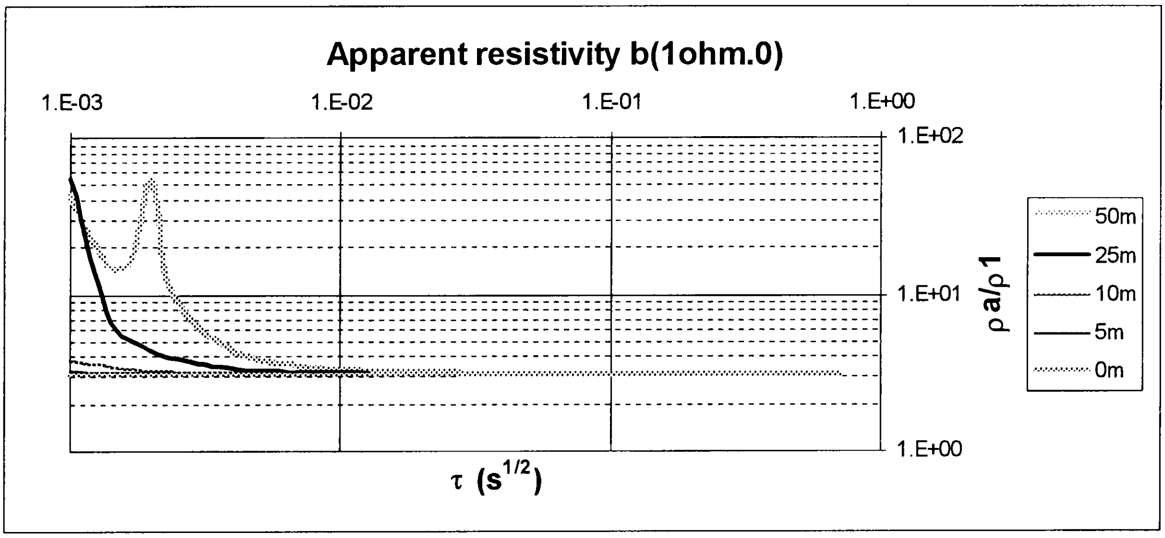

Figure 5.34 Apparent resistivity plots for the indicated b and shifted to the right for the distances shown in the legend.

5.5.2 Current filament elongated in the y-direction and shifted

Just like the previous section, the only change in apparent resistivity with that of 100Ω.m is because of the elongation and not the shift. (Compare Figure 5.14.) At very early times there is an irregular anomaly which forms a sharp upward curve for a horizontal shift of 25m and 50m when the emf changes sign.

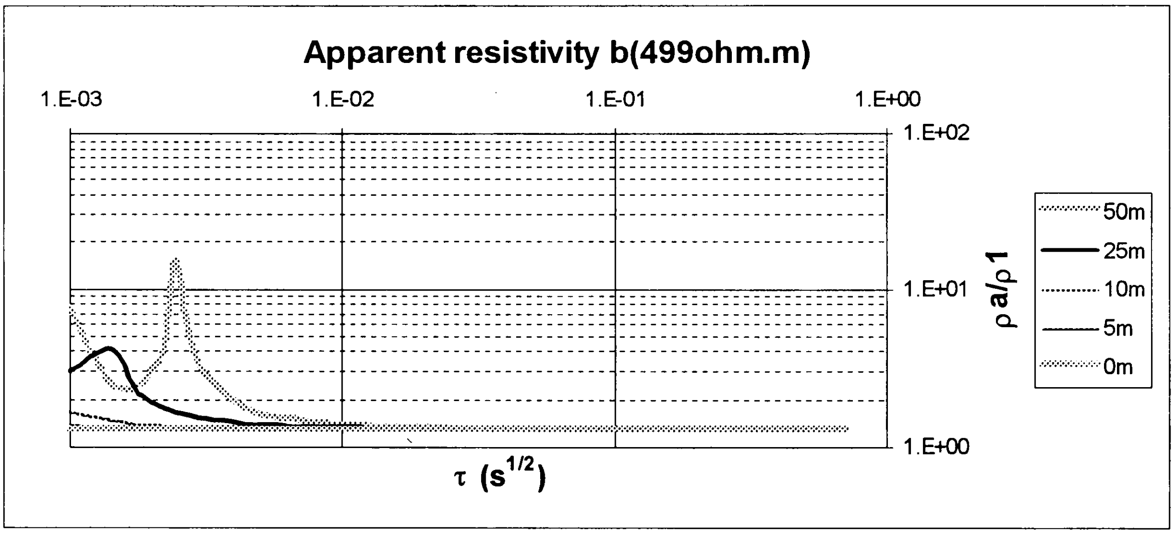

Figure 5.35 Apparent resistivity plots for the indicated b and shifted to the right for the distances shown in the legend.

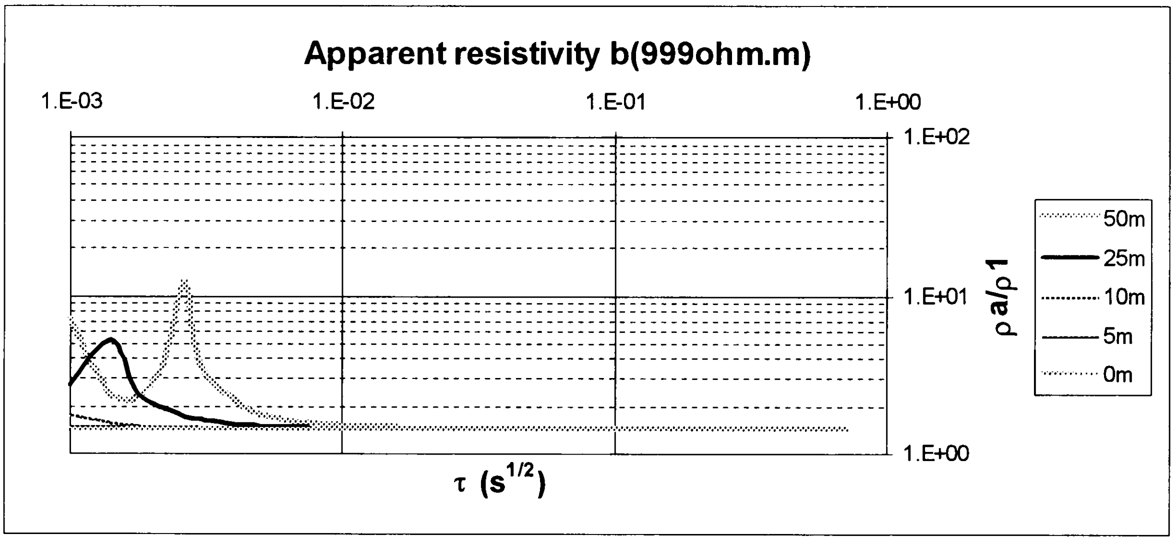

Figure 5.36 Apparent resistivity plots for the indicated b and shifted to the right for the distances shown in the legend.

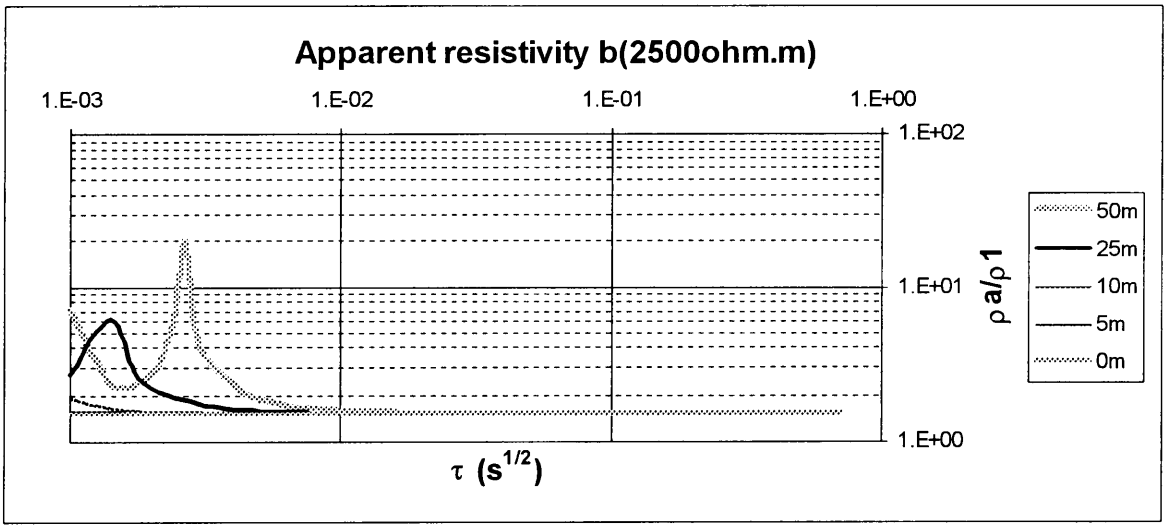

Figure 5.37 Apparent resistivity plots for the indicated b and shifted to the right for the distances shown in the legend.

5.6 VERTICAL BOUNDARY FROM A LOW TO HIGHER RESISTIVITY

After investigating possible changes of the different components of moving current filaments, this section is an attempt to approximate a physical situation of a vertical geo-electrical boundary shown in Figure 5.38. The vertical magnetic dipole is situated at some distance away from the boundary. First of all the current filament will move outwards and downwards as a horizontal circle, until it touches the contact when some deformation, horizontal and vertical shifting and tilting will take place. Two situations will be considered: 1) A boundary with a higher resistivity (discussed in this section) and 2) A boundary with a lower resistivity (discussed in the next section).

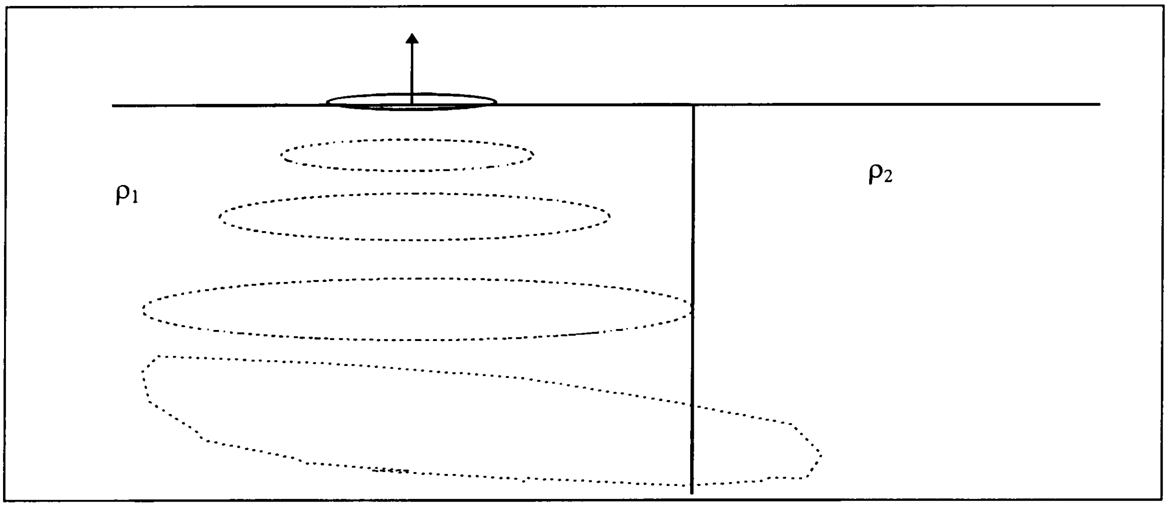

Figure 5.38 Physical model of vertical geo-electrical boundary with the vertical magnetic dipole situated at some distance away from the contact. At some time the horizontal circular current is distorted by the contact.

Consider a vertical boundary with a higher resistivity. The question is what the effect will be on a horizontal circular filament of current. When the filament touches the boundary it will start to move faster outward and downward in that region, with a lower current. So the filament will deform, becoming longer in a direction perpendicular to the contact as seen in Figure 5.39.

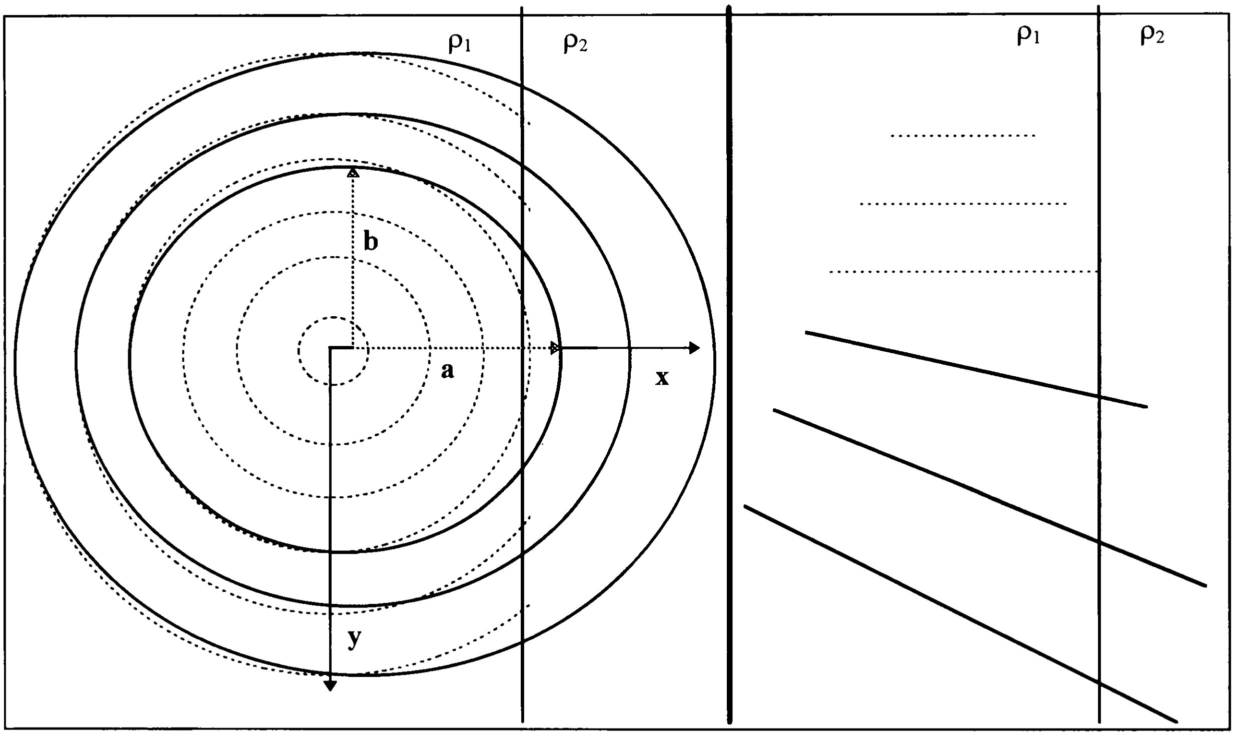

Figure 5.39 Possible model for deformed current filament tilted towards the higher resistivity ρ_2.

A possible approximation for this situation is an ellipse shifted and tilted towards the boundary shown in Figure 5.39, with **b** the axis calculated as the radius for ρ_1 and **a** the calculated radius of some weighted average function $\Sigma(\rho_1,\rho_2)$. The dotted lines depict a system of circular horizontal current rings before it touches the contact. The boundary conditions of eq 2-14 to 2-17 are not taken into account. The current and depth of this ellipse is also calculated for a resistivity $\Sigma(\rho_1,\rho_2)$. Apparent resistivity plots for various tilts are calculated. Two aspects remain to be considered and those are the horizontal shift and what the weighted average function should be.

Because this is a qualitative model any arbitrary weighted function should be satisfactory. For example:

$$\Sigma(\rho_1,\rho_2)=\frac{g}{s}\rho_1+\frac{h}{s}\rho_2 \tag{5-4}$$

where $g+h=s$, to determine if there will be a sufficient difference in apparent resistivities to detect a vertical boundary and if there is a characteristic response for this specific situation. For the results shown, s was chosen to be 11 and different values were assigned to g and h.

Keeping in mind the results of section 5.5 for a circular horizontal current filament, where a horizontal shift resulted in either no change of the apparent resistivity at later times, or serious distortion (because of a sign change) of the values in time, the horizontal shift of a deformed tilted ellipse was done for 25m and 50m. Figure 5.40 shows the apparent resistivity plots for a circular current filament in a 100Ω.m earth, shifted 25m to the right.

At very late times the values are the same as for an unshifted tilted circular filament (compare Figure 5.3), but significant distortions occur for tilts of pi/6 and pi/4. Moving the point of observation 50m to the left (Figure 5.41) produces even bigger distortions for the last two tilts and at later times, but eventually the values conform to those of Figure 5.3. The sharp curves in both graphs indicate a sign change in the emf. In Figures 5.42 and 5.43 the apparent resistivity plots for deformed horizontal current rings are displayed. The a-axis of the current ellipse was calculated using the resistivity values shown in the legends. These values are generated using eq 5-4 and g and h assigned the values 9 and 2, respectively, and for the following resistivities: ρ_2=100, 500, 1000, 2500. The 25m in the title refers to the amount of horizontal shift of the current filament to the right.

For a(100Ω.m) the shifted horizontal filament is a circle and the apparent resistivity values are not distorted. For the 25m shift in Figure 5.42, the values for the distorted rings level out very quickly. In Figure 5.43 it can be seen that this process happens at a later stage, even though it is still less than 0.0001s. Taking into account that for example the Geonics EM-37 only starts recording at $0.089*10^{-3}$s, a shift up to 50m should not be too serious for that instrument.

Obviously more radical horizontal shifts of a current filament will distort the apparent resistivity values even more, but this will certainly be noticed as not being the response of a symmetrical earth. It is again evident that the horizontal shift does not change the apparent resistivity, as previously shown in section 5.5. Its effect is either insignificant, or a significant peak is generated if the measured emf changes sign.

Assuming a horisontal shift of the current filament due to the horisontal change in resistivity, the rest of the apparent resistivities were calculated for a shift of 25m to the right.

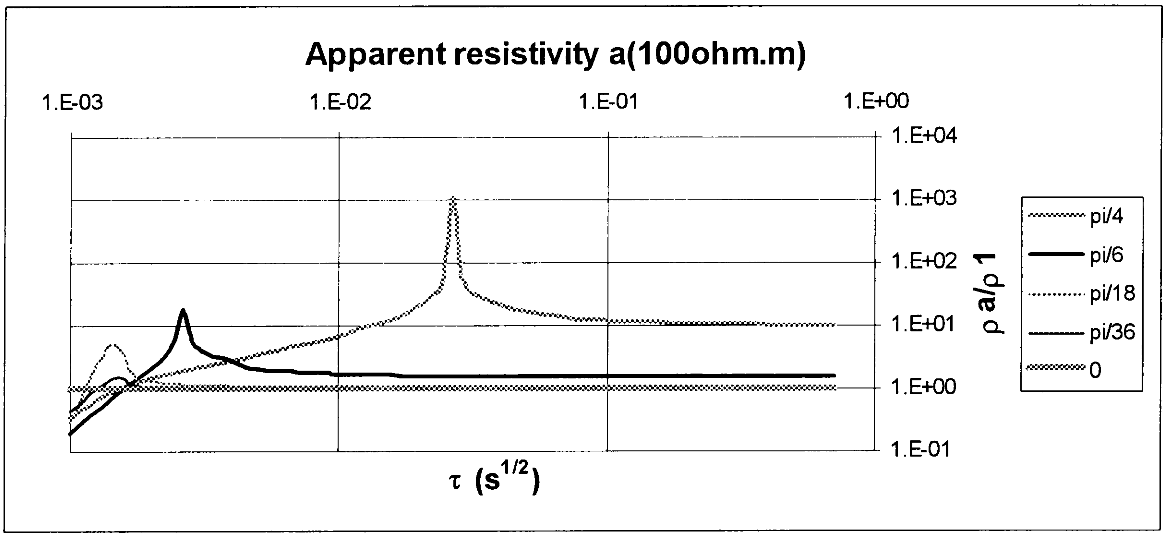

Figure 5.40 Apparent resistivity plots for a circular current filament in a 100Ωm earth, shifted 25m to the right and tilted from x to z for angles displayed in the legend.

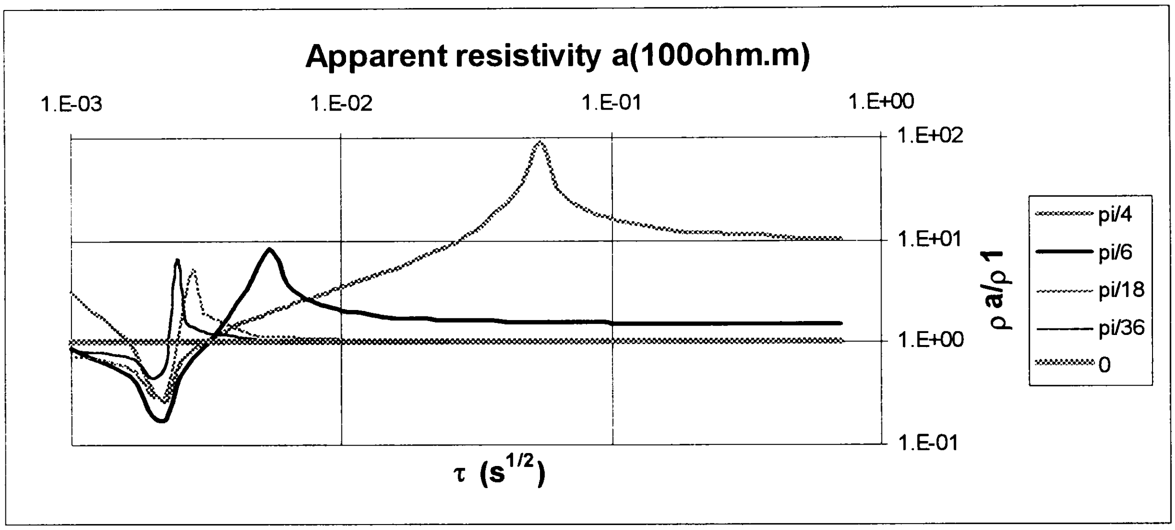

Figure 5.41 Apparent resistivity plots for a circular current filament in a 100Ωm earth, shifted 50m to the right and tilted from x to z for angles displayed in the legend.

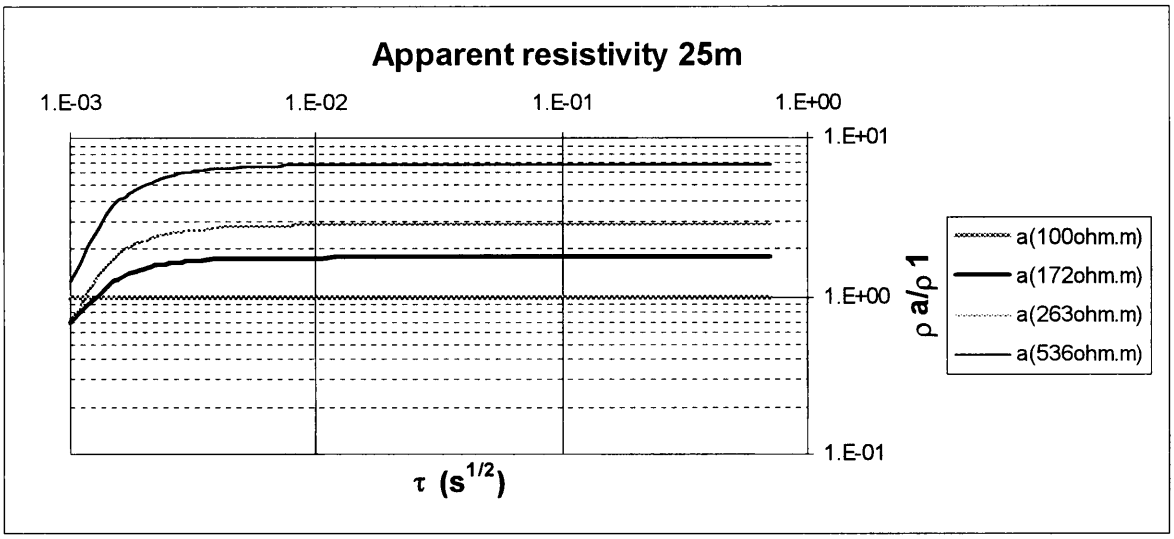

Figure 5.42 Apparent resistivity plots for a horizontal deformed current filament.

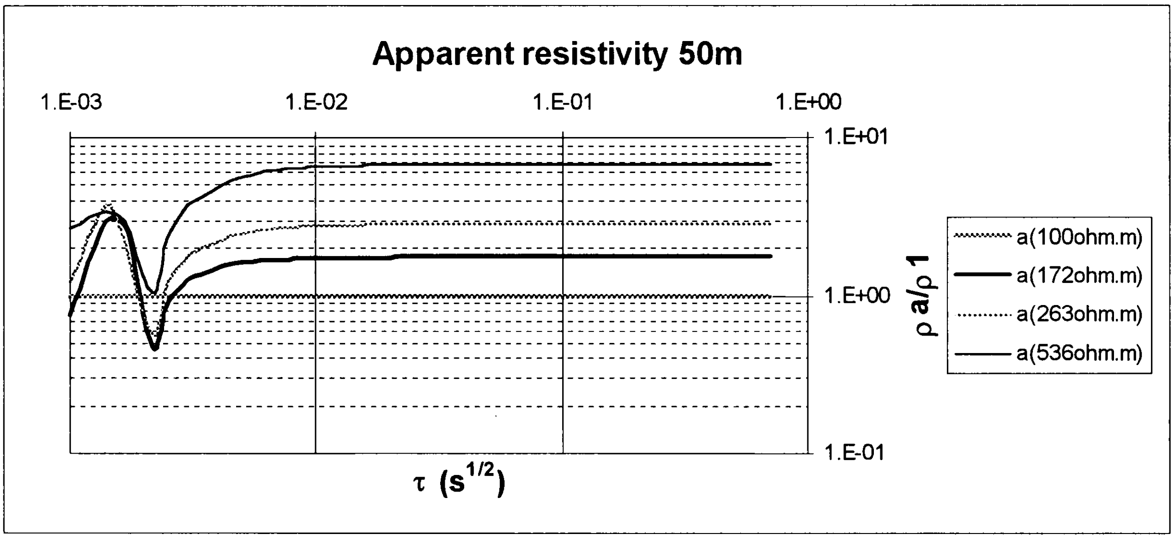

Figure 5.43 Apparent resistivity plots for a horizontal deformed current filament. The 50m in the title refers to the amount of horizontal shift of the current filament to the right.

5.6.1 Apparent resistivities for g=9, h=2

Figures 5.42 and 5.44 to 5.46 display the calculated apparent resistivities for a deformed tilted current filament that is shifted 25m to the right. The deformation is calculated for the a-axis in Figure 5.39 using the resistivities in the legend of Figure 5.42. These resistivities were calculated with eq 5-4 and g=9, h=2. The only reason for the specific values is that it is needed for the calculation of the fields. So these relations are only guidelines to aid in the process of understanding the physical phenomena by developing a qualitative model. Because the vertical magnetic dipole is situated away from the contact, there will be at some time be some influence on the propagation of the current filament. These influences are modeled by increasing the chosen ratios in eq 5-4 to determine what their effects are.

In Figure 5.42 the apparent resistivity values calculated using the described model and the resistivities in the legend, result in slightly higher ratios with 100Ω.m as it would have been for a horizontally layered earth with the legend resistivities. This probably happens because of the deformation of the current filament as was found in section 5.1, which results in higher apparent resistivity values.

In Figures 5. 44 to 5.46 deformation is achieved by calculating the a-axis of the ellipse for the resistivity shown in the title. The tilts from x to z are listed in the legend. Tilting these distorted current filaments gives a similar result as tilting a circular current filament, compare Figures 5.8 to 5.10 and 5.15 to 5.17. For the first two tilt angles (pi/36 and pi/18) there is an insignificant change in the untilted value. For bigger tilts a higher apparent resistivity value is found. This is the case for all three deformations.

Sharp curves coincide with sign changes in the emf.

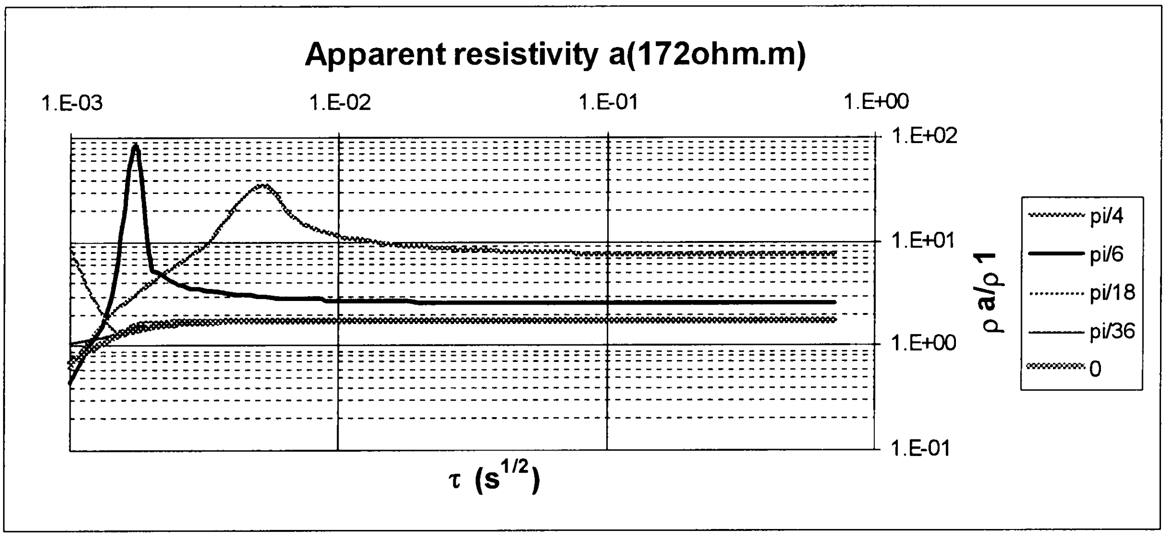

Figure 5.44 Apparent resistivity plots for a deformed tilted current filament.

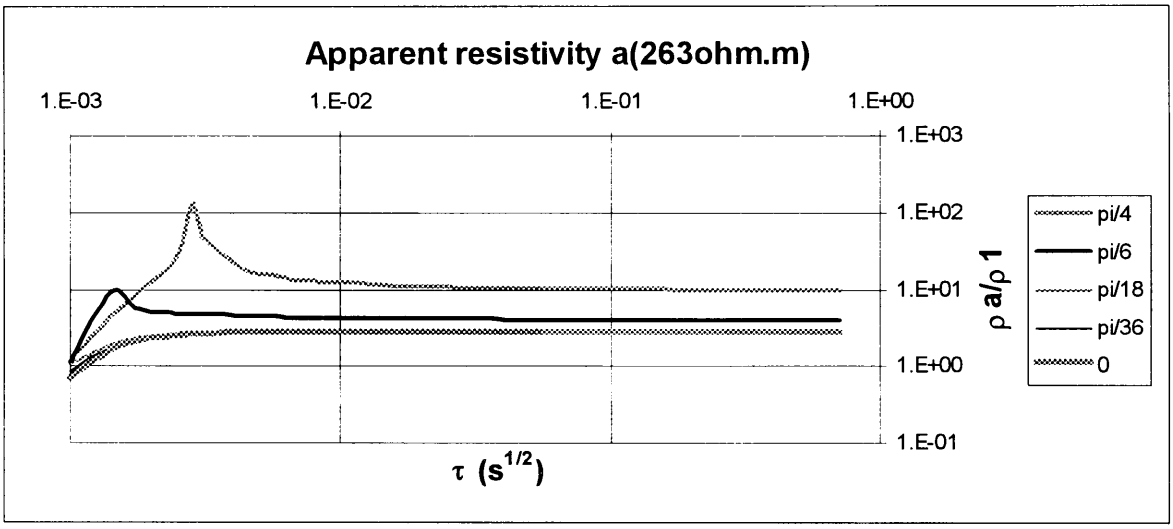

Figure 5.45 Apparent resistivity plots for a deformed tilted current filament.

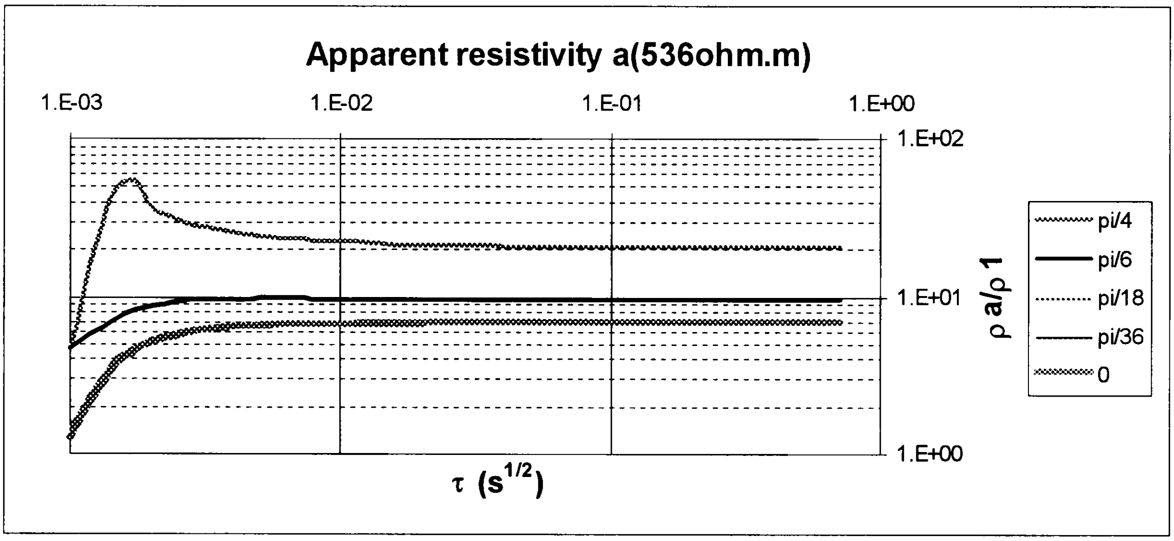

Figure 5.46 Apparent resistivity plots for a deformed tilted current filament.

5.6.2 Apparent resistivities for g=7, h=4

Increasing the effect of the resistivities of the second region is done by choosing g=7 and h=4. The calculated resistivities are listed in the legend of Figure 5.47. Deformation is achieved by calculating the a-axis of the ellipse for the resistivities shown in the legend, while the b-axis is for 100Ω.m. The current filament is shifted 25m to the right. Again the resultant apparent resistivity values for the horizontal deformed rings are slightly higher than those of the weighted average resistivity.

In Figures 5.48 to 5.50 the results of tilting the deformed shifted current filament show the same trend as before, where the first two tilts have little effect. It becomes more significant for the last two.

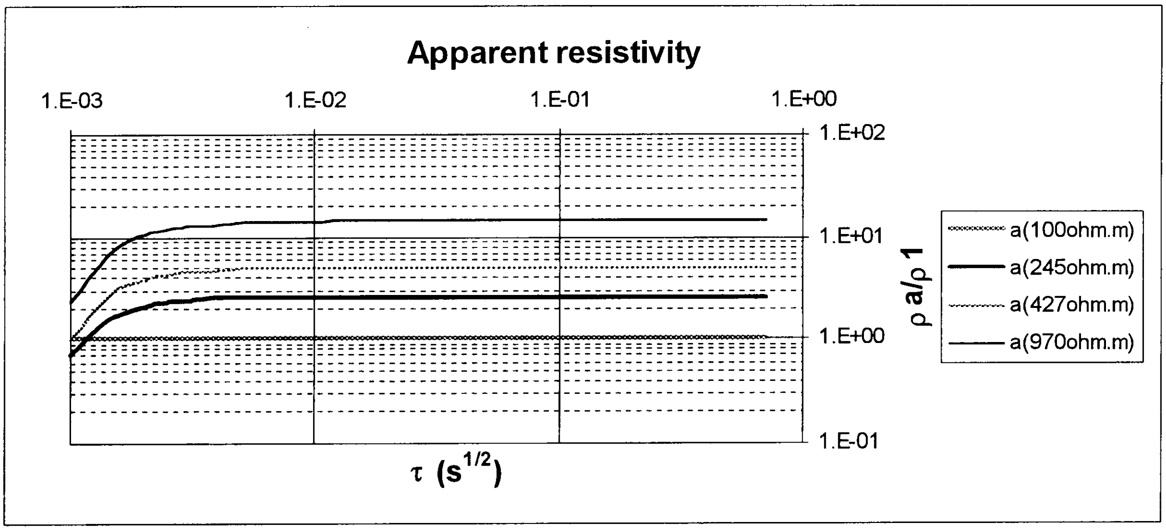

Figure 5.47 Apparent resistivity plots for a deformed and shifted horizontal current filament.

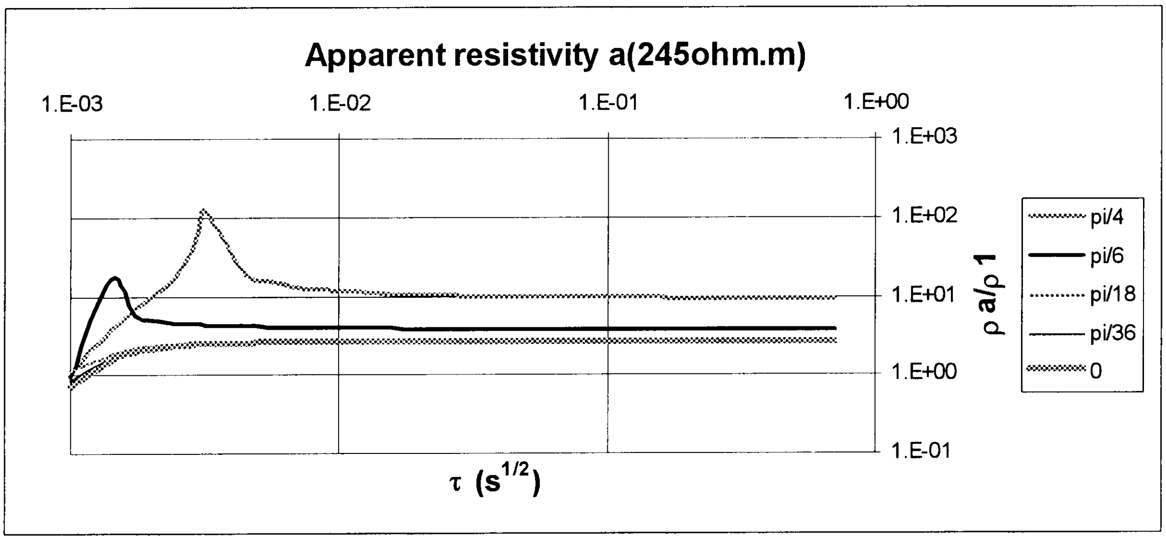

Figure 5.48 Apparent resistivity plots for a deformed, tilted and shifted current filament.

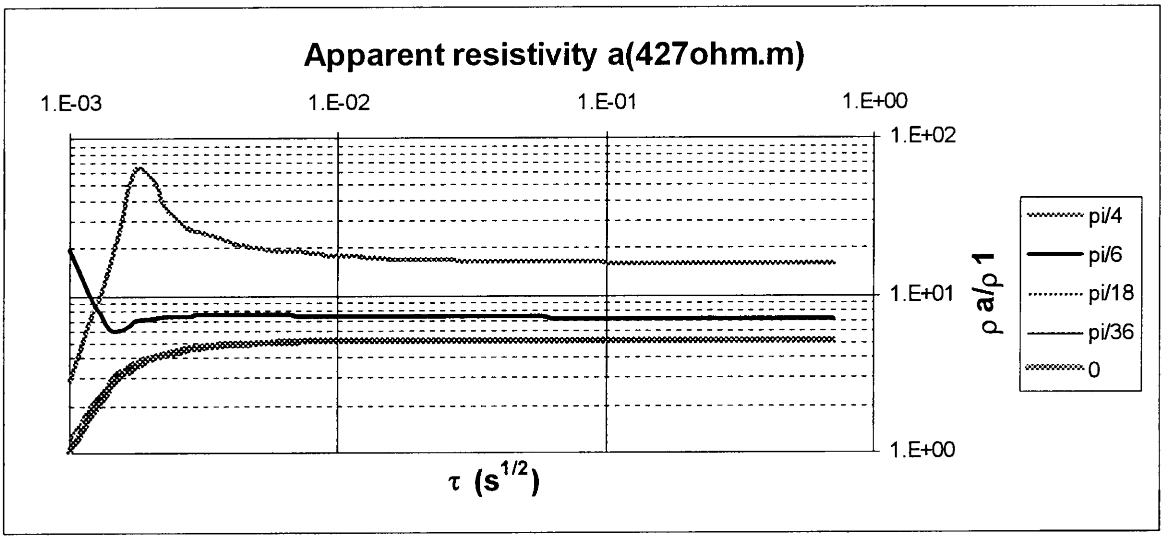

Figure 5.49 Apparent resistivity plots for a deformed, tilted and shifted current filament.

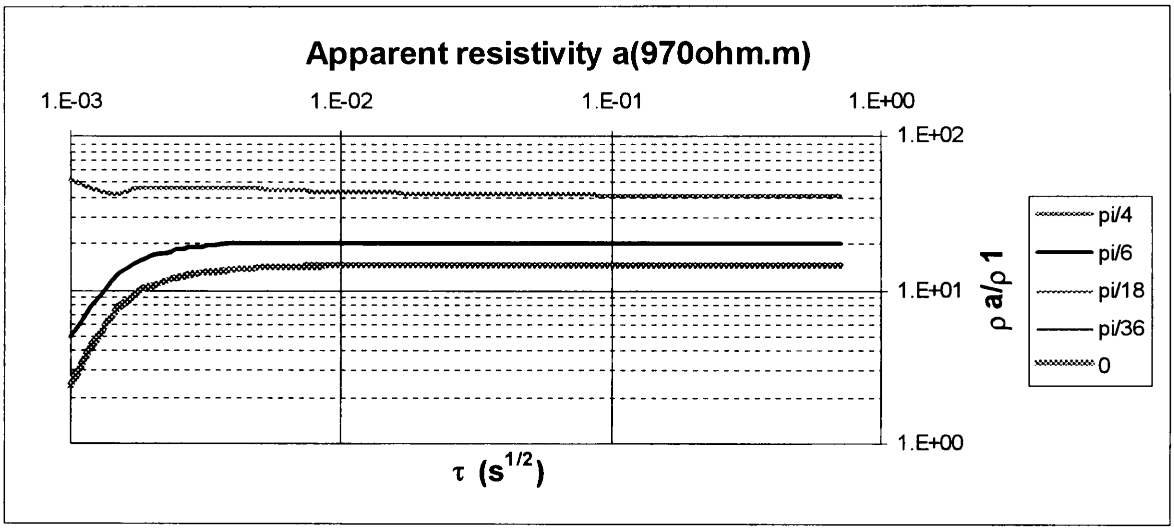

Figure 5.50 Apparent resistivity plots for a deformed, tilted and shifted current filament.

5.6.3 Apparent resistivities for g=5, h=6

Increasing the effect of the resistivity of the second region even more results in resistivities listed in the legend of Figure 5.51. Again the apparent resistivities for the horizontal filament are slightly higher than those of the legend, except for a(1408Ω.m) where the apparent resistivity value is slightly less. Nonetheless, all these 'apparent resistivities' are very close to the 'chosen' resistivity value.

Tilting the deformed filament yields exactly the same results as before as can be seen in Figures 5.52 to 5.54.

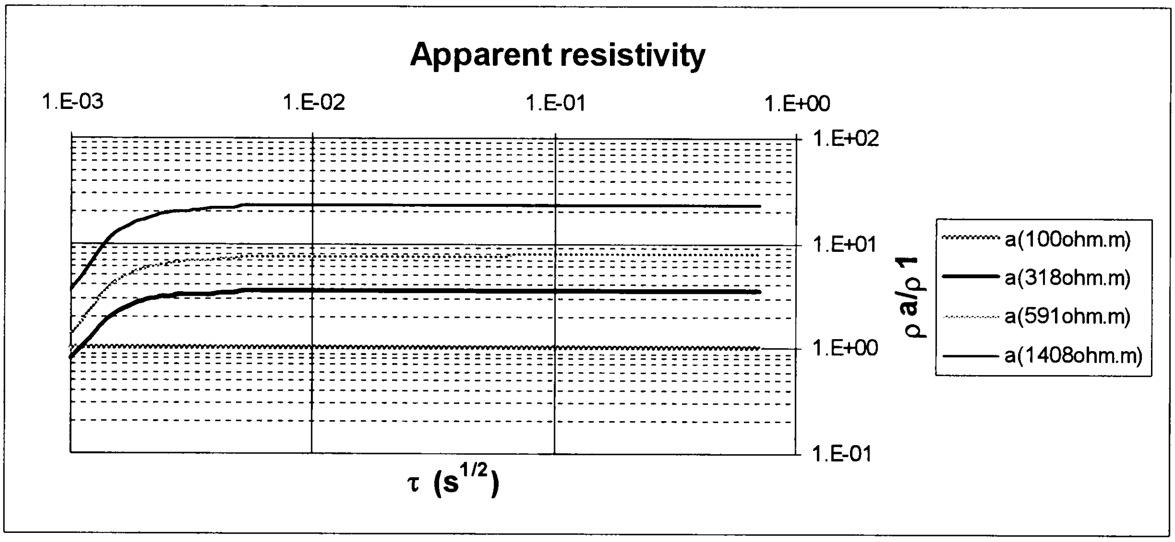

Figure 5.51 Apparent resistivity plots for a deformed and shifted horizontal current filament

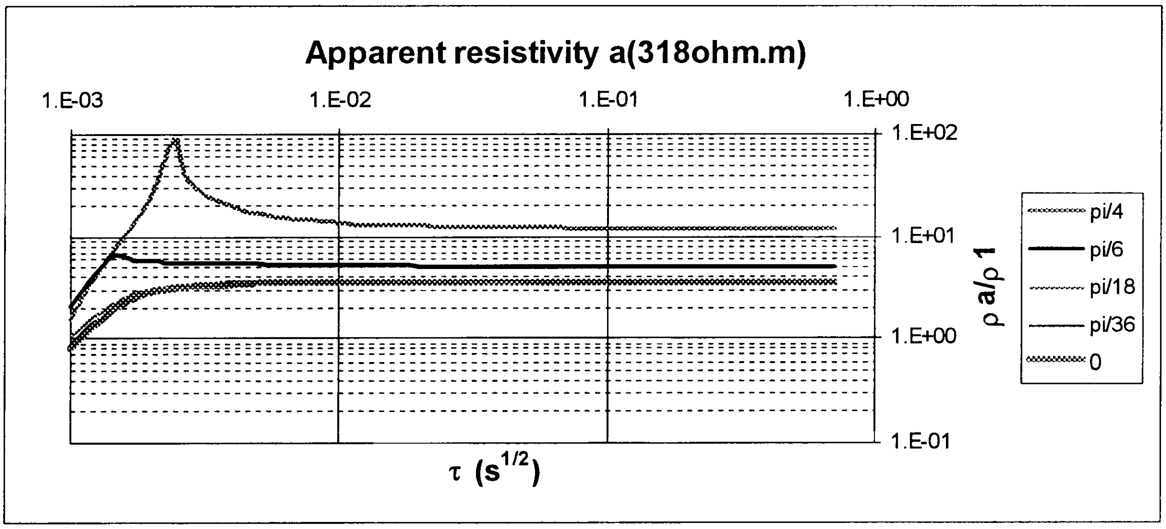

Figure 5.52 Apparent resistivity plots for a deformed, tilted and shifted current filament.

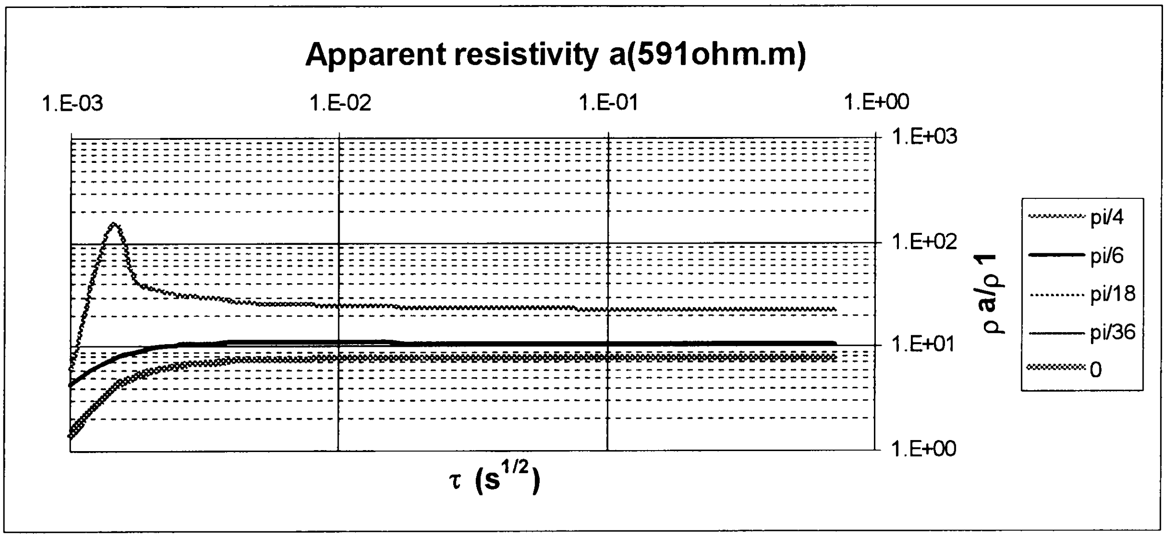

Figure 5.53 Apparent resistivity plots for a deformed, tilted and shifted current filament.

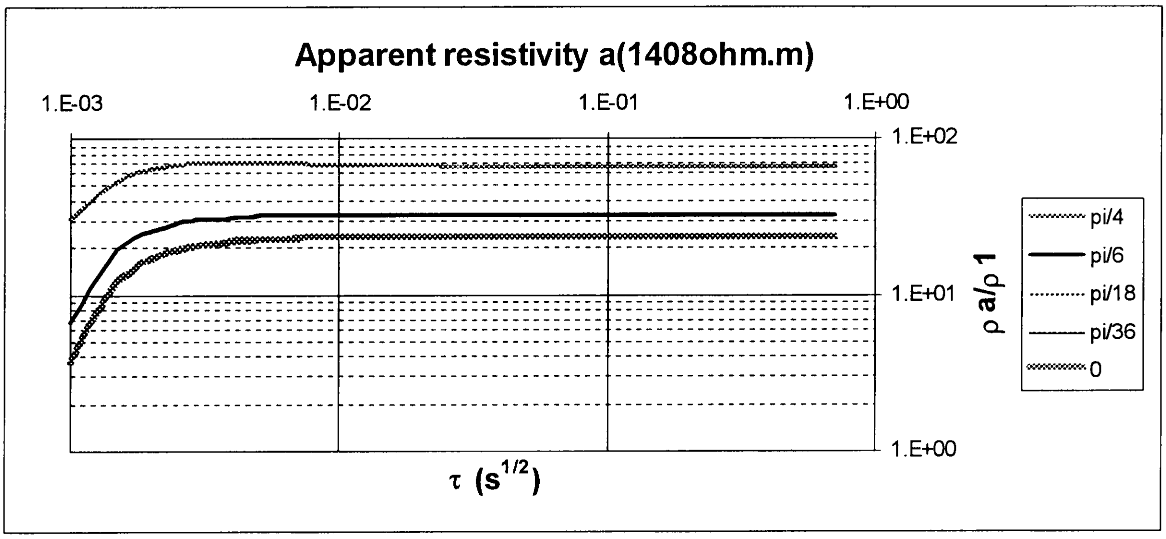

Figure 5.54 Apparent resistivity plots for a deformed, tilted and shifted current filament.

5.7 VERTICAL BOUNDARY FROM A HIGH TO LOW RESISTIVITY

Consider the effect of a vertical boundary with a lower resistivity on a travelling horizontal current filament. When the filament touches the contact it will start to move slower outwards and downwards in that region. The filament will then be tilted away from the boundary as shown in Figure 5.55 where the dotted lines depict a system of circular horizontal current rings before it touches the contact. On the left is a plan view and on the right a section. The b-axis will change as if for a 100Ω.m earth and the a-axis to the right will grow slower for some weighted average function. Because this is an approximation, the whole current filament is chosen to be an ellipse with axes **a** and **b**. This ellipse is moved to the left and tilted from the negative x-axis to the z-axis, which points into the page. The lower resistivities are ρ_2=100, 25, 5, 1 and are again used with eq 5-4 to calculate a(ρΩ.m). These lower resistivities will have the effect of a shallower current filament with more current flowing in it, than for the 100Ω.m earth. The shift is again 25m, but this time to the left. It has a more pronounced effect through time, because the lower resistivities cause a slower diffusion process.

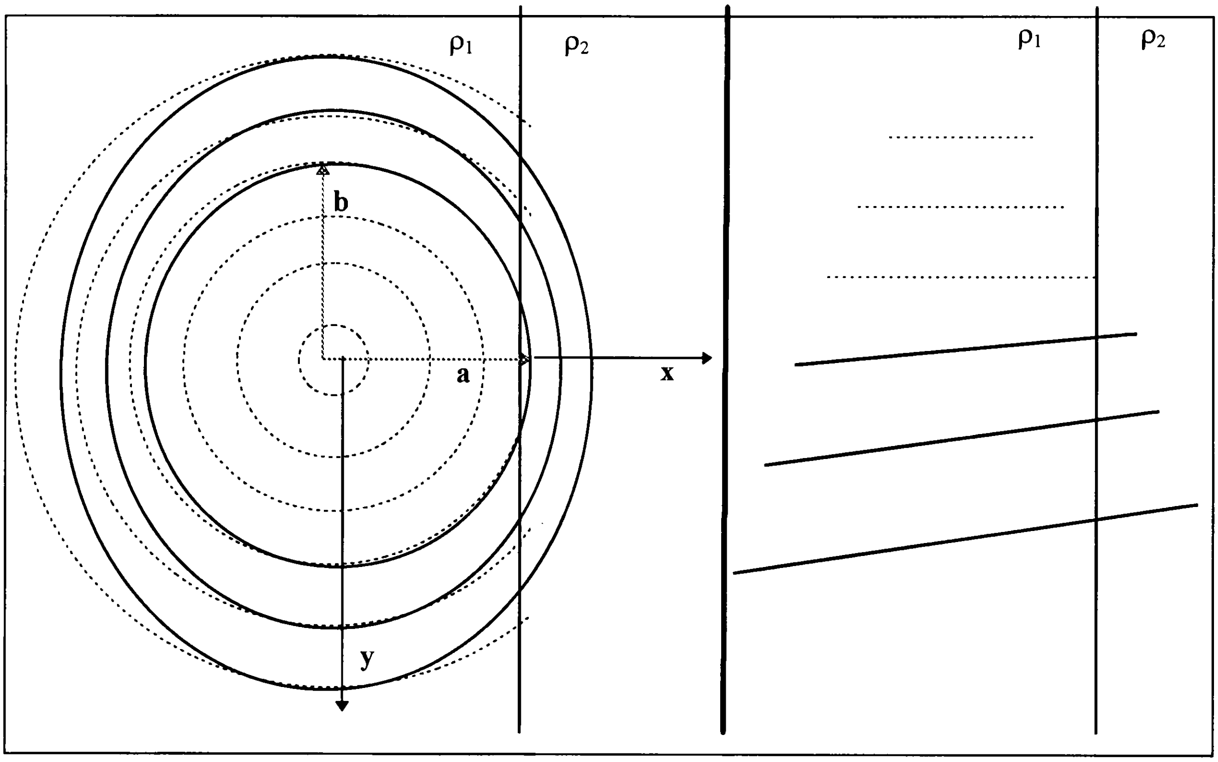

Figure 5.55 Possible model for deformed current filament tilted away from the lower resistivity ρ_2.

5.7.1 Apparent resistivities for g=9, h=2

In Figure 5.56 the resistivities calculated for g=9 and h=2 using eq 5-4 can be seen. Deformation of the ellipse is achieved by calculating the a-axis for the resistivities shown in the legend,while the b-axis is for 100Ω.m. The current filament is shifted 25m to the left.

Even though the ratio between 100Ω.m and 1Ω.m is 100, the resultant resistivity is only 0.81 of 100Ω.m. For the opposite situation in section 5.6.1, the ratio between 100Ω.m and 2500Ω.m was 25 and the resultant resistivity was 500Ω.m. There is thus a distinct difference between crossing over a higher or a lower resistivity boundary.

The fact that the resistivities calculated using eq 5-4 are so close to the value of 100Ω.m manifests in the calculated apparent resistivity values as shown in Figure 5.56. There is an insignificant difference between the plotted values. Even if it were a layered earth situation, the contrast would not have been enough to distinguish between different values.

For the filament shown in Figures 5.57, tilted from the negative x to the z-axis, the apparent resistivity values exhibit sharp edges indicating a sign change, except for the pi/4 tilt which only changes after 1s. The reason for this is that the horizontal shift has a more pronounced effect because the decaying process takes longer for lower resistivities, meaning that these times correspond to the earlier part of the previous section's data. Otherwise tilting seems to have the same effect where a higher apparent resistivity is found for a tilt of pi/6. At very late times the apparent resistivity of the tilt of pi/4 levels out in Figures 5.58 and it is higher as the one for pi/6, as seen previously. The tilts for a(81Ω.m) are not shown, because they are almost exactly the same as in Figure 5.58 where a(83Ω.m).

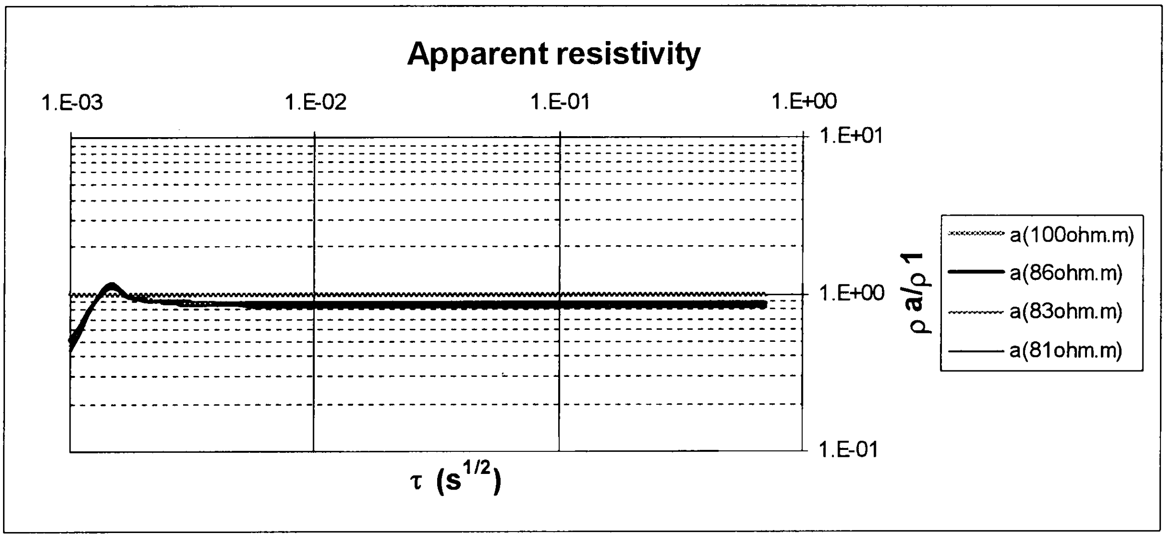

Figure 5.56 Apparent resistivity plots for a deformed and shifted horizontal current filament.

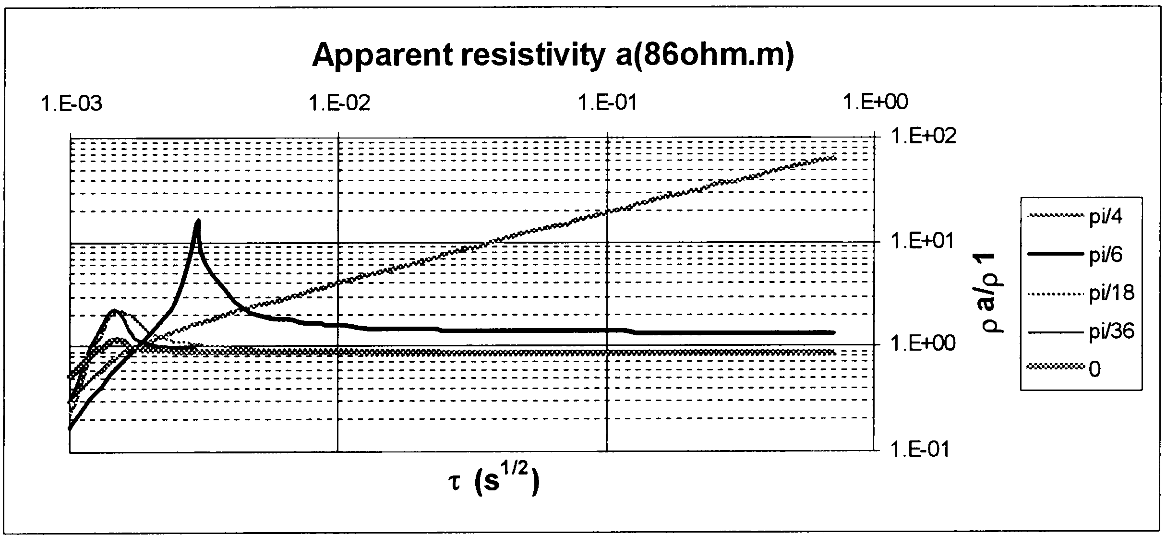

Figure 5.57 Apparent resistivity plots for a deformed, tilted and shifted current filament.

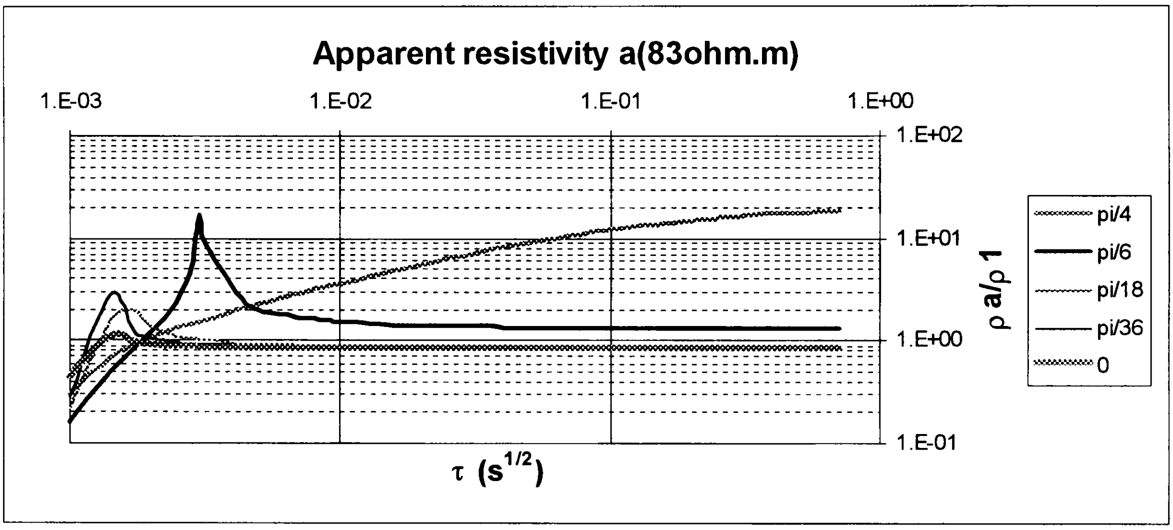

Figure 5.58 Apparent resistivity plots for a deformed, tilted and shifted current filament.

5.7.2 Apparent resistivities for g=7, h=4

Increasing the influence of the lower resistivity boundary still has very little effect and results in very low apparent resistivity contrasts as seen in Figure 5.59. Tilting these deformed rings has the same effect as before, where the tilts for pi/4 and pi/6 have much higher apparent resistivities when they stabilize as shown in Figures 5.60 to 5.61. Note that the pi/6 tilt produces apparent resistivity values which are the same as for a 100Ω.m half-space. The tilt for pi/4 does not change sign like the rest.

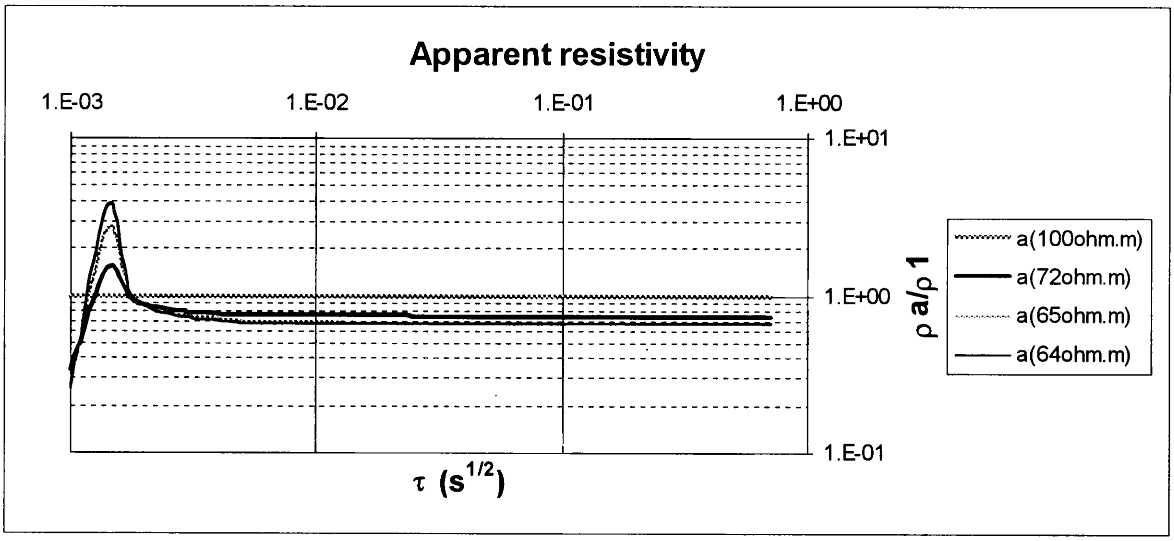

Figure 5.59 Apparent resistivity plots for a deformed and shifted horizontal current filament.

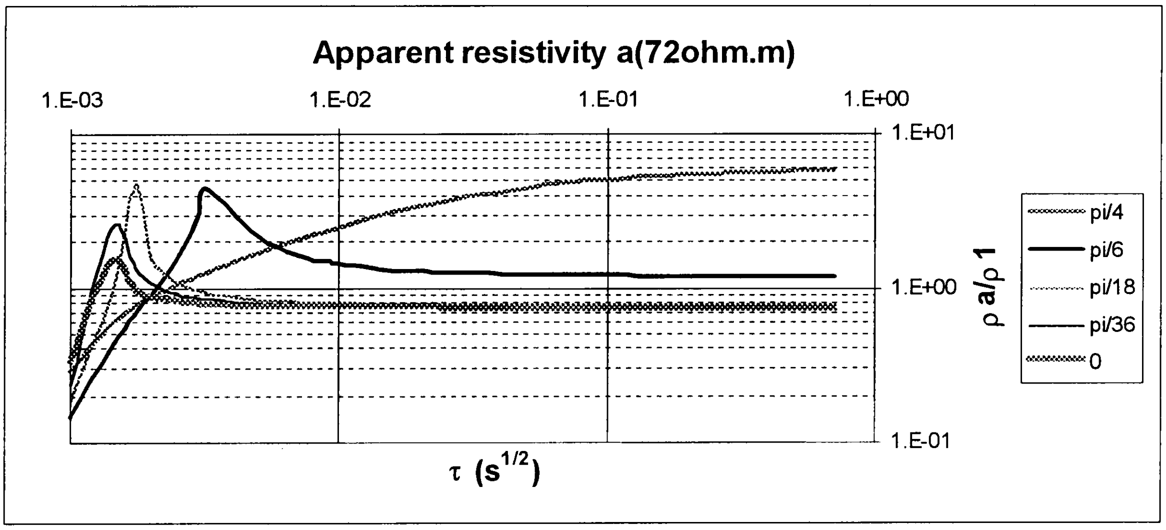

Figure 5.60 Apparent resistivity plots for a deformed, tilted and shifted current filament.

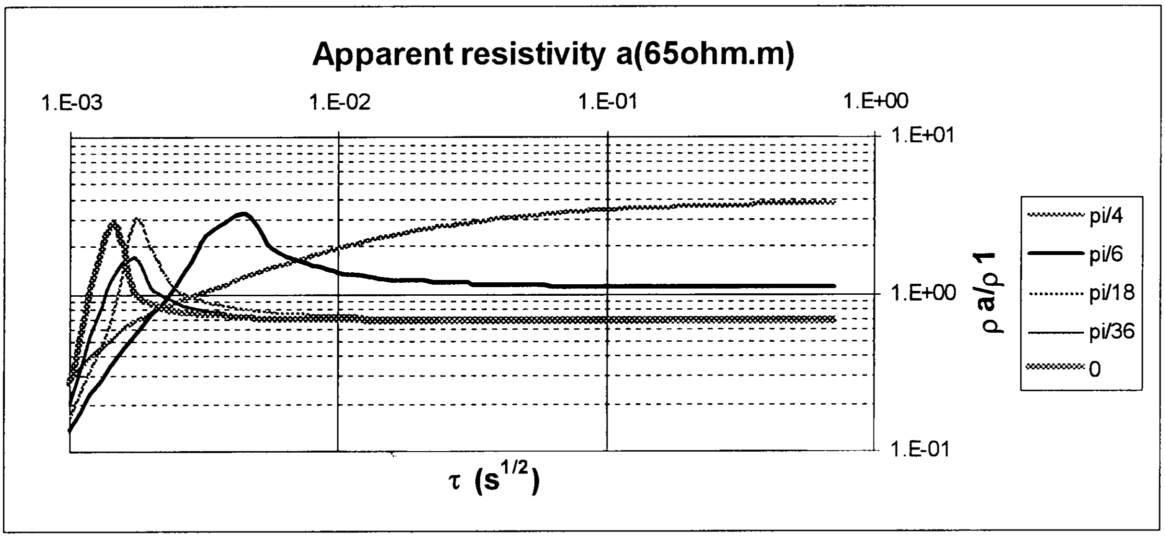

Figure 5.61 Apparent resistivity plots for a deformed tilted current filament.

5.7.3 Apparent resistivities for g=5, h=6

Increasing the effect of the lower resistivity to more than half for the composite resistivity, results in apparent resistivity contrasts which might be significant as shown in Figure 5.62. It can be seen that the apparent resistivity values for the horizontal deformed rings are slightly higher than the indicated resistivities in the legend. Again this is probably the effect of changing the shape of the filament.

The effect on the apparent resistivities of the tilted deformed rings is shown in Figures 5.63 and 5.64. Again the bigger tilts produce noticeably higher values. The pi/4 tilt does not change sign and the pi/6 tilt results in almost the same values as for a half-space of 100Ω.m.

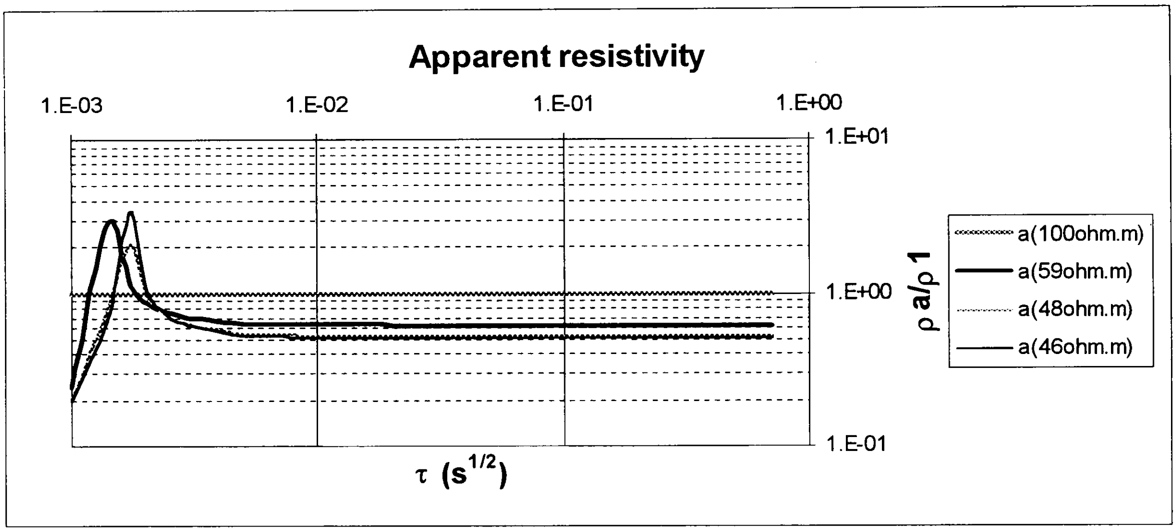

Figure 5.62 Apparent resistivity plots for a deformed and shifted horizontal current filament.

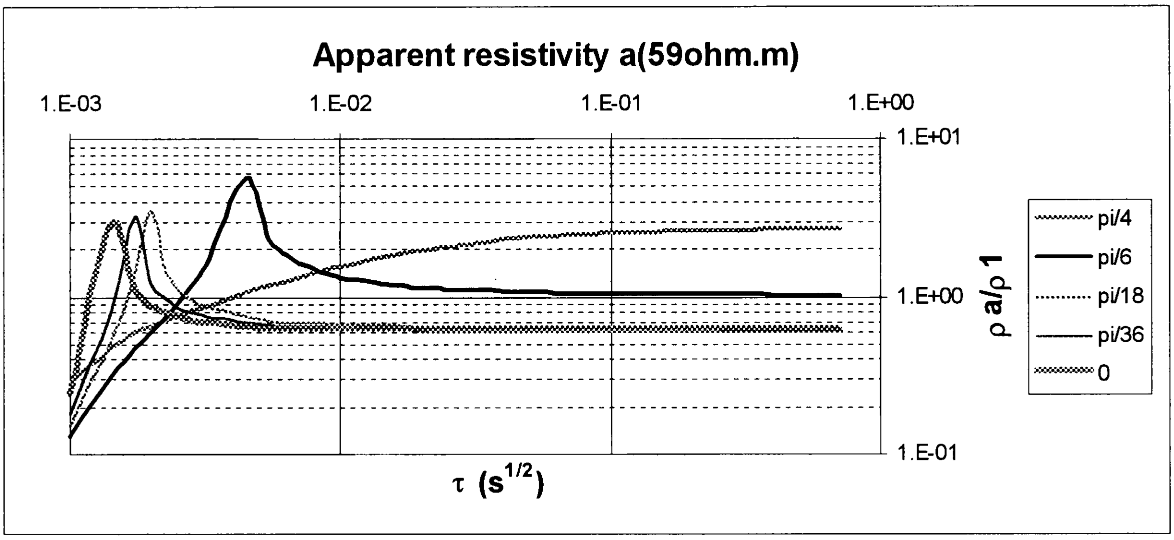

Figure 5.63 Apparent resistivity plots for a deformed, tilted and shifted current filament.

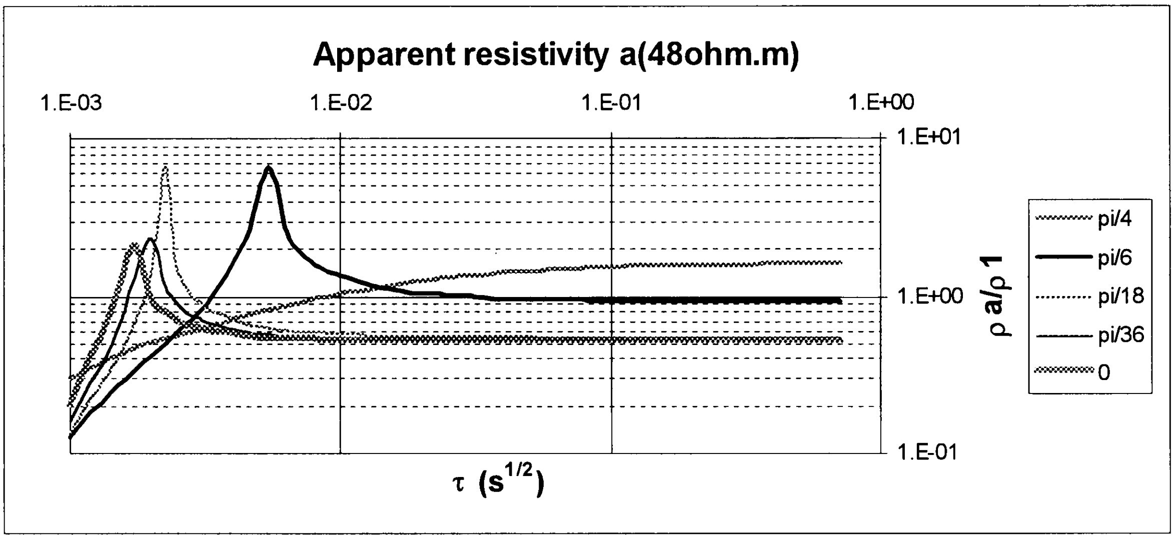

Figure 5.64 Apparent resistivity plots for a deformed, tilted and shifted current filament.

5.8 COMPARISON OF THE EMF WITH THE MAGNETIC FIELD

It Chapter 2 it was mentioned that Spies and Eggers (1986) preferred the magnetic field definition of the apparent resistivity and in Chapter 3 reference was made to the fact that Newman, Anderson and Hohmann (1987) had concluded that it made very little difference in their investigation of a 3D earth whether the apparent resistivity definition for the magnetic field or its derivative (emf) was used.

Spies and Eggers (1986) list the definition of the late-time apparent resistivity for the magnetic field:

$$\rho_a^h = \frac{I^{2/3}\mu a^{4/3}}{30^{2/3}\pi^{1/3}th_z^{2/3}} \tag{5-5}$$

where I is the current in the transmitter, a the transmitter loop radius, t is time and h_z is the measured magnetic field value. This can be written in the form of eq 2-53:

$$\rho_a^h = \frac{\mu}{\pi t}\left(\frac{M}{30h_z}\right)^{2/3} \tag{5-6}$$

with $M = In\pi a^2$ the dipole moment where n is the number of turns of a circular transmitter. Using the model described in Chapter 4, but with eq 4-1 and eq 5-6 it is possible to repeat the procedure of the previous sections for the magnetic field of a moving filament of current.

5.8.1 Layered earth apparent resistivities for the vertical magnetic field

In Figure 5.65 the calculated apparent resistivity values for late times for different half-space resistivities are shown. The relative values perfectly reflect the resistivity ratios. Again the data is presented for half-space values, because of the undefined response of a layered earth for this model. A two layer system, for example, should present over a finite time range distinguishable features in an apparent resistivity curve. The influence of layer thicknesses fall out of the scope of this study, because of the problems mentioned in Chapter 4.3.2. Thus, using the present model with the magnetic field or its derivative, yields the same results.

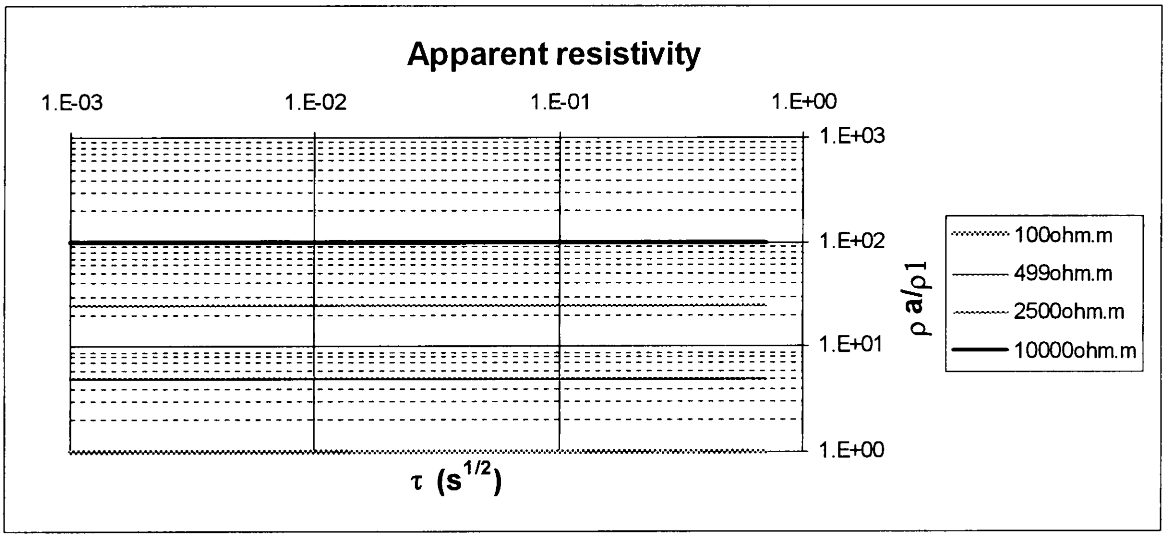

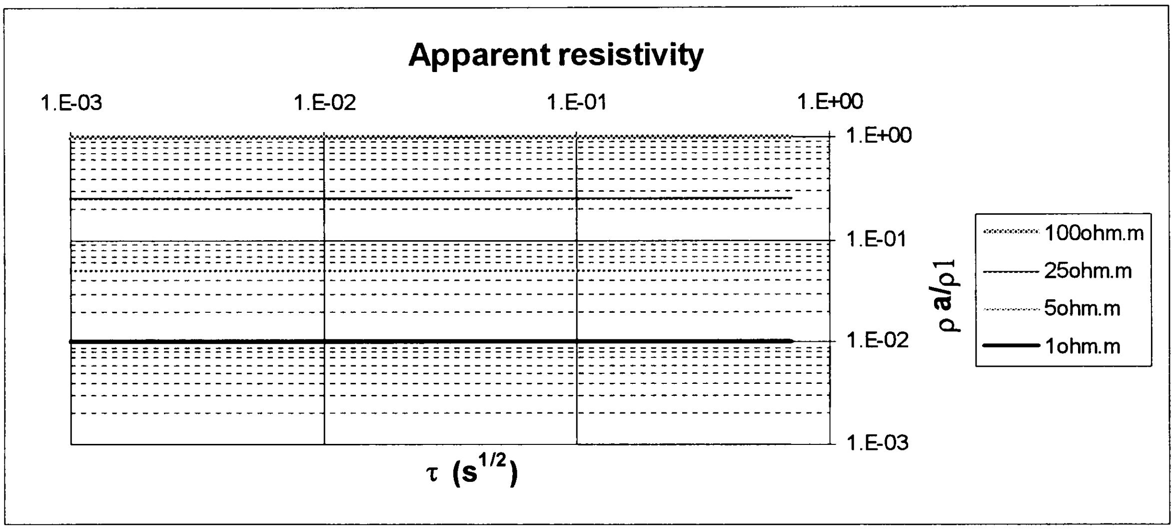

Figure 5.65 Apparent resistivity plots for different half-space resistivities shown in the legend. For the ratio ρ_a/ρ_1, ρ_1 *is taken to be the value for a 100Ωm earth.*

5.8.2 Magnetic field of a circular current filament

In Figure 5.66 the profile plots for the magnetic field of a 100Ω.m earth can be seen. Comparing these to the plots in Figure 5.2 (the derivative), with the exception of the obvious form differences, it can be seen that both components are more sensitive to orientation changes. The z-component also does not easily resemble the x-component for significant tilts, as is the case with the derivative. Another interesting phenomenon is that the z-component changes sign at 0m between tilts of pi/6 and pi/4. This also manifests in the apparent resistivity values in Figure 5.67 where the pi/4 tilt results in lower values than for pi/6. Comparing Figure 5.67 with Figure 5.3 it can be seen that the apparent resistivity is the same for a tilt of pi/6; there is only a difference for pi/4. Tilting the circular current filament still results in higher apparent resistivity values, as before.

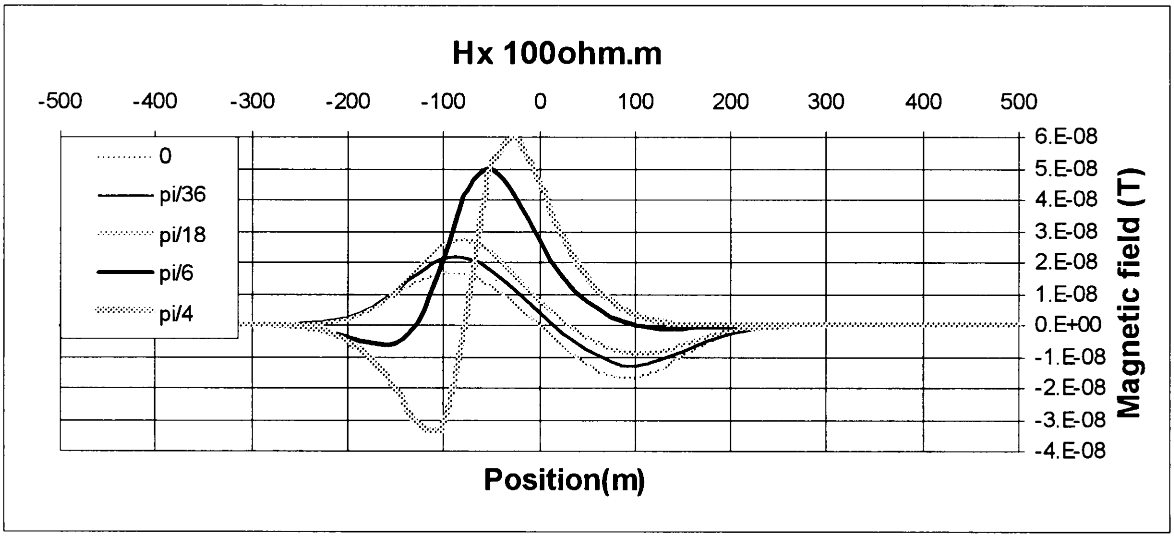

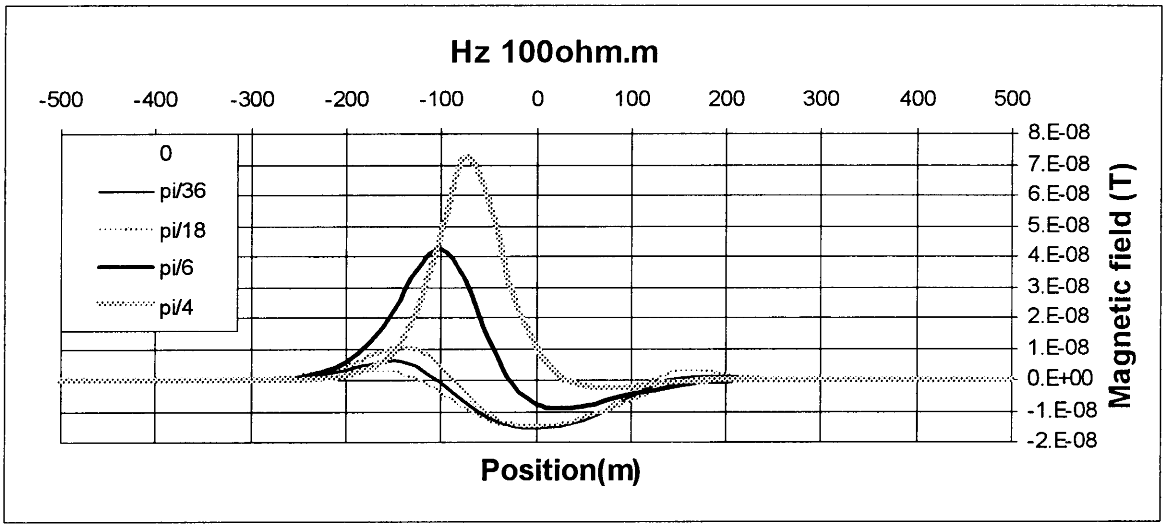

Figure 5.66 Profile plots of the x and z-components of the magnetic field of a circular current filament travelling through a 100Ωm earth. The y-component is zero. The current filament is tilted from the x to the z-axis for the angles shown in the legend.

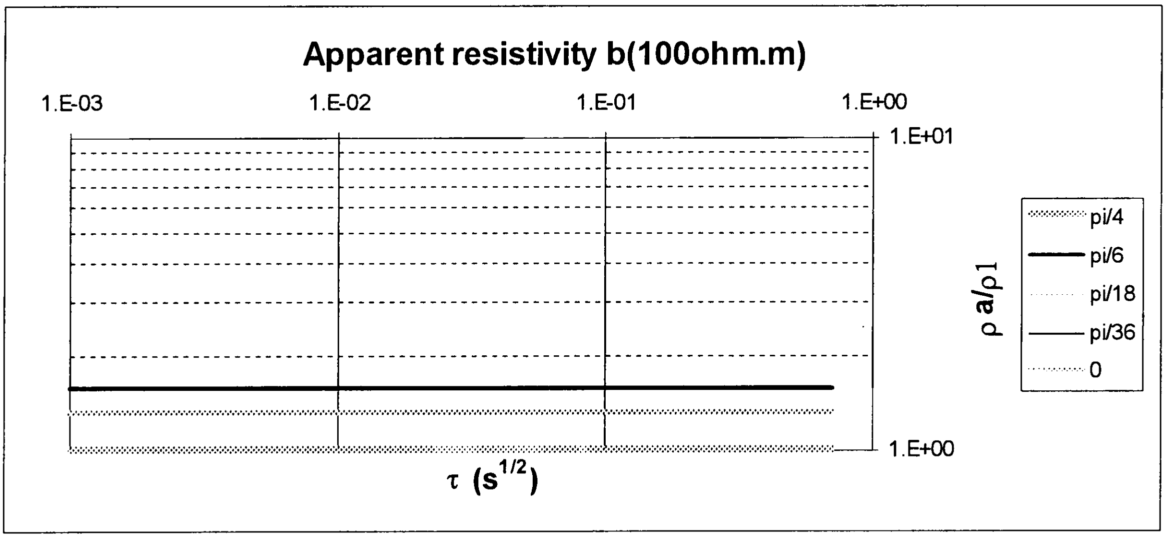

Figure 5.67 Apparent resistivity plots for a circular current filament travelling through a 100Ωm earth, tilted from the x to the z-axis for the angles shown in the legend.

5.8.3 Current filament compressed in the y-direction

As in section 5.1.1 the current filament is compressed in the y-direction to form an ellipse. The short axis of the ellipse is calculated as the radius of a current filament in a lower resistivity area for a specific time instant. Figure 5.1 depicts the deformed filament. The profile is calculated along the x-axis for the distances shown and where y=0. All the profiles are plotted for the same time channel.

In Figures 5.68 to 5.70 it can be seen that the form of the corresponding components for different compressions stay visibly the same as the circular filament, but it is just displaced along spatial axes. The more the compression, the lower the values. The z-component does not change sign between pi/6 and pi/4 as for the circular filament. This was also the case for the derivative of the field of a compressed filament (section 5.1.1).

The apparent resistivity values calculated at 0m for the horizontal deformed rings are shown in Figure 5.71. Compression in the y-direction yields higher apparent resistivity values, but the effect is much less pronounced as for the derivative of the field (Figure 5.7). For the b(25Ω.m) compression there is no difference and the highest ratio is approximately 2.5:1 compared to 3.1:1 for the derivative. Tilting the deformed filament seems to have the same relative effect as for the derivative of the field where an increase in the tilt has the result of an increase in apparent resistivity. Compare Figure 5.72 to 5.74 with 5.8 to 5.10. An exception is the 1Ω.m pi/4 tilt in Figure 5.74 which results in a significant ρ_a/ρ_1 ratio.

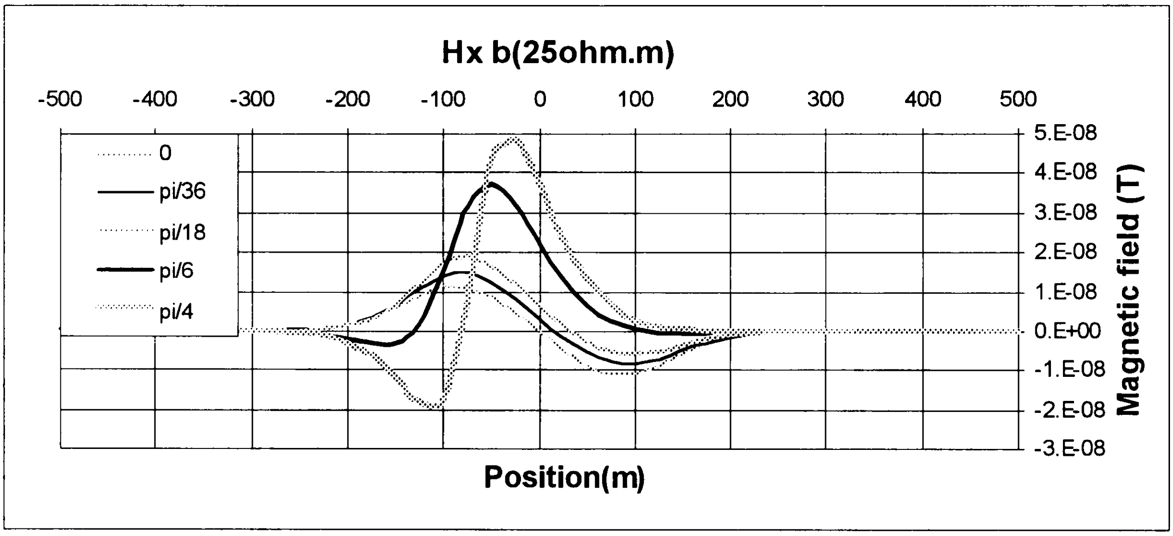

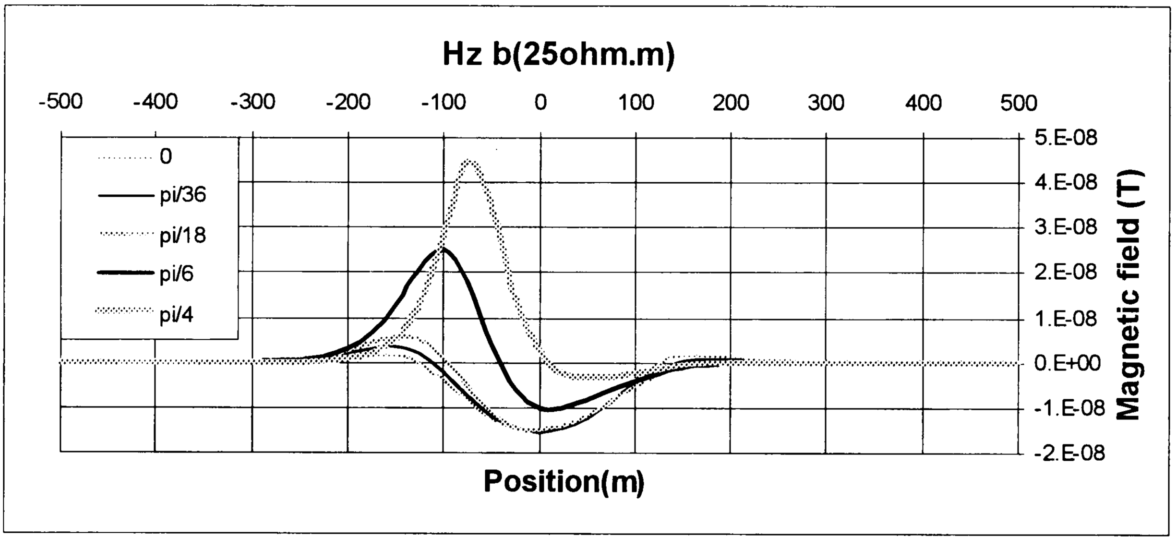

Figure 5.68 Profile plots for the magnetic field of a deformed current filament compressed in the y-direction. The y-component is zero. The legend refers to tilts from the x to the z-axis.

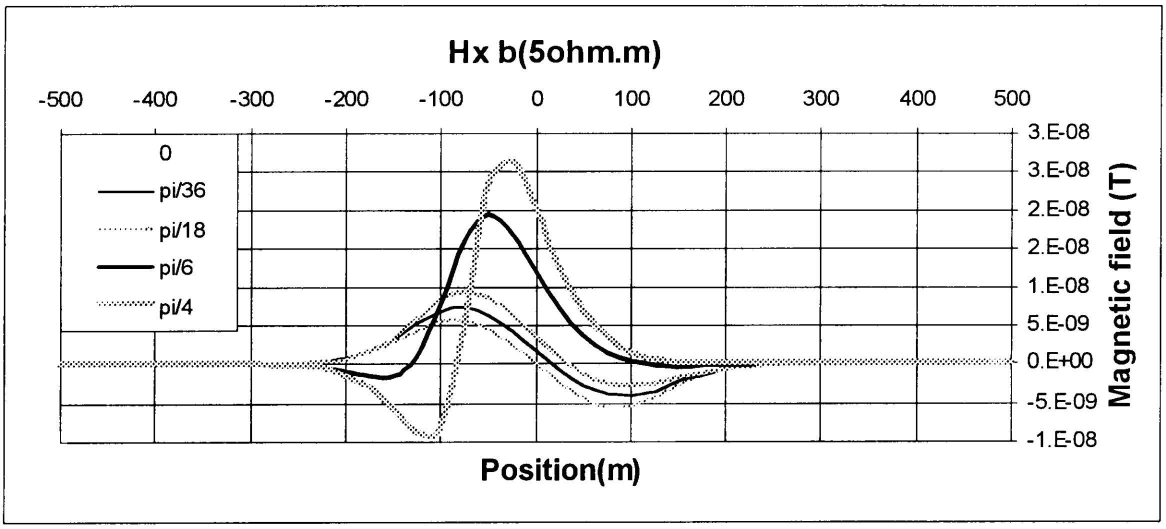

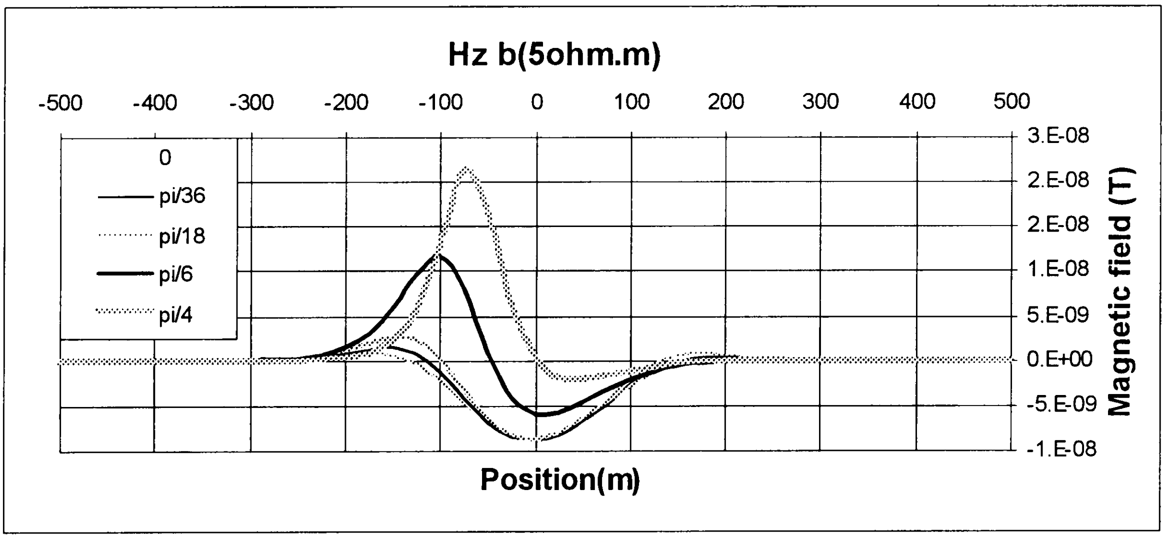

Figure 5.69 Profile plots for the magnetic field of a deformed current filament compressed in the y-direction. The y-component is zero. The legend refers to tilts from the x to the z-axis.

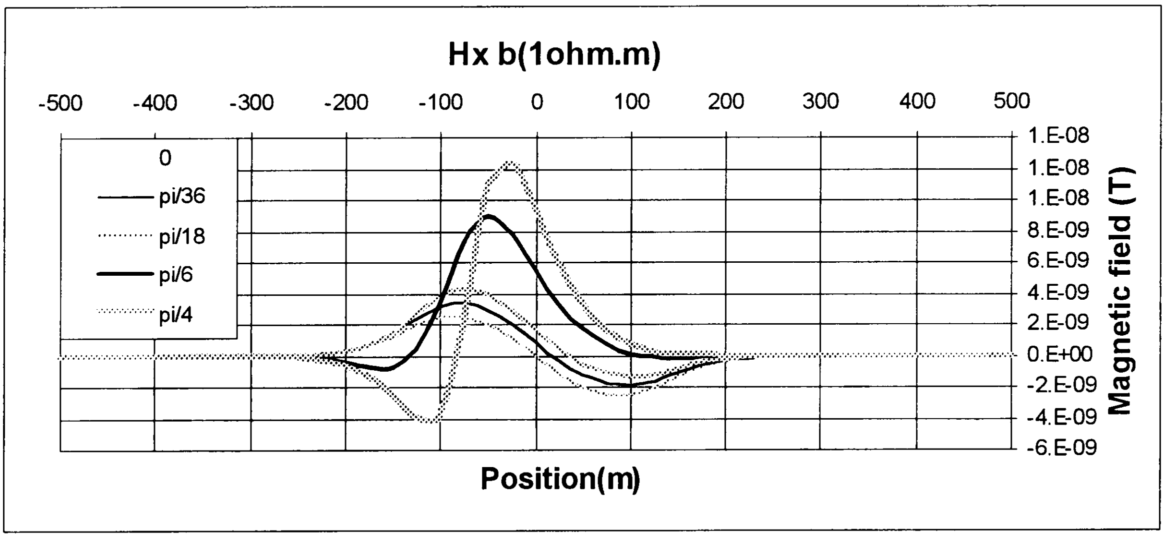

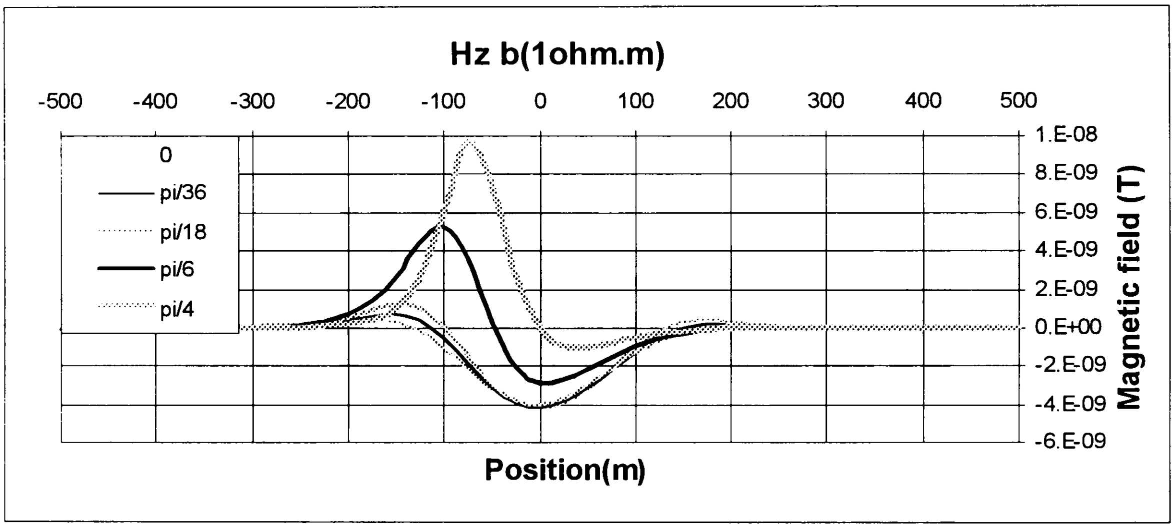

Figure 5.70 Profile plots for the magnetic field of a deformed current filament compressed in the y-direction. The y-component is zero. The legend refers to tilts from the x to the z-axis.

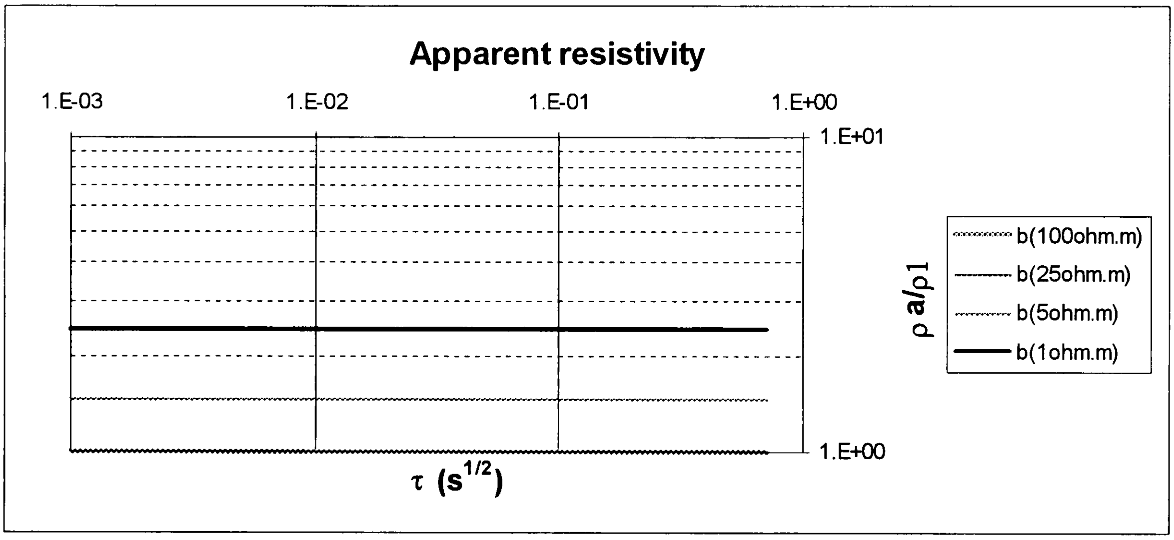

Figure 5.71 Apparent resistivity plots for horizontal current rings compressed in the y-direction. Compression is achieved by calculating the b-axis in Figure 5.1 with the resistivities shown in the legend.

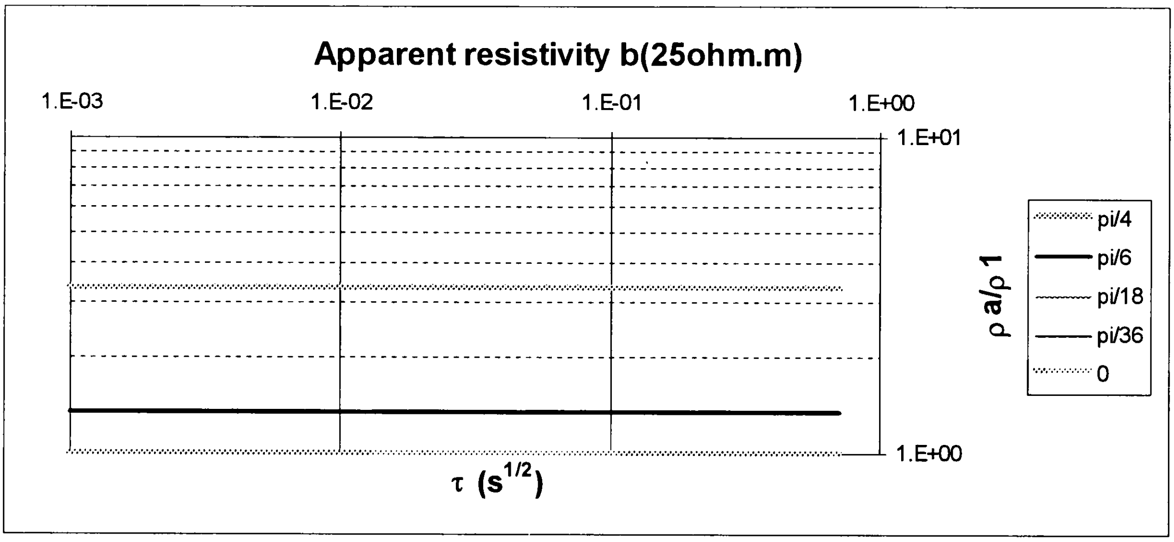

Figure 5.72 Apparent resistivity plots for a deformed tilted current filament. The calculated value is divided by the apparent resistivity of a circular filament in a 100Ωm earth.

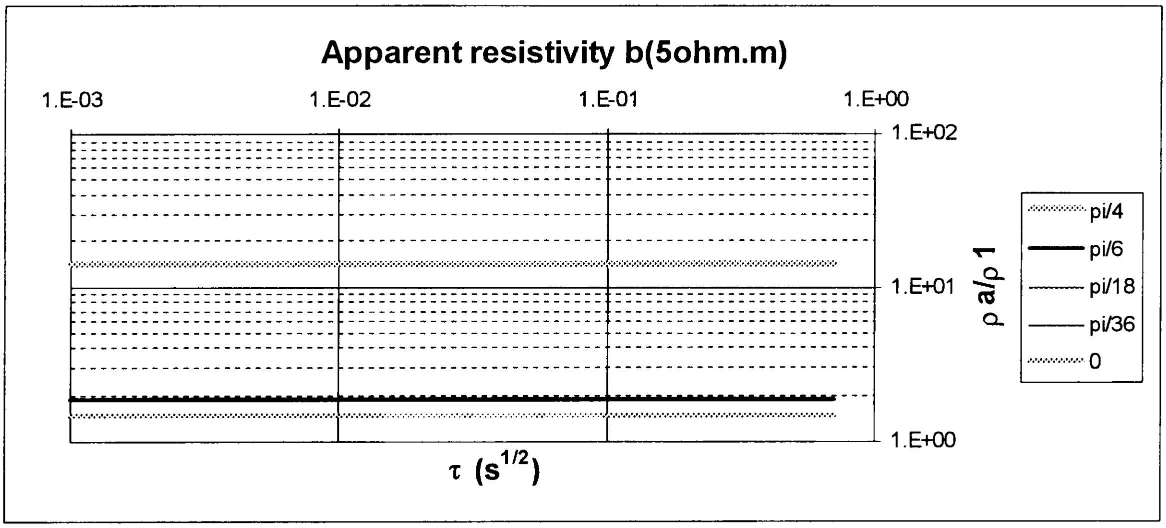

Figure 5.73 Apparent resistivity plots for a deformed tilted current filament. The calculated value is divided by the apparent resistivity of a circular filament in a 100Ωm earth.

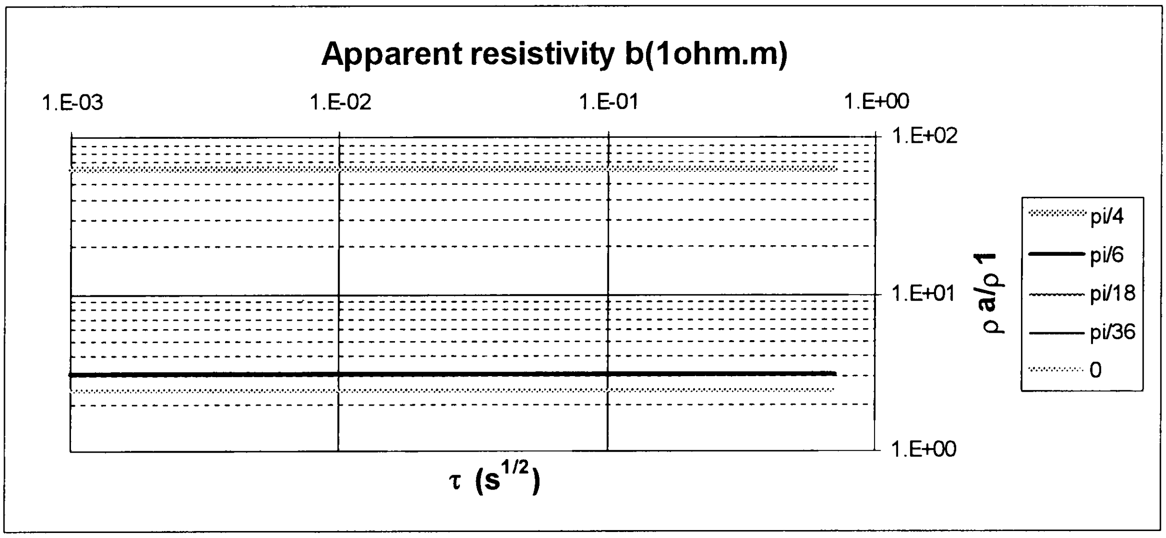

Figure 5.74 Apparent resistivity plots for a deformed tilted current filament. The calculated value is divided by the apparent resistivity of a circular filament in a 100Ωm earth.

5.8.4 Current filament elongated in the y-direction

The current filament is now elongated in the y-direction by calculating the b-axis with the resistivities shown in the titles of Figures 5.75 to 5.77 at the same instant when a is calculated for a 100Ω.m earth. Visually the forms of the corresponding components stay the same with a slight change in the maxima and minima. For all cases there is a change in sign for the z-component at position 0m between pi/6 and pi/4; the same happened for the derivative in Figures 5.11 to 5.13.

Elongation in the y-direction has a similar small effect on the apparent resistivity of the magnetic field as shown in Figure 5.78, when compared to Figure 5.14 for the derivative. There is not even a ratio of 2:1 for b(2500Ω.m). Tilting these deformed rings as shown in Figures 5.79 to 5.81 has the same effect as in section 5.1.2 where the values for the pi/4 are smaller than those for the pi/6 tilt. The reason for this is the sign change of the z-component mentioned before. In the case of the magnetic field it is just more severe than for the derivative. In Figures 5.79 and 5.80 the values for pi/4 result in lower apparent resistivity values as those for a 100Ω.m earth. In Figure 5.81 it is just slightly higher than those for 100Ω.m. The pi/6 tilt yields significant apparent resistivity ratios for all three cases. However, for small tilts there is still no distinction, as was seen for the derivative of the magnetic field.

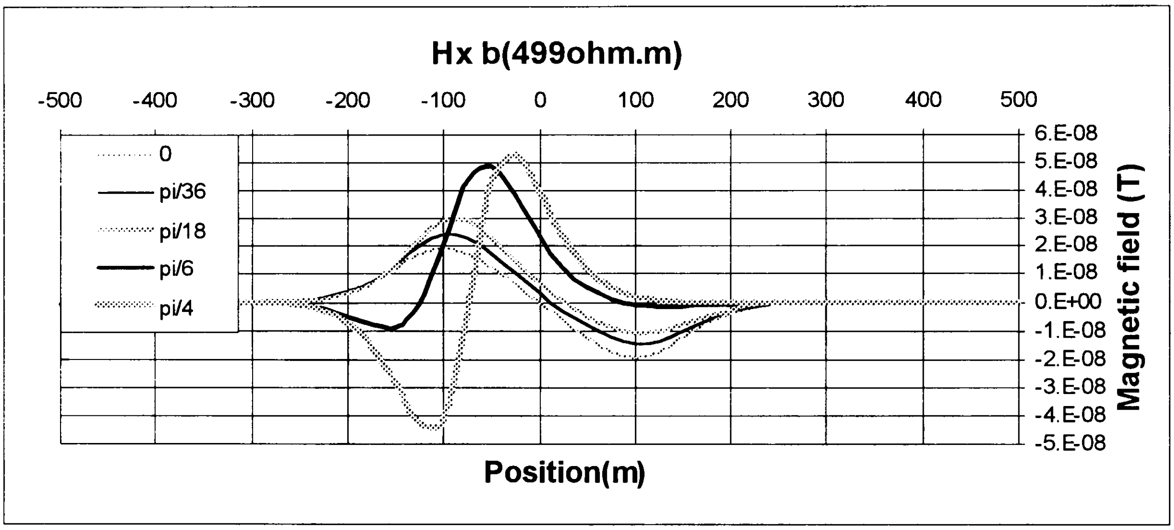

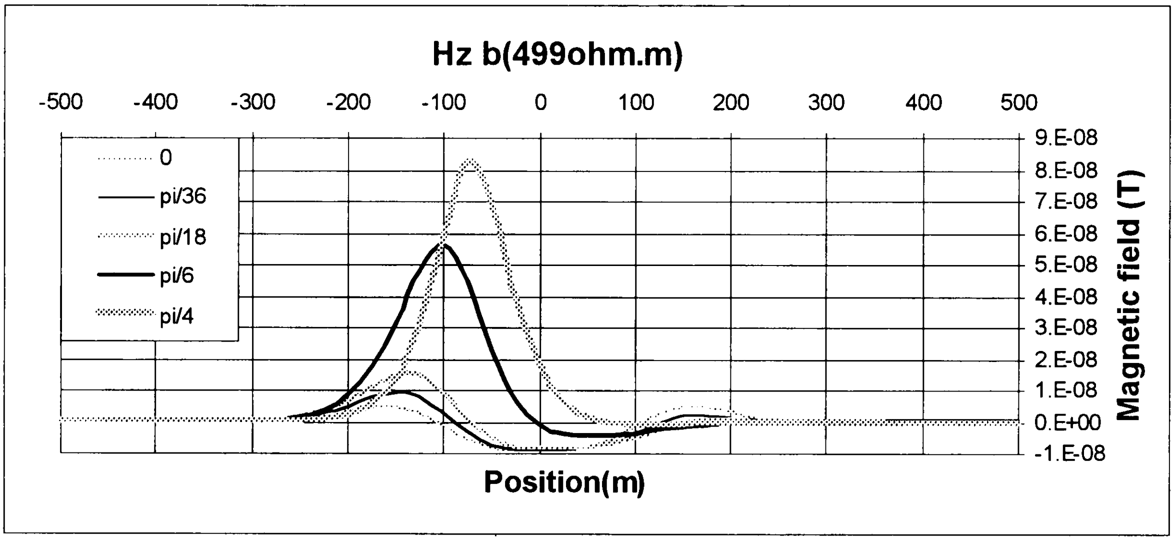

Figure 5.75 Profile plots for the magnetic field of a deformed current filament elongated in the y-direction. The y-component is zero. The legend refers to tilts from the x to the z-axis.

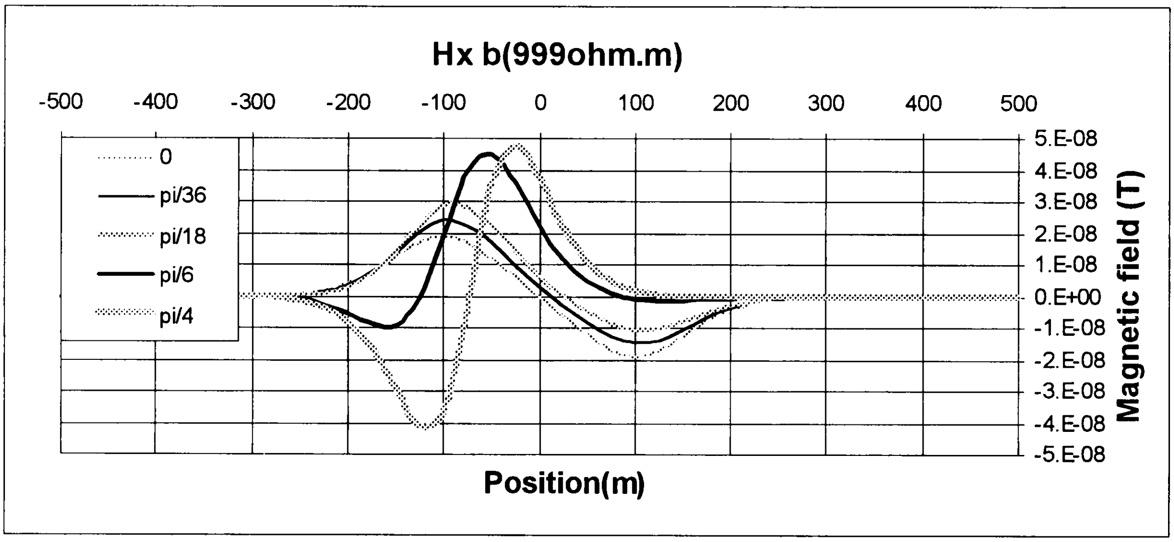

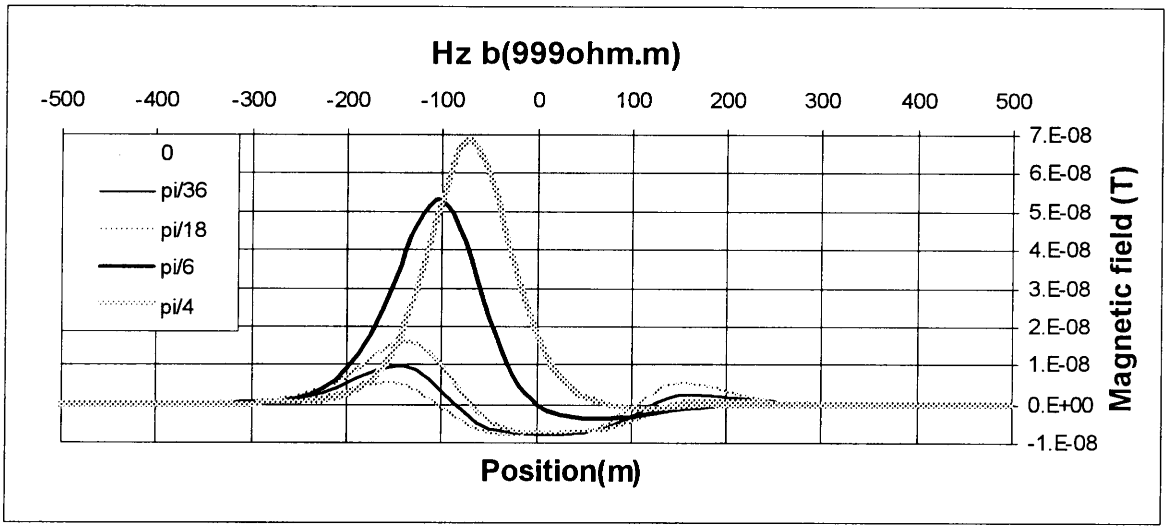

Figure 5.76 Profile plots for the magnetic field of a deformed current filament elongated in the y-direction. The y-component is zero. The legend refers to tilts from the x to the z-axis.

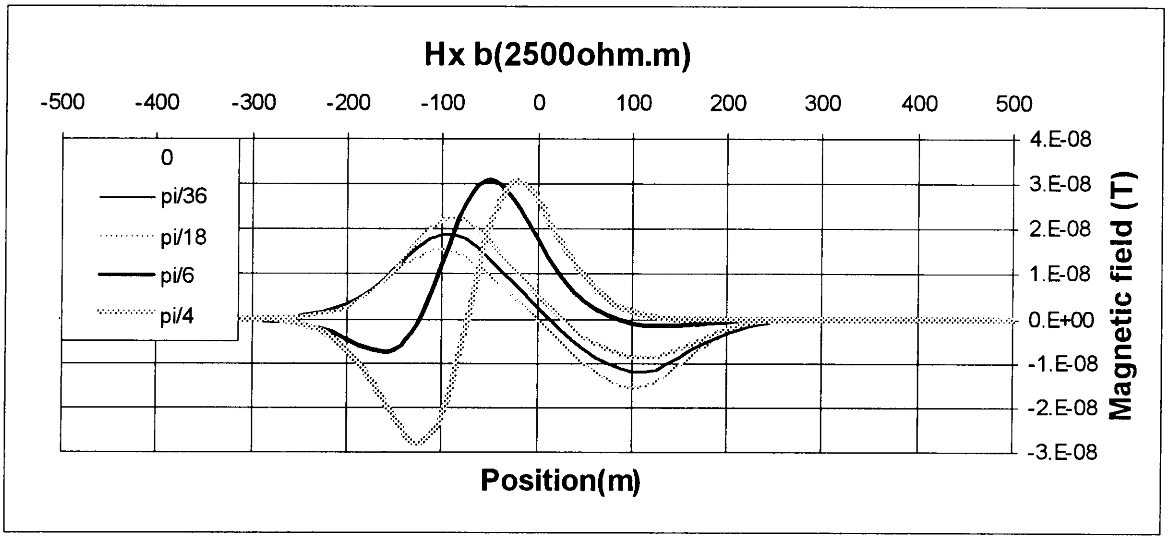

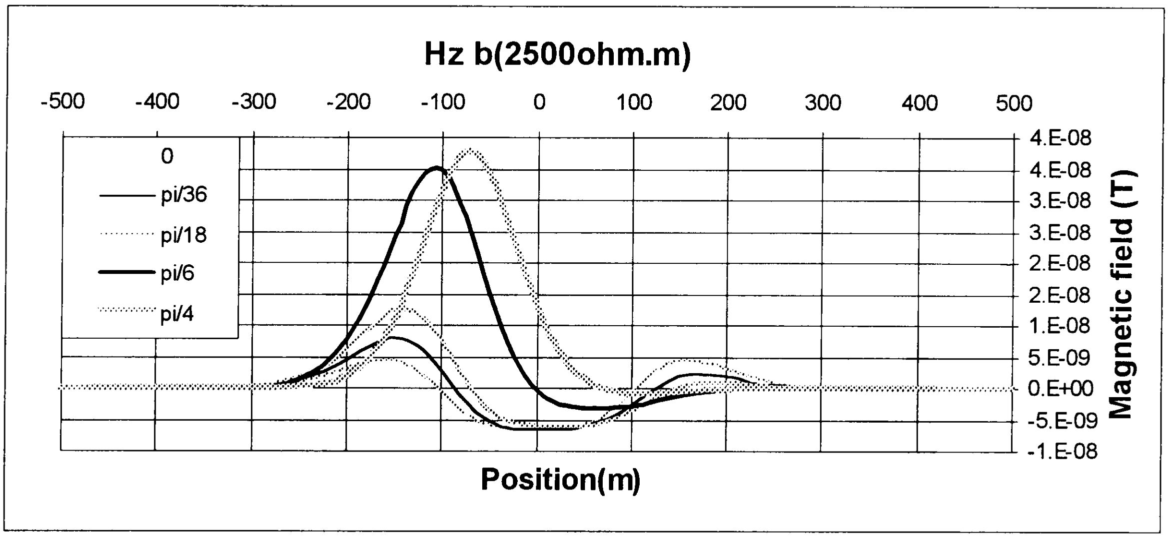

Figure 5.77 Profile plots for the magnetic field of a deformed current filament elongated in the y-direction. The y-component is zero. The legend refers to tilts from the x to the z-axis.

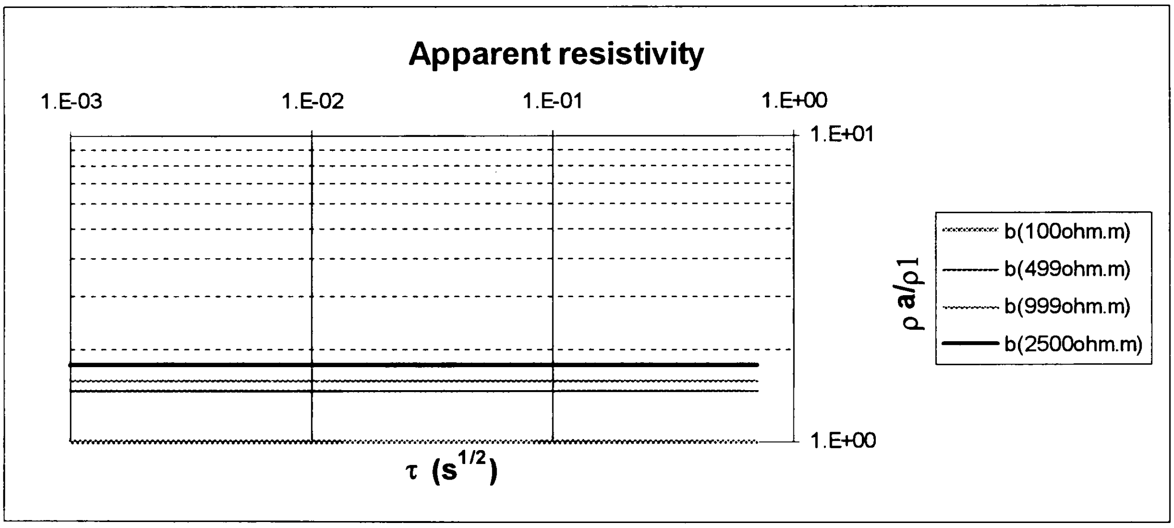

Figure 5.78 Apparent resistivity plots for horizontal current rings compressed in the y-direction. Compression is achieved by calculating the b-axis in Figure 5.1 with the resistivities shown in the legend.

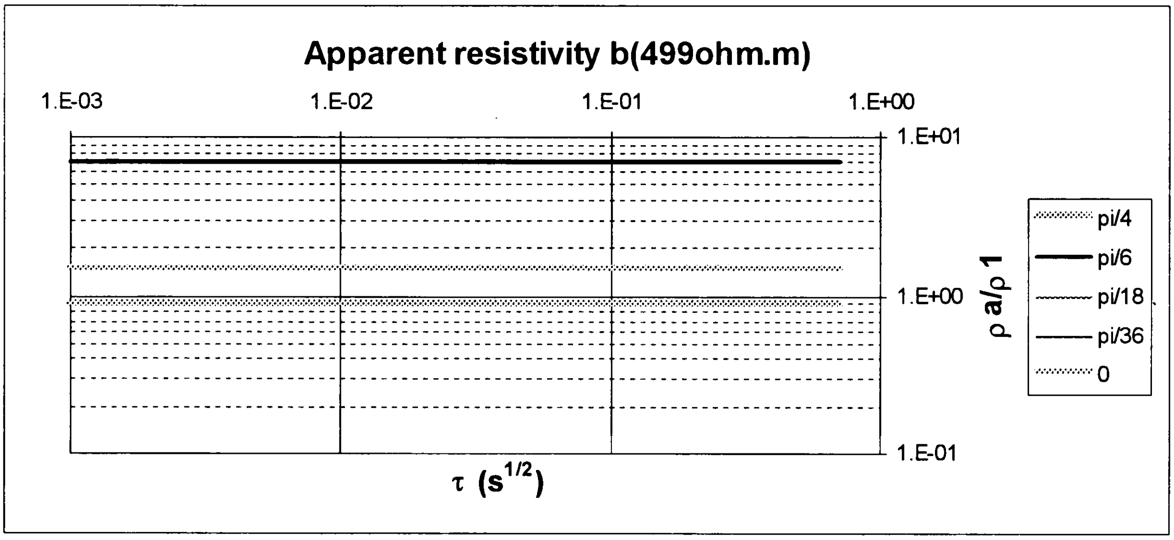

Figure 5.79 Apparent resistivity plots for a deformed tilted current filament. The calculated value is divided by the apparent resistivity of a circular filament in a 100Ωm earth.

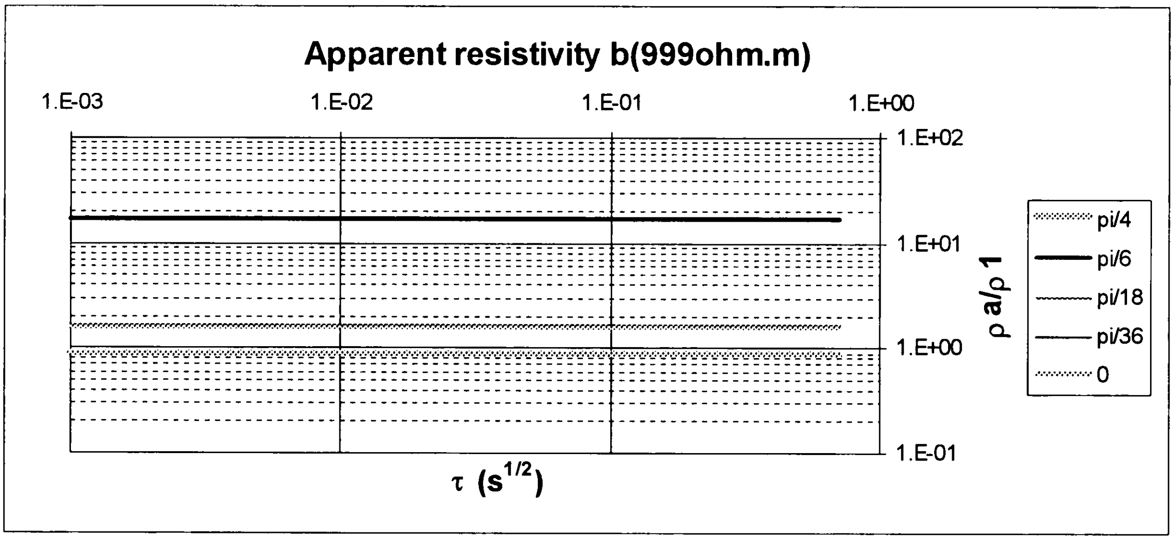

Figure 5.80 Apparent resistivity plots for a deformed tilted current filament. The calculated value is divided by the apparent resistivity of a circular filament in a 100Ωm earth.

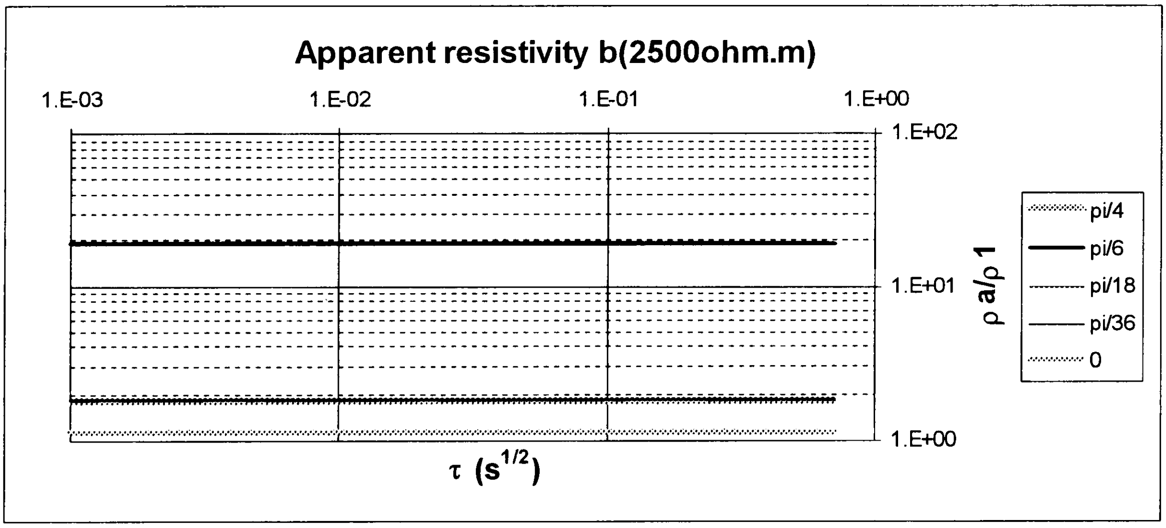

Figure 5.81 Apparent resistivity plots for a deformed tilted current filament. The calculated value is divided by the apparent resistivity of a circular filament in a 100Ωm earth.

5.8.5 Vertical boundary from a low to higher resistivity

The preceding sections showed that there is little difference, for this model, between using the apparent resistivity definition for the derivative and the magnetic field. An approximate physical situation using the magnetic field is presented without all the detail of the sections 5.2 to 5.7. All the previous assumptions for a physical approximation are used.

In Figure 5.82 the apparent resistivity values for a tilted circular current filament in a 100Ω.m earth, shifted 25m in the positive x-direction are shown. The peaks correspond to sign changes for the z-component. Comparing this to Figure 5.40, it is evident that the sign changes happen later for the magnetic field apparent resistivity values. The pi/4 tilt does not change sign, whereas this happened between 10^{-2} and 10^{-1} $s^{1/2}$ for the derivative. Except for the serious early distortions of the apparent resistivities when a sign change happens, there is little difference in the values. As previously seen, it is only the pi/4 tilt, which has a significant influence.

Calculating the depth, current and b-axis for a weighted average resistivity and completing the ellipse with b(100Ω.m), results in the same physical approximation as before. Figure 5.83 shows the apparent resistivity values of the different horizontal current rings. Comparing these results with those for the derivative in Figure 5.42, it seems as if the magnetic field apparent resistivities are slightly less sensitive to changes of the parameters of this model. For a(536Ω.m) the derivative had an apparent resistivity ratio of 7:1, while the magnetic field had a ratio of slightly less than 6:1. This ratio is still higher than the resistivity of 536Ω.m and probably the result of the deformation of the current filament. The magnetic field values for a tilted filament, as shown in Figures 5.84 to 5.86, are very close to each other. The only difference with the derivative is that the pi/4 tilt does not change sign.

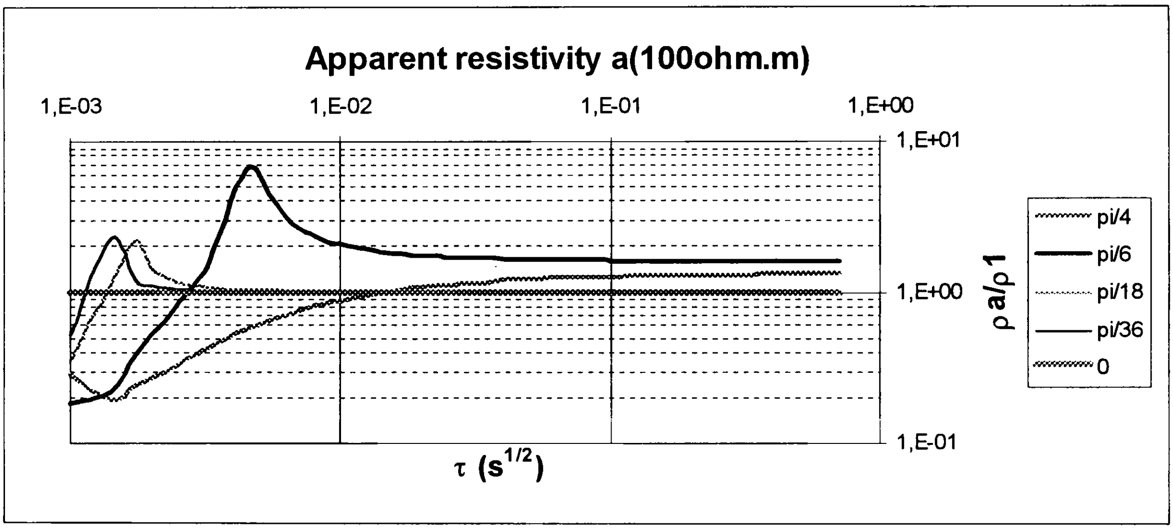

Figure 5.82 Apparent resistivity calculated from the magnetic field for a circular current filament in a 100Ωm half-space and tilted from the x to the z-axis for the angles in the legend.

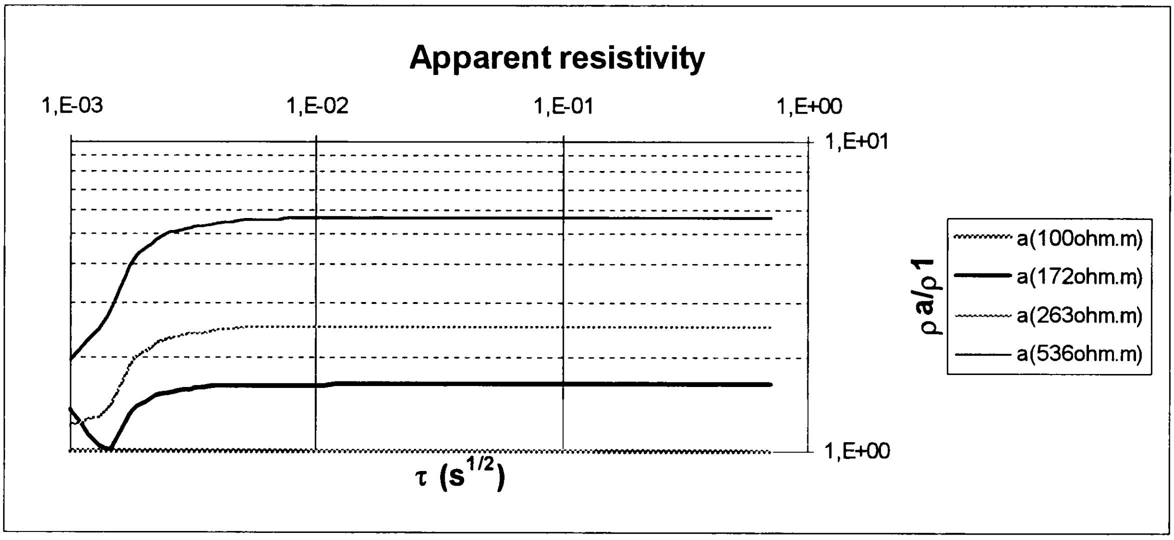

Figure 5.83 Apparent resistivity plots for horizontal deformed current rings. The a-axis is calculated for the resistivities in the legend. All the rings are shifted 25m to the right.

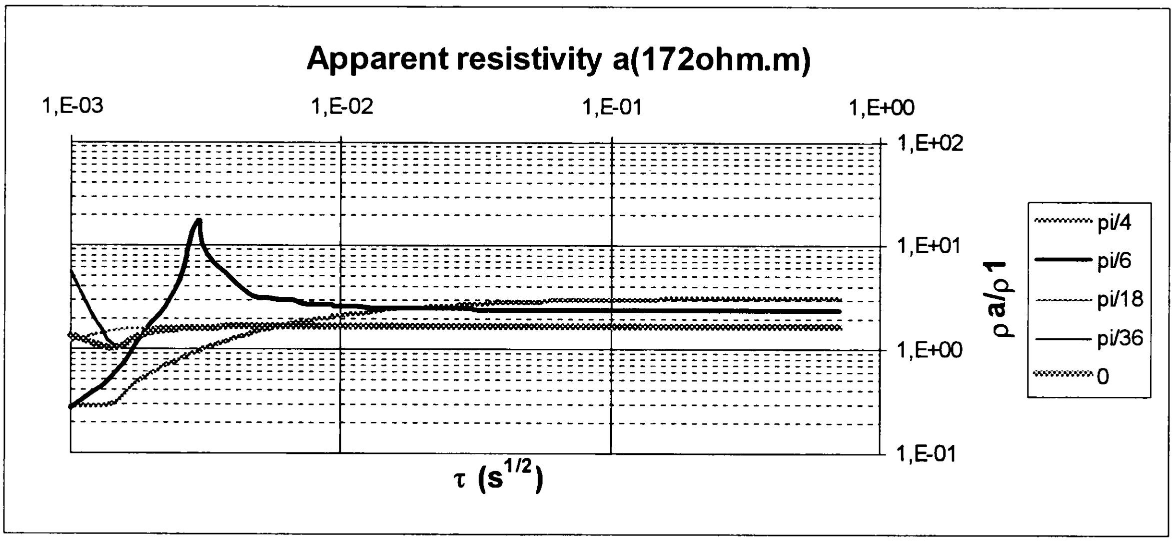

Figure 5.84 Apparent resistivity plots for a deformed tilted current filament. Deformation is achieved by calculating the a-axis for the resistivity in the title. Tilts from the x to the z-axis are shown in the legend.

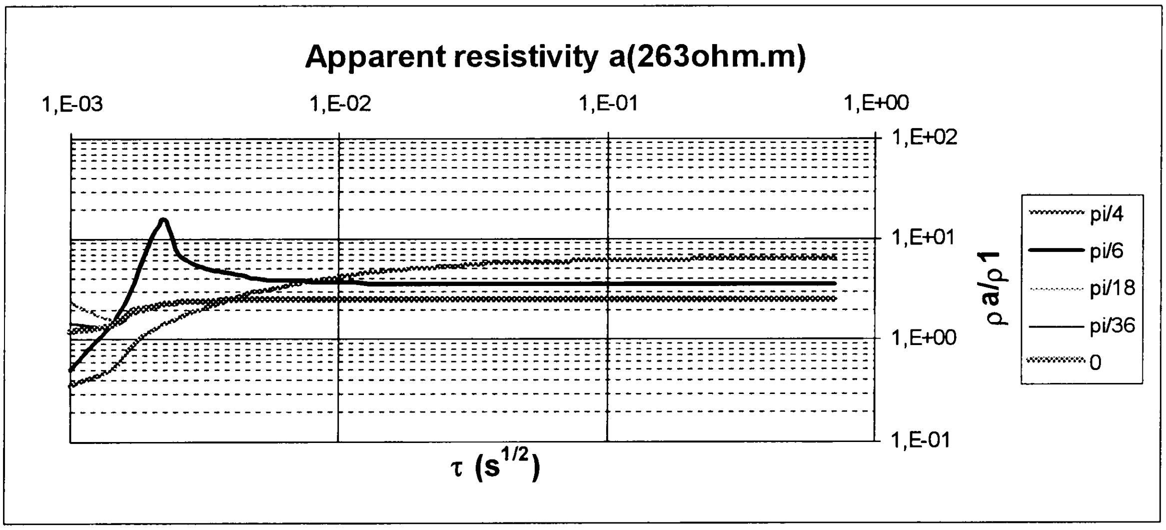

Figure 5.85 Apparent resistivity plots for a deformed tilted current filament. Deformation is achieved by calculating the a-axis for the resistivity in the title. Tilts from the x to the z-axis are shown in the legend.

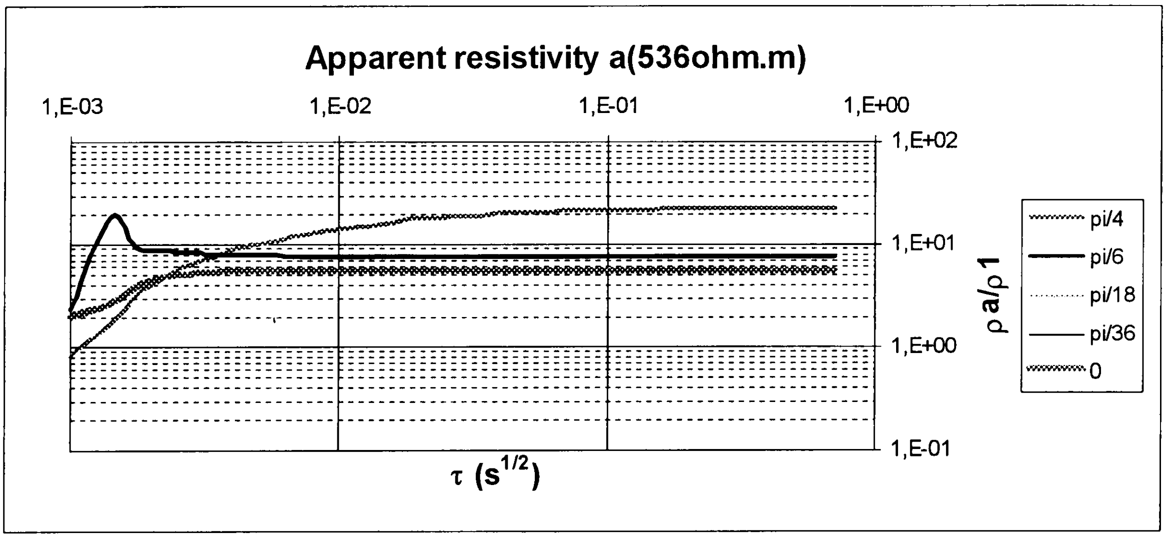

Figure 5.86 Apparent resistivity plots for a deformed tilted current filament. Deformation is achieved by calculating the a-axis for the resistivity in the title. Tilts from the x to the z-axis are shown in the legend.

5.8.6 Vertical boundary from a high to lower resistivity

As in section 5.7 there is very little change in apparent resistivity when applying the model to an approximate physical boundary from a high to a lower resistivity. The problem is mainly that the weighted average resistivity results in a very low contrast, with 100Ω.m as can be seen in the legend of Figure 5.87. Tilting this deformed filament also has very little effect, except for serious tilts like pi/6 and pi/4. But even these resultant apparent resistivity values are too close to each other to be significant, as seen in Figures 5.88 and 5.89. The peaks correspond to sign changes of the z-component, something which does not happen for the pi/4 tilt as was the case with the derivative.

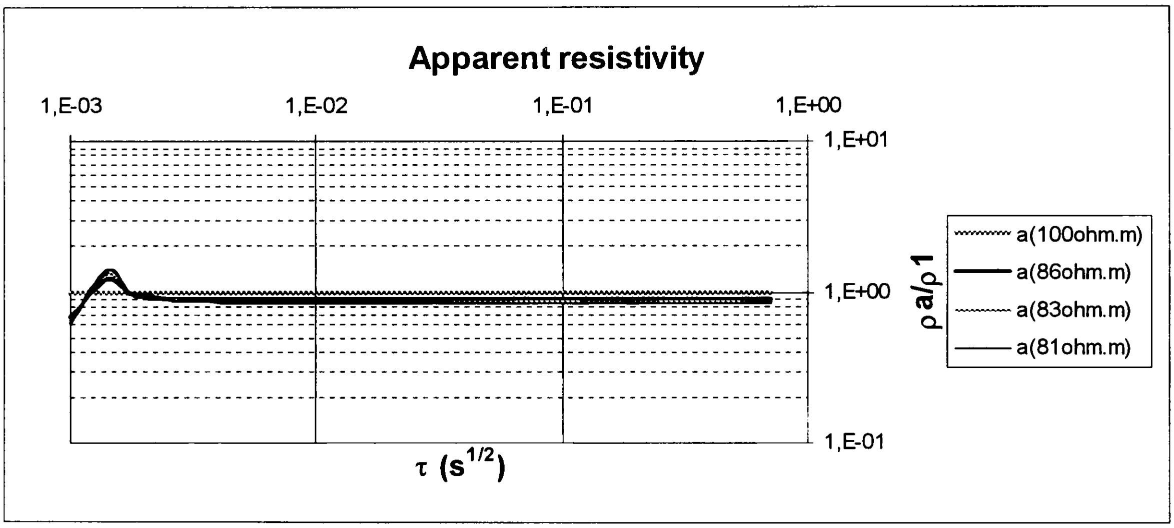

Figure 5.87 Apparent resistivity plots for horizontal deformed current rings. The a-axis is calculated for the resistivities in the legend. All the rings are shifted 25m to the right.

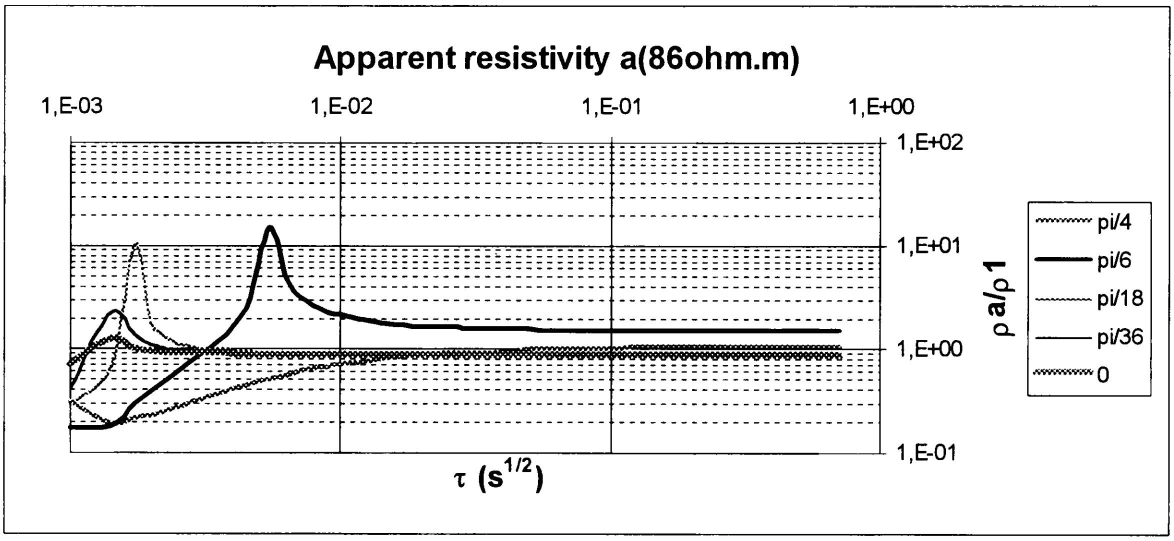

Figure 5.88 Apparent resistivity plots for a deformed tilted current filament. Deformation is achieved by calculating the a-axis for the resistivity in the title. Tilts from the x to the z-axis are shown in the legend.

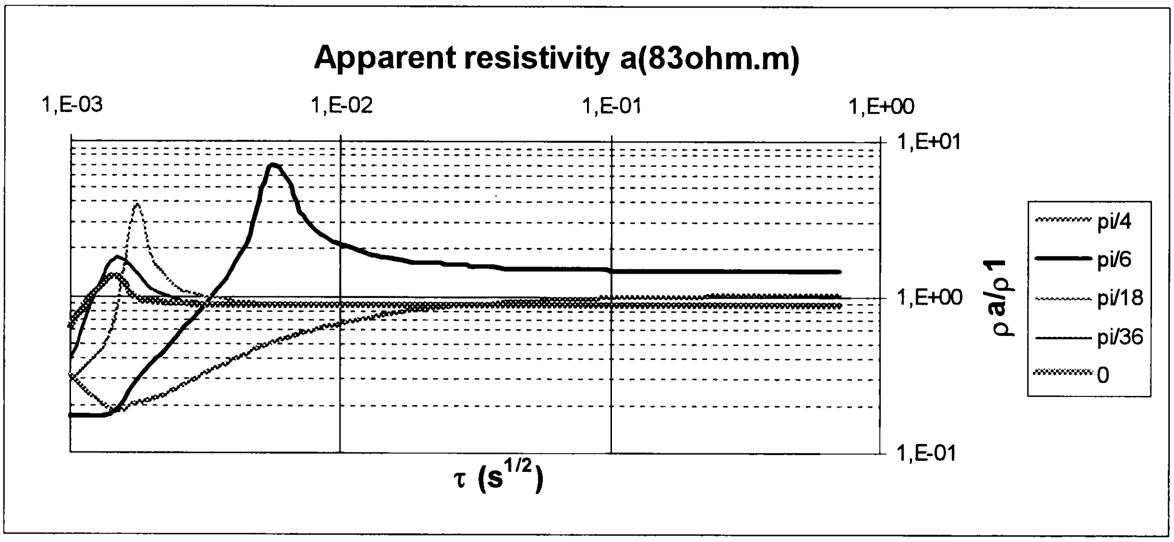

Figure 5.89 Apparent resistivity plots for a deformed tilted current filament. Deformation is achieved by calculating the a-axis for the resistivity in the title. Tilts from the x to the z-axis are shown in the legend.

Chapter 6

Discussion, conclusions and recommendations

The results of the previous chapter will be discussed separately, as well as being compared to the previous chapters. This is followed by the conclusions of this study and recommendations for possible further research on the subject.

6.1 DISCUSSION

6.1.1 Applicability of the TEM sounding method to the detection of lateral boundaries

The correct velocity-current functions to simulate a layered earth using a single current filament, were not determined. However, it was shown that the current filament could reflect the different resistivities of a half-space accurately as apparent resistivities. So although it was not possible to calculate the integrated response of a specific layered earth, the current filament could present differences in apparent resistivity values calculated separately for different input parameters.

Chapter 5 was an attempt to investigate the changes in the measured apparent resistivity, because of changes in orientation and shape of a current filament. It was seen that higher apparent resistivity values were found with the filament when the shape of the filament was changed. The actual diameter of the filament had a significantly smaller influence than the shape of the filament. Overall, the effect was very small when the data was viewed as apparent resistivity or profile plots. Tilting a circular or elliptical current filament did not have much effect, given the fact that the tilt was small and that the z-component used to calculate the apparent resistivity does not change sign. This was the case for a current filament elongated in the y-direction and tilted pi/4, which in turn yielded an apparent resistivity value which was again closer to the untilted value. On profile plots there was a significant distortion of the symmetry of the field for a tilted filament and for severe tilts the response could be mistaken for that of a vertical conductor. The amplitude of this latter response will probably be very small, compared to real vertical conductors.

Changing the current and depth did not have the same effect as changing the radius. In the first two cases the apparent resistivity reflected the resistivities used to calculate it. For example, a higher resistivity yielded a higher apparent resistivity and vice versa, but not to the same extent as would have been the case for a layered earth. In the second case a change in radius manifested itself as a higher apparent resistivity for both cases. So there was no clear relation between the functions used to calculate the position and size and the resultant apparent resistivity when only one parameter is changed. The functions for depth and radius are directly proportionate and are inversely proportionate to the current function, but the resultant magnetic field values do not exhibit any direct relation to these functions. Moving the current filament in a horizontal direction had the effect that the z-component changed sign for certain cases and distorted the apparent resistivity values. When this effect disappears, there is no difference in apparent resistivities between the shifted and unshifted filament.

All these changes of a traveling current filament were put together to develop a qualitative model for the response of a 2D earth with a vertical boundary. For a boundary where the current filament moves into a region with a higher resistivity, it seems logical that it will start to move faster outward and downward in that region. This was approximated by a tilted and shifted ellipse (Figure 5.39), where the one axis was calculated for a weighted average resistivity function $\Sigma(\rho_1,\rho_2)$, eq 5-4. All the results showed that the distortion, tilting and shifting had little effect when applied in moderate quantities and that the most important aspect was the weighted average resistivity function. When the resistivity of this function was significantly different from the resistivity of region 1, there was a distinguishable apparent resistivity ratio. Obviously this can be masked by the effect of the sign changes of the data or severe tilting of the current filament, but in both of these cases it will evidently not be the response of a layered earth.

Proceeding from a higher to lower resistivity in region 2, the fact that a weighted average resistivity function is used, results in a small apparent resistivity ratio from the start. This overshadows any other effect of moderate tilting, shifting and distortion.

These findings were briefly checked with the apparent resistivity calculated using the magnetic field response of a vertical dipole. There were not any difference with the results of the derivative of the field for this current filament.

6.1.2 Comparison of the current filament results with published work

In Chapter 3 published work relevant to this study was discussed and now the results of the forward model will be compared to these earlier findings. The axially symmetrical model of Goldman and Stoyer (1983), shown in Figures 3.1 to 3.3, calculated the apparent resistivity for , respectively, a topographic high and low on a perfectly conducting basement. The data is presented as apparent resistivity curves for different ratios of the body radius to the depth of the basement. In Figure 3.1 it can be seen that a bigger body radius gives an earlier conducting response. As the body radius becomes smaller, this response shifts in time. These two extreme cases are equivalent to two different two layer earth systems where the first layer thickness is varied. In terms of a current filament, which will stay circular for this symmetrical model, it may be possible to explain why there is no difference in the data if the ratio Body Radius/H is increased past 4. H is the depth to the basement. As the current filament travels downwards it will not encounter the vertical boundary for the topographic high, because it has already moved into the bottom layer. The response for this case will then just be that of a two layer earth where the first layer thickness is the depth to the top of the topographic high. Obviously, when the ratio is zero, the response will be that of a two layer earth with first layer thickness being that of the basement depth. Between the extreme cases there will be a response which is the result of a weighted average function of the depth and conductivity effects on the current filament.

Similarly in Figure 3.2, where the results of a topographic low are presented, it can be seen that for a small ratio (body radius to H) the basement response is observed earlier, thus a two layer response with a smaller second layer depth. Increasing this ratio again results in a two layer case where the second layer is deeper. Once more there is no difference if the ratio is increased to a factor of more than 4, which means that the current filament has already passed into the basement without touching the vertical boundary of the topographic low.

In Figure 3.3 the response for a cylindrical conductor of varying body radius to H (depth of basement) is shown. When the ratio is zero there is only a two layer response and for ratios of two to infinity, the response is that of a three layer earth. Again the bigger radius of the conductor means that the current filament passes through it without being influenced by the vertical boundary. The response of smaller radii are the result of the current filament passing through the boundary. They concluded that the interpreted conductivity of smaller bodies, using 1D inversion, is significantly less than the true conductivity, while the interpreted thickness is approximately the same. This could be an indication of the weighted average resistivity function which governs the diffusion of a current filament.

Garg and Keller (1986) found that the distortion of LOTEM data due to 3D structures were significant, but not necessarily diagnostic. They made the assumption that the EM-field consists of different parts where the primary field is due to the layered structure and the secondary field originates from induction and counterinduction of areas where the resistivity deviates from that of a layered earth. This may be the case when dealing with traditional conductors (like sulfide bodies), but smaller contrast 3D bodies could be part of the total resistivity function, as is the case with a layered earth. It was not possible in Chapter 4 to simply add the response of two different layers to get a two layer curve, because there seems to be a singular weighted average resistivity function for a certain resistivity distribution in a layered earth model. Furthermore they concluded that it was more likely for a 3D structure to manifest in spatial than in temporal data. This statement is supported by Fitterman and Stewart (1986). The current filament of this study shows that there is a qualitative response of a 2D earth, which should be significant temporally if the current filament passes into a region with a higher resistivity.

Newman, Hohmann and Anderson (1986) used a 3D modeling program and found lower apparent resistivities over a depression of a resistive basement. The model and results are shown in Figure 3.4. This effect was most pronounced near the center of the depression and the lower apparent resistivities probably resulted from the fact that the current filament could spend more time in the 10Ω.m region where diffusion takes place at a slower rate. The fact that the effect, for the forward model, is apparent even at some distance away at station 2500, could support the previous statement that the 3D structure influences the weighted average resistivity function directly. In Figure 3.5 they show that the response of a basement topographical high is again more pronounced closer to the structure than further away and that it lies between the two 1D cases taking the top and the bottom of the topographical high as third layer depths. This response is also integrated and definitely not that of a 1D case. This is substantiated by their further work (Newman et al, 1987), where they generated results using their 3D model and interpreted these with 1D inversions. The fact that this procedure was relatively successful again shows that for small resistivity contrasts, it is not possible to distinguish between a so-called primary and secondary field.

Spies and Parker (1984) found that the position of the transmitter was important to detect a resistive discontinuity in a model study. In Figure 3.19 they found that the response for the transmitter at position (c) was more pronounced. Comparing this to the current filament study it is possibly the effect of the filament moving from a lower to a higher resistivity, which should have a greater effect than the opposite on the shape and orientation of the filament.

The results of Nelson and Haigh (1990) could also confirm the importance of the transmitter position. They plotted apparent resistivity as a pseudosection of time and found that the values could change radically from one position to another on a doline terrain as in Figure 3.23. A possible explanation could be the difference of distortion of the current filament when it moves laterally from one resistivity region to another, because they found central loop soundings to be more effective for their purposes. Doing profile type measurements could possibly have shown an unsymmetrical response, but the field would just be that of one distorted current filament. Moving the transmitter source would change the position of the current filament and enable it to have different distortions as it moves from high to low and from low to high resistivity regions respectively.

6.2 CONCLUSIONS

- This study proves that it is possible to approximate the response of a vertical dipole over a layered earth, by way of a current filament moving downwards and outwards.
- It is theoretically possible to determine temporal changes of the field of a moving current filament which is being distorted by 2D or 3D structures.
- The effect of a current filament moving from a low to high resistivity area is more pronounced than the opposite.
- The effect of a current filament being distorted yields slightly higher apparent resistivity values as expected, except when the effect is anomalous because of sign changes of the z-component.
- A tilted current filament results in an unsymmetrical profile plot of the data, which could resemble that of a vertical conductor.

6.3 RECOMMENDATIONS

- Investigation of the parameters influencing a current filament in a layered earth. If these can be defined, it will be possible to develop a fast forward model and possibly to better understand the response of a layered earth.
- Using a 3D forward model, like that of Newman et al (1986), to investigate the possibility of defining the propagation influences of a current filament for simple 3D models. If this could be achieved it may be possible to develop a faster forward model which could be used more effectively for interpretation purposes, with the added benefit of a better understanding of complex EM responses.

References

Du Plooy, A., 1985, The electromagnetic field of a vertical magnetic dipole over a layered earth. A theoretical derivation without defining a vector potential.

Feynman, R. P., Leighton, R. B. and Sands, M., 1975, The Feynman lectures on physics, Addison-Wesley Publishing Company, Volume II.

Fitterman, D. V., and Stewart, M. T., 1986, Transient electromagnetic sounding for groundwater: Geophysics, 51, 995-1005.

Frischknecht, F. C., and Raab, P. V., 1984, Time-domain electromagnetic soundings at the Nevada Test Site, Nevada: Geophysics, 49, 981-992.

Garg, N. R., and Keller, G. V., 1986, Spatial and temporal analysis of electromagnetic survey data: Geophysics, 51, 85-89.

Goldman, M. M., and Stoyer, C. H., 1983, Finite-difference calculations of the transient field of an axially symmetric earth for vertical magnetic dipole excitation: Geophysics, 48, 953-963.

Hoversten, G. M., and Morrison, H. F., 1982, Transient fields of a current loop source above a layered earth: Geophysics, 47, 1068-1077.

Kaufman, A. A., and Keller, G. V., 1983, Frequency and transient soundings: Methods in Geochemistry and Geophysics, 16, Amsterdam, Elsevier Publ. Co.

Lewis, R., and Lee, T., 1978, The transient electric fields about a loop on a half-space: Bull. Aust. Soc. Explor. Geophys., v.9, 173-177.

McNeill, J. D., TN-7: Applications of transient electromagnetic techniques, Geonics Limited.

Macnae, J., and Lamontagne, Y., 1987, Imaging quasi-layered conductive structures by simple processing of transient electromagnetic data: Geophysics, 52, 545-554.

Macnae, J., and Lamontagne, Y., 1984, Discussion on "Comparison of apparent resistivity functions for transient electromagnetic methods," by A. P. Raiche: Geophysics, 49, 312-313.

Nelson, R. G., and Haigh, J. H., 1990, Geophysical investigations of sinkholes in lateritic terrains, *in* Ward, S. H., Ed., Geotechnical and environmental geophysics, Investigations in geophysics, vol 5, Soc. Expl. Geophys.

Nabighian, M. N., 1979, Quasi-static transient response of a conducting half-space - An approximate representation: Geophysics, 44, 1700-1705.

Newman, G. A., Hohmann, G. W., and Anderson, W. L., 1986, Transient electromagnetic response of a three-dimensional body in a layered earth: Geophysics, 51, 1608-1627.

Newman, G. A., Anderson, W. L., and Hohmann, G. W., 1987, Interpretation of transient electromagnetic soundings over three-dimensional structure for the central-loop configuration: Geophys. J. R. astr. Soc., 89:3, 889-914.

Poddar, M., and Anderson, W. L., 1992, Transient electromagnetic modeling of shallow A-type sections with 3D inhomogeneities: Geophysics, 57, 774-780.

Raiche, A. P., and Gallagher, R. G., 1985, Apparent resistivity and diffusion velocity: Geophysics, 50, 1628-1633.

Slee, J. C., 1988, Removal of the host rock response from time domain electromagnetic data by transforming to, and filtering in the frequency domain, unpublished MSc dissertation, University of Pretoria.

Spies, B. R., and Eggers, D. E., 1986, The use and misuse of apparent resistivity in electromagnetic methods: Geophysics, 51, 1462-1471.

Spies, B. R., and Parker, P. D., 1984, Limitations of large-loop transient electromagnetic surveys in conductive terrains: Geophysics, 49, 902-912.

Smith, R. S., and West, G. F., 1987, Electromagnetic induction in an inhomogeneous conductive thin sheet: Geophysics, 52, 1677-1688.

Swift, jr, C. M., 1988, Fundamentals of the electromagnetic method, *in* Nabighian, M. N., Ed., Electromagnetic methods in applied geophysics, Investigations in Geophysics 3, vol. 1: Soc. Expl. Geophys.

Van der Walt, J. J., 1991, Evaluation of the time-domain electromagnetic technique for groundwater exploration in the Kalahari, unpublished MSc dissertation, University of Pretoria.

Wait, J. R., 1958, Propagation of electromagnetic pulses in a homogeneous ground, Geophysics, 20, 630-637.

Ward, S. H., and Hohmann, G. W., 1988, Electromagnetic theory for geophysical applications, *in* Nabighian, M. N., Ed., Electromagnetic methods in applied geophysics, Investigations in Geophysics 3, vol. 1: Soc. Expl. Geophys.

Appendix A

Algorithm to model TDEM signal propagation by assuming a travelling current filament (smoke ring) through the earth

```
//
// Version 4.1
// Calculating the derivative of the magnetic field
// by adding line elements lying on a circle
// Advanced depth and radius calculation at contact parallel to x-axis
// 2 layer earth


#include <stdio.h>
#include <math.h>
#include <graphics.h>
#include <conio.h>
#include <stdlib.h>
#include <iostream.h>

#define pi 3.14159265
#define muzero 1.2566370614*pow(10,-6)
#define c2 .546479
#define channels 50
#define positions 40
//#define I 1
#define S 1


//------------------------------------------------//
//      Define variables                         //
//------------------------------------------------//

int n,i,pos,tchan;       // pos=positions, tchan=timechannel, spacing=between stations
int elements;            // Number of elements constituting circle (must be multiple of 4)
float tcon,zcon;

float spacing;
float depth_tcon;                // Depth at which current ring makes contact with vertical
contact
float depth[2][channels],
        currad[2][channels];   // Depth and radius of current rings
float ddepth[2][channels],       // Derivatives of above
    dcurrad[2][channels];

float xobs,yobs,zobs; // Observer position in x'y'z' frame
float xloop, yloop,zloop,loopside;   // Loop centre in x'y'z' frame and sidelength
float l;                   // Length of arc element, angle of rotation
float phi[channels],phival;      // Rotation in XZ plane because of contact

/*float tchanval[]={.089,.110,.140,.177,.220,.280,
```

```
                 .355,.443,.564,.713,.881,1.096,
                 1.411,1.795,2.224,2.850,3.600,
                 4.490,5.700,7.190};              // array with channel times (ms) //
*/
float
tchanval[]={.001,.002,.003,.004,.005,.006,.007,.008,.009,.01,.02,.03,.04,.05,.06,.07,.08,.09,
                 .10,.20,.30,.40,.50,.60,.70,.80,.90,1,2,3,4,5,6,7,8,9,
                 10,20,30,40,50,60,70,80,90,
                 100,200,300,400,500,600,700,800,900};

float I[channels],velocity[channels];
float xl,yl,zl;                          // Magnetic field variable
float dHxtot,dHytot,dHztot;

float dHxe[channels][positions],
     dHye[channels][positions],
     dHze[channels][positions];

float dHX,dHY,dHZ;

float r,alpha;                   // Variables for derivative of electric dipole field

float sigma1,sigma2,mu;                    // Conductivity value,

float dy,dx,dz,gamma,xm,ym,zm; // Variables for field calculation of ellipse
float uoy,uydip,eta,delta,omagn,ox,oy,oz,xd,yd,zd,
        oxrel,oyrel,ozrel,a,b,t,inter,uxdx,uxdy, uxdz,
        uydx,uydy,uydz,uzdx,uzdy,uzdz;

        // Graphics
double xmax,ymax,zmax,
        xmin,ymin,zmin,        // Max&Min values for graphs
        maxdepth;
int left,right,bottom,top,height,color;
float plotxbegin,plotxend,plotybegin,plotyend,posscale,plotzcon;
double xscale,depthscale,zscale;
char axval1[25],axval2[25];

//**************************************************//
//      Define functions                      //
//**************************************************//

        // Calculations
void Phi(float rad1,float rad2,float diff);
void Dipmag_dt(float x,float y, float z,float sig,float ds);
void DepthSize();
void TotOp();
void Ellipse();
void odip(int hom,int inhom);
void Comp();
void WriteF();

        // Graphics
void MaxMin(double x, double y, double z);
```

```
float max(float value1, float value2);
float min(float value3, float value4);
void InitGraph();
void BackCol1();
void BackCol2();
void GraphWin();
void dHlabels();
void Scale();
void Lineplot(double x,double x1,double y,double y1,double z,double z1);
void Curring();
void Valdisplay();
void Graph2();

//**************************************************//
//        MAIN                                      //
//**************************************************//

main ()
{

        clrscr();

        // Transmitter loop
        xloop=0;
        yloop=0;
        zloop=0;
        loopside=400;

        // Traverse line along positive x-axis
        xobs=0;//-2000; //Starting point for traverse in X+ direction
        yobs=yloop;
        zobs=zloop;
        spacing=20;

        // Position of vertical contact
        zcon=100000000;

        // Number of straight elements
        elements=20;

        // Conductivity of earth
        sigma1=.01;   // 0.01 mho/m=1/(100 ohm m)
        sigma2=.0001;
        mu=muzero;


        TotOp();

        InitGraph();
        Graph2();
        closegraph();

        WriteF();
```

```
        return(0);
}



//--------------------------------------------------//
//      Functions                              //
//--------------------------------------------------//

void Phi(float rad1,float rad2,float diff)
{
        phival=acos((rad1+rad2)/(sqrt(pow(rad1+rad2,2)+pow(diff,2))));
}
        // Derivative of field of transient electric dipole
void Dipmag_dt(float x,float y, float z,float sig,float ds)
{
        float Hdt1;
        r=sqrt(pow(x,2)+pow(y,2)+pow(z,2));
        alpha=sqrt(mu*sig/(4*tchanval[tchan]*pow(10,-3)));
        Hdt1=I[tchan]*ds*pow(alpha,3)*r/(2*tchanval[tchan]*pow(10,-3)*pow(pi,1.5))
            *exp(-alpha*alpha*r*r);
        dHX=Hdt1*(-z/r);
        dHY=0;
        dHZ=Hdt1*(-x/r);
}

void DepthSize()
{
        float velocity_tcon,test,inrad,t;
//      inrad=1.1*0.5*loopside;
        inrad=0;
        tcon=sigma1*mu*pi/16*zcon*zcon;
        depth_tcon=4/sqrt(pi)*sqrt(tcon/(sigma1*mu));
      // velocity_tcon=2/sqrt(pi*sigma2*mu*tcon);
cout<<"\nCalculating.\nPlease wait...";
cout<<"\ntcon="<<tcon;
        for (tchan=0; tchan<channels; tchan++){
                t=tchanval[tchan]*pow(10,-3);
      //        velocity=2/sqrt(pi*sigma2*mu*t);
                if(t<tcon){
                depth[1][tchan]=4/sqrt(pi)*sqrt(t/(sigma1*mu));
                currad[1][tchan]=(inrad+sqrt(t/(sigma1*mu)*8*c2));
                I[tchan]=1/(4*pi*c2*t/(sigma1*mu));
                velocity[tchan]=2/sqrt(pi*sigma1*mu*t);
                }
                else{

        currad[2][tchan]=inrad+sqrt(8*c2*tcon/(sigma1*mu))+(sqrt(8*c2*t/(sigma2*mu))
                                -sqrt(8*c2*tcon/(sigma2*mu)));
                depth[2][tchan]=depth_tcon+(4/sqrt(pi)*(sqrt(t/(sigma2*mu))-
                                sqrt(tcon/(sigma2*mu))));
                I[tchan]=1/(4*pi*c2*tchanval[tchan]/(sigma2*mu));
                velocity[tchan]=2/sqrt(pi*sigma2*mu*t);
                }
```

```
/*cout<<"\ntchan="<<tchanval[tchan]*.001<<"\nrad1="<<currad[1][tchan]<<"\nrad2="<<cur
rad[2][tchan];
getch();*/

            /*  if (t<tcon){
                        phi[tchan]=0;
                        }
                else{
                test=depth[2][tchan]-depth[1][tchan];
                Phi(currad[1][tchan],currad[2][tchan],test);
                if (test<0){
                        phi[tchan]=-phival;
                        }
                else{
                        phi[tchan]=phival;
                        }
                }  */
                }
}



        // Calculate the magnetic field of different time channels
        // and different positions
void TotOp()
{
        DepthSize();
        for(pos=0; pos<positions; pos++){
                for (tchan=0; tchan<channels; tchan++){
                   //   MagField();
                     //  if (tchanval[tchan]*.001>tcon){
                          Ellipse();
                 //       }
                 }
//cout<<"\ndHze="<<dHze[tchan][pos];
            }
}

//*************************************************************//
//      APPROXIMATING DISTORTED CURRENT RING WITH ELLIPSE    //
//*************************************************************//

void Ellipse()
{
   float sigma,zeta;
   double dHxetot,dHzetot;
   dHxetot=0;
   dHzetot=0;
   if (tchanval[tchan]*.001<tcon){
    a=currad[1][tchan];
    b=a;}
   else{
    a=currad[2][tchan];
    b=a;}
```

```
    inter=2*pi/elements;
    for (t=0; t<(2*pi); t+=inter){
      /* if (tchanval[tchan]*.001<tcon) odip(1,0);
         else odip(0,1);*/
         odip(1,0);
         if(zd>zcon){ sigma=sigma2;
            /*/  cout<<"\nsigma="<<sigma;
              getch();*/}
         else {sigma=sigma1;}
         Dipmag_dt(oxrel,oyrel,ozrel,sigma,l);
         Comp();
         dHxetot+=xl;
         dHzetot+=zl;
         }
//       zeta=acos(uzdz);
    dHxe[tchan][pos]=-dHxetot;
    dHze[tchan][pos]=-dHzetot;
}



void odip(int hom,int inhom)
{
          float xe,ye,ze,y1,y2,x1,x2,z1,z2,zmagn,
                   e1,e2,zdx,zdy,zdz;
          xe=xloop;
          ye=yloop;
          ze=zloop+depth[1][tchan]+depth[2][tchan];
          e1=depth[1][tchan]-ze;
          e2=depth[2][tchan]-ze;
          if (t<pi){
            z1=inhom*((e1-e2)/pi*t+e2);
            z2=inhom*((e1-e2)/pi*(t+inter)+e2);}
          else{
            z1=inhom*(-(e1-e2)/pi*t+2*e1-e2);
            z2=inhom*(-(e1-e2)/pi*(t+inter)+2*e1-e2);}
          x1=a*cos(t);
          y1=b*sin(t);
          x2=a*cos(t+inter);
          y2=b*sin(t+inter);
          xm=.5*(x1+x2);
          ym=.5*(y1+y2);
          zm=inhom*.5*(z1+z2);
          dz=inhom*(z2-z1);
          dy=y2-y1;
          dx=(x2-x1);//*cos(phi[tchan]);
          l=sqrt(dx*dx+dy*dy+dz*dz);
          xd=xe+xm;
          yd=ye+ym;
          zd=ze+zm;
          ox=(xobs+pos*spacing)-xd;
          oy=yobs-yd;
          oz=zobs-zd;
          // Unit vectors of el dipole and vector perp to it
```

```
        uydy=dy/l;
        uydx=dx/l;
        uydz=dz/l;
        zdx=y1*z2-y2*z1;
        zdy=-x1*z2+x2*z1;
        zdz=x1*y2-x2*y1;
        zmagn=sqrt(zdx*zdx+zdy*zdy+zdz*zdz);
        uzdx=zdx/zmagn;
        uzdy=zdy/zmagn;
        uzdz=zdz/zmagn;
        uxdx=uydy*uzdz-uzdy*uydz;
        uxdy=-uydx*uzdz+uzdx*uydz;
        uxdz=uydx*uzdy-uzdx*uydy;
        oxrel=ox*uxdx+oy*uxdy+oz*uxdz;
        oyrel=ox*uydx+oy*uydy+oz*uydz;
        ozrel=ox*uzdx+oy*uzdy+oz*uzdz;
}

void Comp()
{
        float uxx,uxz,uzx,uzz;
        uxx=uxdx;
        uxz=uzdx;
        uzx=uzdx;
        uzz=uzdz;
        xl=dHX*uxx+dHZ*uxz;
        zl=dHX*uzx+dHZ*uzz;
}



        //********************************//
        // Write data to file            //
        //********************************//
void WriteF()
{
        int xpos;
        FILE *fpointer;
        if((fpointer=fopen("c:\\data\\msc\\Data.dat","w"))==NULL)
          {cout<<"File(s) could not be opened\n";
          getchar();}
        else{
          fprintf(fpointer,"%.3f -> %.3f\n",sigma1,sigma2);
          fprintf(fpointer,"Position Tchannelval dHxe dHze\n");
          for (pos=0; pos<positions; pos++){
          for (tchan=0; tchan<channels; tchan++){
            // pos=20;
              xpos=(xobs+pos*spacing)-xloop;
                                                  fprintf(fpointer,"%d          %.16f          %.16f
%.16f\n",xpos,tchanval[tchan]*.001,dHxe[tchan][pos],dHze[tchan][pos]);
              }
            }
 /*
        for (pos=20; pos<positions; pos++){
```

```
          for (tchan=0; tchan<channels; tchan++){
          //  pos=20;
            xpos=(xobs+pos*spacing)-xloop;
                                    fprintf(fpointer,"%d      %f      %f      %f      %f      %f
%.20f\n",xpos,tchanval[tchan]*.001,currad[1][tchan],currad[2][tchan],depth[1][tchan],depth[2
][tchan],dHze[tchan][pos]);
                }
          }
/*        fprintf(fpointer,"Position T1dBx T2dBx T3dBx ");
          fprintf(fpointer,"T4dBx T5dBx T6dBx T7dBx T8dBx T9dBx T10dBx");
          for (pos=0; pos<positions; pos++){
            xpos=(xobs+pos*spacing)-xloop;
            fprintf(fpointer,"\n%d",xpos);
            for (tchan=0; tchan<channels; tchan++){
            fprintf(fpointer," %.16f",dBx[tchan][pos]);
            }

          } */
          /*tchan=0;
          for (pos=0; pos<positions; pos++){
            fprintf(fpointer,"%d %.16f\n",xobs+pos*spacing,dHz[tchan][pos]);
            cout<<"\ndHz["<<tchan<<"]["<<pos<<"]="<<dHz[tchan][pos];
            getch();
                      }
          fclose(fpointer);*/
          }
}

//------------------------------------------------------//
//      GRAPHICS                                        //
//------------------------------------------------------//
void MaxMin(double x, double y, double z)
{
              xmax=max(xmax,x);
              ymax=max(ymax,y);
              zmax=max(zmax,z);
              xmin=min(xmin,x);
              ymin=min(ymin,y);
              zmin=min(zmin,z);
}

float max(float value1, float value2)
{
        return ( (value1 > value2) ? value1 : value2);
}


float min(float value3, float value4)
{
        return ( (value3 < value4) ? value3 : value4);
}


          // Initialize graphics
```

```
void InitGraph()
{
        int gdriver=DETECT, gmode, errorcode;
        initgraph(&gdriver, &gmode, "c:\\tc\\bgi");
        errorcode = graphresult();
        if (errorcode != grOk){
                cout<<"Graphics error:%s\n"<<grapherrormsg(errorcode);
                cout<<"Press any key to halt:";
                getch();
                exit(1);
        }
}

                        // Background colour //
void BackCol1()
{
        setbkcolor(WHITE);
        setcolor(MAGENTA);
        setlinestyle(SOLID_LINE,0,THICK_WIDTH);
        rectangle(0,0,639,479);
}

void BackCol2()
{
        setbkcolor(YELLOW);
        setcolor(MAGENTA);
        setlinestyle(SOLID_LINE,0,THICK_WIDTH);
        rectangle(0,0,639,479);
}
                // Draw graph windows
void GraphWin()
{
        left=100;
        right=630;
        bottom=460;
        top=10;
        setlinestyle(SOLID_LINE,0,NORM_WIDTH);
        height=(bottom-top-20)/3;
        rectangle(left,top,right,top+height);
        rectangle(left,top+height+10,right,top+10+2*height);
        rectangle(left,top+2*height+20,right,bottom);
}

void dHlabels()
{
        setcolor(BLUE);
        settextstyle(0,HORIZ_DIR,1);
        outtextxy(300,470,"Position (m)");
        settextstyle(0,VERT_DIR,1);
        outtextxy(90,65,"dHx Field");
//   outtextxy(90,200,"By Field");
        outtextxy(90,200,"Current ring");
        outtextxy(90,335,"dHz Field");
}
```

```
        // Calculate scaling values
void Scale()
{
        xscale=height/(xmax-xmin);
        depthscale=height/(maxdepth);
        zscale=height/(zmax-zmin);
        posscale=((right-left)/(positions*spacing));
}

void Lineplot(double x,double x1,double z,double z1)
{
        //X
        color=9+tchan/3;
        setcolor(color);
        plotxbegin=pos*spacing*posscale+left;
        plotxend=(pos+1)*spacing*posscale+left;
        plotybegin=-(x-xmin)*xscale+top+height;
        plotyend=-(x1-xmin)*xscale+top+height;
        line(plotxbegin,plotybegin,plotxend,plotyend);
        //Z
        plotybegin=-(z-zmin)*zscale+bottom;
        plotyend=-(z1-zmin)*zscale+bottom;
        line(plotxbegin,plotybegin,plotxend,plotyend);
}

        //Current ring
void Curring()
{
        if (tchanval[tchan]*.001<tcon){
        circle(left+(currad[1][tchan]+xloop-xobs)*posscale,depth[1][tchan]
             *depthscale+top+height+10,1.5);
          if(left+(-currad[1][tchan]+xloop-xobs)*posscale>=left){
            circle(left+(-currad[1][tchan]+xloop-xobs)*posscale,
                    depth[1][tchan]*depthscale+top+height+10,1.5);}
        }
        else{
           circle(left+(xloop-xobs+currad[2][tchan])*posscale,
                  (depth[2][tchan])*depthscale+top+height+10,1.50);
           if(left+(-currad[2][tchan]+xloop-xobs)*posscale>=left){
                                                        circle(left+(-currad[2][tchan]+xloop-
xobs)*posscale,depth[2][tchan]*depthscale+top+height+10,1.5);}
           }

}

void Valdisplay()
{
        setcolor(RED);
        line(left,xmin*xscale+top+height,right,xmin*xscale+top+height);
        line(left,zmin*zscale+bottom,right,zmin*zscale+bottom);
        //Min & Max values displayed
        settextstyle(0,HORIZ_DIR,1);
        gcvt(xmin,2,axval1);
```

```
        outtextxy(20,top+height-10,axval1);
        gcvt(xmax,2,axval2);
        outtextxy(20,top,axval2);
        gcvt(zmin,2,axval1);
        outtextxy(20,bottom,axval1);
        gcvt(xmax,2,axval2);
        outtextxy(20,bottom-height,axval2);
        gcvt(xobs,2,axval1);
        outtextxy(left,bottom+10,axval1);
        gcvt(positions*spacing-abs(xobs),2,axval2);
        outtextxy(right-60,bottom+10,axval2);
        //Transmitter
        circle(left+(-xobs+xloop+loopside/2)*posscale,top+height+10,2);
        if(left+(-xobs+xloop-loopside/2)*posscale>=left){
        circle(left+(-xobs+xloop-loopside/2)*posscale,top+height+10,2);
        }
        //Current ring
//    outtextxy(80,top+height+10,"0m");
//    outtextxy(70,top+2*height,"600m");
        plotzcon=top+height+10+(zcon-zobs)*posscale;
        line(left,plotzcon,right,plotzcon);
}

void Graph2()
{
        double depth1max,depth2max;
  //    InitGraph();
        cleardevice();
        xmax=0;
        xmin=0;
        zmax=0;
        zmin=0;
        depth1max=depth[1][channels-1];
        depth2max=depth[2][channels-1];
        maxdepth=max(depth1max,depth2max);
        for (pos=0; pos<positions; pos++){
                for (tchan=7; tchan<channels; tchan++){
                MaxMin(dHxe[tchan][pos],dHye[tchan][pos],dHze[tchan][pos]);
            //  MaxMin(dHx[tchan][pos],dHy[tchan][pos],dHz[tchan][pos]);
                }
                }
        BackCol1();
        GraphWin();
        dHlabels();
        Scale();;

                // Plot data
        for(pos=0; pos<(positions-1); pos++){
                for(tchan=7; tchan<channels; tchan++){

Lineplot(dHxe[tchan][pos],dHxe[tchan][pos+1],dHze[tchan][pos],dHze[tchan][pos+1]);
                        Curring();
                        }
        }
```

```
        Valdisplay();
        getch();
//      closegraph();

}
```